Evaluating the antiviral role of thapsigargin against respiratory syncytial virus and influenza A virus

Thesis submitted to the University of Nottingham for the degree of Doctor of Philosophy

January 2025

Cristian Alexandru Preda

Declaration

I hereby declare that this thesis is my own original work and that it has not been submitted for a degree at any other institution. All contributions by other authors and all material from other sources have been duly acknowledged. Any collaboration with others during the course of this work has been fully recognised.

Cristian Alexandru Preda

Abstract

Respiratory syncytial virus (RSV) and influenza A virus (IAV) represent significant global health threats, exacerbated by their ability to co-infect hosts and evade immune responses. Current antiviral treatments are limited by specificity, resistance development, and variable efficacy in co-infection scenarios. This thesis investigates the potential of thapsigargin (TG) as a broad-spectrum antiviral agent targeting RSV, IAV, and their co-infections. TG demonstrated potent inhibition of viral replication across diverse cell models, including immortalised lines and primary human bronchial epithelial cells, with reductions in viral titres exceeding 85% at non-cytotoxic concentrations.

Mechanistically, TG disrupts calcium homeostasis by inhibiting the SERCA pump, triggering endoplasmic reticulum stress and activating the unfolded protein response (UPR). This state induces antiviral pathways, limiting viral protein synthesis and enhancing innate immune signalling. Notably, TG established a prolonged antiviral effect, maintaining efficacy for 48 hours post-treatment. In co-infection models, TG significantly reduced viral replication for both RSV and IAV.

TG's host-centric approach offers advantages over conventional antivirals, reducing the risk of resistance while providing broad-spectrum efficacy. However, challenges remain, including variability in response across cell types, potential off-target effects, and the need for extensive in vivo validation. Future directions include optimising TG delivery

methods, exploring combination therapies, and expanding its evaluation to other RNA viruses. This work establishes TG as a promising antiviral with implications for pandemic preparedness and respiratory disease management, highlighting its potential to redefine the therapeutic landscape against emerging viral threats.

Covid-19 Impact statement

The onset of the COVID-19 pandemic had a profound impact on my doctoral research soon after I completed my BBSRC DTP Rotation. I had only just begun establishing my experimental framework when nationwide lockdowns and strict institutional restrictions sharply limited access to critical laboratory facilities. Although I was not self-funded and therefore received financial support, the pandemic necessitated a comprehensive revision of my research plan to ensure continued progress toward my degree.

Due to prolonged closures of key laboratories, I was compelled to pause my original work. Collaborative efforts essential for my experiments were halted or significantly delayed, prompting a shift in research focus to avenues less reliant on immediate laboratory access. This required extensive re-evaluation of my research objectives and methods, especially as operational constraints persisted throughout the three UK lockdowns.

It is important to note that most of the data presented in the first results chapter was obtained prior to the lockdowns, benefiting from full access to laboratory resources and collaborative networks. However, the second results chapter reflects post-lockdown conditions, when reduced lab occupancy, extended supply chain disruptions, and chronic shortages of vital consumables—such as filtered sterile pipettes essential for RNA work—hampered experimental progress.

These constraints slowed experimental timelines, and I needed considerable flexibility in scheduling to secure the lab time necessary for data collection.

Despite financial support mitigating some concerns, the widespread disruptions of COVID-19 created significant challenges. They highlighted the importance of adaptability, collaboration, and resilience when striving to maintain academic momentum under exceptional circumstances.

Publications

Al-Beltagi, S., Preda, C., Goulding, L., James, J., Pu, J., Skinner, P., Jiang, Z., Wang, B., Yang, J., Banyard, A., Mellits, K., Gershkovich, P., Hayes, C., Nguyen-Van-Tam, J., Brown, I., Liu, J. and Chang, K., 2021. Thapsigargin Is a Broad-Spectrum Inhibitor of Major Human Respiratory Viruses: Coronavirus, Respiratory Syncytial Virus and Influenza A Virus. *Viruses*, 13(2), p.234.

Oral Presentations

Insights into the host antiviral mechanisms of store operated calcium entry, BBSRC DTP Spring Conference, Nottingham, 10th of May 2019

Thapsigargin Is a Broad-Spectrum Inhibitor of Coronavirus, Respiratory Syncytial Virus and Influenza A Virus, Nottingham, 15th of April 2021

Thapsigargin – A promising broad-spectrum antiviral against RSV, 26th of April, Nottingham, 2019

Poster Presentations

Improving innate immunity against emerging viruses: A novel approach to antivirals, BBSRC DTP Spring Conference, Nottingham, 3rd of July 2020

Acknowledgements

I would like to express my deepest gratitude to my principal supervisor, Ken Mellits, and my secondary supervisor, Leah V. Goulding, whose unwavering support, mentorship, and expertise have guided me throughout this research journey. I also extend my heartfelt thanks to my previous main supervisor, Professor Kin-Chow Chang, for originally welcoming me into this research group and for his invaluable contributions in shaping the foundations of my doctoral work. Their collective patience, insight, and encouragement have been instrumental, especially during the unprecedented challenges posed by the COVID-19 pandemic.

I wish to acknowledge Leah Goulding for her foundational research, which served as the inspiration for my own project. I am also immensely thankful to Jiayun Yang and Lamyaa Al-Dalawi for being both exceptional laboratory colleagues and wonderful friends; their advice, camaraderie, and the lively chats between experiments greatly enriched my time in the lab. A special note of appreciation goes to Belinda Wang, whose guidance during my initial RSV experiments was invaluable, as well as to my internal assessor, Tania Dottorini, for her patience, kindness, and genuinely helpful feedback during my annual reviews.

My doctoral experience would not have been the same without the support of my friends Nisha, Valeria, Matthew, and Chris, whose companionship made every challenge more manageable and every success more meaningful. Finally, and most importantly, I dedicate this thesis to my wonderful parents, whose unwavering love, encouragement, and belief in me have been the bedrock of my achievements. I owe my gratitude for this accomplishment to their steadfast support.

Table of contents

List of figures

List of tables

Abbreviations

- **A2**: RSV A2 strain
- **AIDS**: Acquired Immune Deficiency Syndrome
- **ALRIs**: Acute Lower Respiratory Infections
- **AM**: Alveolar Macrophage
- **ANOVA**: Analysis of Variance
- **APHA**: Animal and Plant Health Agency
- **ARDS**: Acute Respiratory Distress Syndrome
- **ATF6**: Activating Transcription Factor 6
- **ATP**: Adenosine Triphosphate
- **BBSRC**: Biotechnology and Biological Sciences Research Council
- **BiP**: Binding Immunoglobulin Protein (GRP78)
- **BSA**: Bovine Serum Albumin
- **Ca^{2+}**: Calcium Ion
- **Calreticulin (CRT)**: A chaperone protein in the ER
- **Calmodulin (CaM)**: A calcium-binding messenger protein
- **CDC**: Centers for Disease Control and Prevention
- **CHOP**: C/EBP Homologous Protein (encoded by **DDIT3**)
- **COPD**: Chronic Obstructive Pulmonary Disease
- **COVID-19**: Coronavirus Disease 2019
- **CRAC**: Calcium Release-Activated Channel
- **CRM1**: Chromosome Region Maintenance 1 (export receptor)
- **DAB**: 3,3′-Diaminobenzidine

- **DDIT3**: DNA Damage-Inducible Transcript 3 (gene encoding CHOP)
- **DMSO**: Dimethyl Sulfoxide
- **DMEM**: Dulbecco's Modified Eagle Medium
- **DNA**: Deoxyribonucleic Acid
- **dsRNA**: Double-Stranded RNA
- **DTT**: Dithiothreitol
- **eIF2α**: Eukaryotic Initiation Factor 2 Alpha
- **EIF2AK2 (PKR)**: Eukaryotic Translation Initiation Factor 2-Alpha Kinase 2 (Protein Kinase R)
- **ER**: Endoplasmic Reticulum
- **ERAD**: Endoplasmic Reticulum-Associated Degradation
- **FFA**: Focus Forming Assay
- **FFU**: Focus Forming Unit
- **F (RSV-F)**: Fusion Glycoprotein (RSV)
- **FCS**: Foetal Calf Serum (often "FBS" foetal bovine serum)
- **FDA**: Food and Drug Administration
- **G3BP1**: Ras GTPase-Activating Protein-Binding Protein 1 (stress granule component)
- **GAGs**: Glycosaminoglycans
- **G (RSV-G)**: G Glycoprotein
- **GRP94**: 94 kDa Glucose-Regulated Protein (encoded by **HSP90B1**)
- **h**: Hour(s)

- **H/N**: Haemagglutinin and Neuraminidase surface glycoproteins that define Influenza A virus subtypes (e.g., H1N1, H3N2)
- **hpi**: Hours Post-Infection
- **H1N1, H2N2, H3N2**: Subtypes of Influenza A Virus
- **HAT**: Human Airway Trypsin-Like Protease
- **HERPUD1**: Homocysteine-Inducible, Endoplasmic Reticulum Stress-Inducible, Ubiquitin-Like Domain Member 1
- **HIV**: Human Immunodeficiency Virus
- **HSP90B1**: Heat Shock Protein 90 Beta Family Member 1 (GRP94)
- **HSPA5**: Heat Shock Protein Family A (Hsp70) Member 5 (BiP/GRP78)
- **IAV**: Influenza A Virus
- **IB**: Inclusion Body
- **ICU**: Intensive Care Unit (mentioned in broader context)
- **IFN**: Interferon (general)
- **IFNβ**: Interferon Beta
- **IL**: Interleukin
- **IRF/IRF3**: Interferon Regulatory Factor (3)
- **IRE1**: Inositol-Requiring Enzyme 1 (ER stress sensor)
- **ISR**: Integrated Stress Response
- **ISGs**: IFN-Stimulated Genes
- **KDa**: Kilodalton
- **L (RSV-L)**: Large Polymerase Protein (RSV)
- **M (RSV-M)**: Matrix Protein

- **M (IAV-M)**: Matrix Segment (Influenza)
- **M1, M2**: Matrix Proteins of Influenza A
- **MAVS**: Mitochondrial Antiviral-Signalling Protein
- **MDCK**: Madin-Darby Canine Kidney Cells
- **MF**: Molecular Function (in gene ontology contexts)
- **min**: Minute(s)
- **MOI**: Multiplicity of Infection
- **MERS**: Middle East Respiratory Syndrome
- **MERS-CoV**: Middle East Respiratory Syndrome Coronavirus
- **NA**: Neuraminidase (Influenza)
- **NAI**: Neuraminidase Inhibitor
- **NHBE**: Normal Human Bronchial Epithelial Cells
- **NLR**: NOD-Like Receptor
- **NLS**: Nuclear Localisation Signal
- **NP**: Nucleoprotein (Influenza) / Also used for Nucleoprotein in RSV context
- **NPTr**: Newborn Pig Tracheal Cells
- **NS**: Non-Structural Proteins (RSV/IAV)
- **NS1, NS2**: Non-Structural Proteins (RSV) or Non-Structural Proteins (IAV)
- **NS2/NEP (IAV)**: Non-Structural Protein 2 / Nuclear Export Protein
- **NTC**: No Template Control (general PCR term)
- **P (RSV-P)**: Phosphoprotein (RSV)
- **PB1, PB2, PA**: Polymerase Basic 1, Polymerase Basic 2, and Polymerase Acidic Proteins (Influenza)

- **PBS**: Phosphate-Buffered Saline
- **PCA**: Principal Component Analysis
- **PFU**: Plaque-Forming Units
- **PKR**: Protein Kinase R (also known as EIF2AK2)
- **PM**: Plasma Membrane
- **PRR**: Pattern Recognition Receptor
- **qPCR**: Quantitative Polymerase Chain Reaction
- **qRT-PCR / RT-qPCR**: Quantitative Reverse Transcription PCR / Reverse Transcription–Quantitative PCR
- **Rab11**: Ras-Related Protein Rab-11
- **RIG-I**: Retinoic Acid-Inducible Gene I
- **RNA**: Ribonucleic Acid
- **RNAse L**: Endoribonuclease L
- **RNA-Dependent RNA Polymerase (RdRp)**: Viral polymerase
- **RPM**: Revolutions Per Minute
- **RSV**: Respiratory Syncytial Virus
- **SARS**: Severe Acute Respiratory Syndrome
- **SARS-CoV-1**: Severe Acute Respiratory Syndrome Coronavirus 1
- **SARS-CoV-2**: Severe Acute Respiratory Syndrome Coronavirus 2
- **SCID**: Slow Ca^{2+}-Dependent Inactivation (context-dependent acronym)
- **SERCA**: Sarco-Endoplasmic Reticulum Ca^{2+} ATPase
- **SH**: Small Hydrophobic Glycoprotein (RSV)

- **SI**: Selectivity Index
- **SOCE**: Store-Operated Calcium Entry
- **STIM**: Stromal Interaction Molecule
- **Su**: Sunitinib
- **TBS**: Tris-Buffered Saline
- **TG**: Thapsigargin
- **TMPRSS2**: Transmembrane Protease Serine S-1 Member 2
- **Tris**: Tris (Hydroxymethyl) Aminomethane
- **UPR**: Unfolded Protein Response
- **vRNPs**: Viral Ribonucleoproteins (Influenza)
- **VERO E6**: African Green Monkey Kidney Epithelial Cells (IFN-deficient line)
- **WHO**: World Health Organization
- **XBP1**: X-Box Binding Protein 1
- **4u8C**: A chemical inhibitor of the IRE1 RNase domain
- **Sunitinib**: (Appears as “Su” in text) Tyrosine kinase inhibitor used here to inhibit RNAse L

General introduction

Human susceptibility to RNA viruses is a persistent concern, given factors such as population growth, migration, close contact with animals and wildlife. These pathogens have short generation times, high mutation rates, and can co-infect hosts, increasing the likelihood of widespread outbreaks. The COVID-19 pandemic serves as a stark reminder of the devastating consequences of these pathogens in the absence of adequate prevention and treatment.

This introduction reviews the historical impact and risks of major RNA virus outbreaks and further focuses on two important airborne pathogens, influenza A and respiratory syncytial virus, which can co-infect individuals. Finally, thapsigargin (TG), a compound with established biological activity, is proposed as a promising means to inhibit these viruses by targeting a shared mechanism - the unfolding protein response.

1.1 The burden of viral outbreaks

Outbreaks are defined as an unexpected rise in the number of people displaying a health condition in a specific geographic area, whereas endemic conditions occur at a predictable rate (Grennan, 2019). An epidemic is an outbreak that spreads to a larger area, while a pandemic is an epidemic that spreads globally (Piret and Boivin, 2021). Although

these terms can also be used to describe non-infectious diseases, in the context of this thesis they will specifically refer to viral RNA infections. Pandemics caused by viral RNA outbreaks throughout history have resulted in significant human and economic damage, including deaths, economic instability, political regime changes, and psychosocial burdens (Sampath et al., 2021). Notable pandemics of the twentieth and twenty-first centuries include infections caused by SARS-CoV-2 (2019), SARS-CoV-1 (2002), influenza A/H1N1 (1918; 2009), influenza A/H2N2 (1957), influenza A/H3N2 (1968), and HIV (1981) (Table 1.1).

Table 1.1 Viral pandemics in the twentieth and twenty-first century.

Pandemic	Timeline	Pathogen	Area of origin	Vector	Death toll
Spanish Flu	**1918-1919**	**Influenza A (H1N1)**	**Not clear**	**Likely avian origin**	**50-100 million (Johnson and Mueller, 2002)**
Asian Flu	**1957-1958**	**Influenza A (H2N2)**	**China**	**Likely avian origin**	**1-2 million (Viboud et al., 2016)**
Hong Kong Flu	**1968**	**Influenza A (H3N2)**	**China**	**Likely avian origin**	**500,000-2 million (Viboud et al., 2005)**
HIV/AIDS	**1981-ongoing**	**HIV**	**Central Africa**	**Non-human primates**	**36 million (UNAIDS, 2013)**
Severe acute respiratory syndrome coronavirus	**2002-2003**	**SARS-CoV-1**	**China**	**Bats**	**774 (Stockman et al., 2006)**
Swine Flu	**2009-2010**	**Influenza A (H1N1)**	**Mexico**	**Pigs**	**20,000-500,000 (Simonsen et al., 2013)**
COVID-19	**2019-2023**	**SARS-CoV-2**	**China**	**Not clear, likely bats or pangolin**	**>6 million (Wang et al., 2022)**

The following section will briefly discuss each of these pandemics, with emphasis on the prevention and treatment methods used at the time.

1.1.1 Brief history of pandemics

1.1.1.1 Spanish flu (1918)

The unfortunate record of deaths caused by viruses is set by the 1918 H1N1 “Spanish flu”, when 20 to 100 million people died (Taubenberger and Morens, 2010). However, this wide range reflects the challenge of severe underreporting during the pandemic (Edwin O. Jordan, 1928). More rigorous demographic analysis suggests the death toll was likely in the upper portion of this range, between 50 to 100 million (Johnson and Mueller, 2002). When adjusting for today’s human population (~4.5 times higher), it would account for 225 to 450 million deaths. The pandemic occurred at the end of World War I and its transmission was facilitated by the close contact of troops.

In three waves (spring, autumn, and winter) the virus is presumed to have infected one third of the world’s population (≈500 million people) (Burnet and Clark, 1942). The pandemic was characterised by an exceptionally high case fatality rate of greater than 2.5%, compared to less than 0.1% in other influenza pandemics, and a distinctive age-specific mortality pattern in which young adults aged 20-40 years were disproportionately affected, accounting for nearly half of all deaths (Taubenberger and Morens, 2006). The animal origin has not been fully elucidated, but since the natural reservoir for all influenza A is avian and more recent genetic, phylogenetic, and functional analyses of the 1918 H1N1 indicate an avian lineage, it increases the likelihood that a close

precursor of the pandemic virus was of bird origin, mutated in a mammalian host, likely pigs, before reaching humans (Rabadan, Levine and Robins, 2006; Qi et al., 2012). Almost all influenza A pandemics that followed have been linked with a descendant of the 1918 H1N1, including the reassorted H2N2 (1957) and H3N2 (1968), which have incorporated important genes from the 1918's pathogen. For its importance in influenza A's transmission and evolution it was labelled the "Mother of All Pandemics" (Taubenberger and Morens, 2006). At the time there were no effective drugs or vaccines, and prevention was achieved by wearing a face mask while schools, theatres and businesses were shut down. The bodies were piled up in morgues until the virus ran its course (Knobler et al., 2005). After the Spanish flu was first isolated in 1931, a great deal of effort was spent towards diagnosis, surveillance, and vaccine development, with the first influenza A vaccine developed during the late 1930s and early 1940s (Shope, 1931; Smith, Andrewes and Laidlaw, 1933; Francis and Salk, 1942; Francis et al., 1945).

1.1.1.2 Asian flu (1957)

The "Asian flu" was caused by influenza A/H2N2 virus, a reassortment of the human 1918 H1N1 with the avian H2N2 (Schäffr et al., 1993). From 1957 to 1958, the approximate number of deaths was between 1 to 2 million people (Saunders-Hastings and Krewski, 2016). The Asian flu came in waves, with a stronger second wave similarly to the Spanish flu. However, the illness was much milder than the Spanish flu, with a maximum case fatality rate of ≈0.67%, but with a similar mortality curve shifted towards young adults (Viboud et al., 2005; Viboud et al., 2016). Society was not much disrupted, the economic impact was small, and recovery was rapid. In the United States, only 3 to 8% of the population were absent from work (Trotter et al., 1959).

The Asian flu was the first time when comprehensive surveillance was used to track an emerging disease and the first time to study the immunological response to influenza vaccination (Kilbourne, 2006; Henderson, 2016). The development and distribution of vaccines was slow, with limited circulation in 1957, in the United States and Europe (Jackson, 2009). There was great emphasis on vaccination campaigns, with a vaccine effectiveness of 53 to 60%. However, the adoption was low, with only 30 million doses distributed worldwide, not enough to have a significant impact on the outcome of the disease (Jackson, 2009; Henderson et al., 2009). There were no antivirals available on the market. Some physicians were prescribing antibiotics which are not effective against viral infections but might have helped with secondary

bacterial infections. The pandemic slowed down by itself, and H2N2 became part of the regular wave of seasonal flu until 1968 (Jackson, 2009).

1.1.1.3 Hong Kong flu (1968)

Ten years later, the previous Asian flu strain reassorted to H3N2 and influenza A turned pandemic once again, known as the Hong Kong flu. It was highly transmissible but even milder than the Asian flu. The death toll is estimated at ≈500,000 to 2 million (Guan et al., 2010; Reperant, Moesker and Osterhaus, 2016). The Hong Kong flu was the first pandemic to show an increased spread due to air travel (Cockburn, Delon and Ferreira, 1969; Longini, Fine and Thacker, 1986). Like previous influenza A pandemics, it tended to infect young adults, but mortality was low due to pre-existing immunity to the neuraminidase antigen (N2) from previously circulating influenza (Saunders-Hastings and Krewski, 2016). The economic and social impact was minimal, and the low severity and mortality rates did not endorse the need for major disruption (Taubenberger and Morens, 2010). The infection control involved a combination of vaccination, antibiotics for secondary (bacterial) pneumonia and hospitalization. Vaccines were only made available after the peak of the pandemic (Saunders-Hastings and Krewski, 2016). Importantly, at this point still no antivirals were used in the treatment of a pandemic.

1.1.1.4 HIV/AIDS (1981)

Acquired immune deficiency syndrome (AIDS) is caused by human immunodeficiency virus type 1 and 2 (HIV-1 and HIV-2). While both are positive-sense, single-stranded RNA viruses that lead to progressive failure of the immune system and increased risk of other illnesses such as cancers, bacterial or viral infections (Powell et al., 2016), they have markedly different global distributions and transmission characteristics. HIV-1 is responsible for the global pandemic and accounts for most HIV infections worldwide, whereas HIV-2 is largely confined to West Africa and has significantly lower transmissibility rates (Marlink et al., 1994; Campbell-Yesufu and Gandhi, 2011). The global HIV/AIDS pandemic was first recognised as an illness in 1981 when young homosexual men reported unusual infections and malignancies (Greene, 2007). HIV/AIDS is primarily a sexually transmitted disease, occurring through contact or transfer of blood, semen, and vaginal fluids (Breskin, Adimora and Westreich, 2017). Non-sexual transmission is possible from mother to infant through pregnancy and breast milk (Mabuka et al., 2012). The pandemic is still ongoing and as of July 2022, more than 40 million people have died as a result of contracting HIV. Currently, 38.4 million live with the disease globally, out of which 25.6 million live in the African continent (WHO, 2022).

The management of HIV/AIDS is done using multiple antiretroviral drugs. These antiviral drugs have a profound effect in keeping the viral load under detectable levels (<50 copies/ml) in patients who consistently

adhere to treatment. It was shown that sexual transmission of HIV is not possible when viral loads remain undetectable in treated patients; therefore, modern antivirals help millions of people live with the illness (Cohen et al., 2016).

1.1.1.5 Severe acute respiratory syndrome (SARS-CoV-1) (2002)

Caused by the SARS coronavirus (SARS-CoV-1), it was the first pandemic of the 21st Century. It emerged from China, Guandong province, and was first noted in November 2002 as an outbreak of acute pneumonia (Cheng, Chan, To and Yuen, 2013). It was identified as a global threat by the World Health Organization (WHO) in March of 2003 and it went on to spread to over 30 countries (Peiris et al., 2003). The animal origin was initially thought to be palm civets, but it was later established to be horseshoe bats (Wang and Eaton, 2007). SARS-CoV-1 is an RNA-positive airborne virus with ability for efficient person-to-person transmission. At the time it had a case fatality rate of >9.6%. Fortunately, the outbreak was short-lived, ending in July 2003 with 8096 cases reported, leading to 774 deaths (Olowokure et. al, 2004). While no vaccines were available, various antiviral treatments were used, including ribavirin (used in over 50% of reported cases), lopinavir/ritonavir, and interferon-α, though their clinical efficacy remained uncertain due to the lack of randomized controlled trials (Cheng et al., 2013).

1.1.1.6 Swine Flu (2009)

The 2009 influenza A pandemic was caused by a novel H1N1 virus that, while sharing the same subtype designation as the 1918 pandemic virus, had a completely different origin and genetic makeup. It emerged as a re-assortment of bird, swine, and human influenza, and it began in Mexico, April of 2009. It reached pandemic status within weeks and ended by May 2010. The death toll was estimated to be 20,000 to 500,000. The virus infected >10% of the global population. Notably, the 2009 influenza A marked the first pandemic with available influenza antivirals in the form of neuraminidase inhibitors (NAIs) such as Oseltamivir (Tamiflu) and Zanamivir. Oseltamivir was approved by the FDA in 1999 for children aged 13+ and for adult prophylaxis treatment (preventive use). In early 2004 growing awareness of a potential H5N1 pandemic triggered a surge in preparedness (Berera and Zambon, 2013). In 2005 the WHO issued a checklist to guide preparations for a future influenza pandemic which included references to antiviral prophylaxis treatments. The guidance was reiterated in 2007 outlining a “rapid containment strategy” (WHO, 2007). During the Swine flu pandemic, the infected immunocompromised patients receiving antivirals posed a major risk - potential antiviral resistance. Since the nature of the antivirals was to block H1N1’s neuraminidase, the virus could have mutated and adapted. The WHO strongly advised against the use of antivirals for prophylactic purposes and instead encouraged the use of antivirals post-symptoms (WHO, 2009). The FDA has issued

an emergency-use authorization for oseltamivir and zanamivir to be used in infants. Following the authorization, the Centers for Disease Control and Prevention (CDC) offered guidelines for adequate dose use (CDC, 2009) (Table 1.2). In September 2009, the FDA allowed the use of a new H1N1 pandemic influenza vaccine, containing inactivated or attenuated influenza. They were offered either as a jab or as nasal spray. The vaccines offered greatest benefit to younger recipients as older individuals had some immunity from exposure to similar viruses in the past (Collignon, 2010). The Swine flu came with a great deal of fear, but with mild repercussions. The virus ran its course and in August 2010 the WHO had officially declared the end of the pandemic (WHO, 2010).

Table 1.2 Historical recommended dosage of antivirals against swine flu.

Adapted from CDC (2009).

Agent, group	Treatment	Chemoprophylaxis
Oseltamivir Adults	75 mg capsule twice/day for 5 days	75 mg capsule once/day
Children		
By weight:		
15 kg or less	60 mg/day divided into two doses	30 mg once/day
15–23 kg	90 mg/day divided into two doses	45 mg once/day
24–40 kg	120 mg/day divided into two doses	60 mg once/day
>40 kg	150 mg/day divided into two doses	75 mg once/day
Zanamivir Adults	Two 5 mg inhalations (10 mg total) twice/day	Two 5 mg inhalations (10 mg total) once/day
Children	Two 5 mg inhalations (10 mg total) twice/day, age 7 years or older	Two 5 mg inhalations (10 mg total) once/day, age 5 years or older

1.1.1.7 COVID-19 (2019)

The latest pandemic was caused by the SARS-CoV-2 coronavirus. First identified in December of 2019 in Wuhan, China, is the third coronavirus outbreak after SARS-CoV-1 and MERS-CoV. Infection with SARS-CoV-2 led to COVID-19 disease, with nonspecific symptoms such as fever, shortness of breath, cough, headache, myalgias, diarrhoea, fatigue, sore throat, anosmia, ageusia, chest pain, haemoptysis, sputum production, rhinorrhoea, nausea, vomiting, skin rash, impaired consciousness, and seizures (Chan et al., 2020; Xu et al., 2020). SARS-CoV-2 is transmitted from person to person via respiratory droplets, making it a very fast spreading illness (Li et al., 2020). Furthermore, SARS-CoV-2 can be carried by asymptomatic people and since symptoms only appear 2 to 14 days after the viral encounter, it can lead to false-negative testing results and can therefore increase the expansion of the virus within the population (Esakandari et al., 2020; Zhao et al., 2020). Since it was declared a global pandemic by the WHO, the virus spread to 223 countries with more than 472 million cases and >6 million deaths as of March 2022 (Cascella et al., 2022).

SARS-CoV-2 had a case fatality rate between 1% and 4% varying between individual and their comorbidities; countries and percentage of population vaccinated (Sorci, Faivre and Morand, 2020; Haider et al., 2022). Black, Hispanic, and Asian ethnic minorities that contract the virus had an increased risk of death (Sze et al., 2020). The original variant of SARS-CoV-2 shared 82% genomic similarity with human SARS-CoV-1

and while the exact origin remains difficult to establish with absolute certainty, it is widely accepted to have evolved from a strain found in bats (Chan et al., 2020). It has been hypothesised that SARS-CoV-2 evolved from bats through intermediate hosts such as pangolins, then to humans (Zhang, Wu and Zhang, 2020).

In attempt to stop COVID-19 from spreading and overwhelming the medical system most countries had adopted restrictive measures. It included quarantines, lockdowns, social distancing, mandatory face masks, mass testing, travel restrictions, encouraging working from home etc. (Han et al., 2020). Important preventative methods included extraordinary efforts to develop vaccines at an unprecedented speed. Notably, this was the first instance where mRNA vaccines (BNT162b2 and mRNA-1273) were rolled out for mass adoption, within a year from the start of the pandemic. Both mRNA and conventional vaccines were produced for public use, with multiple “booster” shots being offered as variations of the original SARS-CoV-2 emerged: Alpha (B.1.1.7), Beta (B.1.351), Gamma (P.1), Delta (B.1.617.2) and Omicron (B.1.1.529) (Cascella et al., 2022).

Several pharmacological advancements have been achieved for the treatment of COVID-19. FDA approved emergency use of drugs like Remdesivir, Molnupiravir, and Paxlovid. Additional treatments include immunomodulatory agents and products that contain anti-SARS-CoV-2 neutralizing antibodies (FDA, 2022).

1.2 Future causes of concern

Humans have always been affected by epidemics originated from animals and wildlife (Taylor, Latham and woolhouse, 2001). There is consensus that human-animal contact is essential for cross-species transmission of infectious disease. This phenomenon is known as *zoonosis*. Although humans have coexisted with animals and wildlife for millennia, the increased population growth, globalisation, farming at scale and unsustainable exploitation of natural resources have inflated the risk of disease spill over in recent decades (Magouras et al., 2020).

1.2.1 Wet and live animal markets

The concept of a “wet market” is popular in Asia, especially in China, where up to 77% of people prefer them over regular supermarkets as a source of fresh meat (Goldman, Krider and Ramaswami, 1999; Zhong, Crang and Zeng, 2019). Here plants and live animals are sold as food or medicine and are slaughtered at the market. Wet markets usually sell live fish, crustaceans, poultry, various mammals but some markets also sell wild animals such as reptiles, porcupines, and other species (Magouras et al., 2020). Furthermore, in countries like China, consuming wild animals is a symbol of wealth as it is thought to be more nutritious (Zhang and Yin, 2014). Wet markets are known to have poor hygiene standards (Lo et al., 2019). Animals are removed from their habitat and kept in crowded conditions, sometimes in cages holding multiple

species, with poor hygiene and limited health monitoring. Due to these conditions, most suffer from stress which may cause immunosuppression and shedding of pathogens (Martin, 2009; Fischer and Romero, 2019). For example, SARS-CoV-1 and SARS-CoV-2 outbreaks are believed, although still debated, to have emerged from the wet markets of Guandong Province and Wuhan (Magouras et al., 2020).

1.2.2 Wildlife hunting

Hunting has been replaced by agriculture and livestock breeding about 10,000 years ago (Marlowe, 2005). However, in low-income areas of the world wildlife hunting is still a common practice as the major source of animal protein. In various regions of Africa, wildlife meat is known as “bushmeat” (Dawson, 2017). In this context, wildlife is a major source of protein, income, and trading products for medicines (Kümpel et al., 2010; Wright and Priston, 2010). The hunters, traders and buyers are exposed to pathogens present in animal carcasses and body fluids. HIV is believed to have originated from non-human primates and it is often suggested that contact with hunters was the reason of transmission into the human population (Gao et al., 1999; Sharp and Hahn, 2011).

1.2.3 Wildlife farming

Several wild species of mammals, such as deer, rodents, civets, and fur mammals are bred to provide protein and income (Jori et al., 2013). The living conditions are poor, and animal health is rarely monitored, exposing the farmed species to stress and immunosuppression, which can lead to the emergence of spill over diseases (Martin, 2009). The spillover can also come from humans to animals, where further mutations may occur. An example is the detection of SARS-CoV-2 in mink farms in Netherlands (Oreshkova et al., 2020).

1.2.4 Domestic animals

Intensive farming is expanding due to increasing global population and urbanization, causing changes in land use, and creating shared environments between wildlife and domestic species. This may lead to spillover events, such as the emergence of the Nipah virus in Malaysia, 1998, where pigs were farmed near mango plantations allowing for viral transmission from bats to pigs through consumption of food contaminated by bat urine or saliva (Daszak et al., 2012).

1.2.5 Climate change

Well-known for its destabilising effects on ecosystems, climate change may also play an important role in the emergence of future outbreaks.

Changing environmental conditions have an impact on species range and density, allowing novel interaction between species and increasing the risk of zoonotic transmission (Carlson et al., 2020). Historically, periods of drought followed by heavy precipitation, as well as unusually mild winters, are thought to have driven upsurges in rodent populations, contributing to the emergence of pulmonary hantavirus in the United States in 1993 (Patz, 1996). In Australia, populations of the black flying fox (or black fruit bat)—a key reservoir of Hendra virus—originally found in the northern regions of the country have shifted approximately 100 km southward due to climate change. This geographic transition has facilitated spillover events into the southern horse population, which in turn led to human infections (Martin et al., 2018; Yuen et al., 2021). These shifts in bat populations are occurring globally, yet they are underappreciated. Bat populations are a major reservoir host for several high-fatality pathogens (Brook et al., 2020).

Some respiratory pathogens such as influenza are more seasonal in temperate climates and more persistent in tropical locations. Although more endemic, respiratory syncytial virus exhibits seasonal surges driven by similar climatic factors as influenza A, including temperature, humidity, and precipitation (Viboud, Alonso and Simonsen, 2006; Baker et al., 2019). For both viruses, transmission tends to increase during periods of low humidity in temperate regions or during rainy seasons in tropical climates (Baker et al., 2019).

1.2.6 Close contact

The growth of the human population and increasing globalisation have contributed to heightened pandemic risk, both by expanding human–animal interfaces and through the rapid spread of pathogens across borders via international air travel. Domestic animals and wildlife are constantly adapting to their changing environments, which increases the risk of viral spillover with major epidemic and pandemic potential, particularly for RNA viruses (Carrasco-Hernandez et al., 2017; Woolhouse and Brierley, 2018). As the most common class of new human pathogens, RNA viruses pose a major threat to public health (Rosenberg, 2014). Zoonotic pathogen transmission has caused major epidemics and pandemics resulting in significant morbidity and mortality throughout the human population (Taubenberger and Morens, 2010).

1.2.7 Lack of wide-range antivirals

The development of broad-spectrum antivirals remains a formidable challenge for multiple reasons: while viruses are intracellular parasites that depend on host cells for replication, they co-opt numerous stages of the host cellular life cycle, and most antiviral drugs target specific phases of viral multiplication. It is difficult to find compounds that exclusively interrupt viral replication without affecting the host cells. Additionally, some viruses can rapidly develop resistance to these drugs or suffer

unwanted mutations (Littler & Oberg, 2005; Chaudhuri et al., 2018; Andrei, 2021).

Currently, 106 drugs have been authorised for the treatment of viral diseases. Despite the vast diversity of human viruses (over 200 known types), antivirals have only been approved for a select few, including HIV, HCV, influenza virus, RSV, HBV, HPV, herpesviruses, and SARS-CoV-2 (Tompa et al., 2021). Half of these approved drugs are utilised for HIV treatment. The antiviral medications available to treat viral infections have saved tens of millions of lives over recent decades and will remain fundamental in the treatment of both current and (re)emerging viral infections. Although significant progress has been achieved, considerable challenges remain. While the development of broad-spectrum antiviral compounds remains a crucial strategy for responding to (re)emerging viral threats, it is not the only viable approach. Targeting conserved viral components, such as polymerases, has enabled the use of nucleoside and nucleotide analogues—such as ribavirin, tenofovir, and cidofovir—against a wide range of unrelated viruses, illustrating the feasibility of broad-spectrum antivirals (Andrei, 2021). These agents interfere with viral genome replication, a process shared across many virus families, making them particularly amenable to cross-viral application. However, many currently approved antivirals are virus-specific, designed to inhibit unique viral proteins such as proteases, integrases, or neuraminidases. These compounds, while highly effective, typically have a narrow spectrum of activity and require tailored development for each virus or viral family. A balanced approach that

includes both broad-spectrum agents for rapid outbreak response and virus-specific therapies for targeted treatment is therefore ideal for strengthening our preparedness against future pandemics. Furthermore, there is a massive need for antiviral drugs that not only effectively suppress viral replication but also limit drug resistance and viral adaptation.

1.2.8 Co-infections

Viruses are intracellular pathogens that replicate by infecting specific types of cells, a phenomenon known as *tropism*. As various viruses share similar tropisms, certain cells and tissues are at risk of being targeted by a diverse array of viruses from different taxonomic groups. From this perspective, a particular tissue or body compartment can be seen as an ecological niche where multiple members of a viral community coexist. It's notable that dual infections by more than one virus occur in approximately 10–30% of all respiratory viral infections, with a higher prevalence observed in children (Franz et al., 2010, Nickbakhsh et al., 2016).

Influenza A is a virus capable of infecting both avian and mammalian hosts with historical and future importance (Mostafa et al., 2018). During the COVID-19 pandemic, it was reported that patients suffering from co-infections of SARS-CoV-2 and Influenza A were associated with a higher risk of intensive care unit (ICU) admission, and that SARS-CoV-2 and RSV co-infection was also occurring (Cong et al., 2022). At the cellular

level, the mechanisms behind the interactions that influence the outcomes of coinfections remain poorly understood. Direct interactions among viruses within coinfected cells may lead to alterations in the viral progeny. These alterations can encompass genomic rearrangements that have the potential to create new pathogens with pandemic capabilities, similar to SARS-CoV-2 and Influenza A (Salzberg, 2009; Boni et al., 2020). Another mechanism includes pseudotyping, which involves the incorporation of surface proteins from one virus into another (Zavada, 1982; Akkina et al., 1996; Duvergé & Negroni, 2020). More recently, in vitro studies have shown that co-infection with Influenza A and RSV can result in the formation of infectious hybrid viral particles (HVP). While the clinical significance of this finding remains to be determined, these particles have been observed to sustain multiple rounds of infection and to assist in the propagation of Influenza A by utilising a modified RSV glycoprotein (F) to facilitate viral entry (Haney et al., 2022). These concerning findings emphasize the urgent need for a broad-spectrum antiviral capable of effectively suppressing both Influenza A and RSV, especially in cases of co-infection. This need forms the central foundation of this thesis.

To better grasp the shared traits and potential mechanisms that could be leveraged to create an antiviral effect, it is essential first to understand both Influenza and RSV, then, explore the common cascade of events that can disrupt their replication.

1.3 Influenza Virus

1.3.1 Taxonomy and nomenclature

Influenza viruses belong to the family *Orthomyxoviridae* and consist of four genera: Influenza A virus (Alphainfluenzavirus, IAV), Influenza B virus (Betainfluenzavirus, IBV), Influenza C virus (Gammainfluenzavirus, ICV) and Influenza D virus (Deltainfluenzavirus, IDV) (Asha and Kumar, 2019). They are envelope viruses with a segmented genome, comprising single stranded negative sense-RNA (vRNA) (Hause et al., 2014). Influenza viruses share a common ancestry but have been genetically diverged. The exchange of vRNA only occurs within each genus (Breen et al., 2016).

1.3.2 Impact

IAV is responsible for 14 pandemics since the 1500s and in 1918 it led to the worst viral pandemic ever recorded (Johnson and Mueller, 2002). The ability of IAV to rapidly undergo genetic and antigenic changes through reassortment between subtypes enables it to evade host adaptive immune responses by altering surface proteins targeted by neutralising antibodies. In addition, specific mutations—particularly in viral RNA structures and immune-antagonistic proteins such as NS1—can interfere with innate immune detection by modifying pathogen-associated molecular patterns (PAMPs) or disrupting pattern recognition

receptor (PRR) signalling, notably RIG-I and interferon pathways, thereby further complicating the development of effective vaccines (Su et al., 2024). On a yearly basis seasonal influenza-associated respiratory diseases account for 291,243 to 645,832 deaths worldwide with the highest impact on low and middle economy countries. High risk groups are young children (<5 years old), pregnant women and 65 years or older adults (Iuliano et al., 2018).

1.3.3 Structure

IAV and IBV contain 8 viral RNA (vRNA) gene segments which encode transcripts for at least 10 viral proteins while ICV and IDV contain only 7 vRNA segments (Dou et al., 2018). The 10 structural proteins are: three RNA-dependent RNA polymerase (RdRp) subunits known as polymerase basic protein 1 (PB1), polymerase basic protein 2 (PB2) and polymerase acidic protein (PA); hemagglutinin (HA), nucleoprotein (NP), neuraminidase (NA), matrix protein (M1 and M2) and non-structural proteins (NS1 and NS2 or nuclear export protein [NEP]) (Mostafa et al., 2018). IAV is surrounded by the envelope, a host-derived lipid membrane that contains the viral proteins HA, NA and M2. The M1 protein coat encloses ribonucleoproteins (vRNPs) complexes. Each vRNP comprises a vRNA segment wrapped round numerous NPs and bound by PA, PB1 and PB2 which form the heteromeric viral polymerase (Arranz et al., 2012). Each vRNA forms base pairing between the semi-complementary 5’ and 3’ ends to create a hairpin (Pflug et al., 2014).

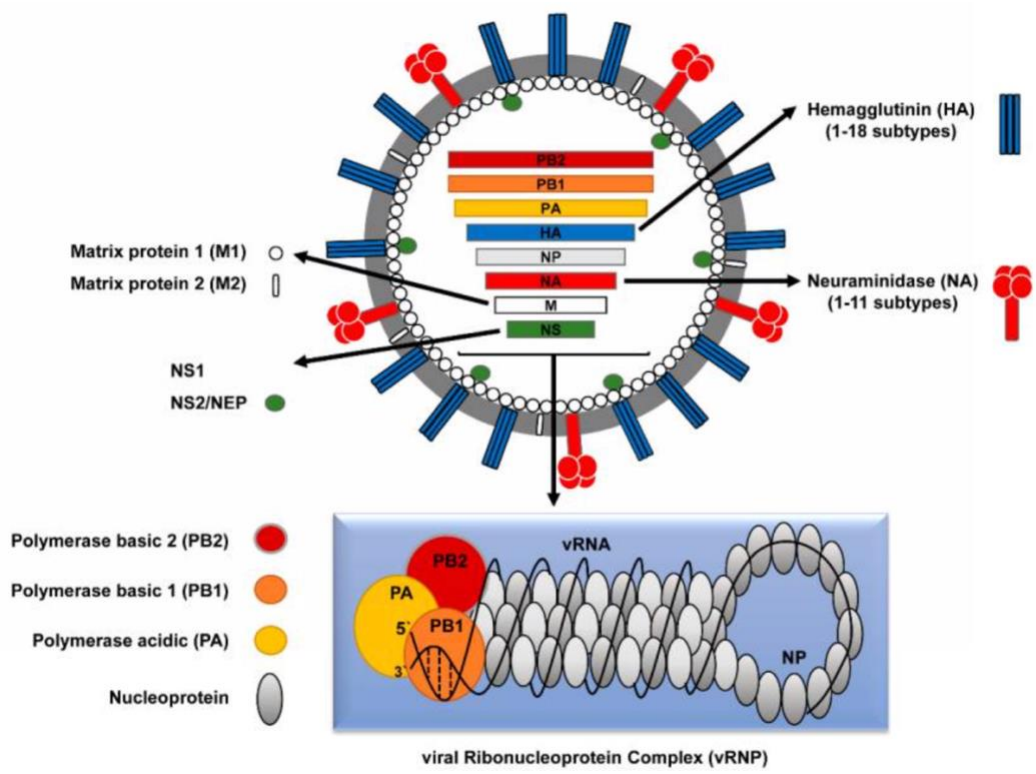

Figure 1.1 Structure of IAV virus.

From Mostafa et al., 2018.

1.3.4 Subtypes

IAVs are further distinguished through their surface glycoproteins, the hemagglutinin (HA) (H1-H18) and neuraminidase (NA) (N1-N9) (Wahlgren, 2011). All IAVs originate from avian hosts except for bat-originated influenza viruses H17N10 and H18N11 (Table 1.3) (Tong et al., 2012). In the human population, although there are numerous possible subtype combinations, only three have persisted and caused pandemics: H1N1 in 1918 and 2009, H2N2 in 1957 and H3N2 in 1968 (Morens, Taubenberger and Fauci, 2009). However, only two IAV subtypes, H1N1 and H3N2 and two IBV lineages (Victoria and Yamagata) are currently within the human population (Rota et al., 1990).

Table 1.3 Distribution of Influenza A virus subtypes across species.

Adapted from Short et al., 2015.

Host species	Influenza A Subtypes Reported
Humans	**Established:** H1N1, H3N2 (current seasonal); H2N2 (1957 pandemic, extinct) **Zoonotic (sporadic):** H5N1, H5N6, H6N1, H7N2, H7N3, H7N7, H7N9, H9N2, H10N7, H10N8
Wild waterfowl/shorebirds	H1-H16 in combinations with N1-N9 (all possible combinations can occur; H3N8, H4N6, H6N2 particularly common)
Domestic poultry	**Endemic lineages:** H5 (including H5N1, H5N2, H5N8), H6 (including H6N2), H7 (including H7N3, H7N7, H7N9), H9 (especially H9N2) Note: Many other combinations possible through spillover from wild birds
Swine	**Endemic:** H1N1, H1N2, H3N2 **Sporadic:** H4, H9
Horses	H3N8 (currently circulating); H7N7 (emerged 1950s, now extinct)
Dogs	H3N8, H3N2
Marine mammals	**Seals:** H3, H4, H7, H10N7 **Whales:** Isolated cases reported
Cats	H5N1 (sporadic infections)
Bats	H17N10, H18N11 (unique bat influenza viruses)
Other mammals	**Tigers/Leopards:** H5N1 **Camels:** H3N8 **Mink/Ferrets:** H5N1 (experimental and natural)

1.3.5 Viral evolution

There are two mechanisms by which the surface antigens (HA and NA) evolve in the hosts: 1) antigenic drift due to the lack of proof reading of the RdRp leading to nucleotide changes that may result in amino acid changes (Figure 1.2A) and 2) antigenic shift due to reassortment of different viral segments present from two or more subtypes of IAV during co-infection (Figure 1.2B) (Mostafa et al., 2018).

Since both the antigenic drift and antigenic shift create changes in the structure of the virus, the host immune system may or may not provide proper defence against the new mutant.

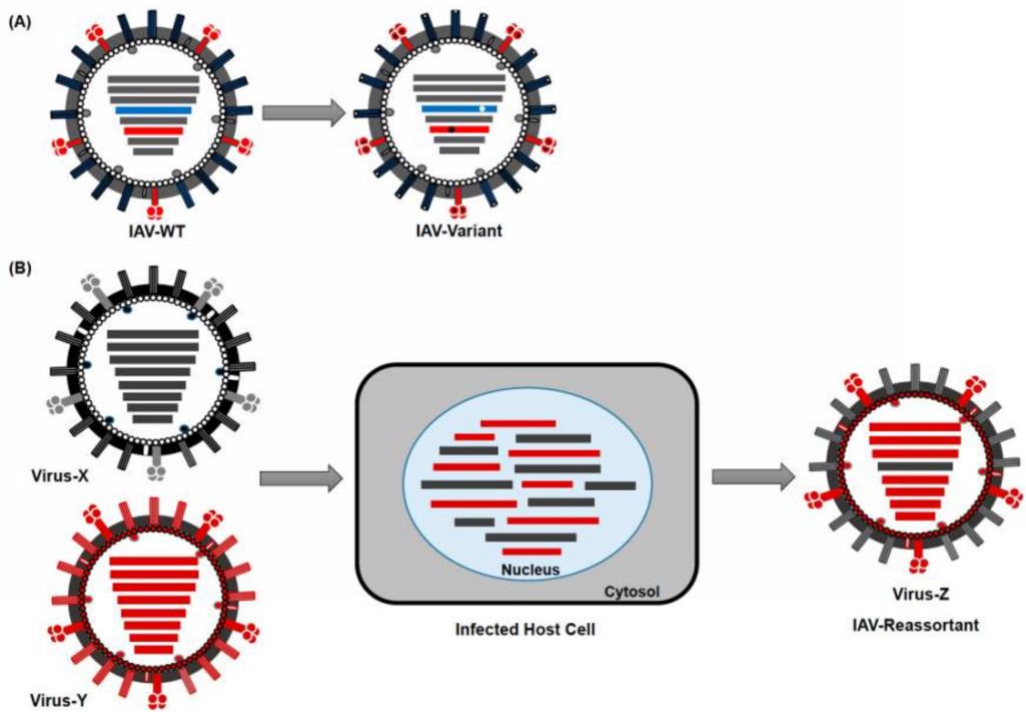

Figure 1.2 Mechanisms of IAV evolution.

(A) Antigenic drift due to mutations in IAV genome leads to new variants. Blue represents mutations in HA; red is NA. (B) Antigenic shift due to the exchange or reassortment of RNA segments from two or more IAV in a host cell leads to distinct subtypes (Mostafa et al., 2018).

1.3.6 Binding and fusion

IAV hemagglutinin plays a key role in the viral replication and adaptation to new hosts (Böttcher-Friebertshäuser et al., 2014). Its affinity for specific sialic acid (SA) is the main determinant of host range. Avian influenza (AIV) preferentially attaches to galactose via α-2,3-linkage (α2,3-SA) which is found mainly in the intestinal tract of birds, human

lower respiratory tract (LRT) and conjunctive cells (Suzuki et al., 2000; Kumlin et al., 2008; França, Stallknecht and Howerth, 2012). Human IAVs show a marked preference for SA termini attached to galactose via an α2,6 linkage on complex N-glycans that are abundant throughout the upper respiratory tract—namely the nasal cavity, paranasal sinuses, pharynx, larynx, trachea and bronchi (Shinya et al., 2006). However, the traditional dichotomy that assigns avian strains exclusively to α2,3-SA receptors and human strains to α2,6-SA receptors is now known to be an oversimplification. Recent biophysical work using synthetic glycan gradients and gene-edited cell lines has shown that influenza virions can exploit hetero-multivalent interactions: low-affinity α2,3 and α2,6 receptors cooperate on the same surface, and even a small admixture of one linkage can markedly enhance binding and entry driven by the other (Liu et al., 2022). Pigs and quails do express both α2,3- and α2,6-linked SA across their respiratory epithelia, which means they can support attachment of both avian- and human-adapted viruses (Wan and Pérez, 2006; Romero-Tejeda and Capua, 2013; Asha and Kumar, 2019). Nevertheless, the idea that pigs are uniquely efficient “mixing vessels” is now considered overstated. A systematic lectin-histochemical survey found that the distribution of α2,6- and α2,3-SA in porcine trachea, lung and other organs is very similar to that in humans, indicating that swine are no more—and no less—permissive to dual-receptor infection than people themselves (Nelli et al., 2010). Moreover, co-expression of both linkages has also been documented in several cell types of chickens and ducks (Kuchipudi et al., 2009),

underscoring that multiple avian and mammalian hosts provide the anatomical substrates required for reassortment.

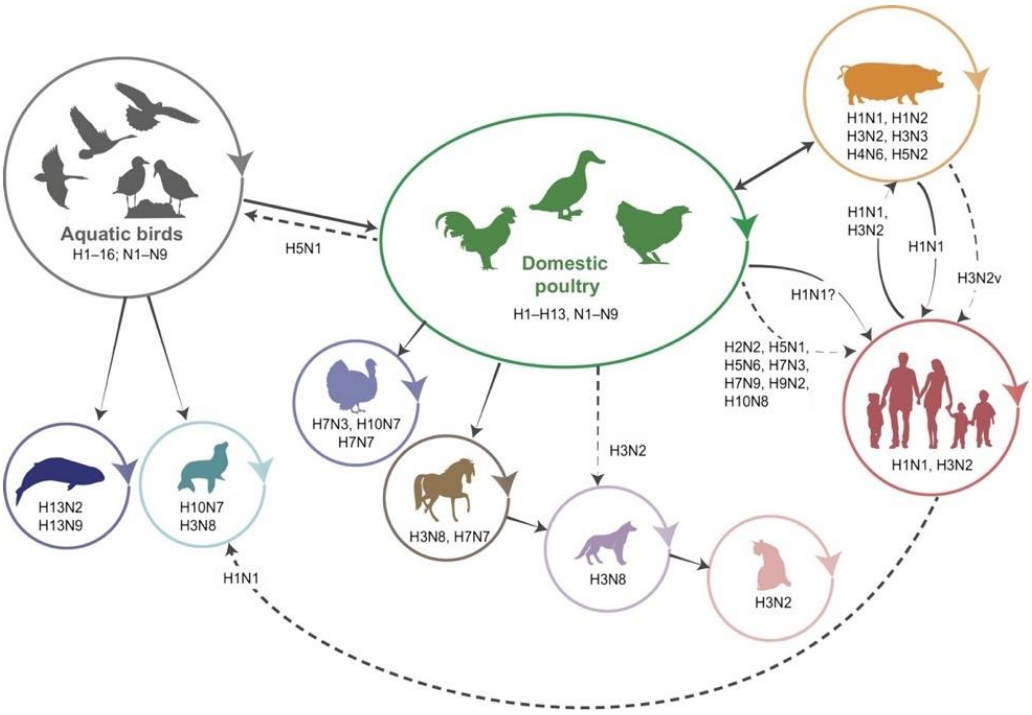

Figure 1.3 Illustration of zoonotic transmission of IAV.

Solid arrows represent direct transmission events; dashed arrows show limited infection of subtypes (Joseph et al., 2016).

Upon attachment to SA receptors, NA facilitates lateral scanning of the cell surface by removing decoy moieties and resolving non-productive HA interactions, thereby enhancing virion mobility (Rota et al., 1990). This promotes stable engagement with entry receptors and allows internalisation of the virus. Although clathrin-mediated endocytosis has long been considered the main uptake route, IAV can also enter via macropinocytosis, and in some cases through SA-independent mechanisms involving alternative receptors such as major histocompatibility complex class II (MHC II) and dendritic cell-specific

intercellular adhesion molecule-3-grabbing non-integrin (DC-SIGN) (Dou et al., 2018; Sempere Borau and Stertz, 2021).

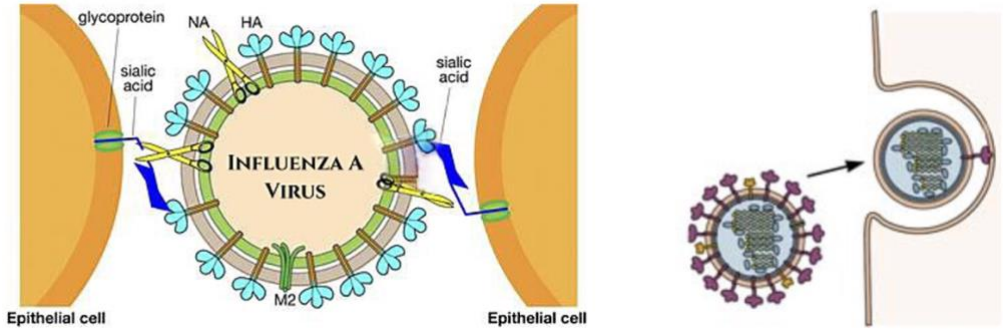

Figure 1.4 Schematic representation of IAV attachment to host.

HA attaches to sialic acid while NA removes the non-productive attachments enabling the endocytosis of the virion, adapted from Rappuoli & Del Giudice, 2019.

1.3.7 Host cell entry

IAV uptake occurs through clathrin-dependent receptor-mediated endocytosis or macropinocytosis, after which viral components are trafficked within endosomal compartments (Hutchinson and Fodor, 2013; Baharom et al., 2017). As endosomes mature, the internal pH decreases to approximately 5.2, triggering conformational changes in HA that enable membrane fusion and subsequent release of the viral genome into the cytoplasm (Meanwell and Krystal, 1996). When the IAV endosome reaches a low pH, the M2 ion channel becomes activated (Roy et al., 2000; Lakadamyali et al., 2003). The M2 functions as an ion channel, acidifying the virion interior and causing M1 protein to dissociate from the RNPs (Martin and Heleniust, 1991; Pinto and Lamb, 2005). The acidic environment inside the endosomal lumen causes a conformational change in HA, exposing the fusion peptide and inserting

it into the endosomal membrane (Pinto and Lamb, 2005). HA folds on itself, forcing the endosomal membrane and the viral envelope to fuse and releasing the vRNPs into the host cytoplasm (Martin and Heleniust, 1991; Harrison, 2015). The vRNPs gain entry to the cell nucleoplasm via the importin-α and importin-β nuclear import (Figure 1.5) (Wu, Weaver and Panté, 2007). Delivery of vRNPs from the cell surface to the nucleus is typically completed within approximately one hour, and newly assembled virions begin to emerge after 4–6 hours post-infection. (Frensing et al., 2016; Dou et al., 2017).

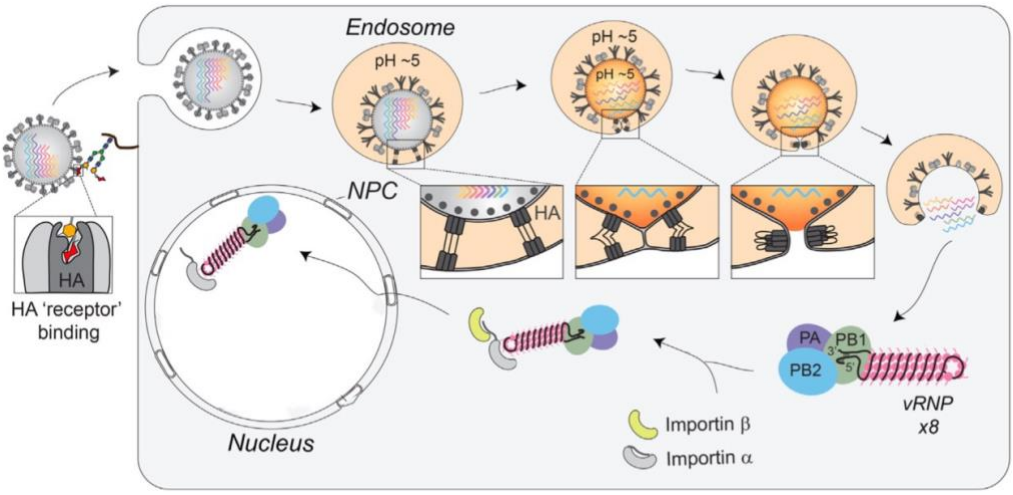

Figure 1.5 IAV entry and delivery of the vRNPs to host cytoplasm and nucleus.

From Dou et al., 2018.

1.3.8 Transcription and replication

Inside the nucleus vRNA undergoes replication via the heterotrimeric viral RNA-dependent RNA polymerase (RdRp [PA, PB1 and PB2]) (Pflug et al., 2017). The genome is replicated in two steps: transcription to cRNA and transcription to vRNA from cRNA as a template. The cRNA

production relies on complementation of free ribonucleoside triphosphates (rNTPs), GTP and ATP, with the 3' end of the RNA as template. The nucleotide locks the vRNA template into the PB1 subunit forming an A-G dinucleotide and allowing cRNA elongation from the polymerase (Robb et al., 2016). Upon exiting the polymerase, cRNA associates with an NP molecule and a copy of the RdRp complex to form a cRNP unit (York et al., 2013). New cRNPs then serve as templates for the synthesis of multiple vRNA copies. vRNP assembly follows a similar mechanism, involving the encapsidation of nascent vRNA by NP and its association with a newly synthesised RdRp complex to form a transcription- and replication-competent vRNP (Fodor, 2013).

mRNA transcription from vRNA is more efficient than cRNA and vRNA transcription (Newcomb et al., 2008). During cap snatching, the viral RdRp associates with the C-terminal domain (CTD) of host RNA polymerase II to access nascent capped transcripts that provide primers (Plotch et al., 1981). PB2 binds to the 5' cap of host transcript and the PA subunit cleaves 10-13 nucleotides downstream of the 5' cap (Dias et al., 2009; Yuan et al., 2009). The PB2 subunit then rotates and places the acquired primer into PB1's catalytic center where it is extended using the vRNA template (Reich et al., 2014). When the polymerase encounters the short poly-U sequence at the vRNA 5' end the transcripts are polyadenylated by a process termed reiterative stuttering (Siegert, Bauer and Hofschneider, 1973; Stridh, Datema and Scholtissek, 1985). The vRNP polymerases transcribe the initial mRNAs which are exported from the nucleus for translation by cytoplasmic ribosomes (Jorba,

Coloma and Ortín, 2009; Reich, Guilligay and Cusack, 2017). Once assembled, the new vRNP can transcribe more viral mRNAs, create cRNA copies or interact with M1 and NS2 in order to recruit CRM1 which mediates the nuclear export of the vRNPs (Guilligay et al., 2008; Dias et al., 2009; Yuan et al., 2009; Chenon et al., 2011). Newly synthesized NP proteins and RdRp subunits are brought back in the nucleus via importin-α-importin-β pathway for cRNPs and vRNPs formation.

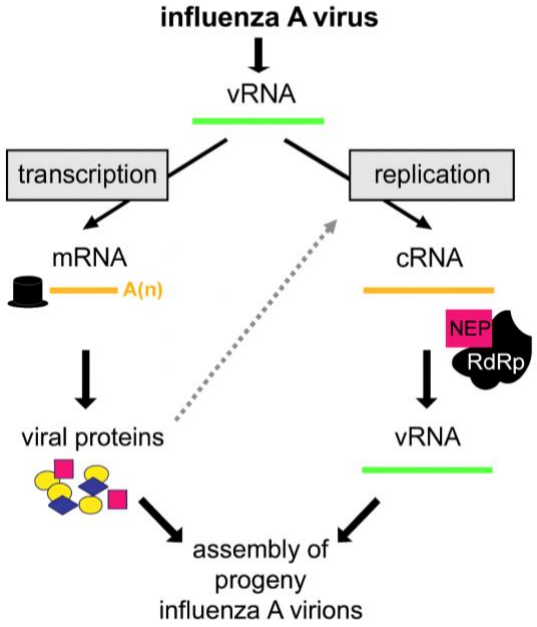

Figure 1.6 Differential pathways undertaken by IAV for replication and virion assembly.

NS2/NEP protein reduces the accumulation of transcript products but increases accumulation of replication products (Robb et al., 2009).

1.3.9 Translation

The translation process is divided between cytosolic ribosomes (for PB1, PB2, PA, NP, NS1, NS2 and M1) and endoplasmic reticulum (ER) associated ribosomes for the membrane proteins HA, NA and M2

(Fodor, 2013). The vRNA binding protein NS1 is synthesized early and imported into the nucleus where it can act as an inhibitor of type I IFN signaling as well as contributing to the mRNA export (Marc, 2016). NS2 and M1 are also imported into the nucleus; NS2 connects the vRNPs with the CRM1 nuclear export pathway to the cytoplasm while the M1 protein prevents the vRNPs from re-importing. In the cytoplasm, the vRNPs are carried for viral assembly by Rab11 which also ensures that vRNPs contain the PB2 subunit (Amorim et al., 2011). Rab11 associates with recycling endosomes (REs) and allows the viral polymerase to bind to RE, enabling RNPs to use the vesicular transport system, required to reach the plasma membrane as well as offering a platform for RNPs to interact (Amorim et al., 2011; Eisfeld et al., 2011; Momose et al., 2011). The viral membrane proteins (NA, HA and M2) are synthesized by the ribosomes associated with the ER. As NA, HA and M2 are synthesized, their hydrophobic target sequences interact with the signal recognition particle (SRP). Interaction between the ribosome SRP and the ER membrane transfers the ribosome to a Sec61 protein-conducting channel referred to as translocon. The transcolon allows passage of HA, NA and M2 into the ER lumen (Deshaies, 1987; Görlich et al., 1992; Karamyshev et al., 2014). HA is exported from the ER as an incompetent precursor referred to as HA0. To gain function HA0 must be cleaved into HA1 and HA2. In highly pathogenic avian IAV, this cleavage is mediated by furin; in low pathogenic avian IAV, by extracellular trypsin-like proteases; and in human IAV, by transmembrane protease serine 2 (TMPRSS2) and human airway trypsin-like protease (HAT). HAT is

found at the plasma membrane while TMPRSS2 and furin are found in the *trans-Golgi* network (Stieneke-Gröber et al., 1992; Bottcher et al., 2006; Chaipan et al., 2009). Following the cleavage of HA in the trans-Golgi network, the M2 protein ion channel balances the pH between the Golgi lumen and cytoplasm which slows the intracellular rate of membrane glycoprotein transport (Steinhauer et al., 1991; Sakaguchi, 1996).

1.3.10 Viral assembly and release

IAV envelope is formed at distinct host apical plasma membrane regions rich in cholesterol and sphingolipids, regions referred to as “rafts” (Lingwood and Simons, 2009; Gerl et al., 2012). Following the migration of M2, HA and NA through ER and Golgi apparatus, as well as the eight vRNPs via Rab11 through the cytoplasm, the viral components are gathered at the raft regions of the plasma membrane to form viral buds (Figure 1.7) (Veit and Thaa, 2011; Zhang, Pekosz and Lamb, 2000; Noton et al., 2007). Virion formation is possible by promoting a curvature of the plasma membrane: HA and NA induce budding, M1 influences the virion shape and M2 functions as a membrane-bending protein, facilitating bud neck formation and scission (Elleman and Barclay, 2004; Chen et al., 2007; Hilsch et al., 2014; Rossman and Lamb, 2013; Chlanda et al., 2015). Once the IAV bud is assembled, virion release is critically dependent on the sialidase activity of NA, which facilitates

detachment by removing local SA residues and preventing HA from re-binding to the cell surface (McAuley et al., 2019; Du et al., 2019).

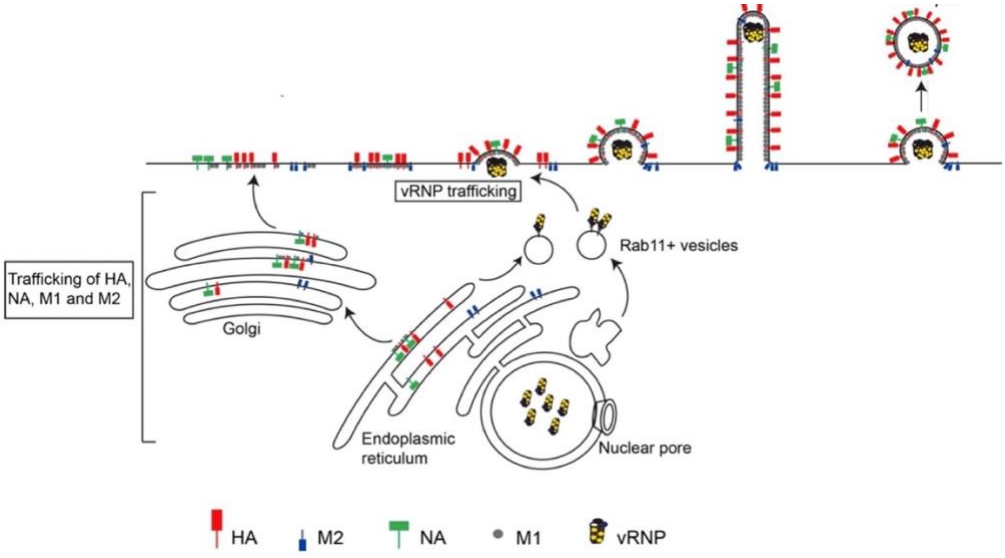

Figure 1.7 IAV viral protein recruitment and virion assembly.

vRNP complexes (PB1, PB2, PA, NP, NS1, NS2 and M2) are carried to the plasma membrane by Rab11 via RE. HA, NA and M2 are carried by ER-associated ribosomes (Bedi & Ono, 2019).

1.4 Influenza A and RSV: similarities and distinctions in viral strategy

An RNA virus similar to IAV in some features is RSV (Gutiérrez-Ortega, Sánchez-Hernández and Gómez-García, 2008). Comparisons between the two pathogens began shortly after the discovery of RSV (Caul et al., 1976). Both pathogens affect the upper and lower respiratory system and can lead to bronchiolitis and pneumonia (Pavia, 2011; Cervantes-Ortiz, Zamorano Cuervo and Grandvaux, 2016). RSV infection in early life has been associated with an increased risk of developing asthma later in childhood, a link that has not been observed with IAV infection

(Veerapandian, Snyder and Samarasinghe, 2018). Understanding the similarities and differences in replication between IAV and RSV, and host immune response to infection may provide important clues to developing novel approaches to the control or treatment of both viruses.

1.5 Respiratory syncytial virus

RSV, which comprises subgroups A and B, is the only member of the genus Pneumovirus in the Paramyxoviridae family that infects humans. It is not only the most frequent cause of lower respiratory tract illness (LRTI) and bronchiolitis in children and the elderly population but can also affect adults with compromised immunity or cardiovascular disease (Monto and Sullivan, 1993; Goka et al., 2014). Globally, RSV causes 64 million infectious cases and 160,000-600,000 deaths each winter (Krilov, 2011; Caly, Ghildyal and Jans, 2015). Until recently, there was no approved seasonal vaccine or effective treatment for RSV (Bawage et al., 2013). This changed with the rollout of the first RSV vaccines for older adults and pregnant women in 2023–2024, including in the UK, marking a major shift in prevention strategy (Atkins and Hodgson, 2023; Kelleher, Subramaniam and Drysdale, 2025). A major characteristic of RSV is syncytia formation of infected cells. A syncytium is formed through the fusion of an infected host cell with uninfected neighboring cells. RSV fusion protein (F) allows viral spread between cells leading to multi-nucleate enlarged cells (Figure 1.8). Viral load

peaks by the fourth day and slowly diminish by the eighth day (Turner et al., 2014).

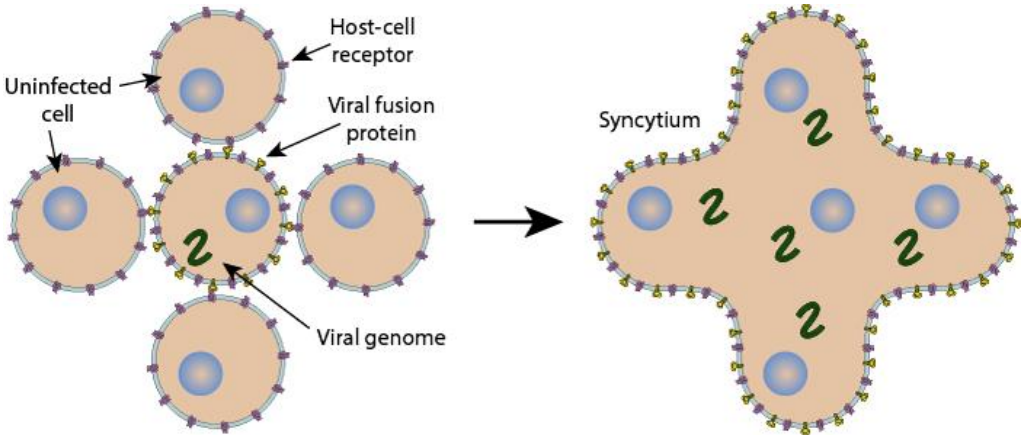

Figure 1.8 Formation of a multi-nucleated syncytium during RSV replication.

1.5.1 Structure

RSV is an enveloped non-segmented negative-sense single-stranded RNA virus with a 15-kb genome transcribed into 10 mRNAs that encode 11 proteins (Rameix-Welti et al., 2014). The large polymerase protein (L), the phosphoprotein (P) and the nucleoprotein (N) form the helical ribonucleoprotein complex around the genomic RNA. The nucleocapsid is surrounded by the non-glycosylated matrix protein (M) and the envelope is derived from the cell membrane. Further internal proteins are all associated with the construction of the nucleocapsid. These include the products of the M2 gene, which are two polypeptides resulting from overlapping open reading frames: a nucleocapsid-associated transcription factor (M2-1) and the associated polypeptide

involved in genome replication (M2-2) (Ascough, Paterson and Chiu, 2018). On the envelope, the glycoprotein (G), the fusion glycoprotein (F) and the small hydrophobic glycoprotein (SH) are anchored (Figure 1.9A) (Collins and Melero, 2011). RSV also houses the highly conserved non-structural proteins, NS1 and NS2 (Collins and Melero, 2011). A comparison of RSV and IAV reveals both structural parallels and important differences. Both viruses are enveloped and contain surface glycoproteins essential for host cell entry—F, G, and SH in RSV (Figure 1.9A), and HA and NA in IAV (Figure 1.9B). However, RSV has a non-segmented negative-sense RNA genome, whereas IAV's genome is segmented into eight RNA segments, each associated with a nucleoprotein (NP) and polymerase components PB1, PB2, and PA. Additionally, IAV possesses the M2 ion channel and a nuclear export protein (NEP), which are not found in RSV. The figure below summarises these differences and similarities in structural organisation.

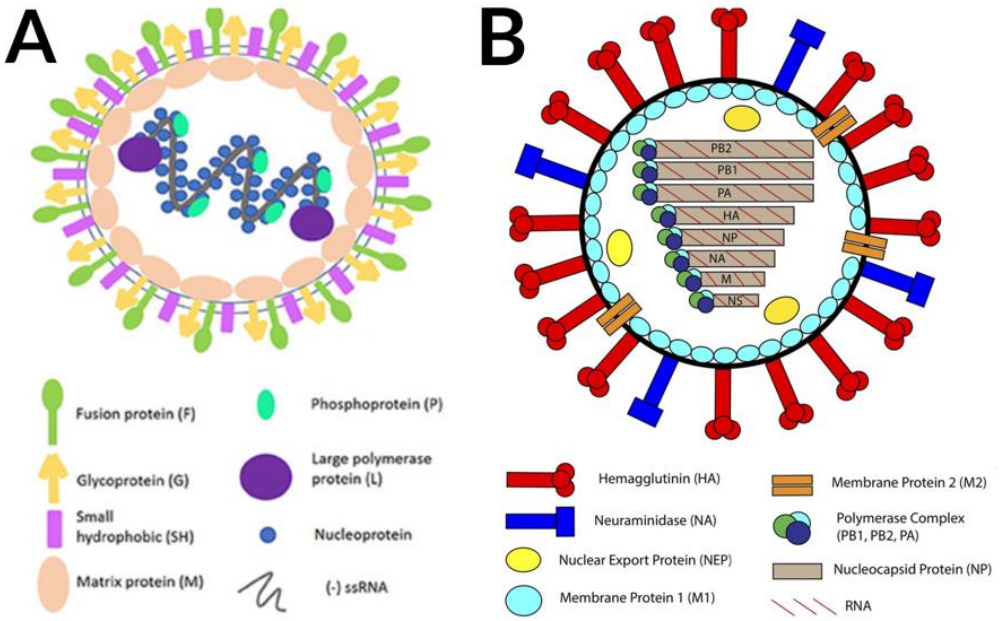

Figure 1.9 Schematic comparison of RSV (A) and IAV (B) structural components.

Adapted from Canedo-Marroquín et al., 2017 and Mostafa et al., 2018.

1.5.2 RSV replication cycle overview

RSV primarily infects and replicates within the ciliated epithelial cells of the respiratory tract, spreading locally from cell to cell via direct membrane fusion. Attachment is mediated predominantly by the G glycoprotein through interactions with cell-surface glycosaminoglycans (GAGs), while the F glycoprotein also contributes to attachment via nucleolin and is essential for fusion of the viral envelope with the host cell membrane (Figure 1.10) (Tayyari et al., 2011). Following attachment, the virus enters via macropinocytosis and releases its vRNP into the cytoplasm in a pH-independent manner, where transcription and replication occur (Krzyzaniak et al., 2013).

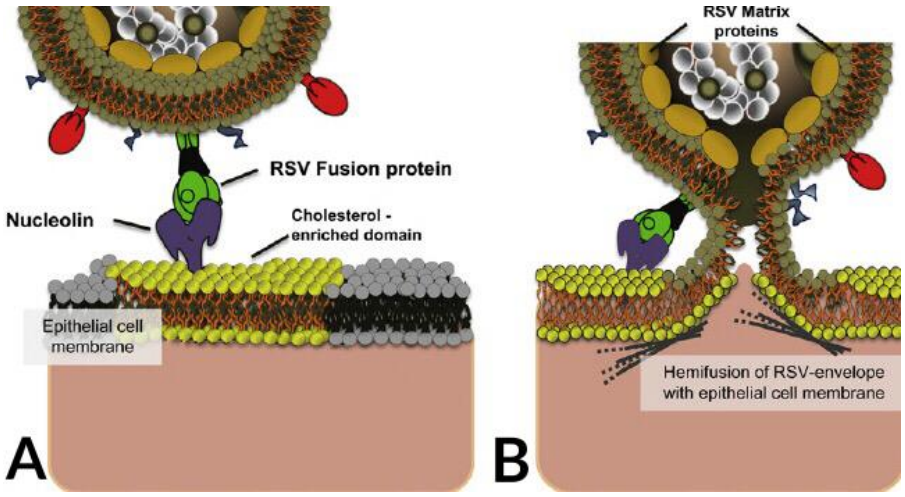

Figure 1.10 Visual representation of RSV binding.

Achieved via F protein (A) and fusion (B) to host epithelial cell via fusion protein (Lay et al., 2013).

1.5.3 Transcription

Upon entry, vRNPs are released into the host cytoplasm. Transcription is carried out by the viral RNA-dependent RNA polymerase (the L protein), which functions with the phosphoprotein P and the M2 gene product M2-1 (ORF1) on the N-encapsidated genome template to produce viral mRNAs (McGivern, Collins and Fearns, 2005). Viral transcripts are capped and polyadenylated prior to release. The first genes transcribed by the viral polymerase are NS1 and NS2, which are crucial for viral survival as they encode proteins that antagonise the host's antiviral responses (Rameix-Welti et al., 2014). The RSV RdRp is capable of transcribing mRNA transcripts and synthesis of positive-sense RNA- referred to as the antigenome. The antigenome serves as a template for genome synthesis (Figure 1.11) (Boyer and Haenni, 1994). The 5' region inhibits the formation of cellular stress granules (SGs) during viral replication (Hanley et al., 2010). The trailer region, a

non-coding sequence located at the 5′ end of the negative-sense RSV genome, also functions as a promoter when replicated into positive-sense RNA (Fearns, Collins and Peeples, 2000).

The new genomic RNA is used to produce additional antigenomes for virion incorporation or as a template for secondary transcription (Griffiths, Drews and Marchant, 2016). Both the genome and antigenome are encapsidated by the N protein, which protects the RNA and organises it into a template that remains accessible to the viral polymerase. The newly synthesised mRNA is then translated by the host ribosome machinery using mechanisms similar to those employed for cellular mRNAs (Bermingham and Collins, 1999).

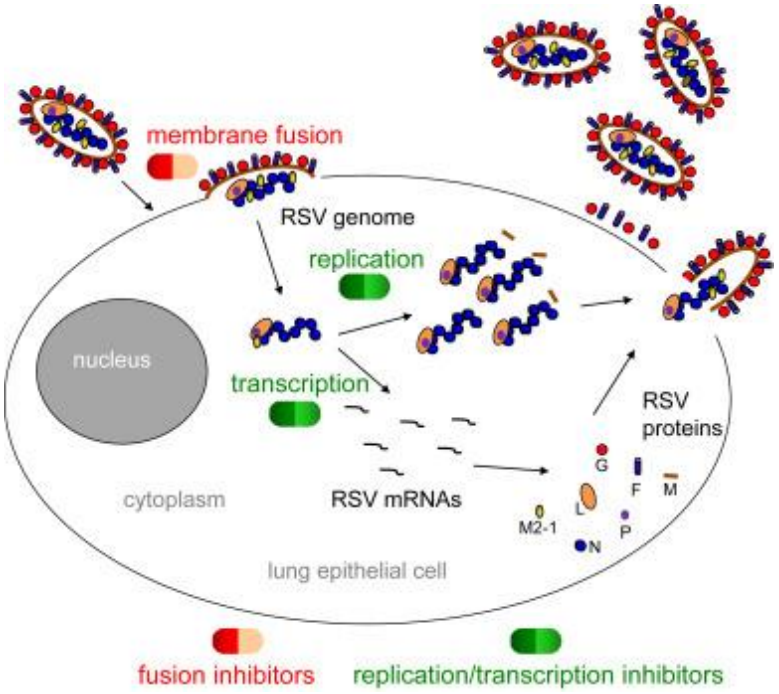

Figure 1.11 Major events in RSV replication cycle.

From Fearns & Deval, 2016.

1.5.4 Inclusion bodies and stress granules

One of the main features of RSV replication is the presence of large cytoplasmic protein inclusions referred to as inclusion bodies (IBs). Although not fully understood, they emerge around the same time as viral protein synthesis begins (~6 hours post-infection) (Lifland et al., 2012). IBs contain all components required for transcription and replication: RSV-N, M2, L and P; and are often observed near Golgi apparatus (McDonald et al., 2004; Carromeu et al., 2007; Lindquist et al., 2010). In close proximity to IBs, antiviral proteins, chaperone and signaling proteins are present: MAVS, MDA5, p38, *O*-linked *N*-acetylglucosamine transferase and HSP70 (Brown et al., 2005; Fricke et al., 2012; Lifland et al., 2012). *O*-linked *N*-acetylglucosamine transferase enables RSV to prevent stress granule (SG) formation (Ohn et al., 2008). SGs are aggregations of mRNA and proteins produced by the innate immune system when infected cells are under stress and protein kinase R (PKR) detects pathogen (Lindquist et al., 2011). PKR is a pathogen recognition receptor (PRR) and when is activated it shuts down the activity of eukaryotic initiation factor 2α (eIF2α), a necessary component of the translation initiation and therefore viral protein synthesis. RSV-N bypasses this mechanism by binding to PKR and preventing phosphorylation of eIF2α (Figure 1.12) (Groskreutz et al., 2010).

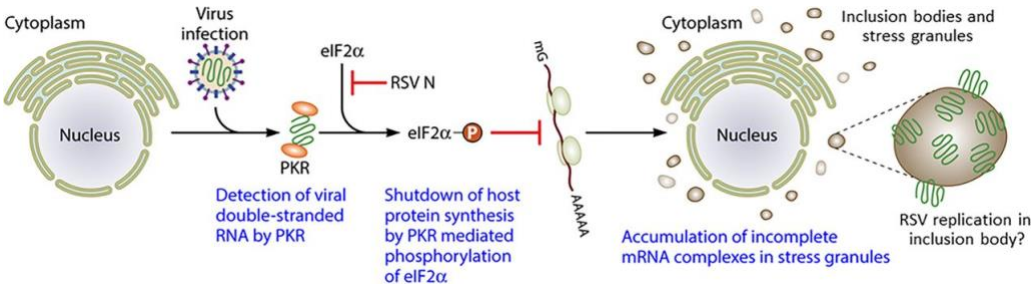

Figure 1.12 RSV-N aids in IBs and SGs formation.

Achieved by preventing eIF2α and O-linked N-acetylglucosamine transferase phosphorylation (Griffiths et al., 2017).

RSV has evolved mechanisms to overcome the stress granule (SG) response; notably, the 5′ trailer region of the genome—a non-coding sequence at the end of the negative-sense RNA—has been shown to actively inhibit SG formation in infected cells. In addition, the NS1 and NS2 proteins suppress both innate and adaptive immune responses (Hanley et al., 2010). NS1 blocks type I interferon signalling, T cell responses, and dendritic cell maturation, while NS2 inhibits RIG-I and promotes degradation of STAT-2 (Ling, Tran and Teng, 2009; Meng et al., 2014).

1.5.5 Translation

Transcribed viral genes are translated by host ribosomal machinery (Collins and Melero, 2011). Viral proteins M, N, P, L, M2-1, M2-2 and vRNA first accumulate and form RNPs in the IBs (Lindquist et al., 2010). The RNPs and matrix (M) protein then traffic to the apical membrane where they meet with F, G and SH proteins that arrive from the ER and Golgi apparatus (Figure 1.11). Virion assembly is enabled with the help

of Rab11 and apical recycling endosomes (ARE) (Goldenring et al., 1996).

1.5.6 Viral assembly and release

RSV proteins must deform the cell membrane outwards to initiate bud formation, surround the bud with host membrane and release the membrane by scission (Chen and Lamb, 2008). For RSV the coordination of both internal and surface proteins is required for bud formation and release: the viral genome, N, P and L associate with M proteins which are in turn capable of associating with F and G surface proteins. The F protein is critical for the formation of filamentous virion structures and for stabilising the plasma membrane around the emerging viral bud. Lipid raft microdomains are areas of choice for viral bud assembly (Brown and Rose, 1992; Fearns and Deval, 2016). RSV proteins and vRNA assemble into viral filaments and after the bud formation, the vesicle membrane scission occurs (Utley et al., 2008).

1.6 Influenza A and RSV

Influenza's haemagglutinin (HA) and RSV's fusion glycoprotein (F) perform analogous roles in mediating host cell entry. HA confers host specificity by binding to sialic acids on the surface of epithelial cells (Gamblin and Skehel, 2010), while RSV F is responsible for viral attachment and membrane fusion, though unlike HA, it does not possess

haemagglutinating activity. RSV binds to host cell glycosaminoglycans (GAGs) and cellular receptors such as nucleolin (Figure 1.10) (Tayyari et al., 2011). In both viruses, neutralising antibodies targeting HA or F can effectively inhibit viral entry (Huang et al., 2010; Li, Ma and Wang, 2015). Vaccination remains the most effective strategy for preventing IAV infection. In contrast, RSV vaccine development has historically faced challenges, but this landscape has changed recently. As of 2023–2024, vaccines for RSV have been authorised and rolled out in several countries, including the UK, targeting older adults and pregnant women (Atkins and Hodgson, 2023; Kelleher, Subramaniam and Drysdale, 2025). A key distinction between IAV and RSV lies in their replication kinetics and intracellular replication sites. IAV produces progeny virions within 4–6 hours post-infection, while RSV requires 30 to 48 hours, with viral titres typically peaking after 4 days (Collins and Graham, 2007). IAV replication occurs in the host nucleus, requiring host proteins such as importin-α, importin-β, and CRM1 for nuclear import and export of viral RNPs. RSV, in contrast, replicates entirely in the cytoplasm within viral inclusion bodies. Their genome structures also differ significantly: IAV has a segmented negative-sense RNA genome comprising eight segments, allowing for reassortment and a high capacity for genetic recombination. RSV possesses a non-segmented, negative-sense single-stranded RNA genome, which replicates as a continuous molecule and does not undergo reassortment. These differences have direct implications for viral evolution, antigenic variation, and pandemic potential. At the cell surface, IAV uses two glycoproteins—HA for

receptor binding and NA for cleavage of terminal sialic acids—to facilitate entry and release. RSV relies on a single surface glycoprotein, F, for both attachment and fusion. Both viruses enter the host primarily via the naso- and oro-pharyngeal mucosa, where mucus forms a protective barrier. However, only IAV is capable of cleaving sialic acid residues within the mucus layer using neuraminidase, thereby exposing target receptors for HA binding. RSV lacks sialidase activity and is therefore more affected by this mucosal barrier (Hamilton, Whittaker and Daniel, 2012). Although both viruses preferentially infect respiratory epithelial cells, they can also replicate in immune cells such as neutrophils, macrophages, and dendritic cells (Dakhama, Kaan and Hegele, 1998; de Graaff et al., 2005; Tregoning et al., 2008; Biondo et al., 2019). Despite some overlapping features in pathogenesis and host range, the differences in replication strategy, genome organisation, and immune evasion mechanisms underscore the need to consider these pathogens within their distinct biological frameworks.

1.6.1 Escaping immunity

Airway epithelial cells, neutrophils, alveolar macrophages (AMs), dendritic cells (DCs) and innate lymphoid cell (ILC) family members are the first line of immune protection against IAV and RSV. Both pathogens generate specific RNA intermediates known as pathogen-associated molecular patterns (PAMPs) which are sensed by host PRRs. Innate recognition through PRRs triggers type I and III interferon (IFN)-

mediated antiviral response (Marr, Turvey and Grandvaux, 2013). The primary site of innate IFN response for IAV are epithelial cells and plasmacytoid DCs (Wu et al., 2016). RSV activates the interferon (IFN) response in epithelial cells and alveolar macrophages (Ascough, Paterson and Chiu, 2018). IFN initiation is followed by the release of proinflammatory cytokines such as interleukin-6 (IL-6), interleukin-8 (IL-8), and tumour necrosis factor-alpha (TNF-α), which contribute to immune cell recruitment, airway inflammation, and the development of RSV-associated pathology. Retinoic acid-inducible gene I (RIG-I) is the major sensing PRR in both IAV and RSV (Liu et al., 2015; Cervantes-Ortiz, Zamorano Cuervo and Grandvaux, 2016). Besides RIG-I, IAV is recognized by TLR3, TLR7, TLR8 and TLR9 (in humans) as well as NLRP3. While the immune response to viral infection is generally protective, in severe cases—particularly during infection with highly pathogenic IAV strains or RSV—it may involve excessive production of proinflammatory cytokines and chemokines at the infection site. This dysregulated response, often referred to as a “cytokine storm,” can contribute to tissue damage and disease severity (Rosenberg and Domachowske, 2012; Liu, Zhou and Yang, 2015).

Both IAV and RSV have evolved mechanisms to evade the host antiviral state. The NS1 protein of IAV and the NS1 and NS2 proteins of RSV antagonise the type I (IFN-α and IFN-β) and type III interferon responses (including IL-29 [IFN-λ1], IL-28A [IFN-λ2], and IL-28B [IFN-λ3]), which are crucial for initiating antiviral signalling (Kochs, Garcia-Sastre and Martinez-Sobrido, 2007; Barik, 2013; Rajsbaum et al., 2012).

1.7 Endoplasmic reticulum stress

A common feature both viruses exhibit when interacting with the host is endoplasmic reticulum (ER) stress (Hassan et al., 2011; Cervantes-Ortiz, Zamorano Cuervo and Grandvaux, 2016). The ER is a membrane-bound compartment essential for calcium homeostasis, control of protein folding and post-translational modifications (Zhang and Wang, 2012; Koenig and Ploegh, 2014). The organelle therefore contains extremely high concentration of proteins (>100 mg/ml) (Stevens and Argon, 1999; Zhang and Wang, 2012). To manage this constant and heavy demand for protein folding and processing, the ER presents a unique cellular environment that enhances processing and prevents aggregation (Anelli and Sitia, 2008; Schönthal, 2012). As a calcium storage, the ER is central to intracellular signalling cascades that contribute to maintaining cellular homeostasis (Zhang and Wang, 2012; Hetz, 2012). Rich in calcium-dependent molecular chaperones, the ER hosts ER luminal binding proteins (BiP), calmodulin (CAM), and calreticulin (CRT), which assist in folding or refolding of proteins (Ellgaard and Helenius, 2003). Importantly, in certain situations the protein load can exceed the ER processing capacity due to changes in demand for protein synthesis and secretion. The result is the process known as ER stress (Zhang and Wang, 2012). ER stress can be achieved through a variety of external stimuli such as pathogen invasion, chemical imbalances, energy, or glucose deprivation (Ye et al., 2011). These stimuli lead to alterations of

redox equilibrium, changes in calcium homeostasis, failure of post-translational changes and increased protein synthesis (Iwata and Koizumi, 2012; Zhang and Wang, 2012). Changes in ER homeostasis causes proteins to accumulate within the ER lumen. In order to restore balance an evolutionary conserved cytoprotective signalling pathway is activated, the unfolded protein response (UPR) (Zhang and Wang, 2012).

1.7.1 The unfolded protein response

The UPR functions to restore homeostasis by preventing the cytotoxic effect of malformed proteins within the ER via mRNA translation inhibition and activation of adaptive mechanisms (Xu, 2005; Kim, Xu and Reed, 2008; Ye et al., 2011; Zhang and Wang, 2012). The adaptive mechanisms are the upregulation of certain genes aimed at increasing protein folding capacity and ER-assisted degradation (ERAD) (Meusser, Hirsch, Jarosch and Sommer, 2005; Kim, Xu and Reed, 2008). The UPR downstream signals are commonly associated with innate immunity and host defense (Kim, Xu and Reed, 2008; Ye et al., 2011). However, if the UPR cannot restore ER homeostasis the cell will undergo a programmed cell death (apoptosis) with the purpose of protecting nearby cells from the expansion of harmful pathogens and chemicals produced by the damaged cells (Ron and Walter, 2007; Zhang and Wang, 2012).

1.7.2 The three branches of the UPR

The UPR relies on the coordinated response of inositol requiring kinase 1 (IRE1), PKR-like endoplasmic reticulum kinase (PERK) and activating transcription factor (ATF6) (Figure 1.13) (Bernales, Papa and Walter, 2006). When unstressed, the branches are held in check by the folding chaperone BiP/GRP78 (Smith, 2014). During ER stress BiP is released from IRE1, PERK and ATF6 (Ron and Walter, 2007; Smith, 2014). Dissociation of BiP from ATF6 enables ATF6 translocation. Upon transit to the Golgi, the site-specific proteases S1P and S2P cleave ATF6, releasing its cytosolic N-terminal domain, which translocates to the nucleus and functions as a transcription factor to upregulate UPR target genes such as GRP78, GRP94, ERP72, and P58IPK (Adachi et al., 2008).

IRE1 has both endonuclease and kinase activity (Hetz, Martinon, Rodriguez and Glimcher, 2011). Upon activation, the endonuclease domain of IRE1 cleaves a 26-nucleotide intron from XBP1 mRNA in the cytoplasm in an unconventional splicing event, removing a premature stop codon. This enables translation of the full-length XBP1 protein, which contains a transcriptional transactivation domain essential for UPR gene expression (Smith, 2014). Together and independently ATF6 and XBP1 regulate proteins and chaperones involved in folding and ERAD (Lee, Iwakoshi and Glimcher, 2003). In a process known as the regulated IRE1 dependent decay (RIDD), the IRE1 nuclease activity degrades ER membrane associated mRNAs encoding secretory

proteins (Hollien and Weissman, 2006; Smith, 2014). The kinase activity of IRE1 is characterised by the formation of a multi-molecular complex comprising IRE1, TNF receptor-associated factor 2 (TRAF2), and apoptosis signal-regulating kinase 1 (ASK1), which activates downstream signalling pathways such as jun N-terminal kinase (JNK). This cascade contributes to cellular processes including autophagy and apoptosis regulation, as illustrated in the JNK signalling branch of the IRE1 pathway in Figure 1.13 (Woehlbier and Hetz, 2011).

When BiP is released, PERK dimerizes and transphorylates to activate its kinase activity leading to PERK phosphorylation of eIF2α. The result is translational attenuation. The primary target of translational attenuation is the transcription factor ATF4 which regulates amino acid transport, protection against oxidative stress and apoptosis via C/EBP homologous protein (CHOP)(Walter and Ron, 2011). The negative feedback loop of PERK is mediated by the association of DNA damage-inducible protein 34 (GADD34) with protein phosphatase 1, which enables dephosphorylation of eIF2α. The kinase activity of PERK can also be inhibited by XBP1-induced P58IPK (Lee, Iwakoshi and Glimcher, 2003; van Huizen, Martindale, Gorospe and Holbrook, 2003). The UPR induce a gene transcriptional program that enables cells to cope with stress by enhancing folding of proteins and decreasing the protein load in the ER. If homeostasis cannot be restored the UPR initiates apoptosis (Smith, 2014).

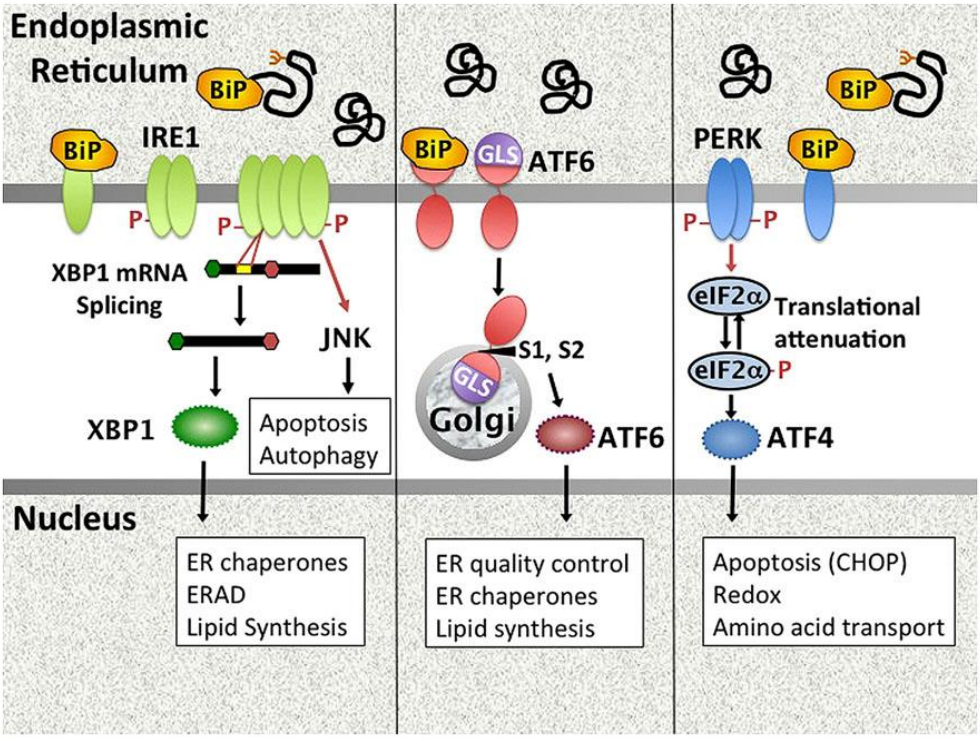

Figure 1.13 UPR signalling pathways activated by ER stress sensors: IRE1, ATF6 and PERK.

From Smith, 2014.

1.7.3 The UPR and viruses

The increase in ER protein load can be both detrimental and beneficial to viral pathogens. The UPR can be antiviral through translational attenuation, ERAD, host apoptosis, UPR-PRR synergy and increased IFN production as well as inflammation (He, 2006). However, viruses have evolved various ways to benefit from the increased protein folding capacity of the UPR (Smith, 2014). The pathway of virus-UPR interaction varies greatly between viruses as both influenza A and RSV have their own way of manipulating the UPR. For example, RSV selectively activates ATF6-dependent promoter activity and XBP1 splicing while

lacking PERK phosphorylation (Hassan et al., 2014). Influenza A selectively activates the IRE1 pathway with little or no activation of PERK and ATF6 (Hassan et al., 2011). Furthermore, as Hassan et al. (2011) has shown, replication of influenza A is decreased by inhibition of IRE1 pathway. Induction of certain parts of the UPR appear to be essential for promoting viral replication (Smith, 2014). Interestingly, multiple parts of the UPR share evolutionary similarities with antiviral pathways: a) PERK is closely related to interferon induced PKR which responds to dsRNA via eIF2α phosphorylation in attempt to reduce viral protein synthesis and b) IRE1 is >40% similar to the antiviral molecule RNAse L both in structure and function. RNAse L and the endonuclease activity of IRE1 can generate small RNA species with 5'OH and cyclic 2'3' phosphodiester 3' ends recognized by RIG-I (PRR) (Smith, 2014; Manivannan, Siddiqui and Malathi, 2020). PRR engagement leads to transcription of type I IFN genes, which function as an early-warning signal during viral infection. IFN binding to type I IFN receptor (IFNAR) induces Janus kinase 1/tyrosine kinase 2 signal activators of JAK1/Tyk2–STAT1/2 signalling that mounts an antiviral transcriptional program and enhances the innate immune response (Smith, 2014; Manivannan, Siddiqui and Malathi, 2020). Aside from UPR–PRR interaction, UPR activation can influence antiviral immunity through modulation of PRR pathways. Although the exact mechanisms are still being investigated, signalling through UPR sensors such as IRE1 and PERK can intersect with PRR-mediated pathways, affecting cytokine expression and viral clearance. UPR activation also triggers

inflammatory signal transduction pathways, including mitogen-activated protein (MAP) kinase signalling via ERK1/2, p38, and JNK, as well as upregulation of transcription factors such as the nuclear factor kappa-light chain enhancer of activated B cells (NF-κB) (Zhang and Kaufman, 2008). NF-κB translocation to the nucleus induces transcription of proinflammatory cytokines such as TNF-α and IL-6, which act to limit viral replication and spread (Hayden and Ghosh, 2008).

A chemical agent widely used to induce ER stress, the UPR, and inflammatory cytokine production is thapsigargin (Peters and Raghavan, 2011).

My colleagues, Goulding et al. (2020), demonstrated that thapsigargin exhibits strong antiviral effects against IAV by activating the host's innate immune response via UPR stimulation instead of directly targeting the virus. This approach could provide a superior alternative to traditional antivirals by reducing the likelihood of drug resistance. These findings have laid the groundwork for this project.

1.8 Thapsigargin

Thapsigargin (TG) is a naturally occurring **sesquiterpene lactone**, a class of compounds composed of three isoprene units and characterised by a lactone ring, many of which exhibit biological activity including cytotoxicity and ER stress induction. It was first isolated in 1978 from the Mediterranean plant *Thapsia garganica* L. (Figure 1.14) (Rasmussen et al., 1978). The abbreviation "L." following the species name refers to Carl

Linnaeus, who first formally described and named the species. The plant belongs to the *Thapsia* genus (Apiaceae family), comprised of herbaceous perennials commonly known as “deadly carrots” due to their long history of toxicity (Gerard et al., 1597; Smitt et al., 1996; Weitzel et al., 2014). *Thapsia garganica* L. is native to the Mediterranean area where it grows on stony, sandy fields (Smitt et al., 1996). Citations referring to the plant date back to Ancient Greece where the name “thapsia” originates, transliterated from the Ancient Greek name "θαψία". The Greeks thought the genus was discovered on Thapsos island (Sicily, Italy). At the time Aristotle’s student, Theophrastus (372-287 B.C.), noted the plant's ability to purge “upwards and downwards” in his famous book series, *Historia Plantarum* (Theophrastus & Hort, 1916). The resin of the plant, extracted from its root, has been noted for medicinal use in both Arabian and European traditions. In 1857, in France, *Thapsia garganica* L. was recommended for treating lung diseases and rheumatic pain through the application of a revulsive plaster—a topical irritant used historically to draw blood to the skin surface and relieve inflammation in deeper tissues (Bertherand, 1857; Tschirch & Stock, 1936; Perrot, 1943). Despite its well-documented toxicity, *Thapsia garganica* L. remains present in medicinal markets such as those in Morocco, consistent with the broader pharmacological principle that many toxic plants, when used in controlled doses, can yield potent therapeutic effects (Kool et al., 2012).

TG is one of the three major herbivore-repelling compounds found in *Thapsia garganica* L., the other two being thapsigargicin and

nortrilobolide (Figure 1.15) (Rasmussen et al., 1978; Christensen et al., 1982; Smitt & Christensen, 1991; Andersen et al., 2015). When topically applied, these compounds can cause erythema, small vesicles, and intense itching within 4-5 hours, which may persist for several days (Christensen et al., 1997). It was noted that TG and thapsigargicin are potent histamine liberators and stimulants of the immune system (Rasmussen et al., 1978; Ali et al., 1985). Towards the end of the 20th century, TG became widely used as a research tool for studying how cells regulate calcium dynamics. It was found to potently inhibit the sarco-endoplasmic reticulum Ca^{2+}-ATPase (SERCA) in mammalian cells, leading to sustained ER stress, apoptosis, and—under certain conditions—tumour promotion (Thastrup et al., 1989; Thastrup et al., 1990). Although SERCA inhibition leads to delayed cellular consequences, it has been suggested that the plant's production of TG may still contribute to herbivore deterrence through cumulative toxicity or physiological stress following ingestion (Martinez-Swatson et al., 2019). Upon the discovery of TG's capacity to inhibit SERCA, it garnered significant interest within the research community, leading to investigations into its laboratory synthesis. Currently, three distinct methods for synthesising TG are reported in the scientific literature (Ball et al., 2007; Chu et al., 2016; Chen & Evans, 2017). Today, the compound is a vital research tool utilised in the study of Ca^{2+} homeostasis, ER stress responses and cell death (Christensen et al., 2021). Firstly, it is essential to examine the mechanism of action,

followed by an assessment of its more recent application: the potent inhibition of viral replication.

Figure 1.14 Thapsia garganica L.

Adapted from Bauer, 2018 and Willing, 2017.

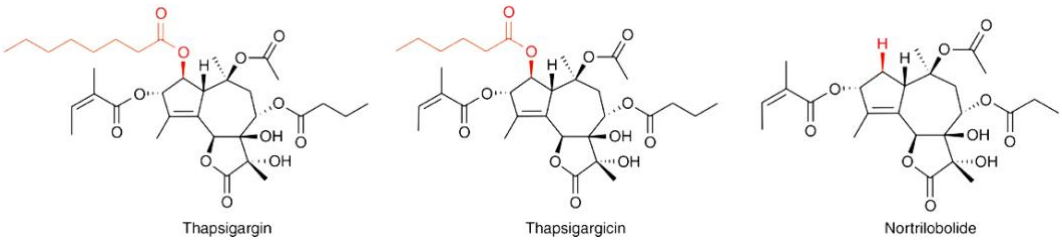

Figure 1.15 Chemical structures of compounds found in Thapsia garganica L.

Structural differences are highlighted in red (Martinez-Swatson et al., 2019).

1.9 Calcium Homeostasis

Calcium ions play a critical role in many functions, influencing almost all cellular processes ranging from cell survival to cell death. In most cells, the cytosolic Ca^{2+} concentration is ~100 n*M*, while inside the endoplasmic/sarcoplasmic reticulum (ER/SR) the concentration is 100–500 µ*M*. The extracellular Ca^{2+} concentration is 1-2 m*M* (Berridge et al., 2000). Maintaining a steady-state with orders of magnitude differences in Ca2+ concentrations between the ER, extracellular environment, and cytosol is crucial for cellular survival, as well as enabling the cellular response through calcium signalling coupled to external stimuli (Lee et al., 2006; Monteith et al., 2007; Berna-Erro et al., 2017). The concentration gradient is maintained mainly by Ca^{2+}-ATPases, ion exchangers and calcium channels, which allow the gradient to stay constant (Monteith et al., 2007). ATPases such as SERCA pumps use the energy generated from ATP hydrolysis to move Ca^{2+} against the concentration gradient to the ER/SR, Golgi apparatus, or external environment (Xu & Van Remmen, 2021).

1.9.1 SERCA

The SERCA family of Ca^{2+} ion pumps (1-3) are transmembrane transport proteins found in the SR of skeletal and cardiac muscle cells and in the ER of non-muscle cells (Møller et al., 2010). SERCA pumps can be found in all eukaryotic cells (Primeau et al., 2018). They transport two

Ca^{2+} from the cytosol into the SR/ER lumen while exporting two protons from the lumen to the cytosol, using the energy from ATP hydrolysis (Yu et al., 1993; Zafar et al., 2008). The SERCA pump operates in two states: E1 and E2. In the E1 state, the pump binds Ca^{2+} ions from the cytosol with high affinity and transports them into the SR/ER lumen. The E2 state has a low affinity for Ca^{2+} ions, allowing them to be released into the lumen while two protons are transported to the cytosol. The pump then returns to the E1 state to repeat the cycle (Figure 1.16) (Toyoshima, 2009).

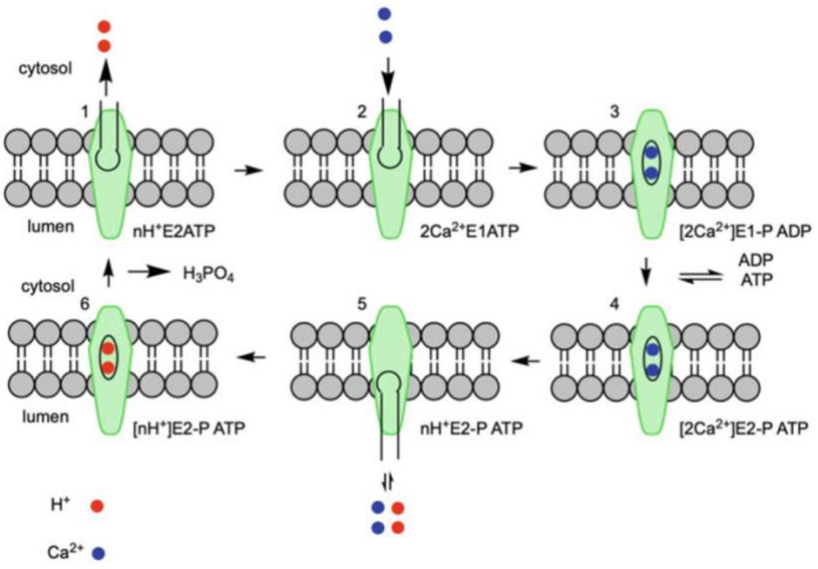

Figure 1.16 The pumping cycle of SERCA.

From Christensen et al., 2021.

TG is the most extensively utilized inhibitor of SERCA (Michelangeli & East, 2011). The transmembrane helix 3 (M3) was first proposed as target of TG-mediated SERCA inhibition (Hua & Inesi, 1997). Mutation of Phe 256 in M3 results in TG resistance (Yu et al., 1998). Later was

discovered that the binding site is a cavity near the cytoplasmic membrane of the SERCA pump, flanked by the M3, M5, and M7 helices, where bulky hydrophobic residues and a hydrogen bond between O8 of TG and the NH group of isoleucine 829 facilitate TG binding to the ATPase (Toyoshima & Nomura, 2002). Within these helices, Phe 256, Ile 765, and Tyr 837, located in M3, M5, and M7, respectively, are essential for TG binding (Figure 1.17) (Xu et al., 2004). It was thought initially that TG caused inhibition of SERCA by inhibiting Ca^{2+} binding and phosphorylation (Sagara & Inesi, 1991). Subsequently, it was found that TG inhibits the SERCA pump primarily in the E2 state, forming an enzymatically inert dead-end complex with the pump (Sagara et al., 1992).

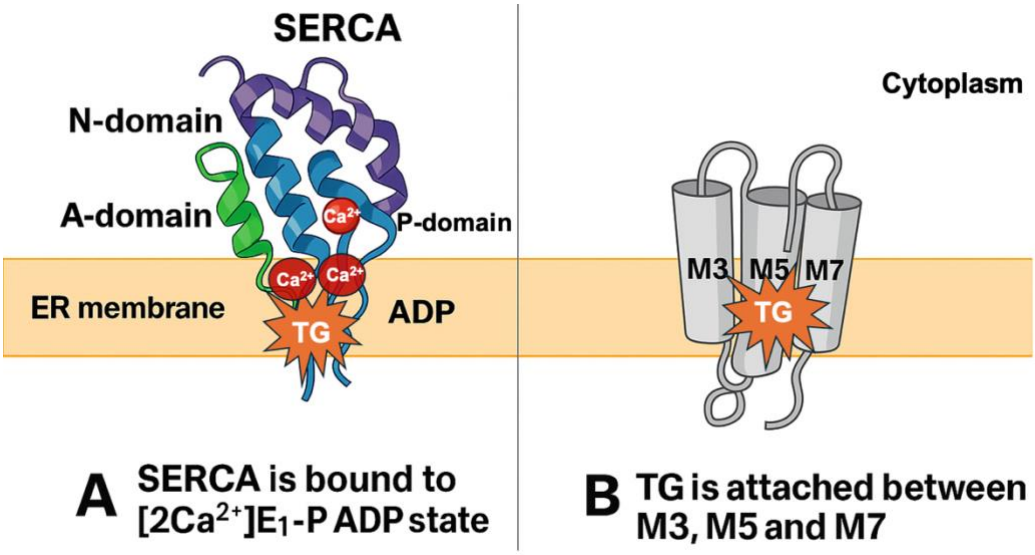

Figure 1.17 TG blocking SERCA's Ca^{2+} cycle.

(A) TG blocks SERCA pump in the $[2Ca^{2+}]$E1-P ADP state. (B) TG is attached between M3, M5 and M7.

TG disrupts the calcium gradient by inhibiting the uptake of Ca^{2+} ions into the ER and preventing the refilling of calcium stores. The primary

mediators of Ca^{2+} efflux from the ER is the inositol 1,4,5-trisphosphate receptor (IP_3R) and the ryanodine receptor (RyR) (Gillespie & Fill, 2008). Depletion of ER calcium stores activates the process of store-operated calcium entry (SOCE) in response (Smyth et al., 2010).

1.9.2 SOCE

SOCE was initially postulated in 1986, and subsequent experimental findings supported this concept (Putney, 1986; Takemura & Putney, 1989). TG was used from the early beginnings to study the mechanism (Takemura et al., 1989). When the levels of Ca^{2+} decrease within the intracellular calcium stores, SOCE facilitates the influx of Ca^{2+} through channels present in the plasma membrane (PM) (Smyth et al., 2010). The CRAC current, also known as I_{CRAC}, is a Ca^{2+}-selective current that was first observed in mast cells when intracellular Ca^{2+} stores were depleted (Hoth & Penner, 1992). This current is mediated by the calcium release-activated calcium (CRAC) channel, a highly selective channel located in the plasma membrane, which is considered a prototypical store-operated calcium (SOC) channel incorporated in the PM (Prakriya & Lewis, 2003). The ER lumen detects Ca^{2+} depletion through stromal interaction molecule (STIM1), found nearby SERCA which then activates the SOC channels and allows for extracellular Ca^{2+} influx (Liou et al., 2005; Roos et al., 2005).

1.9.3 SOC channels

The SOC channels, responsible for Ca^{2+} influx from the extracellular space into the cytosol upon ER Ca^{2+} store depletion, are tetrameric protein complexes composed of ORAI subunits that span the plasma membrane (Penna et al., 2008). Under normal physiological conditions, SOC channels exhibit high selectivity for Ca^{2+} ions when extracellular calcium ion concentration is within the range of 1-2 mM (Hou et al., 2012). ORAI proteins have been well-established as crucial mediators of SOCE. The ORAI subunits consist of ORAI1 (also called CRACM1), ORAI2, and ORAI3. Among the ORAI subunits, ORAI3 is the most recent evolutionary development and is only present in mammals (Shuttleworth, 2012). Each ORAI subunit is composed of four transmembrane α helices (TM1-TM4), a C-terminal M4 extension helix, and an N-terminal M1 extension sequence (Rothberg et al., 2013).

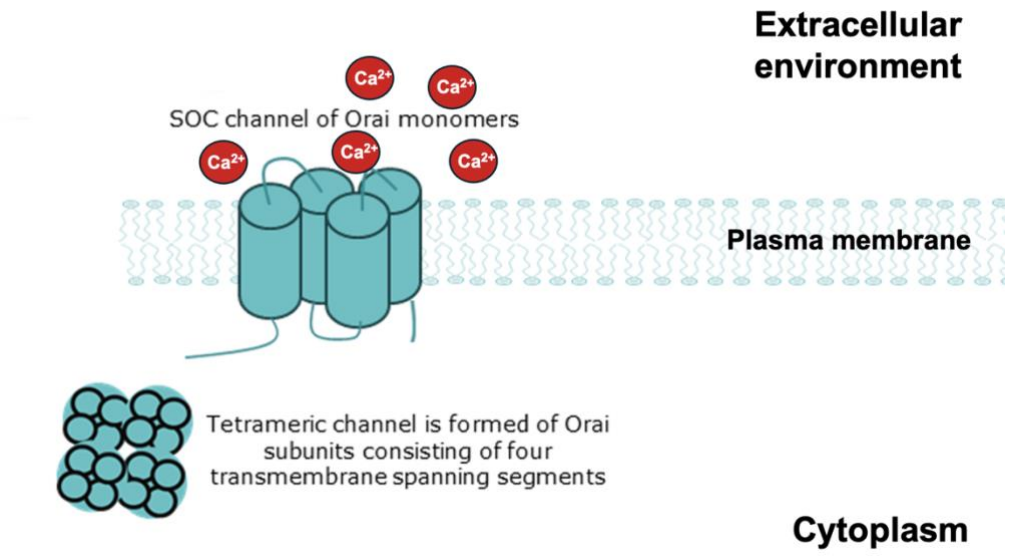

Figure 1.18 SOC channel structure.

1.9.4 Stromal interaction molecule

In response to low calcium levels, a sensor inside cells detects the reduced levels. The stromal interaction molecule (STIM) is a crucial protein embedded in the ER membrane that senses and responds to these changes. STIM activates the calcium entry channels in the plasma membrane when calcium stores are depleted (Liou et al., 2005; Zhang et al., 2005). In mammals, there are two types of STIM proteins, STIM1 and STIM2, which monitor calcium levels in the endoplasmic reticulum/ER (Liou et al., 2005). STIM2 helps keep both cytosolic and ER calcium levels stable, while STIM1 primarily triggers the activation of calcium entry when stores are low (Brandman et al., 2007; Stathopulos et al., 2009; Gruszczynska-Biegala et al., 2011).
When calcium stores are full, STIM1 is evenly distributed across the ER membrane (Zhou et al., 2015; Covington et al., 2010; Penna et al., 2008). However, when it detects a drop in calcium levels through a specific domain, the EF hand domain, located adjacent to a sterile alpha motif (SAM), STIM1 undergoes a conformational change to reach the SOC channels and activate the CRAC activating domain (CAD), the region of STIM1 required for SOC channel activation (Park et al., 2009, Yuan et al., 2009). Evidence shows that STIM1 must cluster before it can move to the junctions between the ER and the plasma membrane, where it works to increase calcium entry from outside the cell (Liou et al., 2007; Luik et al., 2008; Palty et al., 2015 Yamashita et al., 2017). STIM1 clusters form 10-25nm below the plasma membrane, and their development takes place just seconds

before the activation of the calcium entry channels (Wu et al., 2006). Once at the plasma membrane, STIM1 interacts with the SOC channels to help calcium flow into the cell from the outside. The complex formed by STIM1 and the SOC channels includes eight STIM1 proteins and a four-part ORAI channel. Each pair of STIM1 SOAR domains connects with a single ORAI molecule (Penna et al., 2008, Li *et al.*, 2010, Soboloff *et al.*, 2012). It has been suggested that STIM1's attachment to the N and C terminus of ORAI1 triggers structural changes in the ORAI1 TM1 and TM4 regions. These changes disrupt the hydrophobic gate and increase channel hydration, enhancing the movement of calcium through the channel (Yamashita et al., 2017, Palty et al., 2015).

2 Antiviral Effects of TG-Mediated SOCE

TG has emerged as a powerful antiviral agent due to its distinct mechanism of action, which disrupts calcium homeostasis within cells, triggering a cascade of downstream events such as ER stress and the activation of the UPR. These processes, crucial for maintaining cellular equilibrium and survival, become dysregulated upon TG administration, ultimately resulting in antiviral effects. During the COVID-19 pandemic, my colleagues and I demonstrated that TG is indeed a broad-spectrum antiviral, effective against SARS-CoV-2, Influenza A, OC43, and RSV (Al-Beltagi et al., 2021). Despite these promising findings, particularly

against a wide array of respiratory viruses, many questions remain unanswered and require further investigation.

In the subsequent sections, I will provide an overview of how TG interacts with cellular machinery and potentiates an antiviral response.

2.1 Steps by which TG may act as a potent antiviral

The antiviral efficacy of TG begins with its inhibition of the SERCA pump, which is responsible for transporting Ca^{2+} from the cytosol into the ER. By blocking this pump, TG effectively depletes the ER's calcium stores, a crucial component of the organelle's functioning. This depletion disrupts the calcium gradient, triggering the activation of SOCE, a compensatory mechanism that facilitates the influx of extracellular calcium into the cell to replenish the depleted stores (Smyth et al., 2010). SOCE is mediated by the interaction of STIM proteins in the ER membrane with ORAI channels in the plasma membrane, which work together to restore calcium balance within the cell (Liou et al., 2005; Zhang et al., 2005).

The depletion of ER calcium and subsequent activation of SOCE lead to ER stress, a condition where the protein-folding capacity of the ER is overwhelmed due to the accumulation of unfolded or misfolded proteins. This stress response triggers the unfolded protein response (UPR), which employs three complementary signalling branches—IRE1, PERK and ATF6—to restore ER homeostasis by enhancing folding capacity,

promoting degradation of misfolded proteins and attenuating overall protein synthesis (Smith, 2014; Ron & Walter, 2007).

The antiviral effects of TG stem from its induction of ER stress and activation of the UPR, which research shows impairs viral replication by overwhelming the ER's folding capacity and, in some contexts, promoting apoptosis in infected cells (Zhang & Wang, 2012; He, 2006). Emerging studies indicate that UPR activation may also bolster innate antiviral signalling: PERK-mediated phosphorylation of eIF2α can restrict translation in a manner analogous to PKR-driven responses, although its direct antiviral role in TG-treated systems remains under investigation (Manivannan et al., 2020). Likewise, IRE1's endonuclease activity may generate RNA fragments that engage RIG-I and trigger type I interferon production, but this mechanism has so far been demonstrated primarily in vitro rather than in infected tissues (Smith, 2014; Manivannan et al., 2020).

2.2 The unknowns of TG as an antiviral

Although TG has demonstrated significant potential as a broad-spectrum antiviral agent in vitro and in mice against influenza A (Goulding et al., 2020), numerous uncertainties could influence its effectiveness in clinical settings. One major unknown is the precise mechanism through which TG exerts such a potent antiviral response. Further research is needed to clarify these pathways. A critical consideration is TG's function in the context of viral co-infections, which are common in respiratory

illnesses where multiple viruses may infect the same host concurrently. Co-infections complicate antiviral therapy because different viruses interact with the host immune system in diverse ways, potentially interfering with immune signalling pathways or modulating antiviral defences. In some cases, interactions between co-infecting viruses may result in recombination or pseudo-typed viral particles, which can alter tropism or immune recognition, thereby challenging the effectiveness of innate immune responses.

Another significant factor is the safety profile of TG. While the induction of ER stress and activation of the UPR is effective in restricting viral replication, these processes can also have cytotoxic effects on host cells, particularly when TG is administered in high doses. Excessive or prolonged activation of the UPR may lead to apoptosis, which, although beneficial in clearing infected cells, could also result in unintended damage to healthy tissues. Therefore, balancing TG's antiviral effects with its potential toxicity remains a crucial challenge.

Hypothesis

Thapsigargin, by disrupting intracellular calcium homeostasis and triggering endoplasmic reticulum stress pathways, can effectively inhibit the replication of respiratory syncytial virus, influenza A virus, and their co-infections at non-cytotoxic doses in diverse cell systems.

Aim

This thesis focuses specifically on the antiviral effects of TG against RSV, building on the findings of our previous study (Al-Beltagi et al., 2021). The data from our study demonstrated that TG exhibits potent antiviral activity against RSV by inducing ER stress and activating the UPR. However, this thesis will go further by exploring additional aspects of TG's antiviral potential, including its safety profile, its ability to inhibit co-infections, and its impact on the host immune response, with a particular emphasis on RSV and the UPR.

The investigation will address several key matters:

Establish TG’s Antiviral Efficacy - Determine the extent to which TG suppresses RSV and IAV across multiple cell models, including immortalised lines and primary human bronchial epithelial cells, under varying treatment and infection conditions.

Investigate Mechanisms of Action- Elucidate how TG-induced ER stress and activation of the UPR curtail viral replication, particularly focusing on key host factors (e.g., PERK, IRE1, G3BP1, RNase L).

Assess Prophylactic and Therapeutic Potential - Evaluate whether short pulses of TG can establish a durable antiviral state against RSV and IAV, comparing its potency and safety profile to that of conventional antivirals such as ribavirin.

Examine Efficacy in Co-infections - Determine how TG impacts dual RSV–IAV infections, including its effect on hybrid viral particles, overall viral load, and host innate immune responses in a co-infection setting.

Through these objectives, this thesis aims to clarify TG's broad-spectrum antiviral value and appraise its viability as a host-centric therapeutic strategy for respiratory viruses.

General materials and methods

2.1 Materials

All reagents, plasticware, consumables, and technical equipment are listed in the following tables. Reagents include the supplier and catalogue number from which they were obtained. Plasticware, consumables, and technical equipment indicate the manufacturer or their UK distributor. Gifts and donations from other institutions are acknowledged where applicable.

2.1.1 Chemical reagents and kits

Table 2.1 **Laboratory kits and reagents** ***used in experimental procedures.***

Reagent	Company	Catalogue Number
4μ8C	Sigma-Aldrich	SML0949
Bronchial epithelial growth media	Promocell	C-21060
DMEM-Glutamax (high glucose)	Gibco, ThermoFisher	10569010
Foetal calf serum (FCS)	Gibco, ThermoFisher	10270106
Penicillin–streptomycin (P/S)	Gibco, ThermoFisher	15140122
CellTiter-Glo 2.0 Cell Viability Assay	Promega	G9241
DetachKit	Promocell	C-41200
Thapsigargin (TG)	Merck	586005
Ribavirin	Merck	R9644
PBS (Phosphate Buffered Saline)	Gibco, ThermoFisher	10010023
Cryopreservation media (Hybri-Max DMSO)	Sigma-Aldrich	D2650
ProFreeze-CDM Medium	Lonza	BEBP12F300
TPCK Trypsin	Sigma-Aldrich	T1426
0.25% Trypsin-EDTA	Gibco, ThermoFisher	25200056

Lipofectamine 2000	Invitrogen	11668019
Opti-MEM	Gibco, ThermoFisher	31985062
RNeasy Plus Minikit	Qiagen	74134
Superscript III First Strand synthesis kit	ThermoFisher Scientific	18080051
Human ER stress primers (HSPA5, HSP90B1, DDIT3)	Sigma-Aldrich	Custom order
Human IFNβ1 primers	Sigma-Aldrich	Custom order
Human RNASEL primers	Sigma-Aldrich	Custom order
QIAamp Viral RNA Mini Kit	Qiagen	52906
OneStep RT-PCR Kit	Qiagen	210212
Mouse anti-RSV antibody (2F7)	Abcam	ab43812
Tryptose Phosphate Broth	Sigma-Aldrich	T9157
β-Mercaptoethanol	Sigma-Aldrich	M6250
SYBR Green PCR Kit	Qiagen	204141
Protein Assay Dye Reagent	Bio-Rad	5000006
NuPAGE LDS Sample Buffer 4X	Invitrogen	NP0007
NuPAGE Reducing Agent 10X	Invitrogen	NP0009
NuPAGE Bis-Tris Gel (4-12%)	Invitrogen	NP0322BOX
SeeBlue Pre-stained Protein Standard	Invitrogen	LC5625
Sunitinib (malate)	Sigma-Aldrich	1642358
ImmPRESS HRP Anti-Mouse IgG Polymer Kit	Vector Laboratories	MP-7402
Liquid DAB+ Substrate Chromogen System	Dako	K346811

2.1.2 Plasticware and Consumables

Table 2.2 Plasticware and general laboratory consumables.

Item	Company	Catalogue Number
10 mL pipettes	Corning	4488
0.1-10 µL pipette tips	Alpha Laboratories	ZP1010S
1-40 µL pipette tips	Alpha Laboratories	ZP1204S
1-100 µL pipette tips	Alpha Laboratories	ZP1200S
1-200 µL pipette tips	Alpha Laboratories	ZP2250S
10-1000 µL pipette tips	Alpha Laboratories	ZP2250S
50 mL tubes	Falcon	352070
96-well plates	Fisher Scientific	12-565-501

Cell culture plasticware (e.g., flasks, plates)	ThermoFisher Scientific	136196 (Flasks), 140675 (Plates)
Serological pipettes	ThermoFisher Scientific	170358
Sterile filters	Millipore	SLGP033RS
Tubes for centrifugation and storage	Falcon	352096 (15 mL)
Cryovials (sterile)	Nalgene	5000-0020
Acetone	Fisher Scientific	A19-4
Methanol	Fisher Scientific	M/4000/15

2.1.3 Technical Equipment

Table 2.3 Technical equipment utilised in the laboratory.

Equipment	Company	Catalogue Number
Class II Safety Cabinet	ThermoFisher Scientific	51023608 (herasafe KSP15)
Cell culture incubator	ThermoFisher Scientific	51028210
Unstirred water bath	Scientific Laboratory Supplies	BAT2110
Vortex Mixer	Scientific Laboratory Supplies	B2B06222
Centrifuge 1	Fisher Scientific	13-100-675
Centrifuge 2	Eppendorf	5810R
PCR machine	Bio-Rad	1851196
0.5-10 µL pipette	Scientific Laboratory Supplies	B2B06158
2-20 µL pipette	Scientific Laboratory Supplies	B2B06160
5-50 µL pipette	Scientific Laboratory Supplies	B2B06160
10-100 µL pipette	Scientific Laboratory Supplies	B2B06164
20-200 µL pipette	Scientific Laboratory Supplies	B2B06166
100-1000 µL pipette	Scientific Laboratory Supplies	B2B06168

20-200 µL 8-Channel pipette	Scientific Laboratory Supplies	B2B06180
Automatic pipette filler	Scientific Laboratory Supplies	B2B06190
Fluorescent microscope	Leica	DMi8
Real-time PCR system (LightCycler−96)	Roche	05815916001
GloMax® Discover Microplate Reader	Promega	GM3000
ChemiDoc MP Imaging System	Bio-Rad	17001402
Trans-Blot SD Semi-Dry Transfer Cell	Bio-Rad	170-3940
Freezing Container	ThermoFisher Scientific	5100-0001

2.1.4 Cell Lines and Viruses

Table 2.4 Cell lines and viral strains employed in experiments.

Cell Line / Virus	Full Name	Company	Catalogue Number
NHBE cells	Primary normal human bronchial epithelial cells	Promocell	C-12620
NPTr cells	Immortalised neonatal porcine tracheal epithelial cells	University of Nottingham	Stock supplied upon request
HEp2 cells	Human Epithelial type 2 cells	ATCC	CCL-23
A549 cells	Adenocarcinomic human alveolar basal epithelial cells	ATCC	CCL-185
Calu-3 cells	Human lung adenocarcinoma epithelial cells	ATCC	HTB-55
Vero cells	African green monkey kidney epithelial cells	ATCC	CRL-1586
MDCK cells	Madin-Darby Canine Kidney cells	ATCC	CCL-34

Human RSV (A2 strain)	Respiratory Syncytial Virus, A2 strain	ATCC	VR-1540
USSR H1N1 (A/USSR/77)	Influenza A Virus, H1N1 subtype	Animal and Plant Health Agency	Supplied by APHA upon request

2.1.5 Statistical analysis and other software

Table 2.5 Software tools used for statistical analysis, data processing and visualisation.

Software	Purpose	Company	Version / Catalogue Number
Endnote	Reference management	Clarivate	X9
GraphPad Prism	Statistical analysis and graphing	GraphPad	9.0
Microsoft Excel	Spreadsheet software for data analysis	Microsoft	Office 365
ImageJ	Image processing and analysis	NIH	1.53
Primer Express 3.0	Primer design for qPCR	ThermoFisher Scientific	4363991

2.2 Cell culture methods

2.2.1 Cell culture

All procedures involving the use of cell lines were carried out under sterile conditions within a Class II microbiological safety cabinet. The NPTr, MDCK, HEp2, Vero E6, Calu-3, and A549 cell lines were cultured in DMEM-Glutamax (high glucose), supplemented with 10% foetal calf serum (FCS) and 100 U/ml penicillin-streptomycin (P/S) (Gibco). Normal

human bronchial epithelial (NHBE) cells were cultured using specialised epithelial growth medium (Promocell).

Cell cultures were monitored daily using an inverted light microscope to assess their condition. To maintain the cultures, the cells were gently rinsed with phosphate-buffered saline (PBS) and passaged via trypsinisation using 0.25% trypsin-EDTA. For NHBE cells, the DetachKit (Promocell) was utilised according to the manufacturer's instructions. The cells were then diluted in pre-warmed culture medium, either DMEM supplemented with 10% heat-inactivated foetal bovine serum (FBS) and 1% penicillin-streptomycin, or in the specialised epithelial growth medium for NHBE cells. Sub-culturing was performed at appropriate intervals depending on the growth rate and confluence of each cell line, typically using a split ratio between 1:3 and 1:6. Cell lines were maintained in 25 cm^2 or 75 cm^2 tissue culture flasks at 37°C in a humidified atmosphere with 5% carbon dioxide (CO_2).

2.2.2 Cryopreservation

Cryopreservation of NPTr, MDCK, HEp2, Vero E6, Calu-3, and A549 cell lines was carried out using sterile cryovials to store seed stocks. Cells were grown to a confluent monolayer in two 75 cm^2 tissue culture flasks. Following trypsinisation, the cells were diluted to 15 ml with culture media and transferred into 15 ml conical tubes. The cell suspensions were then centrifuged at 500x g for 4 minutes at 22°C. After centrifugation, the culture media was carefully removed, ensuring any

residual media near the lid was discarded. The cell pellets were resuspended in 0.5 ml of DMEM, followed by the addition of an additional 2.2 ml of DMEM to reach a final volume of 2.7 ml. To this, 0.3 ml of dimethyl sulfoxide (DMSO) was added, and the suspension was thoroughly mixed by pipetting.

For primary epithelial cells, the cryopreservation medium consisted of a 1:1 ratio of growth media and freeze media (ProFreeze-CDM Medium, Lonza), supplemented with 15% DMSO. Cells were resuspended in this cryopreservation medium before aliquoting into cryovials. The primary epithelial cells were detached using the DetachKit (PromoCell) according to the manufacturer's recommended subcultivation protocol. The suspended cells were transferred to a bench-top centrifuge and centrifuged at 150x g for 2 minutes. Following centrifugation, the supernatant was removed, and the cells were resuspended in 3 ml of cryopreservation media per T75 flask. From this suspension, 1 ml of the cell mixture was transferred into sterile cryovials.

The cryovials containing the cell suspensions were placed in a Mr. Frosty™ Freezing Container, which controls the rate of freezing at approximately 1°C per minute and stored at -80°C for at least 3 hours. After this initial freezing period, the cryovials were transferred to liquid nitrogen (N_2) for long-term storage.

2.2.3 Cell passage, counting and seeding

To revive frozen cells, cryovials were removed from liquid nitrogen storage and rapidly thawed in a 37°C water bath. Once thawed, the cells were transferred into 10 ml of the appropriate culture medium and seeded into a T75 flask. Both immortalised cell lines and NHBE cells were incubated at 37°C in a 5% CO_2 atmosphere. The culture medium was replaced 24 hours after seeding, with further media changes carried out every 48 hours. When the cells reached approximately 60-70% confluence, they were passaged.

For passaging, the medium was first removed, and the cells were washed with PBS. For MDCK, NPTr cells, and myoblasts, 5 ml of 1X 0.25% trypsin was added to detach the cells from the culture surface, followed by incubation at 37°C. Once detached, 4 ml of growth medium (PM) was added to inactivate the trypsin. For primary epithelial cells, the DetachKit (PromoCell) was used in accordance with the manufacturer's subcultivation protocol. The entire cell suspension was transferred to a Falcon tube and centrifuged at 150x g for 2 minutes. The supernatant was discarded, and the cell pellet was resuspended in 1 ml of growth medium before being diluted to the required volume for reseeding.

Viable cell counts were performed to ensure the correct number of cells was seeded into plasticware according to experimental requirements. For this, after trypsinisation, a 10 µl sample of the cell suspension was mixed with 10 µl of DMEM or Promocell medium (for NHBE cells) and allowed to equilibrate for 1 minute. The mixture was then transferred to

a haemocytometer for total cell counting. The total cell number was calculated based on the defined area of the counting chamber, and appropriate dilutions were prepared to achieve the desired seeding density. The volume of medium required for different tissue culture vessels was as presented in table 2.6.

Table 2.6 Typical media volumes used in tissue culture vessels.

Tissue Culture Vessel	Volume of Medium Required
T75 Flask	10-12 ml
T25 Flask	4 ml
6-Well Plate (per well)	2 ml
12-Well Plate (per well)	1 ml
24-Well Plate (per well)	0.5 ml
48-Well Plate (per well)	0.25 ml
96-Well Plate (per well)	0.1 ml

2.2.4 Cell viability assay

Cell viability was assessed by measuring ATP levels as an indicator of viable cells. The cells were treated with the specified chemicals, such as TG or DMSO, at the concentrations indicated in the experimental protocol. The treatments were administered for either 1 hour or 30 minutes, depending on the experimental design. Following the chemical exposure, the cells were rinsed three times with PBS to remove any residual compounds, and the culture medium was replaced with fresh

media. After 24 hours, cell viability was measured using the CellTiter-Glo® 2.0 Cell Viability Assay (Promega).

The CellTiter-Glo® 2.0 Reagent was prepared according to the manufacturer's instructions. If the reagent was frozen, it was thawed overnight at 4°C, or alternatively in a 22°C water bath. Care was taken to avoid exposing the reagent to temperatures above 25°C. When the reagent was stored at –65°C, it was not directly transferred to a 22°C water bath to prevent potential cracking of the bottle due to rapid temperature changes. Instead, the reagent was allowed to rest at room temperature for 10-15 minutes before being placed in the water bath. Once thawed, the reagent was equilibrated to room temperature by keeping it in a 22°C water bath. Approximately 30 minutes were required to equilibrate 100 ml of thawed reagent, while 500 ml needed around 100 minutes to reach 22°C. Before use, the contents of the reagent bottle were gently mixed by inverting to obtain a homogeneous solution. Care was also taken to prevent contamination during the removal of the seal from the reagent bottle.

To perform the cell viability assay, opaque-walled multiwell plates were prepared with the indicated cell lines cultured in an appropriate medium. The volume of medium and the number of cells seeded were optimised based on the experimental conditions. Multiwell plates compatible with the luminometer used for luminescence detection were selected. Control wells containing only medium (without cells) were prepared to determine background luminescence. The test compounds were added to the experimental wells, and the plates were incubated according to the

specific culture protocol. Before adding the CellTiter-Glo® 2.0 Reagent, the plate and its contents were equilibrated to room temperature for approximately 30 minutes.

An equal volume of CellTiter-Glo® 2.0 Reagent was added to each well, matching the volume of the cell culture medium present (e.g., 100 µl of reagent was added to 100 µl of medium in a 96-well plate). The plate was then gently mixed on an orbital shaker for 2 minutes to induce cell lysis. After lysis, the plate was incubated at room temperature for 10 minutes to stabilise the luminescent signal. The luminescence was recorded using a luminometer (GloMax® Discover Microplate Reader, Promega) providing a direct measure of cell viability based on the ATP content of the samples.

2.3 Viral infection and quantification methodology

2.3.1 Influenza A subtype and stock use

Human influenza A virus, specifically the USSR H1N1 (A/USSR/77) was used in this study. The virus was provided by the Animal and Plant Health Agency. The master virus stocks were propagated in 10-day-old embryonated chicken eggs and stored in liquid nitrogen (N_2) until needed. To minimise the possibility of egg adaptation, an aliquot of the master stock virus was thawed once and used to generate an experimental stock virus, which was stored at -80°C. Each aliquot of experimental stock virus underwent no more than three freeze–thaw

cycles to minimise loss of titre and was not used for further amplification. For each experimental replicate, a fresh aliquot of experimental stock virus was used.

2.3.2 Influenza A propagation

For the propagation of influenza virus, embryonated Dekalb white chicken eggs (Medeggs) were incubated at 37.5°C with humidity maintained between 40-50%. After 10 days, the eggs were inoculated with the virus. The seed virus was diluted in phosphate-buffered saline (PBS) supplemented with 2% tryptose phosphate broth (Sigma-Aldrich) and 5% penicillin-streptomycin (P/S), which had been filtered through a 0.22 µm filter (Fisher Scientific). Small holes were carefully made in the eggshell at the allantoic cavity and air sac sites. Using a sterile 25-gauge needle and syringe, 0.1 ml of the virus dilution was injected into the allantoic cavity, and the holes were sealed with hot wax to prevent contamination. The inoculated eggs were returned to the incubator for an additional 72 hours. Following incubation, the eggs were chilled at 4°C for 12-24 hours to allow for virus collection.

The allantoic fluid containing virus was harvested, aliquoted and stored at –80 °C until use. Virus stocks were titrated by plaque assay, and viral suspensions were then prepared at a target multiplicity of infection (MOI) of 1.0—calculated from the plaque-forming unit titre—using 100 µl of inoculum per well of confluent MDCK cells in a 96-well plate. Infection efficiency was confirmed by staining for viral nucleoprotein, with this

dilution yielding consistently high (≈90 %) NP-positive cells. The diluted virus stock was stored at –80 °C and underwent no more than three freeze–thaw cycles to minimise loss of titre. To avoid cell adaptation of the influenza A virus, all experiments were conducted using virus stocks suspended in allantoic fluid.

2.3.3 Influenza A infection media

The infection medium (IM) for immortalised cells consisted of Opti-MEM I (Gibco) supplemented with 100 U/mL penicillin–streptomycin (P/S), 2 mM glutamine and 200 ng/mL TPCK-treated trypsin (Sigma-Aldrich). The virus stock was titrated by focus-forming assay (FFA), and the multiplicity of infection (MOI) was calculated from the number of focus-forming units. Cells were infected at this calculated MOI and incubated in IM for 2–3 hours. Following adsorption, monolayers were washed three times with PBS and overlaid with fresh, serum-free IM (no FCS) for 24–72 hours, or as specified by the experimental design.

2.3.4 Influenza A spun supernatant and cell lysate collection

After the incubation period, the cell culture medium or infection medium (IM) was carefully removed and centrifuged at maximum speed for 2 minutes. The supernatant was then collected and stored at -80°C until further analysis. The supernatants were subsequently used to quantify progeny virus, either through a 6-hour focus forming assay (FFA) or by determining the viral copy number using RT-qPCR. The remaining cells,

following supernatant removal, were treated with the appropriate lysis buffer for RNA extraction, and the lysates were collected. RNA extraction was performed immediately, or the lysate was stored at –80 °C until needed.

2.3.5 Quantification of influenza A from spun supernatant

The focus forming assay (FFA) was employed to quantify progeny virus via immunostaining methods, without the need for cell lysis. Madin-Darby Canine Kidney (MDCK) cells were seeded into 96-well plates and allowed to reach 100% confluence. Once confluent, the cells were exposed to the appropriate volume of infected supernatant for 2 hours and incubated at 37°C in a 5% CO_2 atmosphere.

The volume of infected supernatant utilised varied depending on the progeny viral output, with serial dilutions determining the minimum representative volume necessary to quantify virus titre. After the 2-hour incubation, the medium was removed, and the cells were washed twice with phosphate-buffered saline (PBS). Subsequently, 100 µl of infection medium was added to each well, and the cells were incubated for an additional 4 hours. Following this, the infection medium was discarded, and the wells were washed with 100 µl of 1X Tris-buffered saline (TBS) (Tris base in distilled water) per well. To fix the cells, a 1:1 acetone:methanol mixture was added at room temperature for 10 minutes, using 40 µl per well. The fixed cells were then washed three

times with 1X TBS to remove the acetone mixture and subsequently stored at 5-8°C in 1X TBS until ready for staining.

2.3.6 Immunostaining Influenza A infected cells

Immunostaining of the infected MDCK cells was conducted using the ImmPRESS HRP Anti-Mouse IgG (Peroxidase) Polymer Detection Kit (Vector Laboratories) and the Liquid DAB+ Substrate Chromogen System (Dako). Initially, the 1X TBS was removed, and 40 µl of ImmPRESS 2.5% normal goat serum blocking buffer was added to each well, followed by incubation for 20 minutes at room temperature. After this step, the blocking buffer was discarded, and the cells were washed three times with 1X TBS. The cells were then incubated for 1 hour at room temperature with 40 µl of primary antibody, Anti-Influenza-A NP (Abcam, ab20343), diluted at 1:8000 in 1X TBS. Once the incubation period was completed, the primary antibody was removed, and the cells were washed three times with 1X TBS. Next, 40 µl of undiluted ImmPRESS (Peroxidase) Polymer Anti-Mouse IgG reagent was added to each well and left to incubate at room temperature for 45 minutes. For the development of colour, one drop of DAB+ chromogen (Dako) was diluted in 1 ml of DAB substrate buffer to achieve the appropriate final volume. The wells were then washed four times with 1X TBS by filling each well with wash buffer, incubating for 5 minutes at room temperature with gentle agitation, and removing the buffer between washes. Subsequently, 40 µl of the prepared chromogen mix was added to the

wells and allowed to develop for approximately 5 minutes until the colour was visible. The cells underwent a final three washes with TBS before being imaged under an inverted light microscope at 100X magnification. Focal-forming units per millilitre (FFU/mL) of supernatant were calculated using the following formula:

FFU/mL = (30 × average number of infected cells per field) ÷ µL of infectious supernatant.

In this equation, the factor of 30 represents the approximate number of microscope fields required to cover the entire well surface at 10× magnification, thereby scaling the mean count of infected cells per field to the total well area. The “average number of infected cells per field” refers to the mean count of discrete infection foci observed across multiple, randomly selected fields.

2.3.7 RSV subtype and stock use

Human respiratory syncytial virus (RSV, A2 strain) was acquired from the American Type Culture Collection (ATCC, VR-1540) for use in this research. The master stock virus was propagated in HEp2 cells and stored in liquid nitrogen (N_2) until required. To ensure consistency and minimise the risk of adaptation, an aliquot of the master stock was thawed once and used to generate the experimental stock virus, which was stored at -80°C. Each aliquot of experimental stock virus was thawed slowly, with exposure to light minimised to reduce the likelihood of virus degradation. Experimental aliquots were subject to no more than

three freeze–thaw cycles overall, but for each experimental replicate a fresh thawed aliquot (i.e. in its first thaw) was used to maintain viral integrity and reliability of results.

2.3.8 RSV propagation

Respiratory syncytial virus (RSV, A2 strain) was propagated using HEp2 cells, following established procedures. Prior to infection, 2 x 10^6 HEp2 cells were seeded into a T75 flask containing 15 ml of Dulbecco's Modified Eagle Medium (DMEM) supplemented with GlutaMAX and 10% foetal calf serum (FCS). The flask was incubated overnight at 37°C in a humidified atmosphere of 5% CO_2 until the cells reached approximately 50% confluence. Two flasks were prepared: one for infection with RSV and one as a control.

For infection, the medium was carefully removed from the flask without allowing the cells to dry out, and the cell monolayer was gently washed with 10 ml of serum-free RPMI or serum-free DMEM (no FCS). An inoculum containing 4 × 10^5 plaque-forming units (PFU) in 2 ml of serum-free medium was prepared, corresponding to an intended multiplicity of infection (MOI) of 0.1, assuming the HEp2 cells had doubled overnight to 4 × 10^6 cells. For example, 20 µl of virus stock (4 x 10^7 pfu/ml) was diluted in 4 ml of serum-free medium. In the control flask, 2 ml of serum-free medium was added without virus.

The virus-containing medium was gently distributed across the flask, and the flask was incubated at 37°C for 2 hours. During incubation, the flask

was rotated by 90 degrees every 15 minutes to ensure even temperature distribution and to counteract any potential uneven surface effects in the incubator. After the 2-hour incubation, the medium was topped up to a final volume of 15 ml with a final FCS concentration of 2%.

The flasks were regularly monitored for cytopathic effects, such as the detachment of cells into the medium. Once approximately 50% of the cells exhibited cytopathic effects, usually after 72 hours, the infected cells were harvested using a rubber policeman. If multiple T75s were infected, virus stocks from identical treatments were pooled to reduce batch variability, and the cell debris was pelleted by centrifugation. The supernatant containing the virus was collected and transferred into separate tubes, leaving a small volume with the cell pellet.

The virus stocks could either be stored immediately or further processed. For additional processing, the cell pellets were subjected to sonication for 20 seconds in a water bath sonicator or three freeze-thaw cycles using liquid nitrogen and a 37°C water bath. After further centrifugation to remove cell debris, the supernatant was collected and combined with the previously collected supernatant. The newly formed virus stock was aliquoted into 1 ml cryovials, rapidly snap-frozen in liquid nitrogen, and stored in a liquid nitrogen tank for long-term preservation.

To determine the concentration of the RSV stock, a 96-well plate was seeded with HEp2 cells to full confluence. On Day 1, 2 x 10^4 cells per well were seeded in 100 µl of growth medium. On Day 2, the cells were infected using a serial dilution of the virus stock, starting with a 1:100 dilution and continuing with 12 serial two-fold dilutions. The seeded cells

were washed twice with serum-free medium, and 50 µl of virus was added to each well according to the dilution scheme. Negative control wells received 50 µl of serum-free medium. The plate was incubated at 37°C with 5% CO_2 for 1.5 hours before the medium was topped with 150 µl of DMEM supplemented with 10% FCS. The plate was further incubated for 24 hours, as RSV replicates more slowly than Influenza A, with detectable levels of RSV remaining confined to the initially infected cells.

On Day 3, RSV-infected cells were visualised and counted individually using a plaque-forming unit (PFU) assay, with viral detection achieved through immunostaining using a mouse anti-RSV (2F7) antibody (Abcam). This allowed for quantification of RSV-positive cells, enabling the determination of virus concentration in the stock and subsequent calculation of the volume required to achieve the desired MOI for further experiments.

2.3.9 RSV infection

The desired cell line was seeded into the appropriate plate based on the experimental design. Growth medium for immortalised cells consisted of DMEM supplemented with 10% foetal calf serum (FCS) and 1% penicillin-streptomycin (P/S), whereas normal human bronchial epithelial (NHBE) cells were cultured in Promocell media. The plates were incubated at 37°C in a 5% CO_2 atmosphere until the cells reached 70-

80% confluence. The plates were examined daily using an inverted microscope.

Once the cells were ready for infection, they were gently washed three times with phosphate-buffered saline (PBS) to remove any residual medium and then set aside. Meanwhile, the RSV stock, stored in liquid nitrogen, was slowly thawed to preserve viral viability. Once thawed, the virus was diluted in serum-free medium (DMEM without FCS for immortalised cells, or Promocell media for NHBE cells) to achieve the desired multiplicity of infection (MOI). Typically, an MOI of 0.1 was used for immortalised cells, while a lower MOI was applied for NHBE cells, depending on the experimental requirements.

The prepared virus-containing medium was then added to the cells, ensuring even distribution across the wells. Control wells were treated with plain medium without the virus. The cells were incubated with the virus for 2 hours at 37°C to allow for infection, with gentle rotation every 15-30 minutes to ensure even viral exposure across all cells.

After the 2-hour incubation period, the virus-containing medium was carefully removed, and fresh culture medium was added to the wells. For immortalised cells, this consisted of DMEM supplemented with 2% FCS, while NHBE cells received fresh Promocell media. The infected cells were then incubated at 37°C in a 5% CO_2 atmosphere for the desired duration, typically 48-72 hours, depending on the downstream analysis planned.

2.3.10 RSV spun supernatant and cell lysate collection

At the end of the incubation period, the cell culture or infection medium was carefully collected and centrifuged at maximum speed for 2 minutes to remove cellular debris. The supernatant was then aliquoted and stored at -80°C until further analysis. These supernatants were subsequently used to quantify progeny virus, either through a 24-hour focus plaque-forming unit (pfu) assay or by determining viral copy number using reverse transcription quantitative PCR (RT-qPCR).

Following supernatant collection, the remaining cells were lysed with the appropriate lysis buffer to facilitate RNA extraction. The lysates were collected and either processed immediately or stored at -80°C for future RNA extraction.

2.3.11 Quantification of RSV from spun supernatant

Plaque-forming unit (pfu) for RSV was conducted using HEp-2 cells. Initially, HEp-2 cells were seeded into a 96-well plate containing DMEM-Glutamax media, supplemented with 10% fetal calf serum (FCS) and 1% penicillin-streptomycin (P/S). The plate was incubated at 37°C in a 5% CO_2 atmosphere for 24 hours or until the cells reached 80-90% confluence.

On the day of infection, the cells were washed once with serum-free medium to remove residual FCS. The RSV supernatants, stored in liquid nitrogen, were slowly thawed on ice to preserve viral integrity. Serial

dilutions of the supernatant were prepared in a separate 96-well plate by mixing the supernatants with serum-free medium. The dilutions ranged from neat (pure supernatant) to 1:5, 1:25, 1:125, 1:250, 1:500, 1:1000, and 1:2000, with each dilution performed in triplicate. This dilution series was used to better distinguish RSV plaques for accurate counting.

In the primary 96-well plate containing HEp-2 cells, the media was removed and replaced with 50 µl of the infection media-supernatant mixture from the dilution plate. The cells were incubated for 2 hours at 37°C to allow for viral infection. After this incubation period, 150 µl of full medium (DMEM-Glutamax supplemented with 10% FCS and 1% P/S) was added to each well to top up the volume, and the plate was returned to the incubator for 24 hours.

The following day, the medium was removed from the wells, and the cells were washed once with phosphate-buffered saline (PBS). The cells were then fixed using acetone:methanol (1:1) solution at room temperature for 5 minutes. After fixation, the wells were washed three times with 1X Tris-buffered saline (TBS). The fixed cells were incubated with a 1:1000 dilution of anti-RSV monoclonal antibody (Abcam, ab43812), 40 µl per well, and left at room temperature for 1 hour. Following antibody incubation, the wells were washed five times with 1X TBS.

Next, 40 µl of undiluted ImmPRESS anti-mouse IgG (Vector Laboratories) was added to each well and incubated at room temperature for 45 minutes. The cells were washed again five times with 1X TBS. The Liquid DAB+ Substrate Chromogen System (Dako) was then applied, with 40 µl added to each well, and the plates were left for

a few minutes until RSV plaques became visible. The reaction was stopped by washing the wells three times with 1X TBS. The plates were then stored at 5-8°C.

Plaques were counted by capturing images of the most appropriate dilution under an inverted light microscope at 100X magnification. Three images per well were taken, with each dilution performed in triplicate.

The plaque-forming units per millilitre (pfu/ml) of supernatant were calculated using the following formula:

Titre (pfu/ml) = (average plaque count) x (dilution factor) x 20, where the factor 20 accounts for the use of 50 µl of virus inoculum per well (1 ml ÷ 0.05 ml = 20).

2.4 Quantification methodology

2.4.1 Quantifying gene expression by RT-PCR

RNA extraction for immortalised cells, as well as normal human bronchial epithelial (NHBE) cells, was conducted using the RNeasy Plus Mini Kit (Qiagen), adhering strictly to the manufacturer's protocol.

The process began with cell lysis, achieved using Qiagen's RLT buffer, which was supplemented with β-mercaptoethanol (β-ME) (Sigma-Aldrich) at a concentration of 100 µl per 10 ml of RLT buffer, as per the manufacturer's instructions. For each RNA extraction, two wells from a 24-well plate were combined and processed as a single sample, or alternatively, one well from a 12-well plate was used per sample. After

extraction, RNA concentrations were determined using the NanoDrop 8000 Spectrophotometer (Thermo Fisher Scientific), ensuring the quality and quantity of RNA were sufficient for downstream applications. This method ensured reliable and consistent RNA yield across different cell types and experimental conditions.

2.4.2 cDNA conversion

For the conversion of RNA to cDNA, 0.5 µg of RNA was first suspended in RNAase-free treated H_2O to achieve a final reaction volume of 11.5 µl. The SuperScript™ III First-Strand Synthesis System (Invitrogen) was employed for the reverse transcription process. Each reaction mix contained 1 µl of 10 mM dNTPs, 1 µl of random hexamers (50 ng/µl), 4 µl of first-strand buffer, 1 µl of 0.1 M DTT, 1 µl of RnaseOUT (40 U/µl), and 0.5 µl of SuperScript III reverse transcriptase (200 U/µl). The mixture was incubated at 50°C for 50 minutes to allow for efficient cDNA synthesis, followed by an incubation at 85°C for 5 minutes to inactivate the enzyme. The synthesised cDNA was subsequently stored at -20°C until required for further use in downstream applications. This method ensured the reliable synthesis of high-quality cDNA, which was critical for the success of subsequent molecular assays.

2.4.3 Quantitative real time PCR

The expression levels of various genes were quantified using SYBR Green-based quantitative real-time polymerase chain reaction (qRT-PCR). This was carried out on the LightCycler® 96 Real-Time PCR System (Roche) using the QuantiNova SYBR Green PCR Kit (Qiagen). Each PCR reaction was prepared in a white LightCycler 480 multiwell 96-well plate (Roche) using the reaction described in Table 2.7. For each experimental condition, three biological replicates were analysed, each measured in three technical replicates to ensure both reproducibility and statistical robustness. The qPCR settings used with the LightCycler® 96 Real-Time PCR System (Roche) are displayed in Table 2.8. This setup allowed for precise quantification and reproducibility of gene expression levels across multiple conditions and samples.

Table 2.7 SYBR Green RT-qPCR reaction mix.

SYBR green

Master mix	Volume
1x SYBR Green master mix	10µl
Forward primer (1:10 dilution of 100pmol/ µl stock)	1µl
Reverse primer (1:10 dilution of 100pmol/ µl stock)	
RNAse-free water	3µl
cDNA (1:100 dilution)	5µl

Volumes are representative for a single well.

Table 2.8 RT-qPCR thermal cycling programme and melt-curve conditions.

Step		**Temperature (^{0}C)**	**Time (s)**	**Cycle**
Initial denature		95	300	1
3-step amplification	Denature	95	10	45
	Annealing	60	10	
	Extension[1]	72	10	
Melting	Denature	95	5	1
	Annealing	60	60	
	Extension	97	1	
Cooling		4	Hold	1

[1)]Fluorescence data were acquired at the 72 °C extension step during each cycle.

2.4.4 Normalisation of target gene expression

18S rRNA was employed as the housekeeping gene, using universal primers (F) 5' ACGGCTACCACATCCAAGGA 3', (R) 5' CCAATTACAGGGCCTCGAAA 3', to normalise the expression levels of target genes. This gene was selected based on published evidence showing that 18S rRNA expression remains stable and unaffected during both RSV and Influenza A (H1N1 USSR strain) infections in respiratory epithelial cell models, including HEp-2 cells (Kuchipudi et al., 2012; Bakre et al., 2017). The ΔΔCq method (Livak & Schmittgen, 2001) was applied for this purpose. In this approach, the Cq value of 18S rRNA was subtracted from the Cq value of the target gene within the same sample, generating the ΔCq value. Next, the ΔCq of the control sample

was subtracted from the ΔCq values of other samples, resulting in the ΔΔCq value (x). The relative expression level of the target gene was then calculated using the formula $2^{-(x)}$, providing a quantifiable comparison of gene expression across different samples.

2.4.5 Quantifying viral gene expression from supernatant

The quantification of viral RNA from the supernatant was conducted via RT-PCR using the QIAmp Viral RNA Mini Kit (QIAGEN) in conjunction with Carrier RNA (QIAGEN). The procedure commenced with warming the Buffer AVL to the appropriate temperature. Three rows of collection tubes were prepared to streamline the processing of samples. To initiate the RNA extraction process, a mixture of 3.36 ml of Buffer AVL and 33.6 µl of Carrier RNA was prepared to accommodate six samples. Subsequently, 560 µl of the Buffer AVL and Carrier RNA mix was added to each sample, which was then vortexed for 15 seconds to ensure thorough mixing. The samples were incubated at room temperature for 10 minutes to allow proper binding of the viral RNA to the buffer. Following incubation, 560 µl of pure ethanol was added to each sample, followed by another 15-second vortex to mix the ethanol with the sample. The resulting mixture (630 µl) was then carefully transferred to a spin column for the purification of viral RNA. The columns were centrifuged for 30 seconds to ensure efficient binding of the RNA to the membrane within the column, after which the flow-through was discarded, and the bottom collection tube was replaced. Another 630 µl of the mixture was

transferred to the same spin column, followed by another 30-second centrifugation. Upon completion, the spin columns were transferred to new collection tubes. To wash the bound RNA, 500 µl of AW1 buffer was added to each spin column, and the columns were centrifuged again for 30 seconds. The bottom tubes were replaced once more, and 500 µl of AW2 buffer was applied to the columns. The columns were centrifuged again for 30 seconds, followed by a final spin of 1 minute to dry the membrane. After this, the spin columns were transferred to Eppendorf tubes, and 60 µl of AVE buffer was added directly to the membrane. This buffer was allowed to soak into the membrane for 1 minute before the columns were centrifuged for 1 minute with the caps down. Finally, 18 µl of the eluted RNA was transferred to a fresh Eppendorf tube for subsequent PCR analysis.

For the RT-PCR, the Quantifast SYBR green (QIAGEN) was taken out and allowed to equilibrate to room temperature, followed by a brief centrifugation. A Master Mix was prepared for five samples, consisting of 281.25 µl of Quantifast SYBR Green, 56.25 µl each of Primer A (forward) and Primer B (reverse), 5.625 µl of Quantifast RT Mix, and 108.125 µl of RNAse-Free Water. A total of 94.5 µl of this Master Mix was added to each sample, and the samples were mixed by gentle pipetting. Subsequently, 24 µl of the prepared mixture was dispensed into each well of a 96-well PCR plate, with four technical replicates per sample included at this stage to ensure reaction consistency. While three technical replicates were used for final quantification, a fourth was included initially to allow for the potential exclusion of any

outliers or pipetting errors. The plate was sealed with an optically clear film and centrifuged at 1500 rpm for 2 minutes to ensure even distribution of the contents. Finally, the plate was loaded into the LightCycler® 96 Real-Time PCR System for amplification and analysis using the thermal profile described in Table 2.8.

2.4.6 Western blot

Protein lysates were obtained using RIPA lysis buffer (Santa Cruz), supplemented with a protease inhibitor cocktail, and prepared according to the manufacturer's guidelines. For each sample, which was derived from either one or two wells of a 12-well plate depending on cell density, 112µl of RIPA buffer was added, and the plate was incubated at 2-5°C for 15 minutes. During incubation, the plate was gently tapped every 5 minutes to redistribute the buffer evenly across the wells. Any remaining cells were scraped from the well using a cell scraper, and the lysate was transferred to an Eppendorf tube. The lysate was centrifuged at 12,000 rpm for 15 minutes at 4°C.

To quantify the protein concentration, a standard curve was generated using serial dilutions of BSA (Thermo Scientific) at concentrations of 50, 25, 12.5, 6.25, and 3.125 ng/µl. The 2 mg/ml BSA stock was diluted in distilled water containing 1% RIPA buffer. A 5µl aliquot of the protein sample was diluted in 500µl of distilled water. Protein Assay Dye Reagent Concentrate (Bio-Rad) was diluted to one-quarter strength, and 100µl of the reagent was added to each well of a 96-well plate. Equal

volumes of standards, samples, and blanks were added to the reagent and thoroughly mixed. Absorbance at 595 nm was measured using a plate reader, and protein concentrations were calculated relative to the standard curve.

For Western blotting, either 5, 10, or 20µg of protein was loaded per well, depending on the abundance of the proteins of interest. The protein samples were diluted in 3.75µl of pre-warmed NuPAGE LDS sample buffer 4X (Invitrogen) and 1.5µl of NuPAGE reducing agent 10X (Invitrogen), and the final volume was adjusted to 15µl with distilled water. The samples were heated for 10 minutes at 70°C and briefly centrifuged. NuPAGE MOPS SDS Running Buffer 20X (Invitrogen) was diluted in distilled water at a ratio of 1:20 (40ml of buffer in 800ml water), and 500µl of NuPAGE antioxidant (Invitrogen) was added to 200ml of the prepared running buffer. The NuPAGE 4-12% Bis-Tris Protein Gel (Invitrogen) was prepared by washing the wells with 10ml of 1X running buffer, after which the gel was placed in the running tank. The inner chamber was filled with 200ml of the running buffer and antioxidant mixture, while the outer chamber was filled with the remaining 1X running buffer. Fifteen microliters of the prepared sample were loaded into each well of the gel, and 7µl of SeeBlue Pre-stained Protein Standard (Invitrogen) was run in one lane. The gels were run at 200V and 115mA for 50 minutes.

The proteins were transferred to a PVDF membrane using the Trans-Blot SD semi-dry transfer cell (Bio-Rad). Whatman 3MM Chr chromatography paper (GE Healthcare Whatman) was cut to the size of

the gel, and sheets were soaked in the appropriate buffers. One sheet was soaked in anode buffer I (0.3M Tris, 10% methanol, pH 10.4), two sheets were soaked in anode buffer II (25mM Tris, 10% methanol, pH 10.4), and three sheets were soaked in cathode buffer I (25mM Tris, 40mM glycine, 10% methanol, pH 9.4). The PVDF membrane (Thermo Scientific) was rehydrated in methanol for 15 seconds, rinsed in water for 5 minutes, and then immersed in anode buffer II. The protein gel was removed from its plastic frame and immersed in cathode buffer I for 5 minutes. The Trans-Blot SD transfer cell was assembled by layering the soaked filter paper, starting with the sheet in anode buffer I, followed by the sheets in anode buffer II, and then the PVDF membrane. The gel was placed on top of the PVDF membrane, and the final three sheets of cathode buffer I-soaked paper were layered over the gel. Air bubbles were carefully removed, and the unit was assembled. Protein transfer was carried out at a constant voltage of 10 V for 1 hour, with an initial current of approximately 70 mA.

Following transfer, the PVDF membrane was marked to indicate protein orientation. The membrane was washed twice in 1X TBST (0.5M Tris, 1.5M NaCl, 1% Tween 20, pH 7.4) for 5 minutes and then blocked at room temperature for 1 hour using blocking buffer (5% Marvel milk powder in 1X TBST) on a bench-top rocker set to approximately 30 rpm. After a further 5-minute wash in 1X TBST, the membrane was incubated overnight at 4°C with the primary antibody, diluted in blocking buffer. The following day, the membrane was washed three times for 5 minutes in 1X TBST and then incubated for 1 hour with the appropriate HRP-

conjugated secondary antibody. The membrane was washed again three times for 5 minutes in 1X TBST. Excess buffer was blotted off, and 500µl of the Amersham ECL Prime kit (GE Healthcare) detection solution was mixed and applied to the membrane. After 2-3 minutes of incubation, the membrane was sealed in saran wrap. Protein bands were visualised using the ChemiDoc MP Imaging System (Bio-Rad), following the manufacturer's instructions. Protein quantification was performed using ImageJ software, with β-actin serving as the housekeeping gene for normalisation.

2.4.7 Cell transfection

Cell transfection was carried out using Lipofectamine-based reagents (Invitrogen) according to a modified version of the manufacturer's recommendations. In preparation, cells were seeded into multi-well plates so that they would reach approximately 60–80% confluence at the time of transfection. On the day of transfection, the culture medium was replaced with either fresh complete medium or a reduced-serum/serum-free medium (following the specific guidelines provided by the reagent manufacturer). Plasmid DNA or siRNA was then diluted in Opti-MEM (Gibco) to the desired final concentration for the particular well format in use (e.g., 24-well plates). In parallel, Lipofectamine reagent (e.g., Lipofectamine 2000 or Lipofectamine RNAiMAX) was also diluted in Opti-MEM at volumes specified by the manufacturer, typically ranging from 1 to 3 µL per well for 24-well plates. After five to ten minutes of

separate incubation at room temperature, the diluted DNA or siRNA was gently combined with the diluted Lipofectamine, ensuring a 1:1 ratio (vol:vol). This mixture was then incubated at room temperature for a further five to ten minutes to allow formation of lipid–nucleic acid complexes. The complexes were added dropwise onto the cells, which were swirled gently to achieve a uniform distribution. Cells were then returned to the incubator (37 °C, 5% CO_2) for 18–48 hours, although in some cases medium changes were performed four to six hours post-transfection to minimise cytotoxicity. Downstream assays, such as measurement of gene or protein expression, were typically carried out between 24 and 72 hours after transfection, depending on whether plasmid DNA or siRNA had been introduced. For siRNA-mediated knockdown experiments, verification of gene silencing (e.g., by quantitative PCR or immunoblotting) was performed two to three days later. For DNA transfection, expression of the transgene (often monitored by fluorescence microscopy or Western blot) was usually assessed 24–48 hours post-transfection. Negative controls, such as scrambled siRNA or empty plasmids, were employed in parallel to rule out non-specific effects, and in most cases, antibiotics were omitted from the transfection medium to reduce cell toxicity. All volumes and concentrations were optimised for the specific cell line and experimental requirements, with reference to the reagent manufacturer's instructions for accurate DNA/siRNA-to-Lipofectamine ratios in each chosen well format.

2.5 Statistical analysis

Statistical analyses were conducted using GraphPad Prism (GraphPad Software). All experiments included a minimum of three replicates, with the standard deviation calculated and represented in the graphical data. Data distribution was assessed using the Shapiro-Wilk normality test, and the appropriate statistical tests were selected based on the distribution outcome. The specific statistical tests employed are detailed within the figure legends.

For comparisons between a single treatment group and the control, an unpaired t-test was applied, which examines the likelihood that the groups originated from the same population based on their means. When comparing multiple treatments to a control group, a one-way ANOVA was utilised, followed by Dunnett's multiple comparisons test as indicated. In cases where the effects of two independent variables were evaluated, a two-way ANOVA was employed, accompanied by Sidak's multiple comparisons test. The control group is identified in each figure legend.

A significance threshold of $p<0.05$ was used. Statistical significance was indicated by asterisks: * for $p<0.05$, ** for $p<0.01$, *** for $p<0.001$, and **** for $p<0.0001$.

Chapter 3: Thapsigargin is a non-toxic and effective antiviral against RSV, Influenza A, and their co-infections

Respiratory infections caused by Influenza A virus and RSV present significant public health challenges, with the risk further exacerbated by the possibility of co-infection, which may lead to the formation of hybrid viral particles. Current antiviral treatments often struggle to manage these infections effectively, and the emergence of drug resistance complicates treatment strategies. Moreover, should a new hybrid virus emerge, the likelihood of rapidly developing an effective antiviral or vaccine remains low. Thapsigargin, a plant-derived compound, has shown promise as a potent, non-toxic antiviral agent with broad-spectrum efficacy. Here, results demonstrate thapsigargin's effectiveness against both Influenza A and RSV infections, and more importantly, against their co-infection, highlighting its potential as a powerful therapeutic option to mitigate the impact of these respiratory viruses and their potential hybrid forms.

3.1 Introduction

Influenza A virus (IAV) and respiratory syncytial virus RSV represent significant global health burdens, particularly given their overlapping seasonal patterns and their ability to cause severe respiratory illnesses across various age groups. RSV is recognised as a leading cause of acute lower respiratory infections (ALRIs), particularly bronchiolitis and pneumonia, in young children. These infections contribute to substantial morbidity and mortality, with an estimated 3.2 million hospitalisations and over 118,000 deaths in young children worldwide in 2015 alone (Chadha et al., 2020). In addition to children, RSV poses a significant threat to the elderly and those with underlying conditions such as heart and lung diseases, leading to annual outbreaks of respiratory illnesses across all age groups. Despite the severity of these illnesses, effective treatments for RSV remain limited, and efforts to develop vaccines have so far been unsuccessful. Similarly, IAV continues to cause millions of infections annually, leading to a significant healthcare burden, especially during the winter months when both viruses typically co-circulate.

The overlapping seasonality of RSV and IAV further complicates the public health challenge they present. The World Health Organization's Global Influenza Surveillance and Response System (GISRS) has been monitoring influenza viruses for over six decades, and recent efforts have been made to integrate RSV surveillance within this existing framework (Chadha et al., 2020). Data from fourteen countries participating in the WHO RSV pilot surveillance programme during 2017–2019 demonstrated that while RSV activity often overlapped with

influenza seasons, distinct patterns of RSV seasonality were observed depending on geographical region and climate. For instance, in temperate countries like the UK, Canada, and Russia, RSV activity typically peaked during the colder months, similar to influenza. However, in subtropical and tropical regions, RSV activity was more closely associated with rainy seasons, and unlike influenza, RSV activity often continued throughout the year, albeit at lower levels (Chadha et al., 2020). These seasonal overlaps and variations underscore the complexity of managing respiratory viral infections during peak transmission periods, especially in the context of co-infections.

Co-infections with IAV and RSV present unique clinical challenges, as they can lead to more severe outcomes than infections with either virus alone. Recent research has shown that co-infection of human lung cells with IAV and RSV can result in the formation of hybrid viral particles (HVPs) that harbour components of both viruses (Haney et al., 2022). These findings were observed in vitro, and while the formation of HVPs is mechanistically intriguing, their clinical significance remains to be determined. These hybrid particles have been shown to evade neutralising antibodies directed against IAV, allowing the virus to infect cells that lack IAV receptors by using the RSV fusion glycoprotein for entry. This viral cooperation suggests that co-infections may expand the tropism of each virus and enable them to evade immune responses more effectively, potentially leading to more severe disease outcomes and complicating treatment efforts. The formation of these hybrid viral particles raises critical questions about the nature of viral pathogenesis

and how co-infections may alter the dynamics of viral transmission and immune evasion.

Given the significant health burden posed by both IAV and RSV, there is an urgent need for effective antiviral strategies that can address not only single infections but also co-infections with these viruses. Current antiviral treatments for IAV, such as neuraminidase inhibitors, directly target viral proteins, making them vulnerable to the development of resistance through viral mutations. This has led to a growing interest in host-centric antiviral strategies that target host cellular pathways instead of the virus itself, thereby reducing the likelihood of resistance (Goulding et al., 2020). TG, a sesquiterpene lactone, has emerged as a promising host-centric antiviral agent. TG acts by inhibiting the sarcoplasmic/endoplasmic reticulum Ca^{2+} ATPase (SERCA) pump, leading to the depletion of calcium stores in the endoplasmic reticulum (ER) and triggering the unfolded protein response (UPR). This ER stress response appears to activate a spectrum of host antiviral defences, including the enhancement of type I/III interferon responses, which are critical for controlling viral infections (Goulding et al., 2020). In our previous work, we demonstrated that brief, non-cytotoxic priming with TG induces a sustained antiviral state that effectively blocks replication of multiple major respiratory viruses — including IAV, RSV, and SARS-CoV-2 — in vitro, and confers protection against lethal IAV infection in vivo (Al-Beltagi et al., 2021). These findings highlight TG's broad-spectrum antiviral potential and its ability to interfere with viral replication at different stages of the viral life cycle.

Studies have demonstrated that brief exposure to non-toxic doses of TG can induce a prolonged antiviral state that dramatically reduces IAV replication. Importantly, oral administration of TG has been shown to protect mice against lethal IAV infection, reducing viral titres in the lungs and improving survival rates (Goulding et al., 2020). These findings suggest that TG could be a viable therapeutic option for IAV infections, offering the potential for a broad-spectrum antiviral effect without the risk of resistance associated with direct-acting antivirals. However, while TG has shown promise against IAV, its efficacy against RSV remains less well established.

The manipulation of intracellular calcium levels has been shown to impact RSV replication. For example, studies by Cui et al. (2016) identified cyclopiazonic acid (CPA), an intracellular calcium ATPase inhibitor, as an effective inhibitor of RSV replication. CPA and other calcium-modulating agents, such as TG, were found to inhibit RSV replication by increasing intracellular calcium concentrations, which interfered with the virus's ability to replicate its genome and transcribe viral RNA. These findings suggest that intracellular calcium plays a critical role in the RSV life cycle and that modulating calcium levels could be a viable strategy for inhibiting RSV replication. However, the relationship between calcium homeostasis and viral replication is complex, and the effects of calcium modulation can vary depending on the specific virus and the cellular context.

For instance, while studies have shown that increased intracellular calcium can inhibit RSV replication, other research has raised concerns

about the potential cytotoxicity associated with prolonged calcium modulation. Prolonged exposure to TG has been shown to induce apoptosis in various cell types by depleting ER calcium stores and triggering the UPR, which can lead to cell death (Jakobsen et al., 2001; Sehgal et al., 2017). This cytotoxicity is particularly relevant when considering the use of TG as a therapeutic agent, as the balance between antiviral efficacy and host cell toxicity must be carefully managed. In the context of RSV, while in a previous publication TG has been shown to reduce viral replication (Jakobsen et al., 2001), prolonged TG exposure can also lead to a significant reduction in cell viability, highlighting the need for careful dosing and timing of treatment.

Further complicating the potential use of TG against RSV is evidence suggesting that ER stress induced by TG may not be universally effective against respiratory viruses. For example, Schögler et al. (2019) found that pre-treatment of human bronchial epithelial cells with TG did not reduce RSV replication, although it effectively inhibited rhinovirus replication. This raises questions about the specific mechanisms by which TG exerts its antiviral effects and whether it can be reliably used against RSV in different cellular contexts. These conflicting findings highlight the need for further investigation into the efficacy of TG as an antiviral agent against RSV and other respiratory viruses.

In addition to its potential use against single infections, TG's effectiveness against co-infections of IAV and RSV, remains an open question. Haney et al. (2022) demonstrated that IAV and RSV co-infections can produce hybrid particles that incorporate structural

components from both viruses, allowing them to evade immune responses and potentially spread more effectively within the host. These hybrid particles pose unique challenges for antiviral therapy, as they may require targeting of both viral components simultaneously. Given TG's broad-spectrum antiviral effects, it is important to explore whether it can inhibit the replication of both IAV and RSV during co-infections and therefore prevent the formation of hybrid viral particles.

Finally, the safety and efficacy of TG as a prophylactic or treatment antiviral must be rigorously evaluated, particularly in the context of co-infections. While brief, low-dose exposures to TG have shown promise in reducing IAV replication without significant cytotoxicity (Goulding et al., 2020), the potential for toxicity remains a concern, especially with prolonged exposure. Sehgal et al. (2017) have highlighted the dual role of calcium as both a regulator of vital cellular functions and a potent inducer of cell death when dysregulated. TG's ability to deplete ER calcium stores and trigger apoptosis underscores the need for a careful balance between therapeutic efficacy and safety.

In conclusion, while TG represents a promising host-centric antiviral with broad-spectrum efficacy against IAV and potential effects against RSV, its use as a treatment for co-infections involving both viruses remains uncertain. This chapter aims to investigate the efficacy and safety of TG as both a prophylactic and therapeutic antiviral agent against RSV, IAV, and their co-infections. Specifically, we will explore whether TG can effectively inhibit the replication of both viruses and provide a non-toxic

antiviral strategy that can be safely deployed to reduce the significant health burden posed by these respiratory pathogens.

3.2 Materials and Methods

3.2.1 Viability assay

HEp-2, Calu-3, A549, NPTr, and NHBE cells were cultured in 96-well plates until near confluence under the conditions detailed in Section 2.2.1. Once the cells reached the appropriate confluence, the medium was replaced with DMEM-Glutamax (high glucose) for HEp-2, Calu-3, A549, and Vero cells, or specialised epithelial growth medium for NHBE cells, containing various concentrations of TG or DMSO (fixed 0.5 μM) as a control for 30 minutes. TG concentrations used for HEp-2, Calu-3, A549, and Vero cells were 0.1, 0.25, 0.5, and 1.0 μM, while for NHBE cells, lower concentrations of 0.001, 0.005, and 0.01 μM were employed due to their sensitivity to TG. NPTr cells were exposed to the same concentrations as HEp-2, Calu-3, and A549. After 30 minutes, the cells were rinsed three times with phosphate-buffered saline (PBS). The cells were then incubated in fresh medium for viability measurements at different time points. For HEp-2, Calu-3, and A549 cells, cell viability was assessed at 24-, 48-, and 72-hours post-exposure to TG or DMSO, while for Vero cells, viability was measured at 24 and 48 hours. NPTr and NHBE cells had viability measured only at 24 hours due to the

experimental design, which dictated shorter exposure times for these cell types to be representative of the experiments carried out in this thesis. All assays were conducted using the CellTiter-Glo® 2.0 Cell Viability Assay (Promega) according to the manufacturer's instructions, as described in detail in Section 2.2.4. The assay plates were equilibrated to room temperature before the addition of the CellTiter-Glo® 2.0 reagent. The CellTiter-Glo® 2.0 reagent was added in equal volume to the culture medium in each well (e.g., 100 µL reagent to 100 µL medium in a 96-well plate), followed by gentle shaking for two minutes to induce cell lysis. After a 10-minute incubation period to stabilise the luminescent signal, readings were taken using the luminometer. The ATP levels were measured as an indicator of cell viability by detecting the luminescence produced during the reaction using the GloMax® Discover Microplate Reader (Promega). This method provided a direct and quantitative measure of ATP production, correlating with the number of viable cells in each well, enabling comparisons between TG-treated groups and the DMSO control.

3.2.2 IAV infection

3.2.2.1 IAV Infection of Immortalised Cells

Immortalised cell lines were infected with IAV following the protocol described in Section 2.3.3. Briefly, the infection media (IM) comprised Opti-MEM I (Gibco) supplemented with 100 U/mL penicillin-streptomycin (P/S), 2 mM glutamine, and 200 ng/mL L-1-tosylamide-2-phenylethyl

chloromethyl ketone (TPCK) trypsin (Sigma-Aldrich). Cells were exposed to the virus at specified multiplicities of infection (MOI), determined by focus forming assay (FFA), and incubated in IM for 2–3 hours at 37 °C with 5% CO_2. Following incubation, cells were washed three times with phosphate-buffered saline (PBS) and maintained in fresh IM for 24–72 hours, as dictated by the experimental design.

3.2.2.2 Collection of IAV Spun Supernatant and Cell Lysates

Post-infection, the IM was carefully removed and centrifuged at maximum speed for 2 minutes to obtain spun supernatant, as outlined in Section 2.3.4. The supernatant was collected and stored at –80 °C for subsequent analysis. Progeny virus quantification was performed using a 6-hour FFA or by determining viral copy number via RT-qPCR, following methods described in Sections 2.3.5 and 2.3.4, respectively. Remaining cells were treated with the appropriate lysis buffer for RNA extraction, and lysates were either processed immediately or stored at –80 °C until required.

3.2.2.3 Quantification and Immunostaining of IAV Virus

The FFA was employed to quantify progeny virus through immunostaining techniques without necessitating cell lysis, as detailed in Section 2.3.5. Madin-Darby Canine Kidney (MDCK) cells were seeded into 96-well plates and cultured to 100% confluence. Confluent cells

were exposed to varying volumes of infected supernatant for 2 hours at 37 °C in a 5% CO_2 atmosphere. After incubation, cells were washed twice with PBS and incubated with 100 µL of IM for an additional 4 hours. Cells were then fixed and immunostained using the ImmPRESS HRP Anti-Mouse IgG (Peroxidase) Polymer Detection Kit (Vector Laboratories) and the Liquid DAB+ Substrate Chromogen System (Dako), following the procedure in Section 2.3.6. The primary antibody used was Anti-Influenza-A NP (Abcam, ab20343), diluted 1:8000 in 1× Tris-buffered saline (TBS). Stained cells were imaged under an inverted light microscope at 100× magnification.

3.2.2.4 RT-qPCR for IAV and RSV-infected cells

Total RNA was extracted from Influenza A- or RSV-infected cells, treated separately (i.e., not co-infected), according to the protocol described in Section 2.4.1. Complementary DNA (cDNA) was synthesised from 0.5 µg of RNA following the procedure outlined in Section 2.4.2. Quantitative real-time PCR (qRT-PCR) was conducted using SYBR Green chemistry and the conditions specified in Section 2.4.3. Relative gene expression levels were determined using the ΔΔCq method (Section 2.4.4), with 18S rRNA as the normalisation control. The primer pairs utilised for each target gene are listed in Table 3.1.

Table 3.1 Viral primers used in RT-qPCR quantification.

Gene	**Sense Primer (5'-3')**	**Antisense Primer (5'-3')**
18S	ACGGCTACCACATCCAAGGA	CCAATTACAGGGCCTCG-AAA
F gene (RSV)	CAAGAACTGACAGAGGATGGTACTG	CATGTTTCAGCTTGTGGGAAGA
L gene (RSV)	AACACTTATCCTTCTTTGTTGGAACTTA	GCAACCGAAACTCACGATAGAAA
M gene (RSV)	ACTCAAGAAGTGCAGTGCTAGCA	AAGGACACATTAGCGCATATGG
M gene (USSR)	AGATGAGCCTTCTAACCGAGGTCG	TGCAAAAACATCTTCAA-GTCTCTG

3.2.2.5 RSV infection of immortalised cells

HEp-2, Calu-3, A549, and Vero E6 cells were cultured until reaching 70-80% confluence. Growth medium was removed, and cells were washed three times with PBS. RSV (A2 strain) was diluted in serum-free DMEM to achieve the appropriate MOI (0.1 MOI for immortalised cells). The virus inoculum was added to cells and incubated for 2 hours at 37°C in 5% CO_2, with gentle agitation every 15-30 minutes. After infection, the inoculum was removed, cells were washed once with PBS, and fresh DMEM supplemented with 2% FCS was added. Infected cells were incubated at 37°C in 5% CO_2 for 24-72 hours. For virus quantification,

supernatants were collected and centrifuged at maximum speed for 2 minutes to remove cellular debris. The clarified supernatants were stored at -80°C until analysis by plaque assay or RT-qPCR. Cell monolayers were processed for RNA extraction as described in Section 2.3.10.

3.2.2.6 Preparation for RSV infection of human primary NHBE cells

Primary normal human bronchial epithelial (NHBE) cells were infected with RSV following the standardised protocol outlined in Section 2.3.9. NHBE cells were cultured using specialised epithelial growth medium (Promocell) supplemented with 2% FCS as described in Section 2.2.1. Cells were maintained in 25 cm² or 75 cm² tissue culture flasks at 37°C in a humidified atmosphere with 5% CO_2 and monitored daily using an inverted light microscope to assess their condition. Cells were passaged via trypsinisation using the DetachKit (Promocell) according to the manufacturer's instructions and seeded into tissue culture plates (12 or 24 well) to achieve 70–80% confluence prior to infection.

3.2.2.7 TG Priming and Infection of NHBE Cells with RSV

TG was previously prepared as a stock solution in DMSO and diluted in PromoCell epithelial growth medium supplemented with 2% FCS to final concentrations of 0.05, 0.025, and 0.1 µM for plates designated for direct immunostaining and protein quantification. For RT-qPCR plates, TG was

used at final concentrations of 0.01 and 0.025 µM, as lower doses were sufficient to elicit measurable transcriptional changes while minimising potential cytotoxic effects during prolonged incubation. Following priming with TG for 30 minutes at 37°C in a 5% CO_2 environment, the medium was removed, and cells were washed thrice with sterile PBS. Fresh medium (Promocell) containing RSV inoculum was added to the plates. For immunostaining and protein quantification, an MOI of 0.01 was used, while for RT-qPCR experiments, an MOI of 0.1 was utilised. Plates were gently rocked to ensure even distribution of the virus and incubated at 37°C for 2 hours to facilitate viral attachment.

After the attachment period, the virus-containing medium was removed, and cells were washed with PBS to remove unbound virus. Fresh PromoCell epithelial growth medium supplemented with 2% FCS was added, and the plates were incubated for 24–72 hours under standard culture conditions, depending on the experimental endpoint.

3.2.2.8 Collection and processing of RSV-infected samples

Samples from both immortalised cells and human primary cells infected with RSV were collected following the protocols outlined in Section 2.3.9 and adapted for downstream immunostaining, RT-PCR, and western blot analysis. For immortalised cells, including HEp-2, Calu-3 and A549, culture and infection were performed as described in Section 2.3.9. At designated time points post-infection, supernatants were carefully aspirated and centrifuged at 10,000 × g for 2 minutes to remove cell

debris. The clarified supernatants were aliquoted and stored at –80 °C for viral quantification via plaque assays or RT-PCR, as detailed in Sections 2.3.10 and 2.3.11. Following supernatant collection, cells were washed three times with cold phosphate-buffered saline (PBS) to remove residual media. For RNA extraction, cells were lysed using RLT buffer supplemented with β-mercaptoethanol, as specified in Section 2.4.1, and stored at –80 °C until further processing. For protein extraction, cells were lysed in RIPA buffer containing protease and phosphatase inhibitors, following the protocol described in Section 2.4.6. Lysates were immediately processed for western blot analysis or stored at –80 °C. For human primary cells, such as normal human bronchial epithelial (NHBE) cells, culture was maintained in specialised epithelial growth media (PromoCell), and infection was carried out as described in Section 2.3.9. At the conclusion of the infection period, supernatants were collected and processed similarly to those from immortalised cells, with clarified aliquots stored at –80 °C. NHBE cells were washed with PBS and detached using the DetachKit (PromoCell). Cell pellets intended for RNA extraction were lysed in RLT buffer and stored at –80 °C, while those intended for protein analysis were lysed in RIPA buffer and prepared for SDS-PAGE and western blotting, as detailed in Section 2.4.6. For immunostaining, NHBE cells were fixed in a 1:1 acetone-methanol mixture at room temperature for 5 minutes, washed with PBS, and stored at 4 °C in PBS. To ensure consistency and quality, all lysates and supernatants were aliquoted into pre-cooled tubes and snap-frozen in liquid nitrogen prior to storage at –80 °C. RNA quality and

concentration were assessed using a NanoDrop spectrophotometer as described in Section 2.4.1, while protein concentrations were measured using the Bradford assay, following Section 2.4.6.

3.2.2.9 Selectivity Index

The selectivity index (SI) of TG was calculated as the ratio of the CC50 over the EC50 (SI = CC50/EC50), representing the therapeutic window of TG in RSV-infected HEp-2 cells. HEp-2 cells were seeded in 96-well plates at a density of ~10,000 cells per well and allowed to adhere overnight. Cells were primed with TG at concentrations ranging from 0.001 μM to 100 μM for 30 minutes, washed with PBS, and infected with RSV (A2 strain, MOI 0.1). Following a 48-hour infection period, viral titres were quantified as plaque-forming units per millilitre (pfu/mL) using immuno-detection with a monoclonal anti-RSV antibody (2F7, Abcam) according to Section 2.3.11. Viral titre data were used to determine the EC50 and EC90 values via non-linear regression analysis. Cytotoxicity (CC50) was determined using the CellTiter-Glo 2.0 Luminescent Cell Viability Assay (Promega). HEp-2 cells were incubated with the same TG concentration range (0.001 μM to 100 μM) for 48 hours, and cell viability was assessed as a percentage of DMSO control. Luminescence data were used to generate dose-response curves and calculate the CC50 value. All experiments were performed in triplicate, and statistical significance was determined using one-way ANOVA with Tukey's multiple comparisons.

3.3 Results

3.3.1 TG demonstrates potent antiviral activity against IAV virus without compromising cell viability

To investigate the influence of TG priming duration and concentration on progeny virus output and cell viability, a stepwise experimental approach was undertaken using NPTr cells. Initially, the effect of TG priming for varying durations (15 or 30 minutes) on progeny virus production was evaluated. NPTr cells were treated with TG at concentrations of 0.5 μM and 1.0 μM, followed by a washing step with PBS three times and subsequent infection with USSR H1N1 virus at 0.5 MOI for 24 hours. Supernatants collected from infected cells were clarified via centrifugation and subsequently used to infect MDCK cells in focus forming assays (FFAs) to quantify progeny virus titres in ffu/μL. The results, presented in Figures 3.1A and 3.1B, demonstrated that TG treatment for both 15 and 30 minutes significantly reduced progeny virus output compared to the DMSO control, indicating a strong antiviral effect. Specifically, at 1.0 μM TG (Figure 3.1A), priming for 30 minutes led to a slightly greater reduction in viral titres compared to the 15-minute priming period. Similarly, at 0.5 μM TG (Figure 3.1B), the 30-minute priming duration yielded more pronounced antiviral activity than the shorter 15-minute exposure. These observations suggested that 30 minutes of TG priming is the optimal duration for suppressing progeny virus production. To ensure that TG treatment did not compromise NPTr cell viability, a

subsequent experiment was conducted to assess cell viability under a range of TG concentrations (0.1, 0.25, 0.5, and 1.0 μM) following 30 minutes of priming. Cell viability was determined via luminescence-based assays, providing a sensitive measure of cellular metabolic activity. The results, presented in Figure 3.1C, revealed that TG at 0.1 μM slightly increased cell viability compared to the untreated control, while higher concentrations (0.25, 0.5, and 1.0 μM) maintained cell viability without any significant cytotoxic effects. These findings confirm that TG treatment, particularly at the 30-minute priming duration, is non-toxic to NPTr cells within the tested concentration range. Together, these experiments demonstrate that TG priming for 30 minutes not only optimally suppresses progeny IAV output but also maintains cellular viability, highlighting its potential utility in antiviral interventions. The luminescence-based viability assay provided further validation that TG concentrations up to 1.0 μM are well tolerated by NPTr cells, ensuring the observed antiviral effects are not confounded by cytotoxicity.

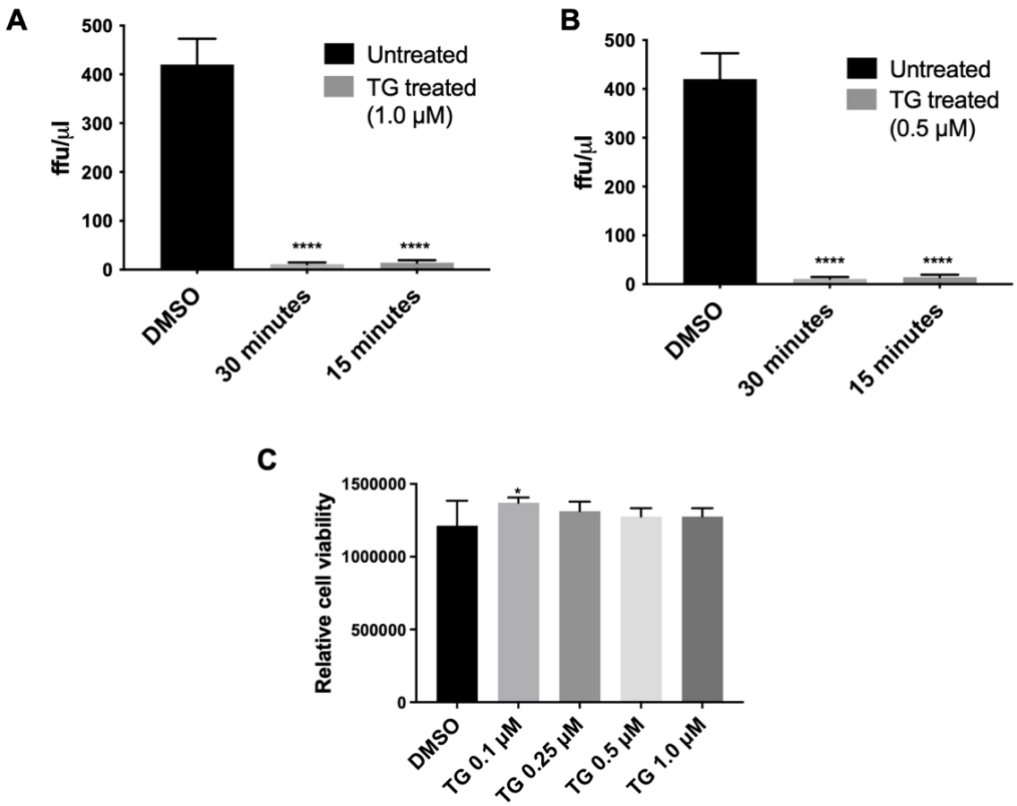

Figure 3.1 TG priming reduces progeny virus output and maintains NPTr cell viability.

*NPTr cells were treated with TG at varying concentrations and priming durations to determine its antiviral efficacy and impact on cell viability. (A) Progeny virus output was quantified following 30 or 15 minutes of priming with 1.0 µM TG. NPTr cells were infected with USSR H1N1 at 0.5 MOI for 24 h, and supernatants were subsequently used to infect MDCK cells for 6 h in focus forming assays (FFAs). (B) Progeny virus output following 30 or 15 minutes of priming with 0.5 µM TG. Viral titres were similarly quantified via FFAs. (C) NPTr cell viability was assessed via the CellTiter-Glo® 2.0 Luminescent Cell Viability Assay after 30 minutes of TG treatment at concentrations ranging from 0.1 to 1.0 µM. Relative cell viability is representative for luminescence levels. Significance was determined by one-way ANOVA (Dunnett's multiple comparisons) relative to the DMSO control (*p < 0.05, **p < 0.01, ***p < 0.001, ****p < 0.0001).*

3.3.2 TG priming inhibits RSV replication in HEp-2 cells

In this study, HEp-2 cells were chosen as a model to evaluate TG's efficacy against RSV (A2 strain). Cells were primed with TG at concentrations ranging from 0.001 μM to 0.5 μM for 30 minutes, immediately followed by infection with RSV at a multiplicity of infection (MOI) of 0.1. After 48 hours of infection (48 hpi), RSV replication was assessed by quantifying viral output in pfu/mL using immuno-detection methods. Cytotoxicity was evaluated using the CellTiter-Glo® 2.0 Luminescent Cell Viability Assay to ensure that observed antiviral effects were not attributable to cellular toxicity.

Results revealed that TG priming significantly reduced RSV replication in a concentration-dependent manner, with the greatest reductions observed at TG concentrations of 0.1 μM and 0.5 μM (Figure 3.2A). At these concentrations, viral titres were reduced to levels near the limit of detection, demonstrating TG's robust antiviral activity in this experimental model.

Importantly, cytotoxicity assays confirmed that TG exhibited no toxic effects at any of the tested concentrations, as shown in Figure 3.2C. The absence of cytotoxicity ensures that the observed antiviral effects are attributable to TG's direct interference with RSV replication rather than off-target effects such as cell death or metabolic disruption.

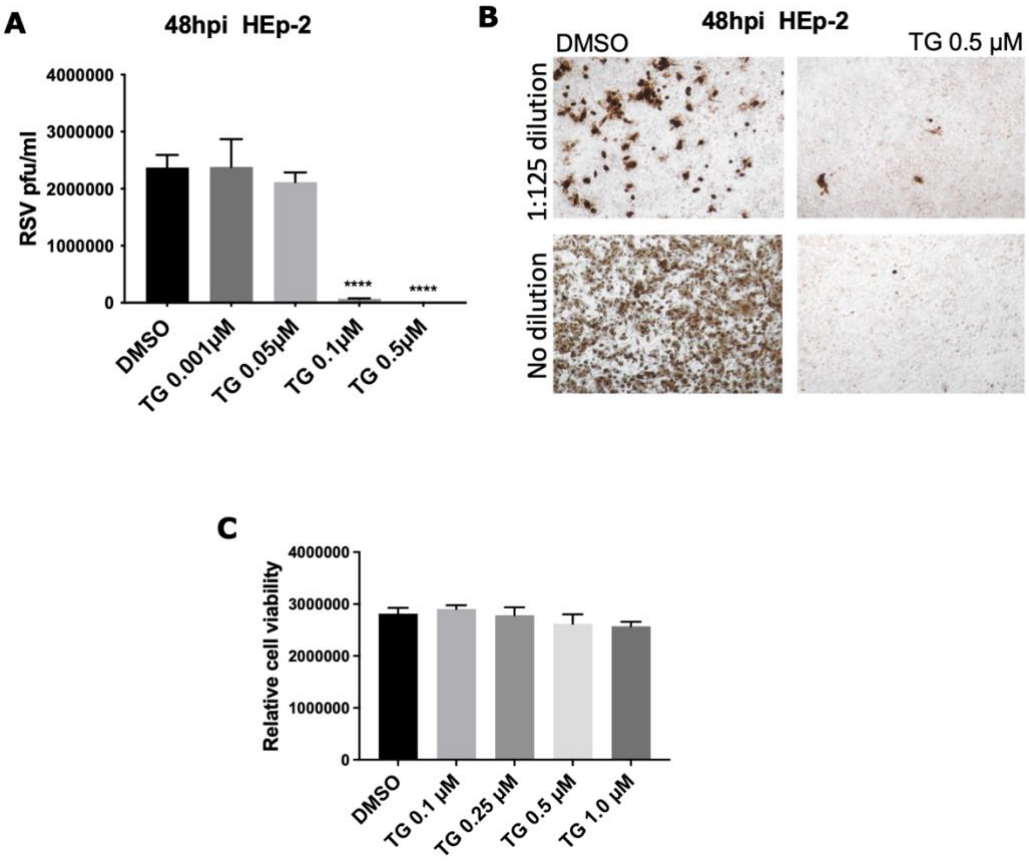

Figure 3.2 TG priming immediately after treatment inhibits RSV replication in HEp-2 cells without cytotoxicity.

*HEp-2 cells were primed with TG at concentrations ranging from 0.001 µM to 0.5 µM for 30 minutes, washing with PBS, followed immediately by infection with RSV (A2 strain, MOI 0.1). (A) RSV replication, expressed as pfu/mL, was quantified after 48 hours of infection from spun supernatant. (B) Immunostaining was performed using HEp-2 cells and anti-RSV antibody (2F7, Abcam) (dilution 1:125). (C) Cytotoxicity of TG in HEp-2 cells was assessed 48 hours post-priming using the CellTiter-Glo® 2.0 Luminescent Cell Viability Assay. Relative cell viability is representative of luminescence levels. Statistical significance in all panels was determined by one-way ANOVA relative to the DMSO control (*p < 0.05, **p < 0.01, ***p < 0.001, ****p < 0.0001).*

3.3.3 TG exhibits a high selectivity index in HEp-2 cells against RSV infection

The selectivity index (SI) is a critical parameter for evaluating the therapeutic potential of antiviral compounds, as it provides a measure of the compound's efficacy relative to its cytotoxicity. A high SI indicates that a compound is highly effective at inhibiting viral replication while having minimal adverse effects on host cells. In this study, TG's SI was determined in RSV-infected HEp-2 cells, a widely used model system for RSV research due to their permissiveness to RSV infection and reproducibility in antiviral assays.

The effective concentration (EC50 and EC90) and the cytotoxic concentration (CC50) of TG were calculated from dose-response curves. Viral titres were measured as pfu/mL according to section 2.3.11, while cell viability was assessed using a luminescence-based viability assay. TG demonstrated an EC50 of 0.06447 μM and a CC50 of 63.43 μM, resulting in an SI of 984 (SI = CC50/EC50). Compounds with SI values ≥10 are generally considered to have significant antiviral activity in vitro. Additionally, the EC90, representing the concentration required to achieve 90% antiviral efficacy, was determined to be 84.55 nM (0.08455 μM). These results highlight TG's exceptional selectivity as an antiviral agent in HEp-2 cells, effectively inhibiting RSV replication at low concentrations while maintaining high cellular viability. The high SI value underscores TG's potential as a therapeutic candidate for RSV

treatment, particularly in the context of HEp-2 cells, which are widely used for preclinical evaluation of RSV antivirals.

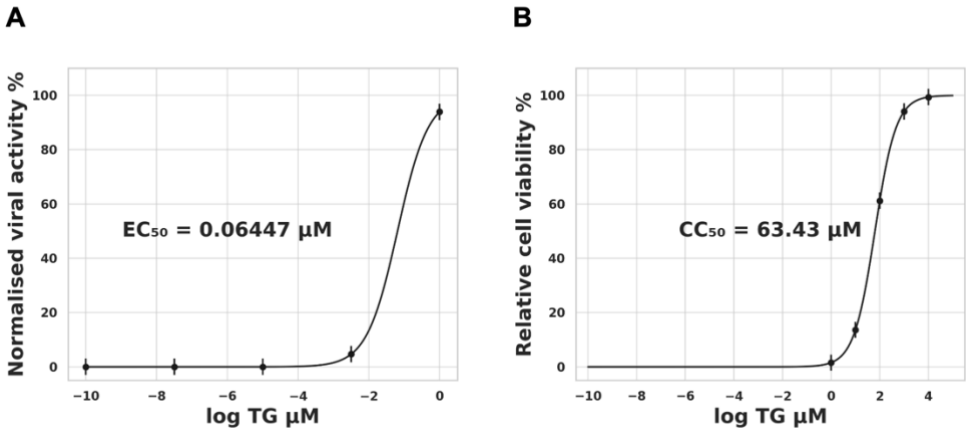

Figure 3.3 TG displays a high selectivity index in HEp-2 cells against RSV infection.

HEp-2 cells were primed with TG at a range of concentrations for 30 minutes, washed with PBS, and infected with RSV (A2 strain, MOI 0.1) for 48 hours. Viral titres were quantified as pfu/mL using immuno-detection with a monoclonal anti-RSV antibody (2F7, Abcam) and cell viability was measured using the CellTiter-Glo 2.0 Luminescent Cell Viability Assay (Promega). Dose-response curves for and antiviral efficacy (EC50) and TG cytotoxicity (CC50) were generated, with EC50 as 0.06447 µM (A) and CC50 calculated as 63.43 µM (B).

3.3.4 TG establishes a long-lasting antiviral state in HEp-2 and A549 cells

Having demonstrated that TG can inhibit RSV replication immediately post-treatment, the next approach was to determine if TG could establish a durable antiviral state when administered prophylactically. To this end, HEp-2 and A549 cells were primed with TG at concentrations of 0.1 µM or 0.5 µM for 30 minutes, followed by washing with PBS to remove residual TG. After priming, cells were returned to normal culture

conditions for either 24 or 48 hours. Subsequently, cells were infected with RSV (A2 strain, MOI 0.1) for 2 hours, after which the infection medium was replaced with fresh DMEM containing 2% FCS. The infection was allowed to proceed for 72 hours, and spun supernatants were collected for viral quantification.

Progeny virus titres were measured as pfu/mL on HEp-2 cells using immuno-detection with a mouse monoclonal anti-RSV antibody (F27, Abcam). The results, presented in Figures 3.4A and 3.4B, revealed that TG priming strongly inhibited RSV replication in both HEp-2 and A549 cells, with significant reductions in viral titres compared to DMSO controls. TG concentrations of 0.1 μM and 0.5 μM were effective in reducing viral output, and the antiviral effect persisted regardless of whether RSV infection occurred 24- or 48-hours post-priming. Notably, HEp-2 cells were more permissive to RSV replication than A549 cells, resulting in higher viral titres in DMSO-treated controls for HEp-2 cells.

To ensure that the observed antiviral effects were not due to cytotoxicity, cytotoxicity assays were performed on HEp-2 and A549 cells at 24-, 48- and 72-hours post-priming using the CellTiter-Glo® 2.0 Luminescent Cell Viability Assay. As shown in Figures 3.4C–F, TG treatment did not significantly impact cell viability at either concentration or time point, confirming that TG's antiviral effects were independent of cellular toxicity. These findings demonstrate that TG induces a robust and durable antiviral state that effectively suppresses RSV replication up to 48 hours post-priming. The ability of TG to maintain antiviral efficacy over

extended periods further highlights its potential as a prophylactic antiviral agent, particularly in settings where viral exposure may be anticipated.

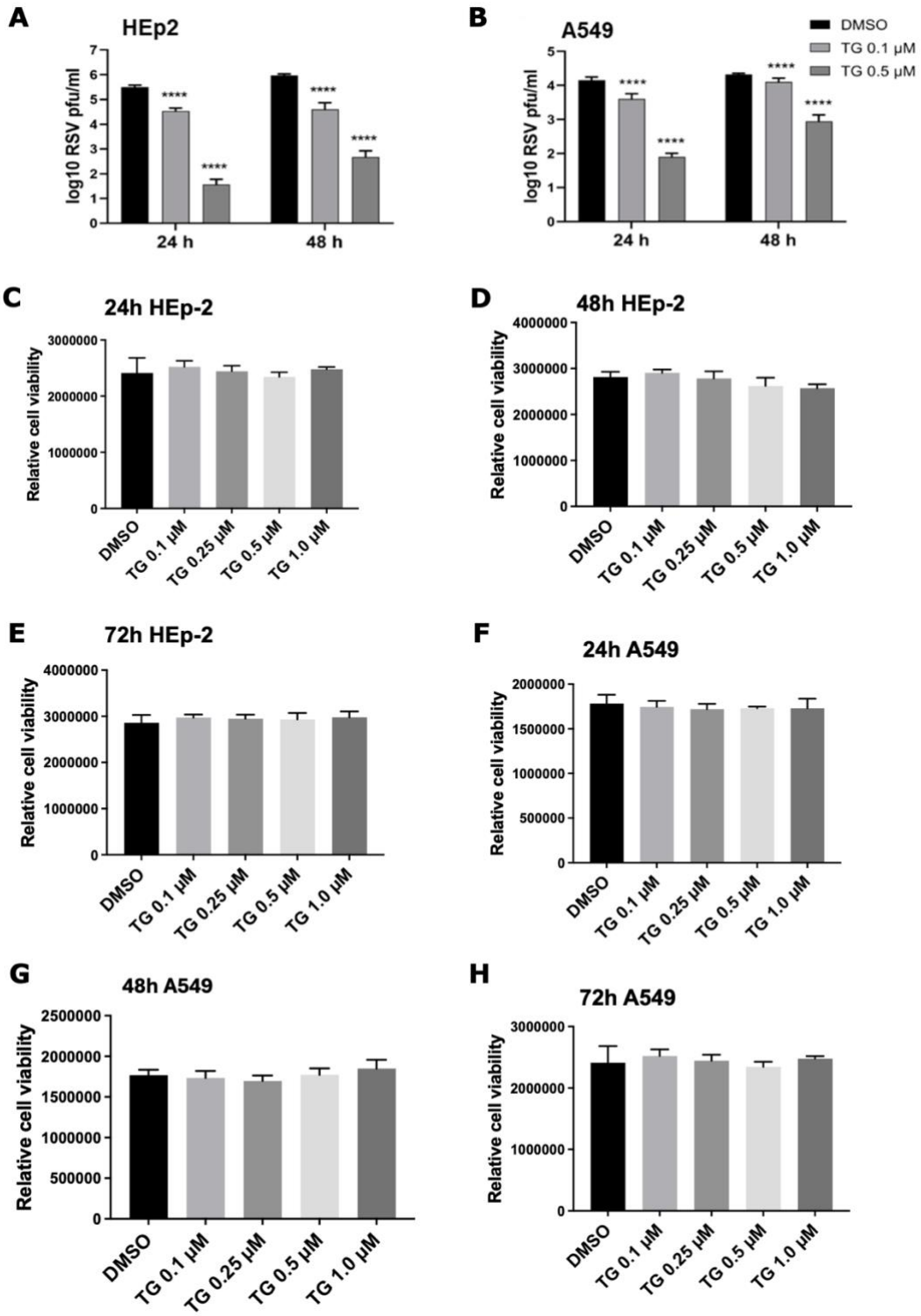

Figure 3.4 TG establishes a durable antiviral state in HEp-2 and A549 cells without cytotoxicity.

HEp-2 and A549 cells were primed with TG at concentrations of 0.1 μM and 0.5 μM for 30 minutes, washed with PBS, and cultured under normal conditions for 24 or 48 hours before

*infection with RSV (A2 strain, MOI 0.1). Cells were infected for 2 hours, after which infection media were replaced with fresh DMEM containing 2% FCS for a total infection duration of 72 hours. (A) RSV replication in HEp-2 cells was quantified from spun supernatants, expressed as log10 plaque-forming units per millilitre (log10 pfu/mL). Quantification was performed using immuno-detection with a mouse monoclonal anti-RSV antibody (F27, Abcam). (B) RSV replication in A549 cells was quantified similarly, using immuno-detection and expressed as log10 pfu/mL. Cytotoxicity of TG in HEp-2 cells was assessed at 24 (C), 48 (D), and 72 (E) hours post-priming using the CellTiter-Glo® Luminescent Cell Viability Assay. In a similar manner, cytotoxicity of TG in A549 cells was assessed at 24 (F), 48 (G), and 72 (H) hours post-priming. Relative cell viability in all cytotoxicity assays was determined by luminescence levels. Statistical significance in all panels was determined by one-way ANOVA relative to the DMSO control (*p < 0.05, **p < 0.01, ***p < 0.001, ****p < 0.0001).*

3.3.5 TG demonstrates antiviral activity as a post-infection treatment in HEp-2 cells

Having established TG's efficacy as a prophylactic antiviral agent, this experiment aimed to investigate its potential as a post-infection treatment for RSV. HEp-2 cells were infected with RSV (A2 strain) at an MOI of 0.1. The infection was allowed to proceed for 2 hours under standard culture conditions, with gentle rotation every 15–30 minutes to ensure even viral exposure. After the 2-hour incubation period, the virus-containing medium was carefully removed, and fresh DMEM supplemented with 2% FCS was added to the cells. Infection was then continued for a total of 24 hours to establish viral replication.

After 24 hours of infection, the medium was removed and transferred to a separate plate, and TG was applied to the infected cells at concentrations of 0.1 µM and 0.5 µM for 30 minutes. Following TG

treatment, the compound was removed, cells were gently washed three times with PBS to eliminate residual TG, and the original infection medium was returned to the cells. The infection was allowed to continue for a further 48 hours, resulting in a total infection duration of 72 hours. Quantification of viral replication was performed by collecting spun supernatants and determining progeny virus titres using immuno-detection with a monoclonal anti-RSV antibody (F27, Abcam). Viral titres were expressed as log10 plaque-forming units per millilitre (log10 pfu/mL). The results, presented in Figure 3.5A, showed that both concentrations of TG (0.1 μM and 0.5 μM) effectively inhibited RSV replication compared to DMSO controls, with the highest inhibition observed at 0.5 μM TG. These findings confirm TG's potent antiviral effects even when administered post-infection, highlighting its therapeutic potential for managing established RSV infections.

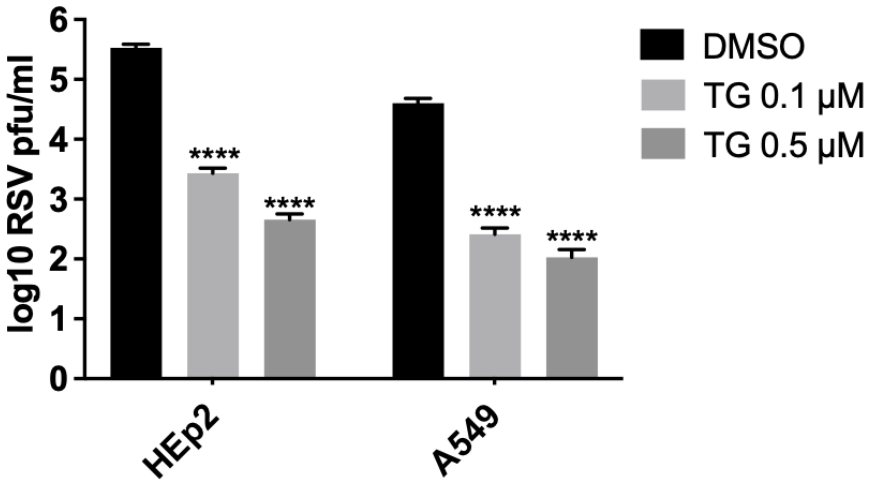

Figure 3.5 TG demonstrates antiviral activity post-infection in HEp-2 cells.

*HEp-2 cells were infected with RSV (A2 strain, MOI 0.1) for 2 hours, with gentle rotation every 15–30 minutes to ensure even viral exposure. After 2 hours, the virus-containing medium was removed and replaced with fresh DMEM containing 2% FCS, and the infection was allowed to continue for 24 hours. Following the 24-hour infection period, the medium was removed and transferred to a separate plate, and TG was applied to the infected cells at concentrations of 0.1 µM and 0.5 µM for 30 minutes. After TG treatment, cells were washed gently with PBS three times to remove residual TG, and the original infection medium was returned to the cells. Infection was then continued for an additional 48 hours, resulting in a total infection duration of 72 hours. (A) RSV replication was quantified from spun supernatants using immuno-detection with a monoclonal anti-RSV antibody (F27, Abcam). Results are expressed as log10 plaque-forming units per millilitre (log10 pfu/mL). Statistical significance was determined by one-way ANOVA relative to the DMSO control (*p < 0.05, **p < 0.01, ***p < 0.001, ****p < 0.0001).*

3.3.6 TG demonstrates superior efficacy compared to ribavirin, a standard RSV treatment

Ribavirin remains the most widely used antiviral treatment for RSV in clinical settings due to its ability to inhibit viral replication, with activity against the viral RNA-dependent RNA polymerase. However, ribavirin's modest efficacy, cytotoxic effects, and requirement for continuous presence during infection pose challenges for its clinical application. This experiment aimed to compare ribavirin's efficacy with TG. By comparing these antivirals under similar experimental conditions, the goal was to evaluate TG's potential as a safer and more potent alternative. For this comparison, HEp-2 cells were primed with TG as described above or treated with ribavirin at final concentrations of 15 μM and 30 μM, with DMSO alone as a control. The ribavirin doses were selected to be approximately 1.5× and 3× the EC_{50} of ribavirin against RSV in HEp-2 cells ($EC_{50} \simeq 11$ μM), as determined by Mirabelli et al. (2018) in plaque-reduction assays. Following the 30-minute priming, TG-treated cells were washed three times with phosphate-buffered saline (PBS) and overlaid with infection medium containing RSV (A2 strain) at a multiplicity of infection (MOI) of 0.1. Ribavirin-treated cells received infection medium supplemented with ribavirin at 15 μM or 30 μM throughout the assay. After 2 hours, all media were removed: TG-primed cells were given fresh infection medium without TG, while ribavirin-treated cells were given fresh medium containing ribavirin at the original concentrations. Infection was then allowed to proceed for a total of 96

hours. At 96 hours post-infection (hpi), media and cell lysates were collected. Progeny virus titres were determined using pfu/mL via immuno-detection with a monoclonal anti-RSV antibody (F27, Abcam). Viral transcription was assessed by detecting *L-gene* RNA using one-step reverse transcription-qPCR. Immunostaining was performed to visualise the extent of RSV replication across treatments, enabling a qualitative comparison of viral inhibition. Progeny virus titres (Figure 3.6A) showed that TG significantly reduced RSV replication compared to ribavirin, even at lower concentrations. At 0.1 μM, TG achieved greater viral suppression than ribavirin at 30 μM. Viral transcription, assessed by L-gene RNA levels (Figure 3.6B), showed a similar trend, with TG exhibiting superior inhibition of viral RNA synthesis. Immunostaining images (Figure 3.6C) visually confirmed these findings, revealing near-complete suppression of RSV-positive cells in samples treated with TG at 0.5 μM. These results further demonstrate TG's antiviral potency and highlight its potential as an alternative to ribavirin for RSV treatment.

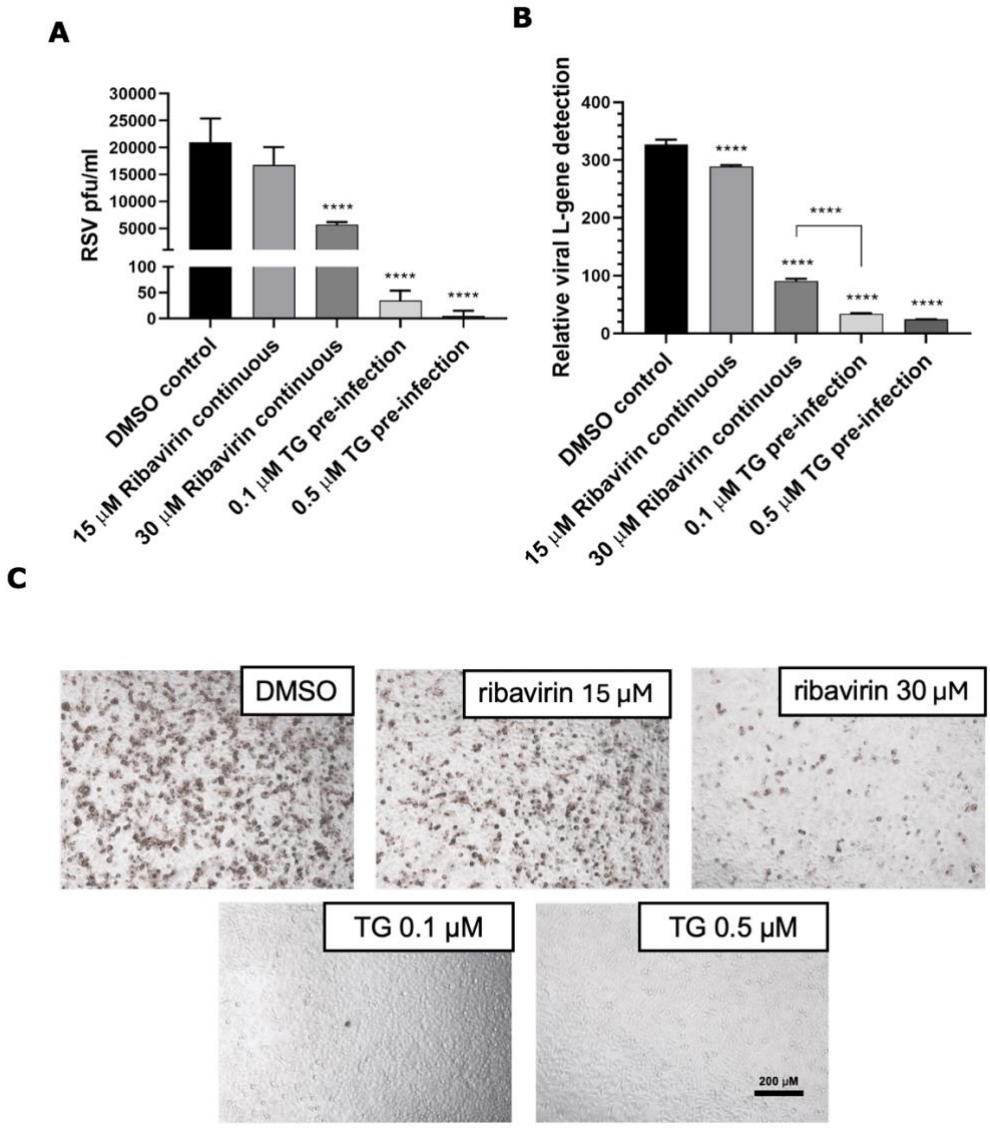

Figure 3.6 TG demonstrates superior antiviral efficacy compared to ribavirin.

HEp-2 cells were primed with TG (0.1 μM and 0.5 μM), ribavirin (15 μM and 30 μM), or DMSO control for 30 minutes. Following TG priming, cells were washed three times with PBS, and fresh infection medium containing RSV (A2 strain, MOI 0.1) was added. For ribavirin-treated cells, ribavirin was added simultaneously with RSV at concentrations of 15 μM or 30 μM. After 2 hours of infection, the media were removed. TG-treated cells received fresh infection medium without TG, while ribavirin-treated cells received fresh medium containing ribavirin at the same concentrations. Infection was allowed to proceed for a total of 96 hours. (A) Progeny virus titres were quantified from spun supernatants at 96 hpi using immuno-detection with a monoclonal anti-RSV antibody (F27, Abcam), expressed as log10 plaque-forming units per millilitre (log10 pfu/mL). (B) Viral transcription was assessed by quantifying RSV L-gene RNA using one-step reverse transcription-qPCR. (C) Representative immunostaining images of RSV-infected HEp-2

*cells, captured at 100× magnification, demonstrate the effects of TG and ribavirin treatments on RSV-positive cells. Statistical significance was determined by one-way ANOVA with Tukey's multiple comparisons (*p < 0.05, **p < 0.01, ***p < 0.001, ****p < 0.0001).*

3.3.7 TG inhibits RSV replication in human primary bronchial epithelial (NHBE) cells

NHBE cells provide a physiologically relevant model for studying RSV infections in the human airway. However, due to their fragility and the virus's preference for replicating in the basal cell layer (Persson et al., 2014), conventional quantification of RSV progeny in supernatants proved inadequate. Initial efforts failed to detect infectious RSV in the supernatant, despite clear syncytial cytopathic effects in the monolayer, in line with previously reported basal replication tropism. To overcome this limitation, experiments were performed using 12-well plates seeded with NHBE cells at ~80–90% confluence, typically between passages 3–5. For each experimental condition, three 12-well plates were used in duplicate (i.e., two wells per condition per plate): one for direct immunostaining of RSV plaques, one for total protein extraction and immunoblotting, and one for RNA extraction to assess viral transcription. This approach allowed parallel quantification of viral replication across multiple biological levels despite the limitations in supernatant-based viral recovery.

3.3.7.1 TG reduces RSV plaque formation in NHBE cells

The first 12-well plate was used to visualise RSV replication through plaque formation. NHBE cells were primed with TG at concentrations of 0.025 µM, 0.05 µM, or 0.1 µM, or treated with DMSO as a control, for 30 minutes. Following priming, cells were washed three times with PBS and infected with RSV (A2 strain, MOI 0.01) in infection medium consisting of airway epithelial cell media supplemented with TPCK-trypsin. The low MOI was selected to facilitate reliable plaque counting in this delicate primary cell model, particularly as the assay involved direct fixation with acetone-methanol. After 2 hours of infection, cells were washed twice with PBS and incubated in fresh PromoCell medium containing 2% FCS for 48 hours.

Cells were then fixed using an acetone:methanol mixture (1:1) and immunostained with a monoclonal anti-RSV antibody (2F7, Abcam). Viral foci were visualised and quantified as plaque-forming units per mL (pfu/mL) (Figure 3.7A), with images captured at 10× magnification (Figure 3.7B). Although a focus forming immunodetection method was used, plaques were readily countable and expressed as pfu/mL to remain consistent with standard virological reporting.

The assay demonstrated a clear, dose-dependent reduction in RSV replication in NHBE cells following TG treatment. At the highest concentration of 0.1 µM, TG treatment nearly abolished plaque formation, with only a few residual plaques detectable compared to the DMSO control.

Importantly, TG was well tolerated by NHBE cells at all concentrations tested. Cell viability assays published by Goulding et al. (2020) demonstrated that short exposures to TG at nanomolar levels had no measurable cytotoxicity in NHBE cells, confirming the suitability of these conditions for antiviral testing in primary airway epithelium.

Even at lower concentrations (0.025 μM and 0.05 μM), TG treatment significantly reduced plaque numbers, indicating strong antiviral activity. These findings highlight TG's potent ability to inhibit RSV replication at the level of infectious virus production, consistent with its mechanism of disrupting cellular processes necessary for viral replication. Importantly, the dose-dependence suggests that TG's efficacy is tightly linked to its concentration, with higher doses leading to greater suppression of viral replication. This reduction in plaque formation aligns with previous observations of TG's antiviral effects in other cell types, supporting its broad-spectrum potential. The success of this approach also underscores the necessity of direct immunostaining for accurate quantification of RSV replication in NHBE cells, given the virus's basal cell tropism.

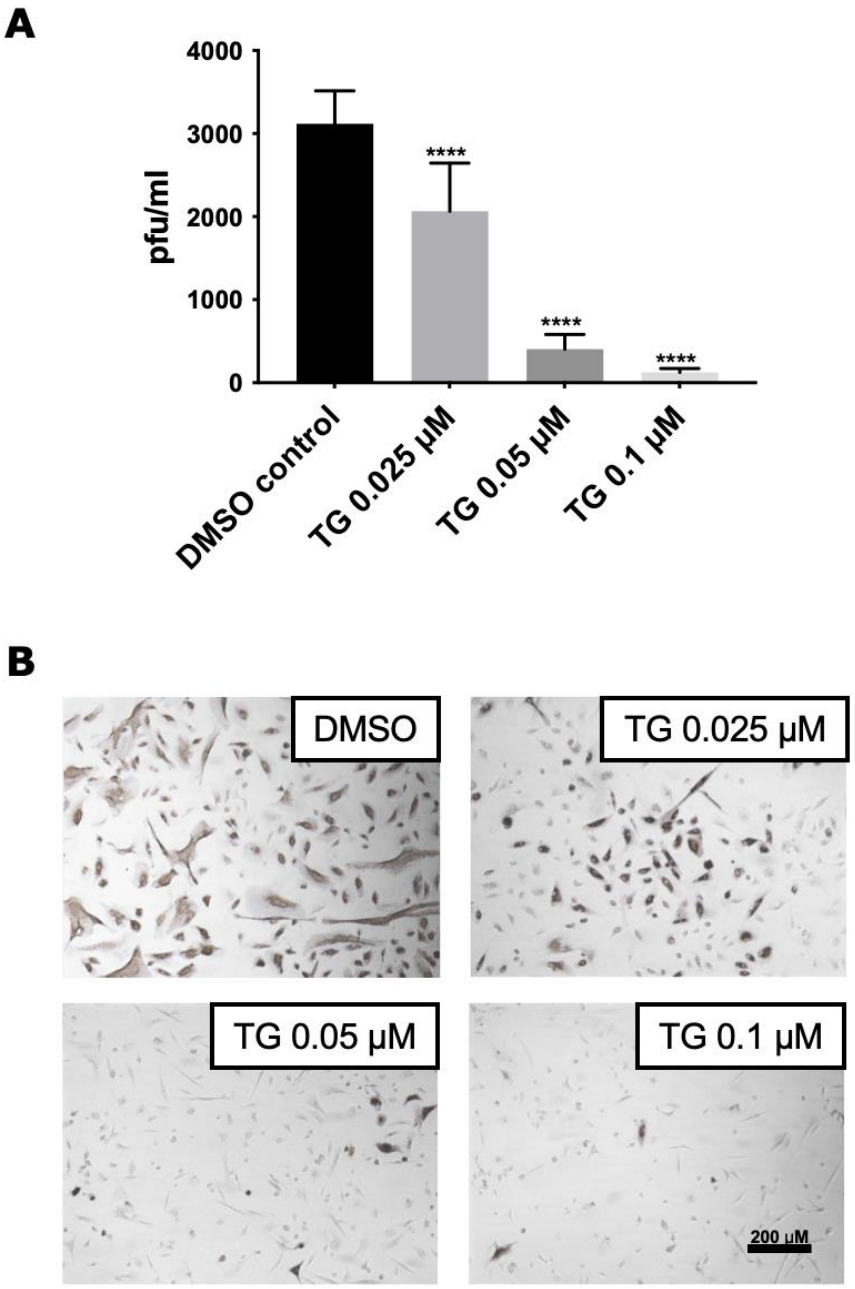

Figure 3.7 TG reduces RSV formation in NHBE cells.

NHBE cells were primed with TG at concentrations of 0.025 µM, 0.05 µM, and 0.1 µM, or treated with DMSO as a control, for 30 minutes. Cells were washed three times with PBS, infected with RSV (A2 strain, MOI 0.1), and incubated for 2 hours with gentle rotation every 15 minutes. Following infection, cells were washed twice with PBS, and fresh PromoCell epithelial growth medium containing 2% FCS was added. After 48 hours of infection, cells were fixed with an acetone-methanol mixture (1:1 ratio) and immunostained with anti-RSV antibody (2F7, Abcam) diluted 1:1000 in TBS. Plaques were visualised under a light microscope and quantified as

*pfu/mL. Statistical analysis was conducted using one-way ANOVA with Dunnett's multiple comparisons relative to the DMSO control (***p < 0.001, ****p < 0.0001). Representative images of RSV plaques in NHBE cells were taken at 10x magnification using an inverted light microscope (Leica).*

3.3.7.2 TG reduces RSV F protein formation in NHBE cells

The second plate was dedicated to protein extraction. NHBE cells were primed with TG at 0.025 μM, 0.05 μM, and 0.1 μM, or treated with DMSO as a control, for 30 minutes. Following infection and incubation as described for the first plate, cells were lysed using RIPA buffer supplemented with protease inhibitors. Proteins were separated via SDS-PAGE, transferred to PVDF membranes, and probed with anti-RSV F protein and β-actin antibodies. The chemiluminescent signals were quantified, and RSV F protein levels were normalised to β-actin. Densitometric analysis of Western blot results confirmed a dose-dependent reduction in F protein levels, with the greatest suppression observed at 0.1 μM TG (Figure 3.8). This reduction suggests that TG inhibits RSV replication at the protein synthesis level, contributing to its antiviral efficacy.

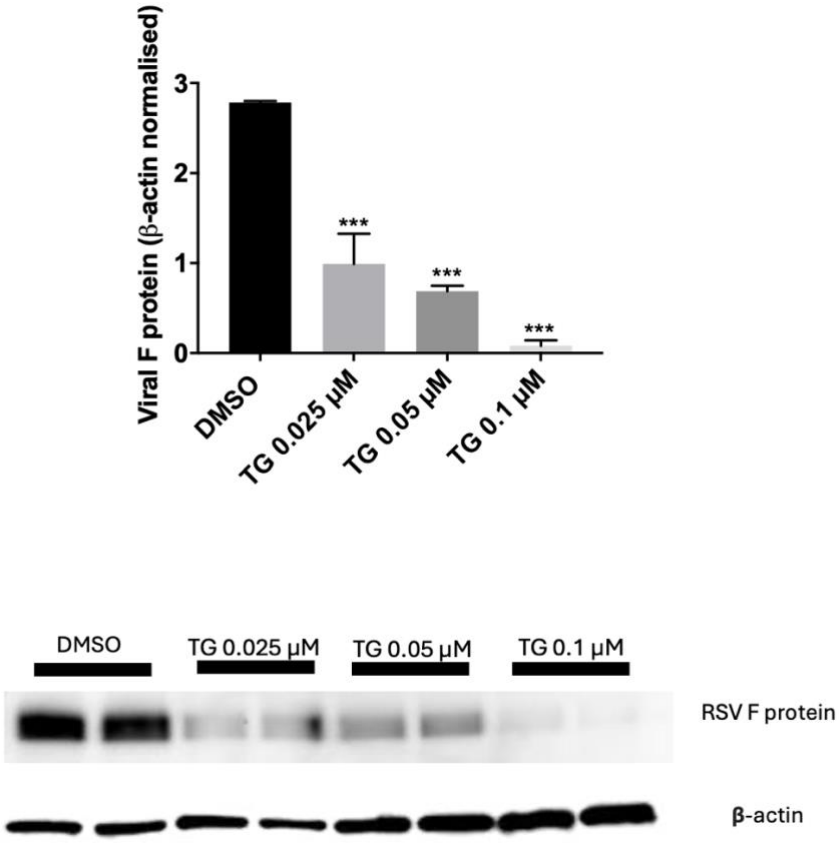

Figure 3.8 TG reduces RSV F protein expression in NHBE cells.

*NHBE cells were primed with TG at concentrations of 0.025 μM, 0.05 μM, and 0.1 μM, or treated with DMSO as a control, for 30 minutes. Cells were washed three times with PBS, infected with RSV (A2 strain, MOI 0.01), and incubated in PromoCell epithelial growth medium supplemented with 2% FCS for 48 hours. At 48 hpi, cells were lysed using RIPA buffer, as described in Section 2.4.6. Protein concentration was determined using the Bradford assay, and samples were prepared with NuPAGE LDS sample buffer and reducing agent, heated at 70°C for 10 minutes, and separated by SDS-PAGE using 4–12% Bis-Tris Protein Gels. Proteins were transferred to PVDF membranes and blocked in 5% milk in TBS-T. Membranes were probed with anti-RSV F protein (1:2000 dilution) and anti-β-actin (1:5000 dilution) primary antibodies overnight at 4°C. Blots were washed with TBS-T and incubated with HRP-conjugated secondary antibodies for 1 hour. Enhanced chemiluminescence (ECL) was used for detection, and bands were visualised using a ChemiDoc MP Imaging System. F protein levels were normalised to β-actin using densitometric analysis. Statistical significance was determined using one-way ANOVA with Dunnett's multiple comparisons relative to the DMSO control (***p < 0.001, ****p < 0.0001).*

3.3.7.3 TG reduces RSV genes transcription in host cells

The last plate was used to determine the transcription levels of three RSV genes—*L*-gene (viral polymerase), *F*-gene (attachment protein), and *M*-gene (matrix protein)—which were analysed to evaluate TG's inhibitory effect on viral RNA synthesis in NHBE cells. Cells were primed for 30 minutes with TG at 0.01 µM and 0.025 µM or treated with DMSO as a control, washed, followed by RSV infection (0.1 MOI) and incubation for 48 hours. Reverse transcription-qPCR revealed significant reductions in *L*-gene and *F*-gene expression at both TG concentrations compared to the DMSO control. These reductions highlight TG's ability to target critical components of RSV's lifecycle, with the *L*-gene essential for RNA synthesis and the *F*-gene crucial for viral entry and attachment. The *M*-gene, which exhibited the highest basal expression levels among the three genes, showed a significant reduction only at the higher TG concentration (0.025 µM). This result suggests that TG's effects may vary depending on the transcriptional hierarchy or functional relevance of the viral genes. Overall, the robust inhibition of the *L*-gene and *F*-gene underscores TG's ability to block the transcription of multiple viral genes, highlighting its multifaceted antiviral properties.

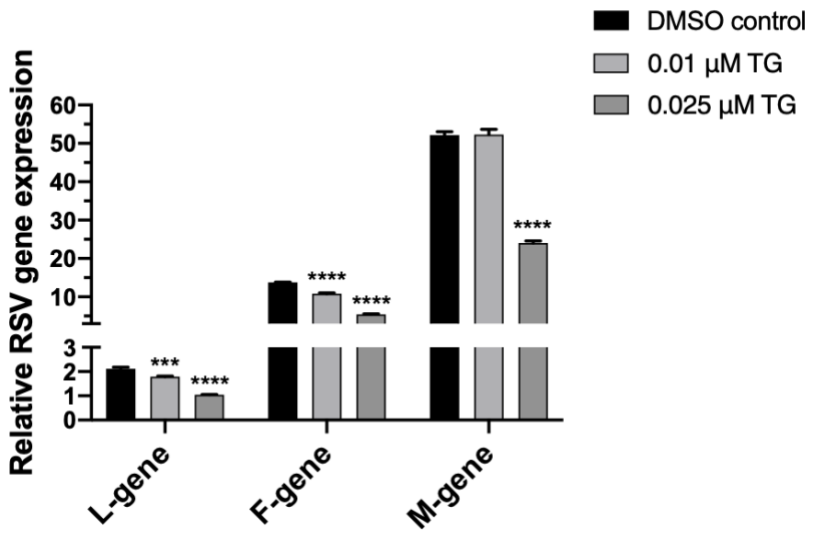

Figure 3.9 TG reduces RSV gene transcription in NHBE cells.

*NHBE cells were primed with TG at concentrations of 0.01 µM and 0.025 µM or treated with DMSO as a control, for 30 minutes. Cells were washed three times with PBS and infected with RSV (A2 strain, MOI 0.1) in serum-free medium. After 2 hours of infection, cells were washed twice with PBS and incubated in PromoCell epithelial growth medium containing 2% FCS for a total infection period of 48 hours.At 48 hpi, total RNA was extracted using the RNeasy Plus Mini Kit. RNA concentration and purity were confirmed using a NanoDrop spectrophotometer, ensuring A260/A280 ratios between 1.8 and 2.0. cDNA was synthesised from 500 ng of RNA using the SuperScript III First-Strand Synthesis System following Section 2.5.1. Reverse transcription-qPCR was performed using SYBR Green chemistry, with primers specific to RSV L-gene, F-gene, and M-gene. 18S ribosomal RNA was used as the internal control for normalisation. Relative expression levels of viral genes were calculated using the ΔΔCt method, comparing TG-treated samples to the corresponding DMSO control group. Statistical significance was determined using two-way ANOVA with Tukey's multiple comparisons relative to the DMSO control (***p < 0.001, ****p < 0.0001).*

Taking together the results from these complementary approaches, TG was shown to offer robust antiviral protection at multiple levels of the RSV replication cycle. Direct immunostaining revealed a significant dose-dependent reduction in plaque formation, demonstrating TG's ability to inhibit infectious virus production in NHBE cells. Western blot analysis further confirmed that TG effectively suppressed the expression of the RSV F protein, a key mediator of viral attachment and entry. Finally, reverse transcription-qPCR highlighted TG's capacity to inhibit transcription of essential RSV genes, including the *L-gene* and *F-gene*, which are critical for RNA polymerase activity and viral entry, respectively. These findings underscore TG's multifaceted antiviral properties, targeting RSV replication at both the transcriptional and translational levels. By effectively reducing viral RNA synthesis and protein production, TG disrupts essential stages of the viral lifecycle, offering a potent antiviral effect in a physiologically relevant human primary cell model. Furthermore, the consistent efficacy of TG across distinct readouts—plaque assays, protein expression, and transcriptional analysis—provides compelling evidence of its broad-spectrum antiviral potential. This study highlights TG's promise as a therapeutic agent, capable of offering significant protection against RSV in fragile and clinically relevant primary cell systems.

3.3.8 TG Demonstrates Broad-Spectrum Antiviral Efficacy Against RSV and IAV Co-Infections in Calu-3 Cells

Calu-3 cells, a widely used in vitro model for respiratory pathogens including SARS-CoV-2, were employed to evaluate the antiviral potential of TG against co-infections of RSV and IAV. Before evaluating TG's efficacy in co-infection, its cytotoxicity in Calu-3 cells was assessed. The toxicity of TG (0.5 μM) was measured at 24-, 48-, and 72-hours post-treatment using the CellTiter-Glo® 2.0 Cell Viability Assay (Promega). As shown in figure 3.10A (24h), figure 3.10B (48h), and figure 3.10C (72h), TG treatment did not significantly impact Calu-3 cell viability over the tested time points, confirming its safety at the applied concentration. For the co-infection experiment, Calu-3 cells were first infected with RSV (MOI 0.1) for 48 hours, followed by sequential infection with IAV (MOI 0.5) for 2 hours. TG treatment significantly reduced RSV replication, as evidenced by the reduction in progeny virus titres (pfu/mL), shown in figure 3.11A. Similarly, TG markedly reduced IAV replication, with a corresponding decrease in progeny virus titres (ffu/μL), as illustrated in figure 3.11B. RNA analysis revealed substantial suppression of RSV L-gene transcription, shown in figure 3.11C, and IAV M-gene transcription, displayed in figure 3.11D, in TG-treated cells compared to the DMSO control.

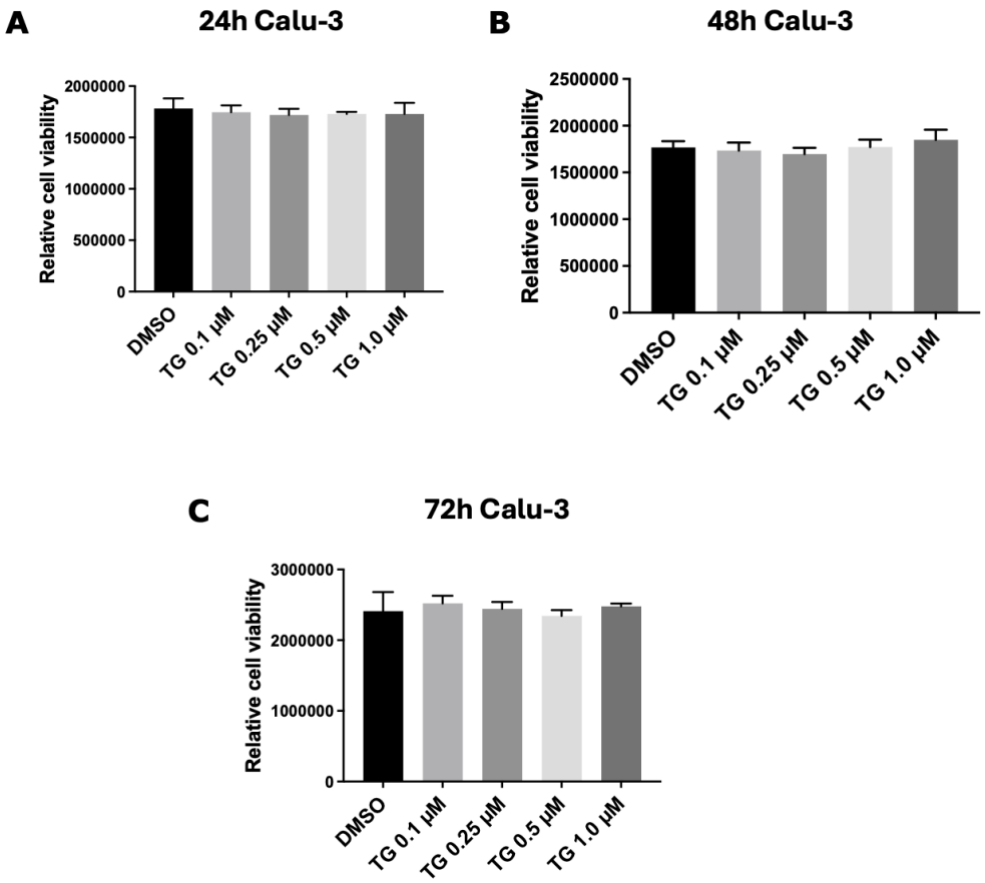

Figure 3.10 TG demonstrates low cytotoxicity in Calu-3 cells.

Calu-3 cells were primed with TG (0.5 µM) or DMSO for 30 minutes, washed with PBS, and incubated in PromoCell airway epithelial growth medium containing 2% FCS. Cytotoxicity was assessed at 24 (A), 48 (B), and 72 (C) hours post-treatment using the CellTiter-Glo® Luminescent Cell Viability Assay. Luminescence levels were measured using a luminometer and normalised to DMSO-treated controls.

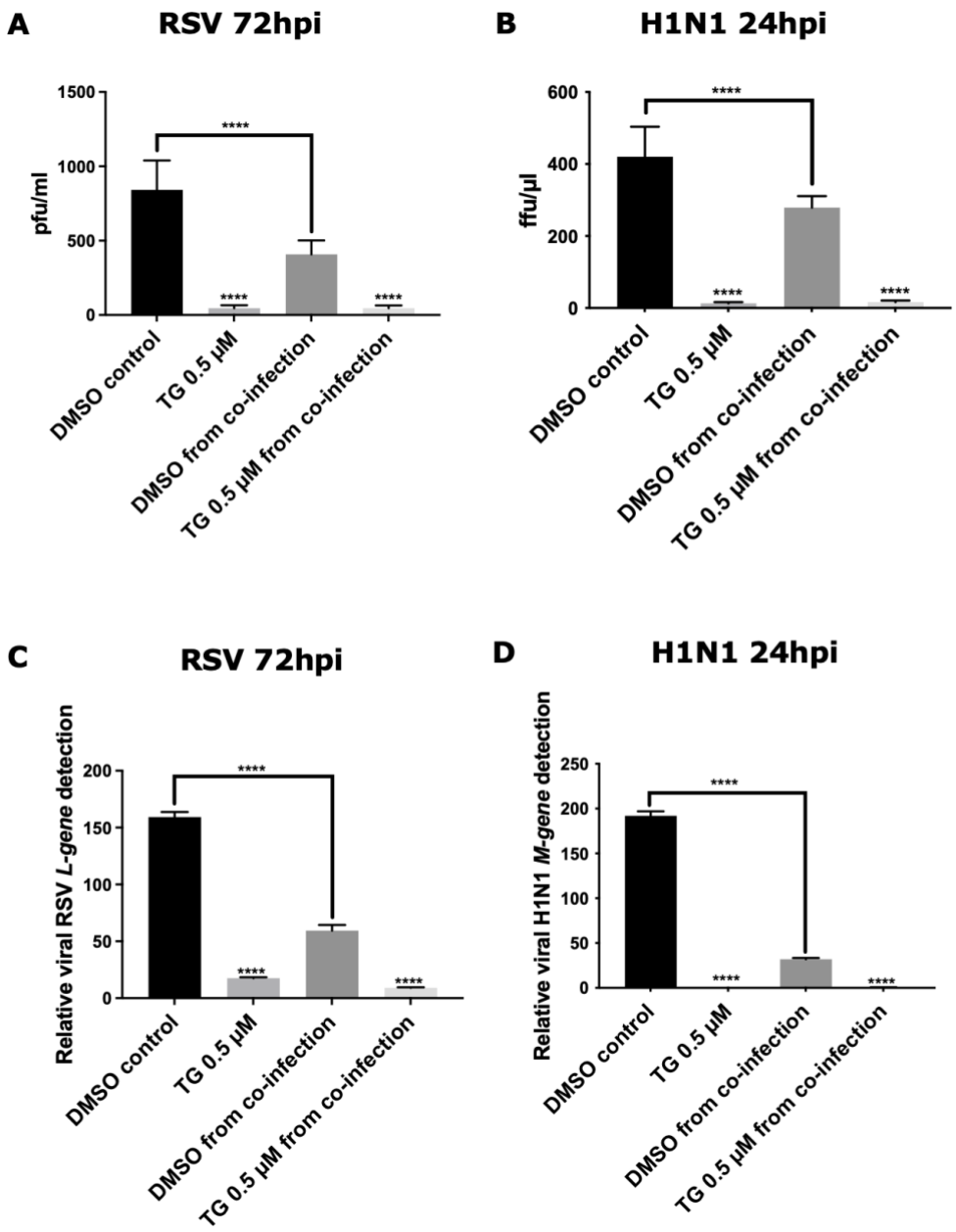

Figure 3.11 TG reduces RSV and IAV replication in co-infected Calu-3 cells.

*Calu-3 cells were primed with TG (0.5 µM) or DMSO for 30 minutes, washed with PBS, and infected sequentially with RSV (MOI 0.1) for 48 hours and H1N1 (MOI 0.5) for 24 hours. (A) Progeny RSV titres were quantified from spun supernatants as pfu/mL using immuno-detection with a monoclonal anti-RSV antibody (2F7). (B) Progeny H1N1 titres from supernatants were measured as focus-forming units per microlitre (ffu/µL) using immuno-detection with an anti-NP antibody. (C) RSV L-gene transcription was quantified by reverse transcription-qPCR using cDNA synthesised from extracted RNA, normalised to 18S rRNA. (D) H1N1 M-gene transcription was similarly quantified using reverse transcription-qPCR. Significance by one-way ANOVA (Tukey's multiple comparisons) is relative to the corresponding DMSO control (****p < 0.0001).*

Chapter 4: Host-focused defence: Thapsigargin as a key modulator of innate immunity against RSV and IAV

4.1 Introduction

TG has recently attracted considerable attention as a broad-spectrum antiviral candidate, an interest that mirrors the longstanding recognition that RNA viruses—particularly those infecting the respiratory tract—represent an ever-present global health threat (Taubenberger and Morens, 2008; Woolhouse and Brierley, 2018). Past pandemics such as the 1918 influenza A/H1N1 “Spanish flu” (Johnson and Mueller, 2002; Taubenberger and Morens, 2010), the 2009 “Swine Flu” (WHO, 2010), and the worldwide spread of coronaviruses including SARS-CoV-1 (Cheng et al., 2013) and SARS-CoV-2 (Cascella et al., 2022) underscore the capacity of RNA viruses to mutate, evade host immunity, and cause significant morbidity and mortality. Although antiviral drugs aimed at viral enzymes have saved millions of lives over the last several decades (Andrei, 2021), their efficacy can be undermined by the rapid evolution of drug-resistant variants (Littler and Oberg, 2005). As a result, research has increasingly pivoted towards host-targeted approaches, leveraging pivotal cellular defences such as the unfolded protein response (UPR) and the integrated stress response (ISR) (Smith, 2014; Hetz et al., 2013). TG, as shown, epitomises this shift by inducing ER stress in ways that appear to thwart viral replication across multiple families of RNA viruses, including IAV, RSV, and coronaviruses (Al-Beltagi et al., 2021). The primary mechanism by which TG initiates ER stress stems from its inhibition of SERCA (Thastrup et al., 1990; Christensen et al., 2021). By blocking the re-uptake of calcium into the ER, TG lowers luminal calcium stores, thereby activating store-operated calcium entry (SOCE) at the

plasma membrane (Putney, 1986; Smyth et al., 2010). The downstream consequence is a state of pronounced ER stress, which in turn triggers the three main sensors of the UPR: inositol requiring kinase 1 (IRE1), PKR-like ER kinase (PERK), and activating transcription factor 6 (ATF6) (Ron and Walter, 2007; Zhang and Wang, 2012). Although these sensors typically function to restore homeostasis by upregulating chaperones, promoting ER-associated degradation (ERAD), and selectively reducing protein translation (Walter and Ron, 2011), viruses such as IAV and RSV have evolved ways to manipulate or partially hijack certain aspects of the UPR for their replication (Hassan et al., 2011; Cervantes-Ortiz et al., 2016). Among the key genes induced during TG-mediated ER stress is *HERPUD1*, which encodes the ER-resident membrane protein HERP. This protein plays a pivotal role in ERAD, facilitating the removal of misfolded or unfolded proteins from the ER to maintain proteostasis (Kokame et al., 2000). By supporting degradation of aberrant proteins, *HERPUD1* links UPR activation to the preservation of ER function during stress. Importantly, some viruses modulate *HERPUD1* expression to benefit their replication (Chan et al., 2008), making it a relevant marker for understanding how TG-driven ER stress intersects with antiviral defence. It appears, however, that TG pushes these stress pathways to a tipping point that undermines viral replication, either by restricting the availability of host resources, triggering apoptosis of infected cells (Zhang and Wang, 2012), or boosting innate immune sensors (Manivannan et al., 2020). One emerging question concerns how TG's activation of ER stress merges

with canonical antiviral programmes orchestrated by retinoic acid-inducible gene I (RIG-I), mitochondrial antiviral-signalling protein (MAVS), and interferon regulatory factor 3 (IRF3). Although these pathways typically respond to foreign RNA by amplifying interferon (IFN) production, growing evidence suggests that RNA cleavage activities within the UPR can feed directly into viral RNA detection (Smith, 2014; Malathi et al., 2007). Two ribonucleases underscore this possibility. The first is RNAse L, activated through the 2′-5′ oligoadenylate synthetase (OAS) pathway, which cleaves viral and host RNA to yield small fragments that further stimulate RIG-I (Chakrabarti et al., 2011). The second is the IRE1 branch of the UPR, whose regulated IRE1-dependent decay (RIDD) function can degrade mRNAs and potentially generate similarly stimulatory RNA fragments (Hollien and Weissman, 2006). Both RNase L and IRE1 thus occupy a nexus where cellular stress responses and innate immune sensing overlap, and TG's broad-spectrum antiviral efficacy might well hinge on how these two nucleases operate—individually or in tandem—to produce immunostimulatory RNAs.

Chemical inhibition studies are needed to probe these hypotheses. One inhibitor, 4μ8C, selectively blocks IRE1's endoribonuclease domain, allowing researchers to determine whether RIDD-driven RNA cleavage is indispensable for TG's antiviral potency (Cross et al., 2012). Another agent, sunitinib, is known to suppress RNase L under certain conditions (Das et al., 2015). By systematically blocking either IRE1 or RNase L in TG-treated cells, the aim is to uncover whether one pathway

compensates for the other or whether TG's antiviral mechanism becomes fully ablated only when both endoribonucleases are silenced. If an interplay exists—for example, if the cleavage fragments produced by IRE1 or RNase L are sequestered within stress granules or directly recognised by pattern recognition receptors such as RIG-I—it would clarify how TG-driven stress might amplify innate immune signalling through MAVS, IRF3, and interferon-β (IFNβ). Moreover, clarifying the contributions of these nucleases has implications for co-infections, since IAV and RSV can collude or compete for host machinery, making it more relevant that TG can direct multiple, parallel antiviral defences.

TG's relationship to the integrated stress response (ISR) offers additional explanatory power. The ISR converges on the phosphorylation of eukaryotic initiation factor 2 alpha (eIF2α), a key modification triggered by multiple kinases, including PERK (Harding et al., 2000) and the interferon-inducible protein kinase PKR (Garcia et al., 2007). PERK, which responds directly to ER stress, diminishes global protein synthesis by phosphorylating eIF2α, thereby hindering both viral protein production and the translation of most host mRNAs (Walter and Ron, 2011). In parallel, PKR, when activated by viral RNA, also phosphorylates eIF2α in an effort to shut down viral replication (Garcia et al., 2007). TG-driven stress might thus synergise with PKR by creating conditions that further decrease viral protein output and push cells closer to an antiviral threshold.

A fascinating extension of PERK-mediated eIF2α phosphorylation is its link to the formation of cytoplasmic stress granules—dynamic, phase-

separated structures containing stalled mRNA-ribonucleoprotein complexes (Reineke and Lloyd, 2015). G3BP1, a crucial scaffolding protein within these granules, helps assemble and stabilise them, while also recruiting PKR and other immune factors. Many viruses, including RSV and IAV, actively disrupt or co-opt stress granules to enable their own replication (Lindquist et al., 2011; Hanley et al., 2010), demonstrating that stress granules pose a genuine threat to viruses. TG, by fuelling ER stress and bolstering the PERK–eIF2α axis, may promote robust stress granule assembly, sequestering viral RNAs and proteins. This phenomenon would tie the UPR even more tightly to classical antiviral defences, since G3BP1 granules can block viral replication, funnel immune activators to RIG-I and other pattern recognition receptors and reinforce the translation block that starves viral progeny formation (Reineke and Lloyd, 2015).

Equally pertinent is the role of key chaperones, such as heat shock 70 kDa protein 5 (HSPA5, also called BiP), which normally binds to IRE1 and PERK, keeping them inactive under non-stress conditions (Bertolotti et al., 2000). When TG sequesters ER calcium stores, HSPA5 is displaced from these sensors, setting off the UPR signalling cascade (Ron and Walter, 2007). It remains to be elucidated whether enhanced HSPA5 expression in TG-treated cells might paradoxically assist some viruses by improving their protein folding or whether the global stress environment offsets any pro-viral chaperoning function. Recent findings have indeed suggested that certain viruses exploit HSPA5 to stabilise their proteins (Smith, 2014). Delineating how TG-mediated ER stress

shapes this chaperone function, and whether the integrated stress response ultimately overrides such pro-viral possibilities, is crucial for understanding the overall antiviral outcome.

A further dimension that underscores the importance of this host-centred antiviral tactic is the increasing frequency and severity of co-infections. RSV and IAV have been shown to co-occupy the human respiratory tract and, in some instances, form hybrid viral particles (Haney et al., 2022). In clinical settings, individuals harbouring both viruses can suffer more severe disease than those infected by either pathogen alone (Cong et al., 2022). Strategies like TG that modulate fundamental host processes—rather than targeting specific viral enzymes—could prove uniquely suitable for limiting the replication of more than one virus at a time, diminishing the risk that the two viruses might swap genetic segments or manipulate shared host factors to exacerbate infection.

Collectively, these threads raise key questions that will be addressed in this study: Does inhibition of IRE1 or RNase L meaningfully reduce TG's broad-spectrum antiviral efficacy? Does PERK signalling—and its downstream formation of G3BP1-laden stress granules—represent a central hub in TG's antiviral function, or do other branches of the UPR, such as ATF6, also contribute significantly? Might overlapping calcium dysregulation mechanisms feed directly into MAVS activation, thereby enhancing IFNβ production in TG-treated cells? And finally, to what extent can TG reshape the intracellular environment to counteract the complexities posed by simultaneous IAV and RSV infections? By scrutinising these pathways and molecules, this chapter seeks to

characterise the host-driven underpinnings of TG's antiviral mechanism. A more granular understanding of how TG mobilises innate immunity and the UPR will not only inform efforts to refine TG-based strategies against persistent respiratory threats but could also foster new treatments that harness the formidable synergy of stress and immune responses in a manner adaptable to future pandemic challenges.

4.2 Materials and Methods

4.2.1 Viability assay

Vero E6 cells were cultured in 96-well plates under the conditions described in Section 2.2.1 until they reached near confluence. Once confluent, the culture medium was replaced with DMEM supplemented with TG at concentrations of 0.25 μM or 0.5 μM, with DMSO (0.5%) serving as the vehicle control. Cells were exposed to TG for 30 minutes at 37°C in a humidified 5% CO_2 atmosphere.

Following treatment, the cells were rinsed three times with PBS to remove residual TG or DMSO, and fresh DMEM was added. Cell viability was assessed at 48 hours post-treatment using the CellTiter-Glo® 2.0 Cell Viability Assay, as detailed in Section 2.2.4. Equal volumes of the CellTiter-Glo® reagent and culture medium (100 μL each) were mixed in each well, followed by gentle shaking for 2 minutes to induce cell lysis. Plates were incubated at room temperature for 10 minutes to stabilise the luminescent signal, which was measured using the GloMax®

Discover Microplate Reader. The luminescence values, reflecting ATP levels, were used as an indicator of cell viability.

4.2.2 IAV Infection of Immortalised Cells (Calu-3 and NPTr)

Calu-3 and NPTr cells were cultured under conditions described in Section 2.2.1 until reaching 70–80% confluence. Following medium removal and washing with PBS, cells were infected with H1N1 (1 MOI) in infection media as detailed in Section 2.3.3. The cells were incubated with the virus for 1 hour at 37°C with gentle rocking every 15 minutes to ensure even viral exposure. After the incubation, the infection medium was replaced with fresh infection media. Infected cells were maintained at 37°C in a 5% CO_2 atmosphere for 24–72 hours, depending on the experimental design.

4.2.3 Collection of IAV Spun Supernatant and Cell Lysates

At the designated post-infection time points, cell culture supernatants were carefully collected and centrifuged at 10,000 × g for 2 minutes to remove cellular debris. The cleared supernatants were aliquoted and stored at –80°C for downstream viral quantification. Remaining cells were washed with PBS and lysed in RIPA buffer for protein analysis or RLT buffer supplemented with β-mercaptoethanol for RNA extraction, following methods described in Section 2.4.1.

4.2.4 Quantification and Immunostaining of IAV

Viral progeny were quantified using immunostaining of infected MDCK cells seeded in 96-well plates, as detailed in Section 2.3.5. The infected supernatant was serially diluted and added to confluent MDCK cells, which were incubated for 6 hours. Following fixation with acetone/methanol (1:1), viral nucleoprotein (NP) was detected using an anti-NP antibody (Abcam) and the ImmPRESS anti-mouse Ig polymer HRP reagent. Development with DAB substrate allowed visualisation of infected cells, and infected foci were counted to determine focus-forming units (ffu). For single-step detection of viral output, RT-qPCR targeting the M gene was employed

4.2.5 RT-qPCR for IAV and RSV-Infected Cells

Total RNA from infected cells was extracted and converted to cDNA, as described in Section 2.4.2-2.4.4. Quantification of viral and host gene expression was performed using SYBR Green-based RT-qPCR. Host response to various stressors was analysed using the genes found in Table 4.1. Viral genes, including the *M* gene for IAV and *F, L,* and *M* genes for RSV, were amplified using primers listed in Table 3.1, following the steps from the section 2.4.5.

Table 4.1* Host-cell p*rimers used in RT-qPCR quantification of host genes.

Gene	**Sense Primer (5'-3')**	**Antisense Primer (5'-3')**
18S	ACGGCTACCACATCCAAGGA	CCAATTACAGGGCCTCG-AAA
RIG-I (DDX58) (human)	GAAGGCATTGACATTGCACAGT	TGGTTTGGATCATTTTGATGACA
RIG-I (pig)	CCCTGGTTTAGGGACGATGAG	AACAGGAACTGGAGAAAAGTGA
OAS1 (human)	AGGAAAGGTGCTTCCGAGGTAG	GGACTGAGGAAGACAACCAGGT
OAS1 (pig)	GAGCTGCAGCGAGACTTCCT	GGCGGATGAGGCTCTTCA
DDIT3 (human)	GGTATGAGGACCTGCAAGAGGT	CTTGTGACCTCTGCTGGTTCTG
HSPA5 (human)	CTGTCCAGGCTGGTGTGCTCT	CTTGGTAGGCACCACTGTGTTC
HSP90B1 (human)	GGAGAGTCGTGAAGCAGTTGAG	CCACCAAAGCACACGGAGATTC
HERPUD1 (human)	TGGATTGGACCTATTCAGCAGC	GCAGGTACATAACAACGGTGGC
G3BP1 (human)	AGCCTGTTCAGAAAGTCCTTAGC	CGAAGGCGATTATCTCGTCGGT

EIF2AK2 (PKR) (human)	GAAGTGGACCTCTACGC TTTGG	TGATGCCATCCCGTAGGTC TGT
MAVS (human)	ATGGTGCTCACCAAGGT GTCTG	TCTCAGAGCTGCTGTCTAG CCA
IRF3 (human)	TCTGCCCTCAACCGCAA AGAAG	TACTGCCTCCACCATTGGT GTC
IFNβ (human)	CTTGGATTCCTACAAAG AAGCAGC	TCCTCCTTCTGGAACTGCT GCA

4.2.6 Chemical Blocking of Host Pathways

IRE1 Blocking with 4μ8C

To investigate the role of IRE1 in the antiviral activity of TG, NPTr cells were seeded in 24-well plates (100,000 cells per well) and allowed to adhere overnight. On the following day, the cells were primed with 4μ8C (Sigma-Aldrich), a specific IRE1 ribonuclease inhibitor, at concentrations of 10 μM or 30 μM in full media for 30 minutes. After this priming, TG groups underwent a second 30-minute priming with TG (0.5 μM). Control cells were treated with DMSO (0.05% concentration) to match the experimental conditions. Between each treatment, cells were washed with PBS three times to remove residual compounds.

After priming, cells were infected with H1N1 at an estimated MOI of 1.0 for 1 hour in infection media (comprising CHO Ultraculture media, 1%

penicillin-streptomycin, 1% L-glutamine, and TPCK trypsin). The MOI was calculated based on prior viral titration using focus forming assays. Following the infection period, cells were washed three times with PBS, and fresh infection media was added to all wells. For groups treated with 4μ8C, infection media contained the inhibitor at the respective concentration to maintain its effect throughout the infection period.

Infected cells were incubated for 24 hours at 37°C in a humidified atmosphere with 5% CO_2. After this period, supernatants were collected, centrifuged to remove cell debris, and stored at –80°C for further viral quantification. Remaining cells were lysed with RLT buffer for RNA extraction or fixed with acetone-methanol (1:1) for immunostaining.

RNAse L Blocking with Sunitinib

The role of *RNAse L* in TG's antiviral effects was examined by blocking its activity with Sunitinib (Sigma-Aldrich). HEp-2 cells were seeded in 24-well plates at a density of 100,000 cells per well and allowed to adhere overnight. Cells were primed with 3 μM Sunitinib for 30 minutes in full media. After washing with PBS three times, cells were treated with TG (0.5 μM) or DMSO for an additional 30 minutes under the same conditions. Cells were again washed three times with PBS to remove residual compounds.

Following priming, cells were infected with RSV at an MOI of 0.1 in serum-free media for 2 hours. During the infection period, cells were gently rocked every 15 minutes to ensure even distribution of the virus. After 2 hours, the infection media was removed, cells were washed twice

with PBS, and fresh media containing 2% FCS was added to the DMSO and TG groups. For Sunitinib-treated groups, media was supplemented with 3 μM Sunitinib to maintain inhibition of *RNAse L* throughout the infection.

Infection was allowed to proceed for 72 hours, after which supernatants were collected, centrifuged, and stored at –80°C for further analysis. These supernatants were subsequently used to infect fresh HEp-2 cells for an additional 24 hours to assess progeny virus infectivity. RNA from the remaining cells was extracted using RLT buffer for RT-qPCR analysis, and fixed cells were subjected to plaque assays to quantify viral replication. Viral titres were determined using pfu/mL, and RT-qPCR targeted RSV *L gene* to assess viral RNA levels.

4.2.7 Functional Knockdown of G3BP1 and PERK via siRNA

siRNA knockdown experiments were performed to investigate the role of specific host genes, targeting G3BP1 and PERK, with negative control siRNAs used as a reference (Table 4.2). The transfection protocol was conducted as described in Section 2.4.7. For each well, 100 μL of Opti-MEM reduced serum medium was mixed with 6 μL of Lipofectamine RNAiMAX in a 1.5 mL tube to create the RNAi Master Mix. Separately, 100 μL of Opti-MEM was combined with 2 μL of 20 pM siRNA stock for G3BP1, PERK, or the negative control in individual tubes. The RNAi Master Mix was added to each siRNA-containing tube (100 μL per tube) and mixed thoroughly to form siRNA-reagent complexes, which were incubated at room temperature for 5 minutes.

Calu-3 Cells were seeded to achieve 60–80% confluence on the day of transfection. For each well, 100 µL of the siRNA-reagent complex was added directly. Medium replacement with fresh DMEM supplemented with 10% FCS was optional after 4–6 hours to minimise potential cytotoxicity. The cells were incubated at 37°C in a humidified 5% CO_2 atmosphere for 48 hours. At designated time points, cell lysates were collected for RNA extraction, as described in Section 2.4.1, and the knockdown efficiency of G3BP1, PERK, and negative control siRNAs was quantified using RT-qPCR (Section 2.4.5). RNA was converted to cDNA and subjected to quantitative PCR, with expression levels normalised to 18S rRNA and relative expression determined using the ΔΔCq method. Upon confirmation of target gene knockdown, the experiment was repeated with TG treatment and the appropriate infection protocols for IAV or RSV, as outlined in Sections 4.2.2 and 4.2.7. Following siRNA transfection, cells were primed with TG (0.5 µM) for 30 minutes before being washed with PBS and infected with the respective virus at the specified MOI. Post-infection, cells were maintained under standard culture conditions with the relevant infection media. At the designated time points, supernatants and cell lysates were collected for viral quantification and gene expression analysis, as described in Sections 2.4.5 and 2.4.6.

Table 4.2 siRNAs used for gene knockdown.

siRNA Gene	**Product type**	**Manufacturer**	**siRNA ID or catalogue no.**
G3BP1 (human)	Silencer® Select	ThermoFisher Scientific, Massachusetts	s19754
EIF2AK3 (PERK) (human)	Silencer® Select	ThermoFisher Scientific, Massachusetts	s18102
Negative Control No. 1 siRNA	Silencer® Select	ThermoFisher Scientific, Massachusetts	4390843

4.3 Results

4.3.1 Evaluating the Role of Interferon Response in TG-Induced Antiviral Activity Using VERO E6 Cells

TG has been shown to induce a potent antiviral state through endoplasmic reticulum (ER) stress and activation of the unfolded protein response (UPR), leading to increased type I and III interferon (IFN) production (Goulding et al., 2021). To investigate whether interferon production is essential for TG-mediated antiviral activity, VERO E6 cells were used. These cells are genetically deficient in interferon production due to a deletion in the IFN gene locus (Emeny and Morgan, 1979), providing a suitable system to distinguish between interferon-dependent and -independent antiviral mechanisms.

VERO E6 cells were primed with DMSO (vehicle control), 0.25 μM TG, or 0.5 μM TG for 30 minutes, followed by PBS washing and infection with RSV at an MOI of 0.1. After a 2-hour incubation, the inoculum was removed, and cells were maintained in fresh DMEM supplemented with 2% FCS for a further 72 hours. Viral replication was assessed by quantifying RSV *L*-gene RNA in cell supernatants using one-step RT-qPCR. To assess cell health and rule out cytotoxicity as a confounding factor, viability was evaluated using a luminescence-based assay. Additionally, supernatants from infected VERO E6 cells were applied to HEp-2 cells for immunostaining to visualise viral spread.

TG treatment did not lead to a measurable reduction in RSV replication in VERO E6 cells, with *L*-gene RNA levels remaining comparable between TG- and DMSO-treated groups. Consistent with this, immunostaining of HEp-2 cells infected with VERO E6-derived supernatants showed no decrease in RSV spread. These observations suggest that the antiviral activity of TG relies on the presence of a functional interferon response, which is absent in VERO E6 cells.

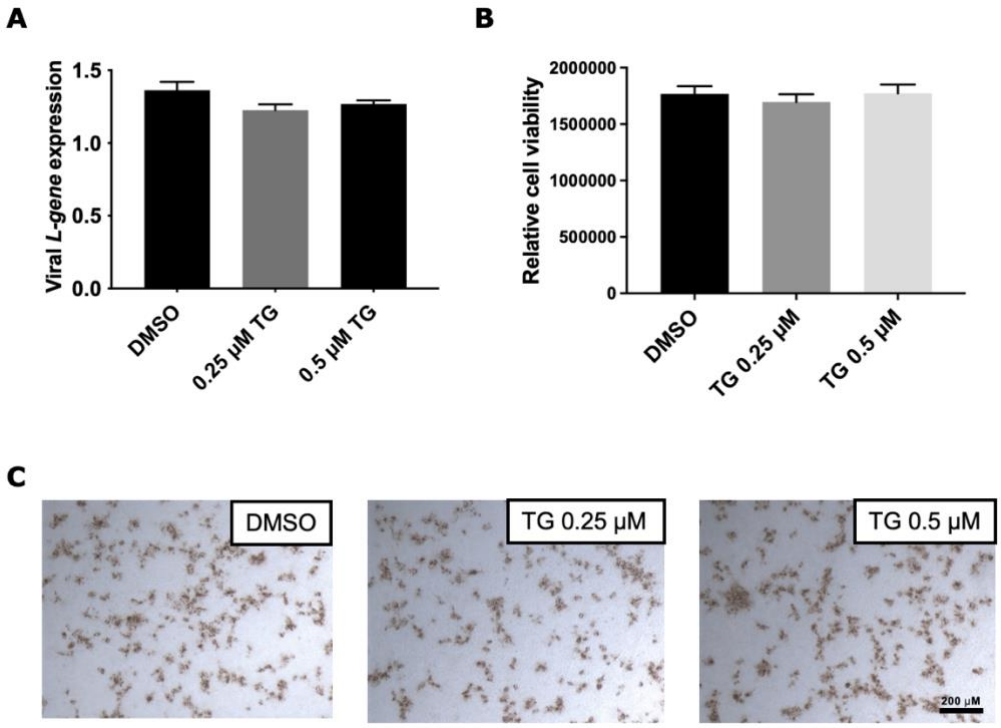

Figure 4.1 TG fails to inhibit RSV replication in interferon-deficient VERO E6 cells.

*(A) Viral replication was quantified by measuring L-gene RNA levels in supernatants collected 72 hours post-infection using one-step RT-PCR, expressed as fold change relative to DMSO controls. (B) Cell viability was assessed using a luminescence-based assay after treatment with DMSO, 0.25 µM TG, or 0.5 µM TG for 30 minutes, showing no significant cytotoxicity. (C) HEp-2 cells infected with supernatants derived from TG- or DMSO-treated VERO E6 cells were immunostained with anti-RSV antibody (10× magnification). Statistical significance was determined by one-way ANOVA relative to DMSO controls (*p < 0.05).*

4.3.2 TG exposure enhances *OAS1* and *RIG-I* expression in H1N1-infected NPTr cells

Exposure to TG has been shown to induce ER stress and activate antiviral pathways. To evaluate its effect on the expression of *OAS1* and *RIG-I*, an experiment was conducted using NPTr cells under infected and uninfected conditions. Cells were exposed to 0.5 μM TG for 15 or 30 minutes, followed by washing with PBS and recovery under normal culture conditions for 24 hours. RNA was extracted, and cDNA synthesis and qPCR were performed to measure relative mRNA levels of *OAS1* and *RIG-I*, normalised to 18S rRNA.

Results demonstrated that TG-induced expression of *OAS1* and *RIG-I* depended on viral infection. In uninfected cells, TG treatment did not significantly alter the expression of either gene, regardless of exposure duration. However, in cells infected with H1N1 (MOI 0.5), TG treatment significantly upregulated both genes, with a stronger response observed following 15 minutes of exposure compared to 30 minutes. This highlights the dependency of TG-mediated gene expression on infection-associated stimuli, reinforcing the role of viral presence in amplifying the cellular response to TG priming.

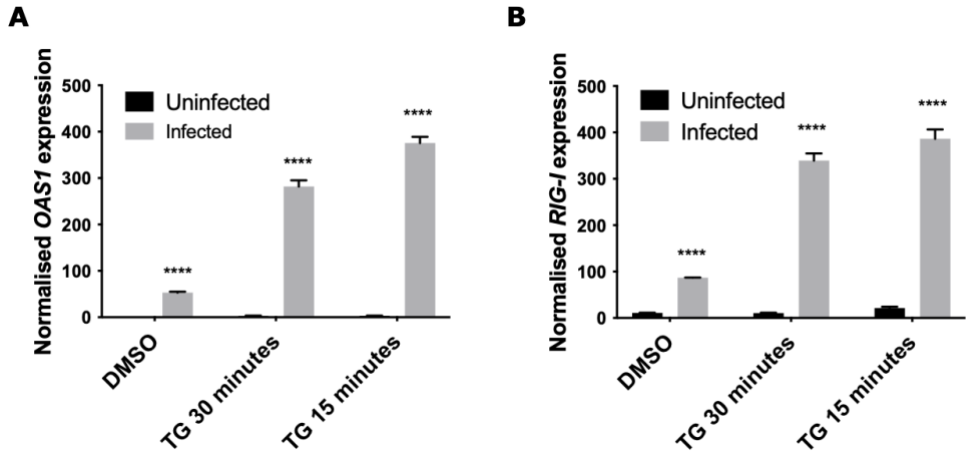

Figure 4.2 TG raises OAS1 and RIG-I expression levels in H1N1 infected cells.

*(A) OAS1 expression was quantified by qPCR in NPTr cells exposed to 0.5 μM TG for 15 or 30 minutes, under uninfected or H1N1-infected conditions (MOI 0.5). Results are normalised to 18S rRNA and expressed as fold change relative to DMSO-treated controls. (B) RIG-I expression was measured under the same conditions. TG-induced upregulation of both genes was observed exclusively in infected cells, with 15 minutes of exposure eliciting a greater response than 30 minutes. Statistical significance was determined by one-way ANOVA relative to DMSO controls (*p < 0.05, **p < 0.01, ***p < 0.001).*

4.3.3 TG induces ER-related host-gene response in NHBE cells

4.3.3.1 *DDIT3* and *HSPA5*

Using the cDNA samples described in Section 3.3.7.3, the transcriptional response to TG was assessed in primary NHBE cells under uninfected and RSV-infected conditions (MOI 0.01). Cells were exposed to TG at 0.01 μM or 0.025 μM for 30 minutes, washed with PBS, and then incubated for 24 hours under standard culture conditions. mRNA levels were quantified by qPCR and normalised to 18S rRNA.

For *DDIT3* (encoding the pro-apoptotic transcription factor CHOP; Figure 4.3), TG increased expression relative to DMSO in both uninfected and infected cells. In uninfected cells, the induction was dose-dependent, with higher transcript levels at 0.025 μM than at 0.01 μM. In infected cells, *DDIT3* expression was already elevated in the DMSO condition and remained high following TG treatment, with only a modest further increase and limited dose dependence. Across all TG conditions (including DMSO), *DDIT3* levels were higher in infected than in uninfected cells, indicating that RSV infection strongly elevates this arm of the stress response. For *HSPA5* (encoding the chaperone BiP/GRP78; Figure 4.4), TG produced a clear dose-dependent upregulation in both uninfected and infected cells, with the largest increases observed at 0.025 μM. In contrast to *DDIT3*, infection alone did not appreciably increase *HSPA5* compared with the uninfected DMSO control. However, at matched TG concentrations (0.01 μM and 0.025 μM), *HSPA5* transcript levels were higher in infected than in uninfected cells, consistent with infection amplifying the TG-driven induction of this UPR chaperone.

Taken together, these data show divergent patterns for the two genes: RSV infection elevates baseline *DDIT3* and blunts the dose dependence seen in uninfected cells, whereas *HSPA5* is primarily driven by TG in a dose-dependent manner, with infection enhancing the magnitude of induction only when TG is present. This distinction suggests that the pro-apoptotic branch marked by *DDIT3* is highly responsive to infection, while the chaperone arm represented by *HSPA5* is predominantly

responsive to pharmacological ER stress, yet further boosted by infection.

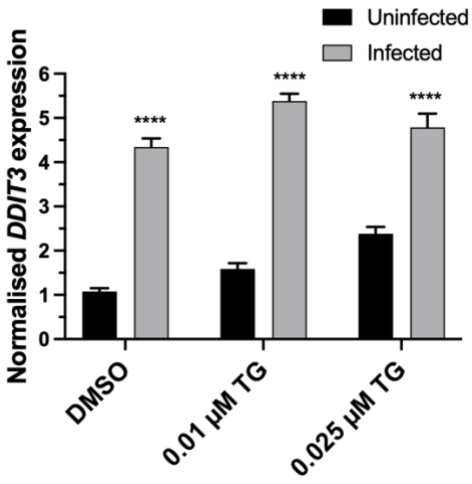

Figure 4.3 TG induces DDIT3 expression in NHBE cells.

*DDIT3 mRNA expression was measured by qPCR in NHBE cells treated with TG at 0.01 µM, 0.025 µM, and 0.1 µM for 30 minutes, under uninfected or RSV-infected conditions (MOI 0.01). Results are normalised to 18S rRNA and expressed as fold change relative to DMSO-treated controls. Statistical significance was determined by two-way ANOVA relative to DMSO controls (*p < 0.05, **p < 0.01, ***p < 0.001).*

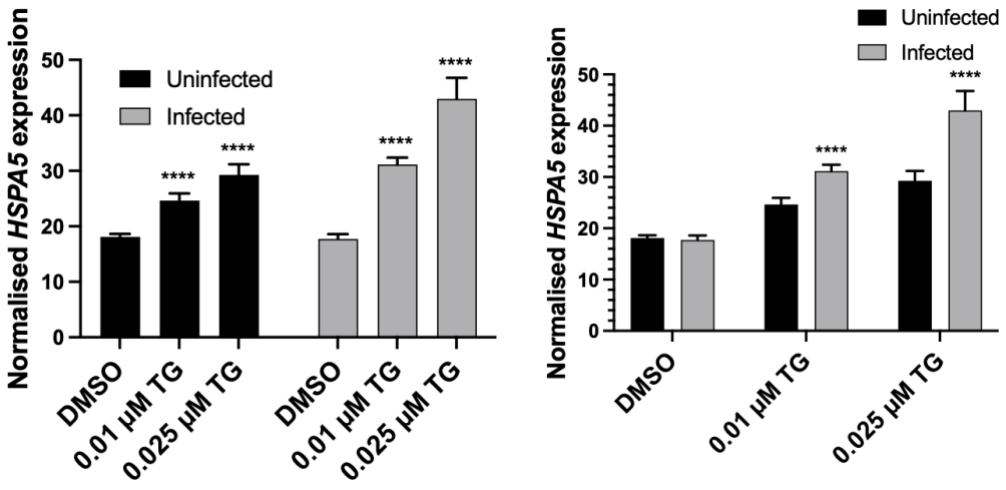

Figure 4.4 TG induces HSPA5 expression in NHBE cells.

*SPA5 mRNA expression was quantified by qPCR in NHBE cells treated with TG at 0.01 µM and 0.025 µM for 30 minutes, under uninfected or RSV-infected conditions (MOI 0.01). Results are normalised to 18S rRNA and expressed as fold change relative to DMSO-treated controls. TG upregulated HSPA5 expression in a dose-dependent manner, with a stronger response observed at 0.025 µM. Statistical significance was determined by two-way ANOVA relative to DMSO controls (*p < 0.05, **p < 0.01, ***p < 0.001).*

4.3.3.2 *HSP90B1*

The expression of *HSP90B1,* which encodes the chaperone GRP94, a key component of the UPR involved in protein folding and stress adaptation, was assessed in NHBE cells. Results demonstrated that TG treatment led to a slight increase in *HSP90B1* expression in uninfected cells, indicating a mild activation of stress pathways even in the absence of infection. In RSV-infected cells, TG treatment significantly upregulated *HSP90B1* expression in a dose-dependent manner, with the strongest induction observed at 0.025 µM TG (**** $p < 0.0001$). In uninfected cells, TG exposure did not produce a statistically significant change compared

to the DMSO control. These findings indicate that RSV infection enhances the host cell's transcriptional response to TG, potentially through the combined activation of stress and immune pathways.

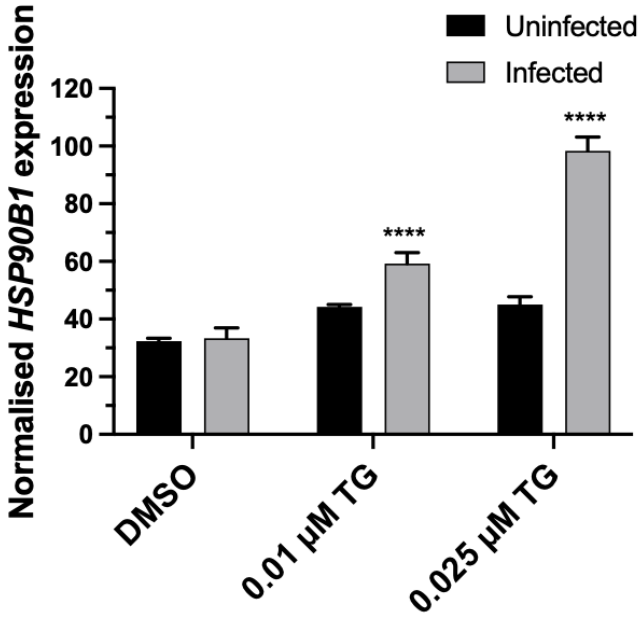

Figure 4.5 TG induces HSP90B1 expression in NHBE cells with enhanced responses in infected samples.

*HSP90B1 mRNA expression was quantified by qPCR in NHBE cells treated with TG at 0.01 µM and 0.025 µM for 30 minutes, under uninfected or RSV-infected conditions (MOI 0.01). Results are normalised to 18S rRNA and expressed as fold change relative to DMSO-treated controls. TG treatment slightly increased HSP90B1 expression in uninfected cells, while a dose-dependent upregulation was observed in infected cells, with the highest expression at 0.025 µM TG. Statistical significance was determined by one-way ANOVA relative to DMSO controls (*p < 0.05, **p < 0.01, ***p < 0.001, ****p<0.001).*

4.3.3.3 *HERPUD1*

The expression of *HERPUD1*, a UPR-associated gene involved in ER-associated degradation (ERAD) to mitigate protein misfolding, was assessed in NHBE cells. Cells were treated with TG at 0.01 μM and 0.025 μM for 30 minutes, followed by washing with PBS and incubation under normal culture conditions for 24 hours. RNA was extracted, and qPCR was performed to measure *HERPUD1* mRNA levels, normalised to 18S rRNA. TG treatment induced a strong, dose-dependent increase in *HERPUD1* expression in uninfected cells, whereas the response in RSV-infected cells was markedly attenuated. At both TG concentrations, *HERPUD1* levels were significantly higher in uninfected compared to infected cells, indicating that RSV infection dampens the transcriptional activation of this ER stress-related gene.

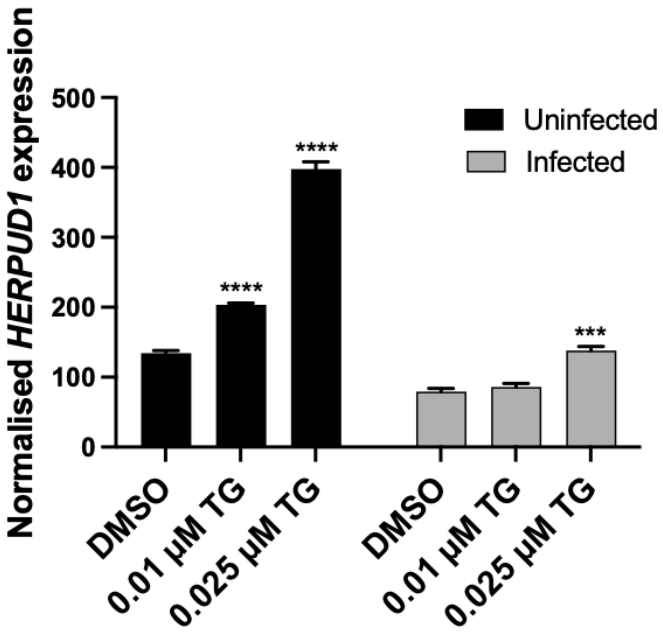

Figure 4.6 TG induces HERPUD1 expression in NHBE cells with distinct dose responses in uninfected and infected samples.

*HERPUD1 mRNA expression was quantified by qPCR in NHBE cells treated with TG at 0.01 µM and 0.025 µM for 30 minutes, under uninfected or RSV-infected conditions (MOI 0.01). Results are normalised to 18S rRNA and expressed as fold change relative to DMSO-treated controls. Statistical significance was determined by two-way ANOVA relative to DMSO controls (*p < 0.05, **p < 0.01, ***p < 0.001).*

4.3.3.4 *G3BP1* and *EIF2AK2*

G3BP1 and *EIF2AK2*, two components of the integrated stress response (ISR), were quantified in NHBE cells after TG exposure (0.01 µM or 0.025 µM for 30 min) under uninfected or RSV-infected conditions (MOI 0.01). qPCR values were normalised to 18S rRNA and expressed as fold change relative to DMSO. Two-way ANOVA (factors: TG concentration and infection status) showed a significant main effect of TG for both genes. For *G3BP1* (Figure 4.7A), expression increased with

dose in both states; infected values were generally lower than uninfected at matched doses, but this separation was modest and not consistently significant after multiple-comparison correction. For *EIF2AK2* (Figure 4.7B), expression increased with dose in both states and was higher in infected than uninfected cells at each matched dose; the between-state separation widened with dose, consistent with an interaction between TG and infection.

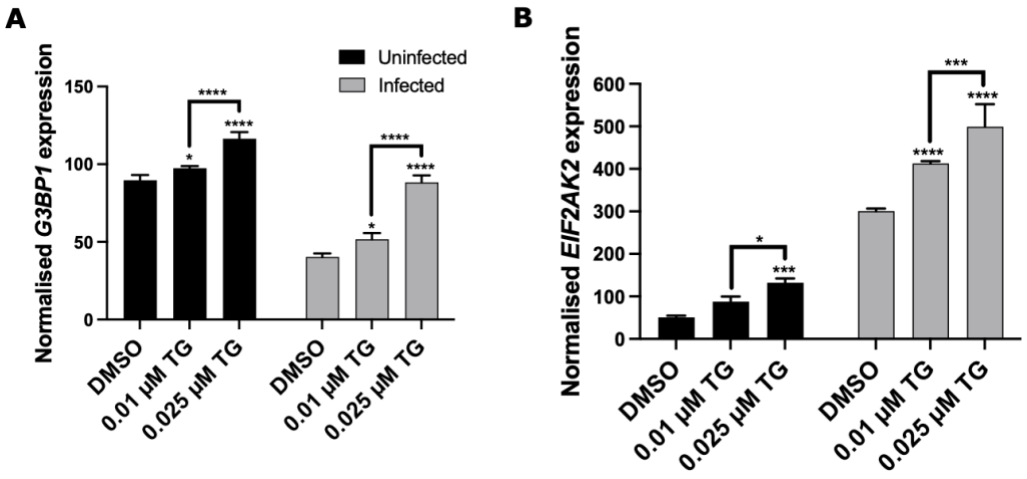

Figure 4.7 TG induces G3BP1 and EIF2AK2 expression in NHBE cells in a dose-dependent manner.

(A) G3BP1 and (B) EIF2AK2 mRNA were measured by qPCR in NHBE cells treated with TG (0.01 or 0.025 µM, 30 min) under uninfected or RSV-infected conditions (MOI 0.01). Data are normalised to 18S rRNA and expressed as fold change relative to DMSO. Statistics: two-way ANOVA with TG concentration and infection status as factors, followed by Sidak's multiple comparisons for within-state dose effects and for infected vs uninfected at each dose ($p < 0.05$, ** $p < 0.01$, *** $p < 0.001$, **** $p < 0.0001$). Note that the asterisks drawn on the panels indicate dose-wise comparisons; infected vs uninfected contrasts were tested but are not annotated on the plots.*

4.3.3.5 *MAVS* and *IRF3*

MAVS and *IRF3* mRNA were quantified in NHBE cells after TG exposure (0.01 or 0.025 μM, 30 min) under uninfected or RSV-infected conditions (MOI 0.01). Transcript levels were normalised to 18S and expressed relative to DMSO. Two-way ANOVA (factors: TG concentration and infection status) showed small but statistically significant effects of TG. For *MAVS* (Figure 4.8A), uninfected cells showed an increase at both TG doses versus DMSO, while infected cells displayed a dose-dependent rise (0.025 μM > 0.01 μM). Between-state differences at matched doses were limited in magnitude. For *IRF3* (Figure 4.8B), uninfected cells showed no clear dose effect, whereas infected cells increased at 0.025 μM compared with 0.01 μM. Overall, the changes were modest; therefore, while statistically significant, their biological impact should be interpreted cautiously.

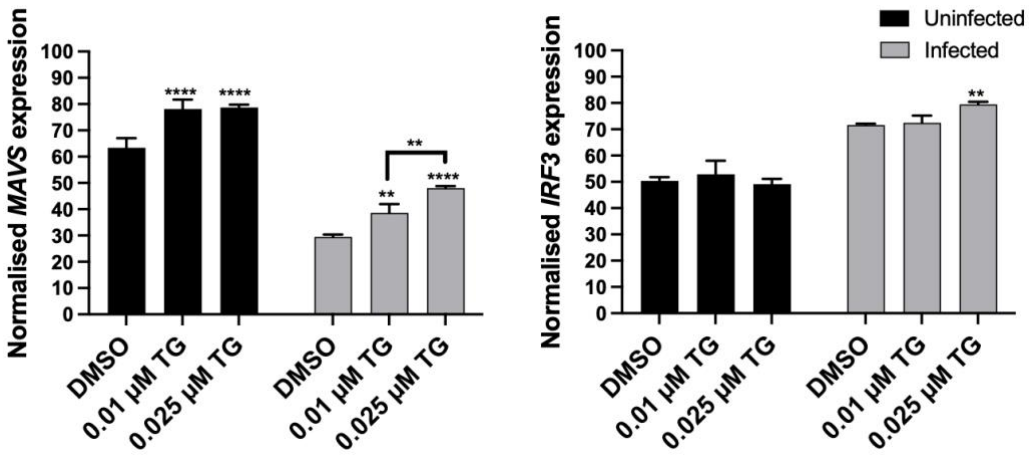

Figure 4.8 TG produces modest changes in MAVS and IRF3 expression in NHBE cells. *(A) MAVS and (B) IRF3 mRNA were measured by qPCR in NHBE cells treated with TG (0.01 or 0.025 µM, 30 min) under uninfected or RSV-infected conditions (MOI 0.01). Data are normalised to 18S rRNA and expressed relative to DMSO. Statistics: two-way ANOVA with TG concentration and infection status as factors, followed by Sidak's multiple comparisons for within-state dose effects and infected-versus-uninfected contrasts at each dose (* $p < 0.05$, ** $p < 0.01$, *** $p < 0.001$, **** $p < 0.0001$).*

4.3.4 TG Enhances the Expression of Antiviral Genes in Co-Infected Calu-3 Cells

The ability of TG to modulate antiviral responses during co-infections was assessed by examining the expression of key antiviral genes in Calu-3 cells under RSV, H1N1, and RSV + H1N1 co-infection conditions. Co-infections pose significant challenges to the host immune system, as simultaneous infections can exacerbate cellular stress and interfere with the coordinated activation of antiviral pathways. Using cDNA samples from Section 3.3.8, the experiment investigated whether TG could enhance the expression of these critical antiviral genes, which are

essential for viral recognition, interferon signalling, and downstream immune defence mechanisms.

4.3.4.1 *RIG-I, OAS1* and *IFNB*

Using cDNA from Section 3.3.8, transcript levels were quantified after a 30-minute pre-treatment with DMSO or 0.5 μM TG, followed by infection with RSV, H1N1 or RSV+H1N1. Values were normalised to 18S rRNA and expressed relative to DMSO.

TG reduced the abundance of *RIG-I* mRNA across all infection conditions (Figure 4.9A). A similar reduction was observed for *OAS1* (Figure 4.9B). For *IFNβ*, TG lowered expression in H1N1-infected and co-infected cells, with little change from the low baseline in RSV-infected cells (Figure 4.9C). Two-way ANOVA with treatment (DMSO, TG) and infection group (RSV, H1N1, RSV+H1N1) as factors showed a significant main effect of treatment for all three transcripts; Sidak-corrected post-hoc tests confirmed lower TG versus DMSO within each infection group. Overall, TG treatment is associated with reduced expression of *RIG-I*, *OAS1* and *IFNβ* under these infection conditions.

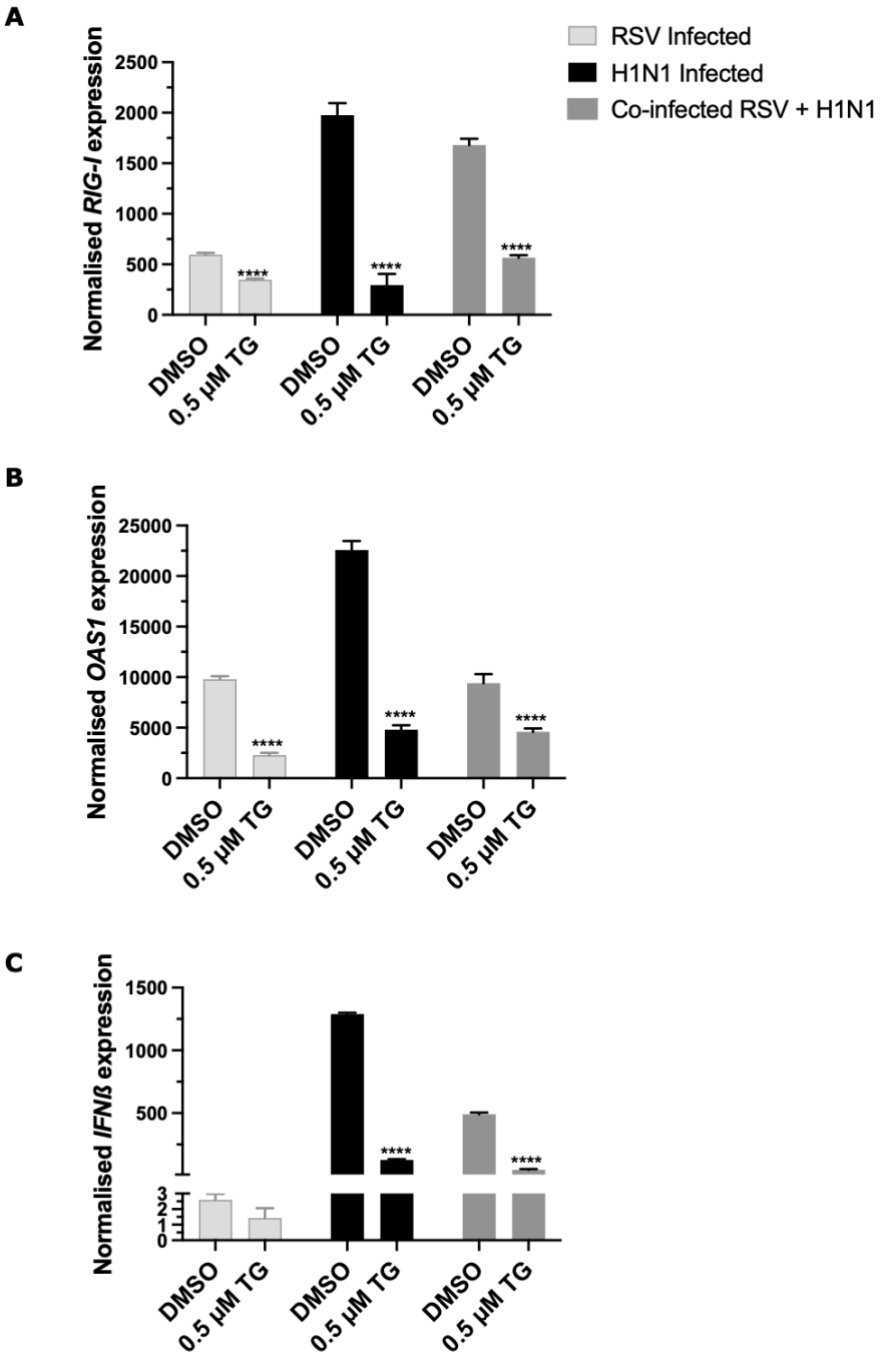

Figure 4.9 TG attenuates RIG-I, OAS1 and IFNβ transcript levels in infected Calu-3 cells. *(A) RIG-I, (B) OAS1 and (C) IFNβ mRNA were quantified by RT-qPCR in Calu-3 cells pre-treated with DMSO or 0.5 μM TG for 30 minutes, then infected with RSV, H1N1 or RSV+H1N1 as in Section 3.3.8. Data are normalised to 18S rRNA and expressed as fold change relative to DMSO. Statistics: two-way ANOVA with treatment and infection group as factors, followed by Sidak's multiple comparisons for DMSO vs TG within each infection group (* $p < 0.05$, ** $p < 0.01$, *** $p < 0.001$, **** $p < 0.0001$).*

4.3.4.2 *G3BP1*, *IRF3* and *PKR*

Using cDNA from Section 3.3.8, mRNA levels were quantified after a 30-minute pre-treatment with DMSO or 0.5 μM TG, followed by RSV, H1N1 or RSV+H1N1 infection as described in Section 3.3.8. Values were normalised to 18S rRNA and expressed relative to DMSO.

For *G3BP1* (Figure 4.10A), TG reduced expression in RSV-infected and co-infected cells (*** $p < 0.001$) and had no detectable effect in H1N1-infected cells. For *IRF3* (Figure 4.10B), TG decreased expression across all three infection groups (**** $p < 0.0001$). For *EIF2AK2* (PKR) (Figure 4.10C), TG lowered transcript levels in each infection group (**** $p < 0.0001$). Two-way ANOVA with treatment (DMSO, TG) and infection group (RSV, H1N1, RSV+H1N1) as factors showed a significant main effect of treatment for *IRF3* and *EIF2AK2*, and TG-by-group differences consistent with the patterns described above; Sidak-corrected post-hoc tests were used for DMSO vs TG within each infection group.

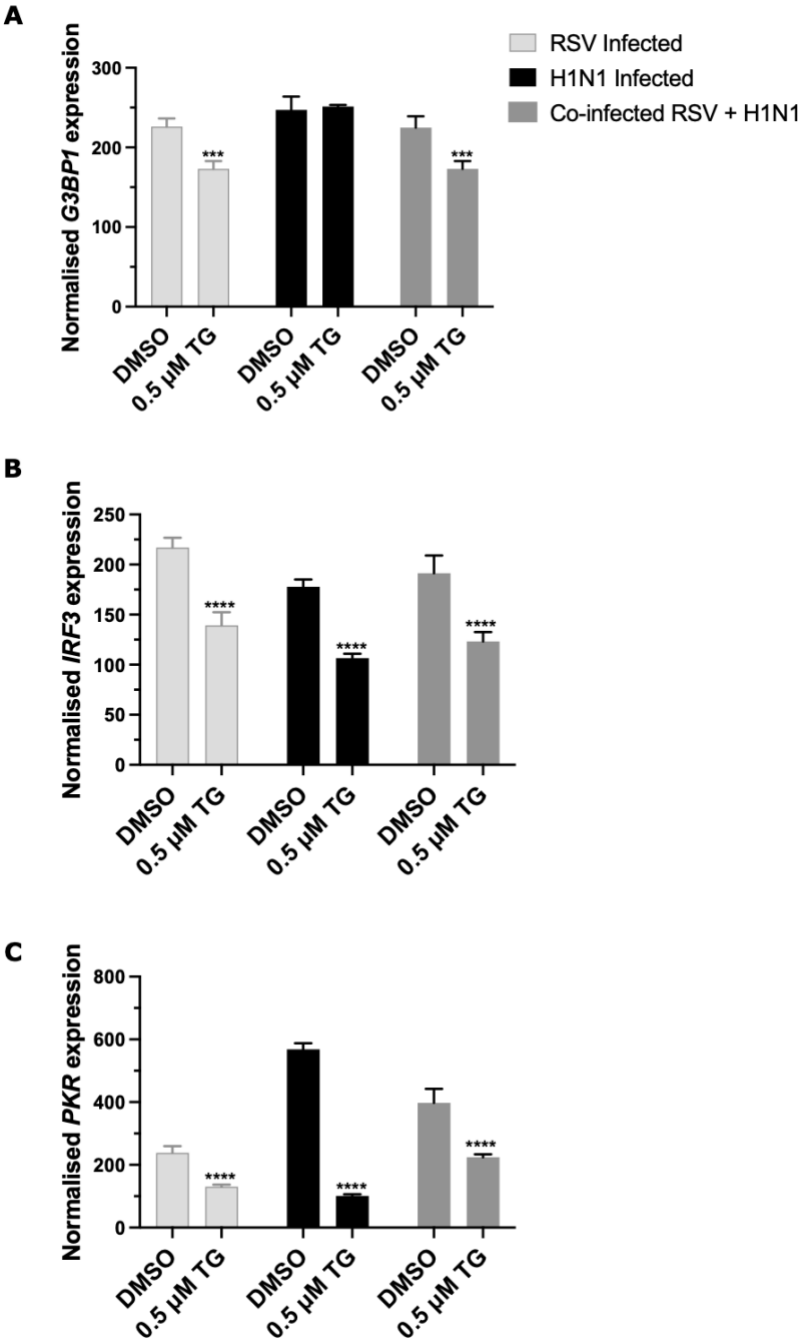

Figure 4.10 TG reduces G3BP1, IRF3 and PKR transcript levels in infected Calu-3 cells. *(A) G3BP1, (B) IRF3 and (C) PKR mRNA were measured by RT-qPCR in Calu-3 cells pre-treated with DMSO or 0.5 µM TG for 30 minutes, then infected with RSV, H1N1 or RSV+H1N1 as in Section 3.3.8. Data are normalised to 18S rRNA and expressed as fold change relative to DMSO. Statistics: two-way ANOVA with treatment and infection group as factors, followed by Sidak's multiple comparisons for DMSO vs TG within each infection group (* $p < 0.05$, ** $p < 0.01$, *** $p < 0.001$, **** $p < 0.0001$).*

4.3.5 Evaluating the Effect of RNAse L Inhibition via Sunitinib on TG-Induced Antiviral Activity Against RSV

To determine whether RNAse L activity is essential for the antiviral effects of TG, HEp-2 cells were treated with the RNAse L inhibitor sunitinib (Su) prior to TG priming and subsequent RSV infection. RNAse L plays a critical role in degrading viral RNA as part of the host's antiviral defence, and this experiment aimed to elucidate whether TG-induced antiviral activity relies on this pathway. Cells were first primed with 3 μM Su for 30 minutes, washed, and then exposed to DMSO (control) or 0.5 μM TG for an additional 30 minutes. After repeated washing, cells were infected with RSV (MOI 0.1) for 2 hours in serum-free media. Following infection, the media was replaced with fresh media containing either 2% FCS (DMSO or TG) or 2% FCS with 3 μM Su (TG + Su). The infection was allowed to proceed for 72 hours, after which supernatants were collected for quantification via pfu/mL and used to infect fresh HEp-2 cells. Viral infection was visualised through immunostaining of fixed cells using anti-RSV antibodies (2F7, Abcam). Quantification of viral titres in supernatants (Figure 4.11A) revealed no significant differences in pfu/mL between TG-treated groups with or without Su. While the viral L-gene RNA levels appeared elevated with Su compared to TG alone, this did not translate into any observable changes in viral progeny output. Immunostaining results (Figure 4.11C) corroborated these findings, showing similar levels of RSV-positive cells across all groups, with no

discernible differences in viral spread between TG-treated cells with and without Su.

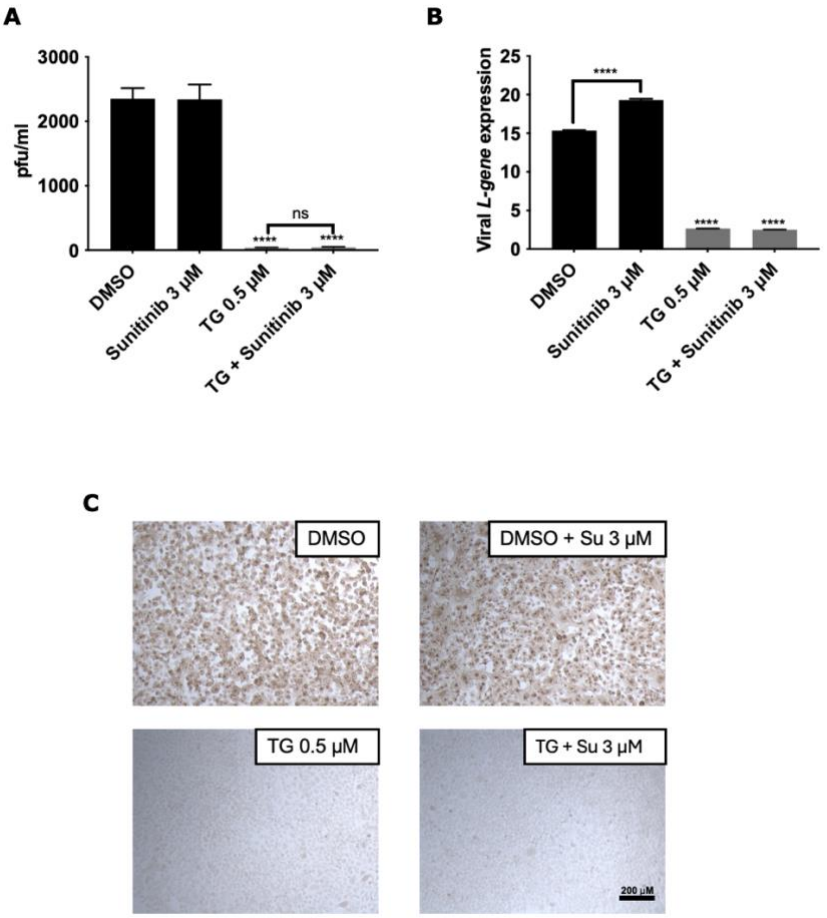

Figure 4.11 Effect of RNase L inhibitor sunitinib on TG-mediated inhibition of RSV in HEp-2 cells.

(A) Infectious RSV titres (pfu/mL) in supernatants from HEp-2 cells treated with DMSO, sunitinib 3 μM, TG 0.5 μM, or TG 0.5 μM plus sunitinib 3 μM. (B) RSV L-gene RNA from the same conditions, measured by RT-qPCR and normalised to 18S rRNA. (C) Representative immunostaining of RSV antigen in HEp-2 cells infected with supernatants from the indicated treatments. Statistics: data were analysed by two-way ANOVA with TG (present/absent) and sunitinib (present/absent) as factors, followed by Sidak's multiple comparisons. TG produced a significant main effect, reducing virus titres and L-gene RNA relative to DMSO; sunitinib alone had no effect on titres but increased L-gene RNA versus DMSO. There was no significant difference between TG and TG plus sunitinib for either readout (ns), indicating that sunitinib did not diminish the antiviral effect of TG. Asterisks denote Sidak-corrected pairwise comparisons ($p < 0.05$, ** $p < 0.01$, *** $p < 0.001$, **** $p < 0.0001$; ns, not significant).*

4.3.6 Synergistic Antiviral Effects of TG and the IRE1 Inhibitor 4μ8C in Calu-3 Cells

To investigate the role of the IRE1 pathway in that TG-induced antiviral activity, Calu-3 cells were treated with the IRE1 inhibitor 4u8C at varying concentrations and assessed for its impact on TG's efficacy against IAV and RSV infections. IRE1 is a key component of the UPR and contributes to antiviral defences by regulating mRNA decay and stress responses. This experiment sought to clarify whether TG's antiviral effects are mediated via IRE1-dependent mechanisms. In IAV-infected cells, immunostaining of supernatants for viral foci (Figure 4.12A) demonstrated a significant reduction in progeny virus from supernatants in TG-treated samples, as expected. Treatment with 4μ8C alone at 10 μM or 30 μM resulted in partial suppression of IAV replication, although less effectively than TG. However, combining TG with 4μ8C further suppressed viral foci, indicating a potential additive effect. One-step PCR detection of the *M-gene* from IAV supernatants (Figure 4.12B) showed a similar trend, with TG alone significantly reducing viral RNA levels. 4μ8C at both concentrations also lowered *M-gene* detection, while the combination of TG with 4μ8C yielded the strongest suppression of viral RNA, further supporting the additive antiviral effects of TG and IRE1 inhibition. In RSV-infected cells, the one-step PCR detection of the *L-gene* (Figure 4.12C) revealed a significant reduction in viral RNA levels in TG-treated cells. 4μ8C alone also reduced *L-*

gene levels, albeit less effectively than TG. The combination of TG with 4μ8C at both concentrations again exhibited a stronger reduction in RSV replication compared to TG or 4μ8C alone, suggesting that inhibiting IRE1 enhances TG's antiviral efficacy against RSV.

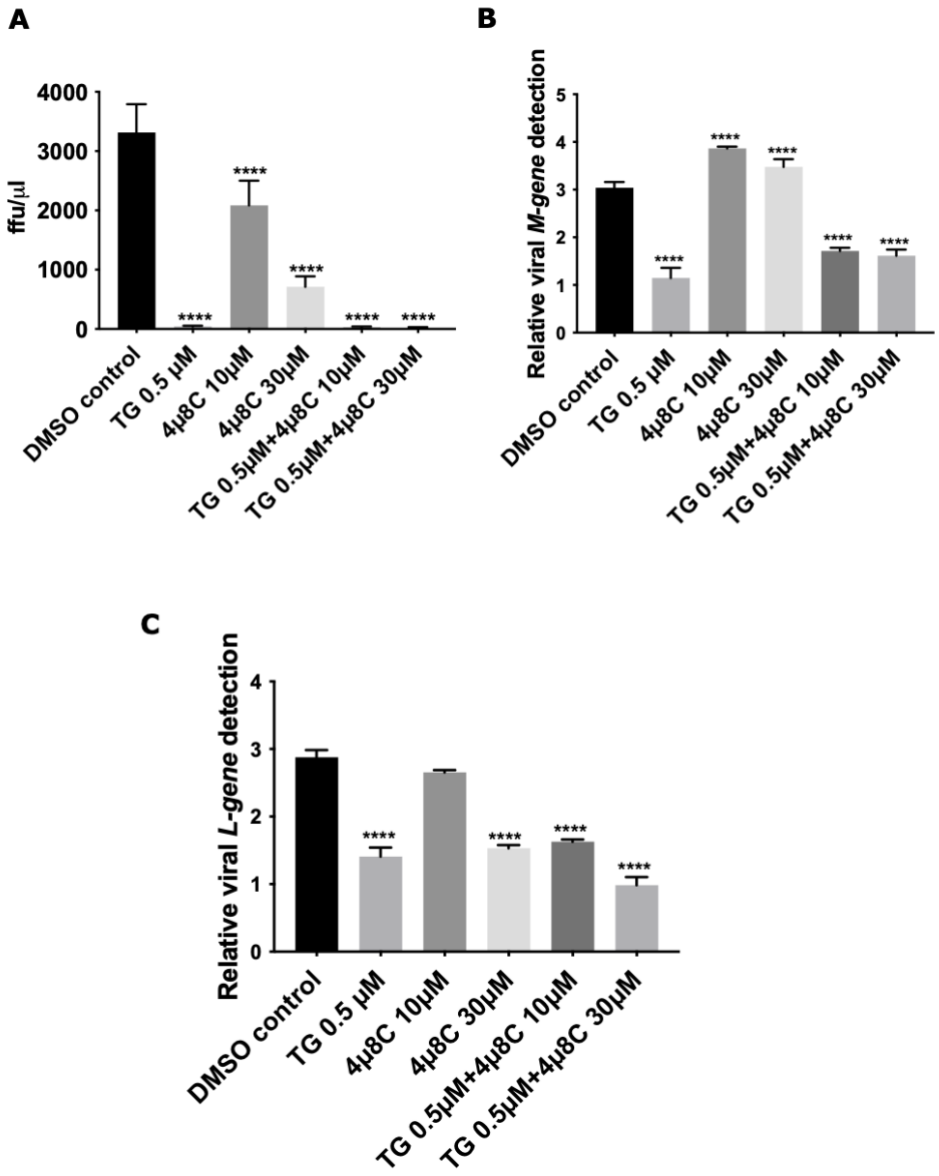

Figure 4.12 Effect of 4u8C on TG-induced antiviral activity in Calu-3 cells.

(A) Viral foci were quantified via immunostaining of supernatants from IAV-infected Calu-3 cells treated with DMSO, TG (0.5 μM), 4u8C (10 μM or 30 μM), or TG combined with 4u8C. (B) M-gene *RNA levels were measured via one-step PCR from IAV-infected supernatants under the same conditions. (C)* L-gene *RNA levels were quantified via one-step PCR from RSV-infected Calu-3 cells treated similarly. Statistical significance was determined using Sidak's multiple comparisons (****p < 0.0001).*

4.3.7 Exploring the Role of G3BP1 and PERK in TG-Induced Antiviral Responses Using Gene Knockdown in Calu-3 Cells

To investigate the contribution of *G3BP1* and *PERK* to the antiviral effects of TG, gene knockdown experiments were performed in Calu-3 cells using specific siRNAs. These experiments assessed whether the silencing of these key stress response genes altered TG's capacity to suppress RSV replication. The efficacy of *G3BP1* knockdown was first validated using qPCR (Figure 4.13A). At 20 pM siRNA, *G3BP1* expression was significantly reduced compared to the negative control, confirming the success of the knockdown. Following this validation, RSV infection was conducted in the presence of *G3BP1* siRNA with and without TG treatment. As shown in Figure 4.13B, TG treatment significantly reduced RSV *L-gene* expression in control cells, demonstrating its antiviral activity. However, *G3BP1* knockdown further amplified the suppression of the *L-gene*, indicating that silencing *G3BP1* enhanced TG's antiviral efficacy. Similarly, the impact of PERK knockdown was evaluated by infecting Calu-3 cells with RSV and assessing viral *L-gene* (Figure 4.13C) and *M-gene* (Figure 4.13D) expression. TG alone significantly reduced both viral genes in control cells, consistent with its established antiviral activity. PERK knockdown also suppressed viral gene expression independently of TG, suggesting that PERK contributes to RSV replication.

In contrast, in our IAV experiments, PERK knockdown alone was associated with an increase in viral M-gene expression, indicating that PERK can act as a restriction factor for IAV while appearing proviral for RSV in Calu-3 cells. This divergence likely reflects virus-specific dependencies on PERK–eIF2α signalling and differences in replication site and host-pathway usage (nuclear replication and cap-dependent translation for IAV versus cytoplasmic replication and ER-processing demands for RSV), as well as potential cell-type effects.

When PERK knockdown was combined with TG treatment, the reduction in L-gene and M-gene expression in RSV-infected cells was more pronounced than with either intervention alone, consistent with at least an additive effect.

These findings highlight the critical roles of *G3BP1* and PERK in regulating stress responses during RSV infection and their interplay with TG-induced antiviral mechanisms. The enhanced suppression of viral replication following *G3BP1* or PERK knockdown suggests that TG operates through both overlapping and independent pathways to inhibit viral replication. This underscores the potential for targeting these pathways in combination with TG to achieve maximal antiviral efficacy.

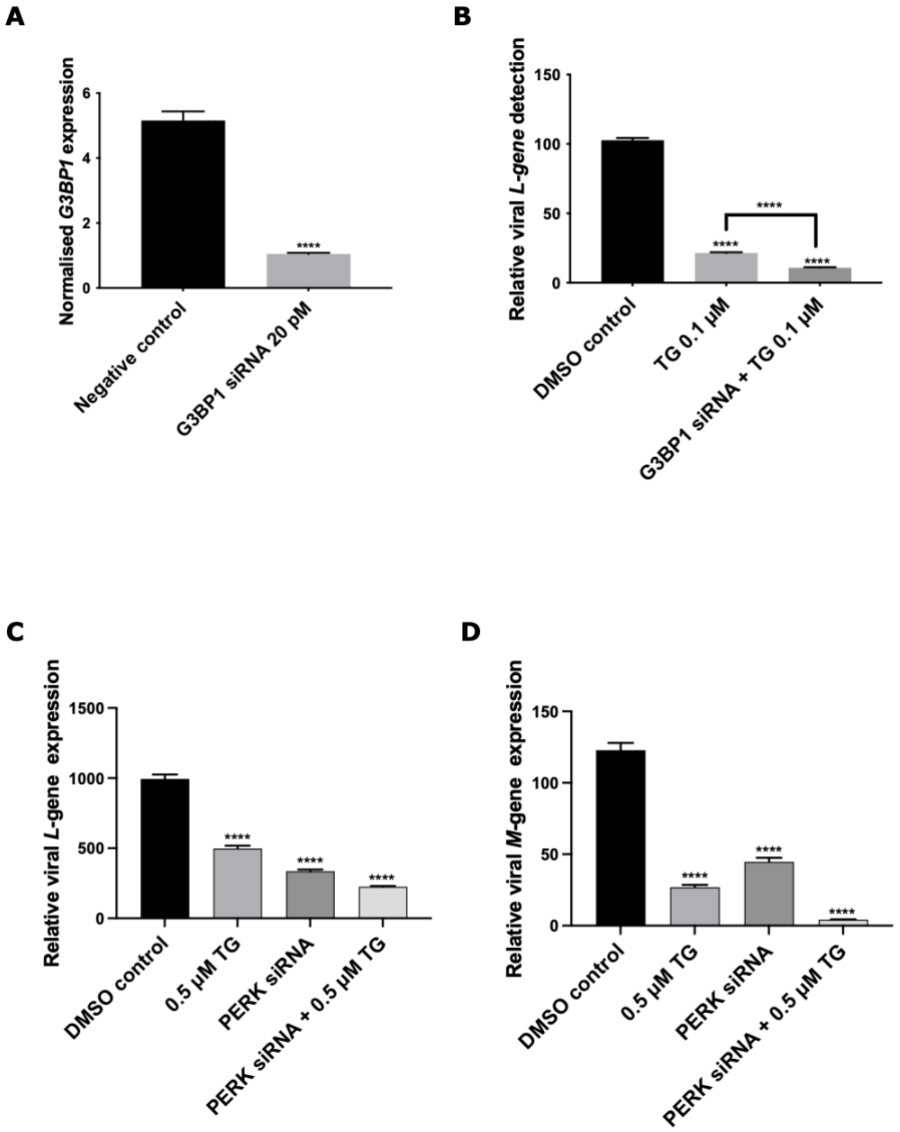

Figure 4.13 Role of* G3BP1 *and PERK in TG-induced antiviral responses in Calu-3 cells.

(A) G3BP1 *knockdown was confirmed by qPCR, following siRNA treatment (20 pM) compared to the negative control. (B) Viral* L-gene *expression was measured via qPCR in RSV-infected cells with* G3BP1 *knockdown, treated with or without TG (0.1 µM). Knockdown of* G3BP1 *amplified TG's antiviral suppression of* L-gene *expression. (C) Viral* L-gene *expression was quantified in RSV-infected cells with PERK knockdown, treated with or without TG (0.5 µM). PERK knockdown and TG treatment each reduced* L-gene *expression, with a synergistic effect observed when combined. (D) Viral* M-gene *expression was similarly quantified in RSV-infected cells with PERK knockdown, treated with or without TG. Both PERK knockdown and TG reduced* M-gene *expression, with the greatest suppression seen when combined. Statistical significance was determined using Sidak's multiple comparisons (****p < 0.0001). Note: "DMSO control" is a representative label for "Negative control siRNA."*

Discussion

This thesis explored how TG, a plant-derived sesquiterpene lactone, exerts potent antiviral activity against both RSV and IAV, including in conditions of co-infection. The primary motivation behind these investigations stemmed from longstanding concerns over rapidly evolving RNA viruses and their capacity to cause substantial health and economic burdens worldwide, as highlighted by numerous historical outbreaks (Burnet and Clark, 1942; Johnson and Mueller, 2002; Taubenberger and Morens, 2006; Wan and Perez, 2006). Despite the availability of selective antivirals, issues around drug resistance and the tendency of many viruses to adapt to virus-directed therapies have created an imperative to develop robust strategies that capitalize instead on host-specific mechanisms (Monteith et al., 2007). A central hypothesis of the present research was that TG's capacity to disrupt sarco-endoplasmic reticulum Ca^{2+}-ATPase (SERCA) activity and trigger endoplasmic reticulum (ER) stress could be harnessed to inhibit viral replication—an approach that does not rely on direct binding to a viral protein but on manipulation of host pathways essential for viral propagation. Across a variety of in vitro systems, the results systematically demonstrated TG's effectiveness against RSV and IAV, clarified some of the underlying cellular processes, and revealed its capacity to impede viral co-infection. Because co-infections may enable genetic exchange or modify tropism (Wan and Perez, 2006), a treatment that simultaneously curtails multiple viruses represents a significant step

forward in mitigating the challenges of emerging and re-emerging respiratory pathogens.

Central to the antiviral findings was a series of experiments confirming that short pulses of TG, in the micromolar or even submicromolar range, significantly reduced viral output without inducing major cytotoxicity. Historically, TG was discovered as a potent inhibitor of SERCA (Rasmussen et al., 1978; Smitt et al., 1996), a pump that maintains ER calcium levels critical to proper protein folding (Monteith et al., 2007). Depleting ER calcium stores forced cells into a state of stress that was evidently incompatible with efficient viral replication. Notably, it can be observed that different concentrations and durations of TG priming achieved consistently strong inhibition of both RSV and IAV replication, underscoring how interfering with calcium homeostasis appears to disrupt essential events in the viral life cycle. Although influenza A virus exploits host nuclear machinery during mRNA synthesis, both influenza A virus and RSV depend on host translation and ER-dependent protein processing (Cox and Subbarao, 1999). By contrast, RSV synthesises its mRNAs with its own polymerase complex in the cytoplasm. Consistent with this, our data show that even brief disruption of ER function severely impairs the viruses' ability to produce or properly fold their proteins. The results illustrate that viruses depend acutely on stable calcium gradients and the correct operation of the host's protein quality-control systems.

One of the most compelling outcomes emerged from experiments investigating the prophylactic angle: TG pretreatment of cells—often for just 30 minutes—was enough to suppress viral replication for extended

periods, even when infection was initiated a day or two afterward. This phenomenon provides insight into how triggering ER stress or the UPR early on can establish a durable antiviral state (Takemura et al., 1989; Putney, 1986). In effect, it was observed that once cells were “primed” by TG, they mounted innate defences that significantly reduced both RSV and IAV yields. The phenomenon persisted long after TG removal, which is notable because it suggests that even if TG itself is cleared from the system, the downstream effects—such as the expression of antiviral factors or changes in protein translation—can remain active. As infections with respiratory RNA viruses often spread rapidly (Cox and Subbarao, 1999), having a robust antiviral state that does not require continuous drug presence could be highly advantageous for both prophylactic and early post-exposure prophylaxis scenarios.

Further deepening the scope of the present work were assays with multiple cell types, including classic immortalised lines such as HEp-2 (for RSV), Calu-3, A549, NPTr and MDCK (for IAV quantification), as well as NHBE cells. The latter hold strong physiological relevance, given that RSV and IAV target the respiratory epithelium, and they also present higher sensitivity to external stressors than do immortalised lines. Although NHBE cells indeed required somewhat lower doses of TG for safe exposure, the same fundamental outcome prevailed: viral replication was substantially reduced, as evidenced by fewer plaques, lower gene transcription levels, and diminished viral protein expression. Such consistency across multiple in vitro models supports the view that TG’s activity is not an artefact confined to a single cell line but rather a

broader phenomenon relevant to the actual cells in the human respiratory tract (Amorim et al., 2011). Importantly, the congruence of the cytotoxicity data—showing that the TG concentrations with antiviral activity did not compromise cell viability—reinforces the notion that TG can be safely deployed at carefully controlled doses. Translation to therapeutic use in vivo, however, will depend on achieving effective airway exposure with minimal systemic distribution. A brief exposure can induce an antiviral programme that persists for at least 48 hours, suggesting that intermittent (pulsatile) dosing could maintain efficacy while limiting off-target exposure (Al-Beltagi et al., 2021). Because TG inhibits SERCA, inadvertent exposure of excitable and contractile tissues—particularly cardiomyocytes reliant on SERCA2a—could disturb Ca^{2+} handling and contractility; similar considerations apply to vascular and airway smooth muscle (Periasamy and Kalyanasundaram, 2007). These risks could be minimised by lung-targeted delivery (for example, inhaled formulations), short-contact dosing that exploits the durable antiviral state, and, where appropriate, tissue-selective prodrugs analogous to mipsagargin to restrict systemic activation (Mahalingam et al., 2016). In parallel, this thesis shows how TG compares with existing antivirals. Ribavirin is used as a benchmark for RSV, as it remains one of the few treatments clinically used against that virus. However, ribavirin's efficacy can be inconsistent, often requires prolonged exposure, and may entail toxicity (Knobler et al., 2005). The data showed that TG consistently outperformed ribavirin in terms of viral gene suppression and subsequent reduction in viral progeny, even though TG

was only applied briefly and then removed. This is a notable finding, not only because it demonstrates the pronounced potency of TG but also because it aligns with the principle that, if one successfully hinders the host pathways essential for viral replication rather than focusing on virus-specific targets, one might see more enduring antiviral effects with fewer opportunities for the virus to mutate away from drug pressure (Burnet and Clark, 1942; Monteith et al., 2007). The fact that a brief host-targeted stress induction can achieve levels of inhibition beyond those realised by a conventional antiviral underscores the potentially transformative character of TG and may prompt future optimisation of this strategy. A central mechanistic question was how TG-induced ER stress disables viruses. From the literature, it is known that viruses like RSV or IAV can manipulate certain aspects of the UPR for replication (Wan and Perez, 2006). For instance, moderate IRE1 activation may facilitate viral protein synthesis or assembly, whereas partial PERK activation might paradoxically help viruses by supporting folding of viral glycoproteins and transiently stabilising ER homeostasis. Nevertheless, once triggered beyond a certain threshold, the UPR can lead to translational attenuation, degrade the quality or quantity of nascent viral proteins, and even promote apoptosis of infected cells (Johnson and Mueller, 2002). The findings support this multi-stage interplay. A strong downregulation of viral transcription was observed in multiple readouts, and this can be mechanistically linked to UPR output as follows. First, PERK-mediated phosphorylation of eIF2α depresses global translation, which is expected to reduce synthesis of viral replicase components;

with fewer polymerase/cofactor proteins available, ongoing transcription and genome replication fall, giving lower *L*- and *M-gene* transcript levels. Second, IRE1 activation both splices XBP1 mRNA to enhance chaperone capacity and engages RNase-dependent decay (RIDD) of select ER-associated transcripts, a process that can reduce the stability of viral mRNAs directed to the secretory pathway. Third, ATF6 signalling augments ER-associated degradation and chaperone expression, limiting the maturation of viral glycoproteins (RSV F/G; IAV HA/NA) and thereby constraining assembly and budding. When sustained, these pressures also increase the probability of apoptosis in infected cells, further reducing the pool of cells capable of producing virus. Additionally, manipulation of selected host factors indicated that coordinated activation across IRE1, PERK and related stress/immune pathways is critical; the combined engagement produced a greater block to replication than single-pathway perturbation, consistent with the additive effects seen when PERK knockdown was combined with TG. Once these pathways are simultaneously engaged by a robust stress signal, it appears viruses cannot easily circumvent the blockade (Rota et al., 1990; Wan and Perez, 2006). An overview of this sequence is provided in Figure 5.1.

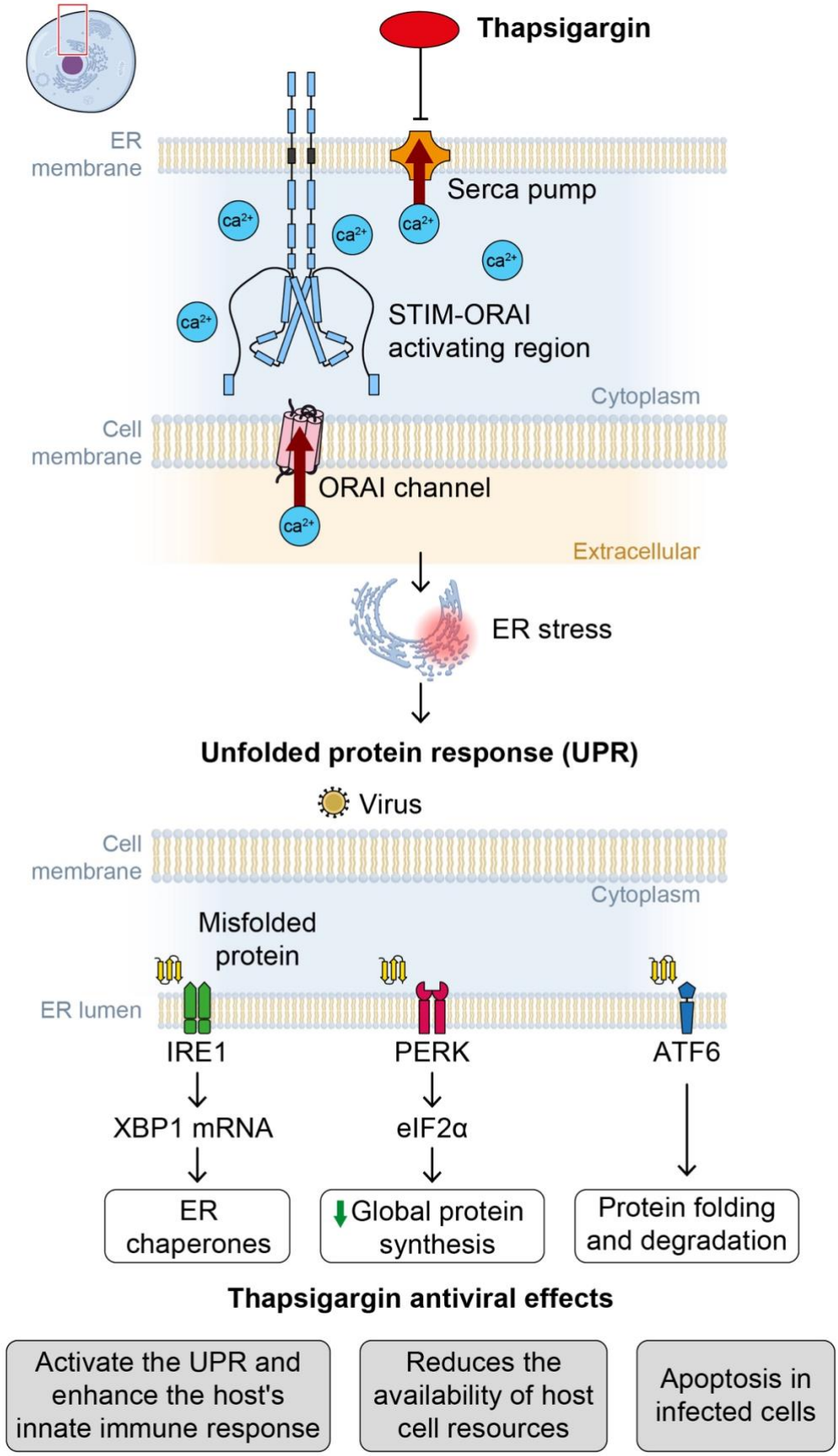

Figure 5.1 Schematic overview of TG-mediated UPR response against viral pathogen

Another fascinating piece of the data set pertains to co-infections. Experiments tested whether TG remained effective in inhibiting both RSV and IAV simultaneously, particularly because co-infected cells can exhibit enhanced or altered viral progeny profiles (Wan and Perez, 2006). In severe influenza seasons, patients may be susceptible to co-infection by RSV or other respiratory viruses. Co-infections have historically been underappreciated, yet they can facilitate gene segment reassortments or at least synergy that modifies virulence.

TG effectively limited replication of both viruses, lowering IAV and RSV gene output and final titres. In the co-infection model, each virus partially constrained the other, and TG further reduced the combined viral output. These in vitro data indicate that TG does not preferentially favour one virus; however, extrapolation to in vivo co-infection dynamics is not warranted from this system alone. From a broader perspective, a host-directed agent with activity against more than one respiratory virus could be valuable when multiple pathogens co-circulate. Historical observations suggest that concurrent pathogens may worsen outcomes in vulnerable hosts (Burnet and Clark, 1942). The critical requirement, therefore, is that antiviral activity is maintained across targets without unintentionally shifting the competitive balance between them—an attribute supported here by the absence of virus-specific escape in the co-infection assays. The durability of the antiviral state in post-infection settings was also examined. Prophylactic application prevented

subsequent infection, and post-infection administration retained substantial efficacy within a defined window. When infection was already well established, the benefit was reduced relative to prophylaxis, consistent with replication processes having progressed beyond points most sensitive to TG-induced stress responses. Even so, delayed administration within the first 24–48 hours still reduced viral titres, implying that once triggered, the host stress response can restrict replication at multiple steps. This aligns with the biology of acute respiratory infections, which typically have short incubation periods, and supports the rationale that early therapy is likely to be the most impactful (Knobler et al., 2005). Even if a fraction of cells had begun producing new virions, subsequent infection cycles in neighbouring cells appeared constrained by TG-induced stress.

Looking toward the broader relevance of these findings, an essential consideration is safety. Although ER stress induction is beneficial in undermining viral replication, it might pose risks if pushed too far, as pro-apoptotic cascades can become widely activated, threatening healthy tissue (Monteith et al., 2007). The consistent demonstration that certain concentrations of TG did not compromise cell viability suggests a broad therapeutic index in vitro, yet the real question is how this translates in vivo. In some earlier contexts, TG was noted for tumour cell cytotoxicity and has even been tested as a chemotherapeutic lead, precisely because it can kill cells with unbridled protein-folding demands (Smitt et al., 1996). But for an antiviral approach, one must carefully select or modulate dose regimens so as to hamper viral replication without

indiscriminately harming normal tissues. The in vitro success in calibrating TG exposure to safe and efficacious ranges is encouraging, as is the robust antiviral effect observed even at modest doses. Importantly, in vivo efficacy has already been shown: in lethal influenza A mouse challenge models, oral thapsigargin administered after infection reduced lung virus titres and improved survival, consistent with an acid-stable formulation suitable for brief dosing (Al-Beltagi et al., 2021; Goulding et al., 2020). These data support the feasibility of a short, pulsatile dosing strategy to trigger a transient antiviral state without prolonged exposure. Further exploration of pulmonary delivery, for example via nebulisation or dry-powder inhalation, could concentrate the drug in the lungs while limiting systemic exposure, as demonstrated for inhaled zanamivir (Peng, Milleri and Stein, 2000) and supported by trials of nebulised interferon-β (Monk et al., 2021), while still conferring strong localised protection.

Additionally, future directions might incorporate synergy with other host factors or established antivirals that target discrete stages of virus entry or assembly (Knobler et al., 2005). By combining TG-induced stress with a direct neuraminidase inhibitor or an RSV fusion blocker, for example, one might further minimize viral spread while lowering the dose of each agent—potentially reducing toxicity and limiting the emergence of resistance. The data in this thesis strongly suggest that host-based approaches can unify with virus-specific inhibitors in a complementary way, a strategy that, historically, has been deployed far less frequently than single-agent therapies. However, given the complexities of real-

world infection, especially in older adults or immunocompromised individuals, such combination strategies may prove valuable.

Besides the immediate translational angle, the present body of work opens a line of inquiry into precisely which stress or immune pathways most powerfully underlie TG's actions on RSV or IAV. Although TG is expected to perturb ER calcium via SERCA inhibition, ER Ca^{2+} depletion was not directly measured here; rather, the data show activation of ER-stress pathways linked to reduced viral replication, with virus-specific mechanisms still to be defined. The results found consistent outcomes across multiple assays—reduced ffu/ml, decreased viral mRNA, diminished protein expression—but do these viruses attempt to counter or modulate the host response in different ways? RSV, for instance, is known for forming large syncytia and for leveraging specialized inclusion bodies in the cytoplasm (Cox and Subbarao, 1999). IAV, meanwhile, coordinates a nuanced interplay of nuclear export signals, splicing events, and surface glycoprotein assembly (Rota et al., 1990). The fact that both viruses succumb strongly to TG indicates that their replication cycles converge on certain essential host dependencies that become unavailable under robust ER stress. Identifying precisely which steps in the life cycle are first affected—whether it is polymerase function, glycoprotein handling, or egress—could be crucial for further improvements in drug design.

It was also observed that the relevant host pathways may extend beyond the canonical branches of the UPR. For instance, the synergy or crosstalk between innate immune sensors (RIG-I–like receptors, for

example) and stress-induced factors (such as chaperones or redox modulators) likely amplifies the overall suppression of viruses. Historically, viruses have evolved ways to block or hijack innate immunity (Monteith et al., 2007). Our findings show that TG treatment consistently suppresses viral replication across assays. This suggests that further experimentation on TG might illuminate a continuum of host defences that link stress detection, immune surveillance, and metabolism. The conclusion from our studies of the co-infection scenario is that the baseline changes in the cell's translational environment and the structural changes in compartments critical to viral assembly (like the Golgi or ER) matter at least as much as direct induction of interferons (Burnet and Clark, 1942). Indeed, many of these results were consistent with the idea that broad disruptions in viral protein accumulation, rather than mere blocking of a single gene or protein, lead to the consistently powerful antiviral effect. From an epidemiological perspective, the consistent action of TG across viruses of such distinct families (Paramyxoviridae for RSV versus Orthomyxoviridae for influenza) is a strong argument for continuing to refine host-based approaches. Influenza A has long been recognized as a threat for pandemic emergence (Johnson and Mueller, 2002), while RSV causes significant illness in infants and the elderly (Cox and Subbarao, 1999). The diversity of these viruses' replication cycles is partly why so few broad-spectrum antivirals exist, particularly in the context of co-infections (Monteith et al., 2007). If the crucial factor uniting them is their reliance on an intact protein-folding environment, it follows that transiently biasing cells

towards a high-stress state that is less permissive to viral protein production may provide broad coverage. Because this strategy targets host processes rather than virus-encoded determinants, its activity may be less sensitive to sequence variation; however, this remains to be demonstrated across diverse strains and in appropriate in vivo models. Furthermore, if new emergent respiratory viruses—like certain coronaviruses—depend similarly on ER homeostasis, TG could hamper them as well (Al-Beltagi et al., 2021). This as relevant to future pandemic preparedness: a host-centric antiviral does not need prior knowledge of a virus's structural antigens or polymerase motifs. Instead, it preys on an unchanging Achilles heel of viral biology—namely, the requirement for correct protein handling in the host.

Of course, the leap from promising in vitro data to actual clinical interventions requires considering how well these results will translate in animals and, ultimately, in humans. Standard toxicology studies would need to confirm the margin between antiviral doses and cytotoxic thresholds in tissues. Pharmacokinetic analyses would clarify how quickly TG is distributed or cleared, and whether localized lung delivery via inhalation is feasible. Notwithstanding these practical constraints, the stability of TG-induced antiviral states that was observed in cell culture suggests that short exposures may suffice. That alone is an attractive property: rather than subjecting patients to continuous infusions or repeated dosing, one might administer a short pulse of TG in a controlled manner to produce an extended period of cellular resistance to infection. Coupling that approach with broad surveillance could, in theory, forestall

an outbreak at early stages. Indeed, short-stint prophylaxis for health care workers or vulnerable individuals might help them avoid infection in high-risk scenarios.

What stands out from the data collected is how frequently a single, relatively short TG priming induced a multi-day inhibition of RSV or IAV. The morphological shift to a “stress-laden” state, which was observed in certain cell lines, correlates well with the decreased production of viral particles. Although it remains to be validated that the same morphological or molecular changes operate in the complex environment of a living lung, the strong parallels observed across the different cell lines tested—NHBE, A549, HEp-2, Calu-3, and others—provide reassurance that the phenomenon is not restricted to an experimental anomaly (Monteith et al., 2007). It should also be noted that in everyday life, airway epithelial cells do endure a variety of mild insults, including changing oxygen levels, pollutants, and inflammatory signals. Our demonstration that these cells can cope with TG stress while mounting antiviral defences adds to the plausibility that carefully dosed TG therapy would be tolerated in the actual airway environment.

Perhaps most revealing is the perspective gleaned from co-infection experiments. Dual RSV–IAV infections, while not the most common scenario, can enhance morbidity if they do occur, and they exemplify the challenge of dealing with multiple pathogens at once. Conventional direct-acting antivirals have to be carefully combined to cover more than one virus, and each virus could still evolve resistance to its specific inhibitor (Wan and Perez, 2006). Our data, by contrast, showed that TG

effectively suppressed both viruses in tandem, thus diminishing overall viral loads in co-infected cells and presumably reducing the probability of synergy or pseudotyping. In real-world epidemics, it is not unusual for individuals to harbour more than one respiratory virus, especially in crowded or high-contact settings (Knobler et al., 2005). Having a single drug that blocks multiple viruses is, therefore, a major advantage. Even if some respiratory viruses are partially or minimally affected, the overall burden and risk of viral complementation might be lower.

Taking a historical lens, one can see that the largest and most consequential influenza outbreaks, such as the 1918 “Spanish flu,” the 1957 “Asian flu,” and others, were associated with co-infections by bacterial or viral agents exacerbating disease severity (Burnet and Clark, 1942; Johnson and Mueller, 2002). Although the primary impetus for many vaccine and therapeutic efforts has been to target single pathogens, our findings serve as a reminder that broad-spectrum strategies remain crucial in preparedness. The data here thus feed into a larger conversation: the future of antiviral development might not rely exclusively on virus-specific small molecules, but rather on harnessing stress or innate immunity in a measured manner. While it is undeniable that virus-specific strategies continue to be essential—particularly for post-exposure prophylaxis or in advanced infection—these results showcase that a host-based approach like TG can function in prophylaxis, early-stage, and co-infection contexts with a single mechanistic principle.

In summary, this thesis has demonstrated the robust antiviral effects of TG against RSV and IAV across multiple in vitro models. Short pulses of TG at non-cytotoxic doses strongly suppress viral protein synthesis, reduce viral plaque formation, and curtail gene expression associated with progeny virions. The efficacy extends to co-infection scenarios, suggesting that the therapy could limit complications arising from the simultaneous presence of more than one virus. The crux of TG's success appears to lie in its capacity to elevate ER stress to levels that viruses cannot withstand, thereby preventing them from efficiently folding and assembling their structural and enzymatic proteins. By leveraging a fundamental host function, TG essentially places the virus at a disadvantage that is difficult for it to circumvent by simple mutational changes. Yet challenges remain in precisely calibrating the drug's dosage to ensure safety in a complex organism, and more data are needed about how TG might be administered in a targeted fashion to spare healthy tissues from excessive stress. Still, the body of data compiled here strongly positions TG among the leading candidates for a new wave of host-centric antivirals, demonstrating that controlled ER stress can decisively hinder multiple respiratory RNA viruses. The broader implications for pandemic preparedness, prophylactic interventions, and synergy with existing inhibitors are substantial, and they point the way to clinical evaluations of TG formulations, potentially in combination with protective strategies against other viruses or secondary pathogens. Ultimately, the findings underscore the power of turning the cell's own stress machinery against invading viruses, setting

a precedent for novel antiviral strategies that strike at the interface of protein homeostasis and immunity.

REFERENCES

Adachi, Y., Yamamoto, K., Okada, T., Yoshida, H., Harada, A. and Mori, K. (2008) 'ATF6 is a transcription factor specialising in the regulation of quality control proteins in the endoplasmic reticulum', Cell Structure and Function, 33(1), pp. 75–89. doi:10.1247/csf.07044.

Akkina, R.K., Walton, R.M., Chen, M.L., Li, Q.X., Planelles, V. and Chen, I.S.Y. (1996) 'High-efficiency gene transfer into CD34+ cells with a human immunodeficiency virus type 1-based retroviral vector pseudotyped with vesicular stomatitis virus envelope glycoprotein G', Journal of Virology, 70(4), pp. 2581–2585. doi:10.1128/jvi.70.4.2581-2585.1996.

Al-Beltagi, S., Preda, C.A., Goulding, L.V., James, J., Pu, J., Skinner, P., Jiang, Z., Wang, B.L., Yang, J., Banyard, A.C., Mellits, K.H., Gershkovich, P., Hayes, C.J., Nguyen-Van-Tam, J., Brown, I.H., Liu, J. and Chang, K.-C. (2021) 'Thapsigargin is a broad-spectrum inhibitor of major human respiratory viruses: coronavirus, respiratory syncytial virus and influenza A virus', Viruses, 13(2), p. 234. doi:10.3390/v13020234.

Ali, H., Christensen, S.B., Foreman, J.C., Pearce, F.L., Piotrowski, W. and Thastrup, O. (1985) 'The ability of thapsigargin and thapsigargicin to activate cells involved in the inflammatory response', British Journal of Pharmacology, 85(3), pp. 705–712. doi:10.1111/j.1476-5381.1985.tb10567.x.

Amorim, M.J., Bruce, E.A., Read, E.K.C., Foeglein, Á., Mahen, R., Stuart, A.D. and Digard, P. (2011) 'A Rab11- and microtubule-dependent mechanism for cytoplasmic transport of influenza A virus viral RNA', Journal of Virology, 85(9), pp. 4143–4156. doi:10.1128/jvi.02606-10.

Andersen, T., Husted, A., Nygaard, S., Weng, S., Christensen, S.B. and Møller, J.V. (2015) 'Thapsigargin—from Thapsia L. to mipsagargin', Molecules, 20(4), pp. 6113–6127. doi:10.3390/molecules20046113.

Andrei, G. (2021) 'Vaccines and antivirals: Grand challenges and great opportunities', Frontiers in Virology, 1, 666548. doi:10.3389/fviro.2021.666548.

Anelli, T. and Sitia, R. (2008) 'Protein quality control in the early secretory pathway', The EMBO Journal, 27(2), pp. 315–327. doi:10.1038/sj.emboj.7601974.

Arranz, R., Coloma, R., Chichón, F.J., Conesa, J.J., Carrascosa, J.L., Valpuesta, J.M., Ortín, J. and Martín-Benito, J. (2012) 'The structure of native influenza virion ribonucleoproteins', Science, 338(6114), pp. 1634–1637. doi:10.1126/science.1228172.

Ascough, S., Paterson, S. and Chiu, C. (2018) 'Induction and subversion of human protective immunity: contrasting influenza and respiratory syncytial virus', Frontiers in Immunology, 9, 323. doi:10.3389/fimmu.2018.00323.

Asha, K. and Kumar, B. (2019) 'Emerging influenza D virus threat: what we know so far!', Journal of Clinical Medicine, 8(2), p. 192. doi:10.3390/jcm8020192.

Atkins, K.E. and Hodgson, D. (2023) 'Vaccination of older adults against respiratory syncytial virus: the final pieces of the puzzle', Clinical Infectious Diseases, 77(3), pp. 490–491. doi:10.1093/cid/ciad162.

Baharom, F., Thomas, O.S., Lepzien, R., Mellman, I., Chalouni, C. and Smed-Sörensen, A. (2017) 'Visualisation of early influenza A virus trafficking in human dendritic cells using STED microscopy', PLOS ONE, 12(6), p. e0177920. doi:10.1371/journal.pone.0177920.

Baker, R.E., Mahmud, A.S., Wagner, C.E., Yang, W., Pitzer, V.E., Viboud, C., Vecchi, G.A., Metcalf, C.J.E. and Grenfell, B.T. (2019) 'Epidemic dynamics of respiratory syncytial virus in current and future climates', Nature Communications, 10(1), 5512. doi:10.1038/s41467-019-13562-y.

Bakre, A.A., Harcourt, J.L., Haynes, L.M., Anderson, L.J. and Tripp, R.A. (2017) 'The central conserved region (CCR) of respiratory syncytial virus (RSV) G protein modulates host miRNA expression and alters the cellular response to infection', Vaccines, 5(3), p. 16. doi:10.3390/vaccines5030016.

Ball, M., Andrews, S.P., Wierschem, F., Cleator, E., Smith, M.D. and Ley, S.V. (2007) 'Total synthesis of thapsigargin, a potent SERCA pump inhibitor', Organic Letters, 9(4), pp. 663–666. doi:10.1021/ol062947x.

Barik, S. (2013) 'Respiratory syncytial virus mechanisms to interfere with type I interferons', Current Topics in Microbiology and Immunology, 372, pp. 173–191. doi:10.1007/978-3-642-38919-1_9.

Bauer, F. (2018) Thapsia garganica, Digital Bodleian – Flora and Fauna Graeca. Bodleian Libraries, University of Oxford. Available at: digital.bodleian.ox.ac.uk/collections/flora-and-fauna-graeca/ (Accessed: 27 February 2023).

Bauernfeind, F.G., Horvath, G., Stutz, A., Alnemri, E.S., MacDonald, K., Speert, D., Fernandes-Alnemri, T., Wu, J., Monks, B.G., Fitzgerald, K.A., Hornung, V. and Latz, E. (2009) 'Cutting edge: NF-κB activating pattern recognition and cytokine receptors license NLRP3 inflammasome activation by regulating NLRP3 expression', The Journal of Immunology, 183(2), pp. 787–791. doi:10.4049/jimmunol.0901363.

Bawage, S.S., Tiwari, P.M., Pillai, S. and Dennis, V.A. (2013) 'Recent advances in diagnosis, prevention, and treatment of human respiratory syncytial virus', Advances in Virology, 2013, 595768. doi:10.1155/2013/595768.

Bedi, S. and Ono, A. (2019) 'Friend or foe: the role of the cytoskeleton in influenza A virus assembly', Viruses, 11(1), p. 46. doi:10.3390/v11010046.

Benitez, A.A., Panis, M., Xue, J., Varble, A., Shim, J.V., Frick, A.L., López, C.B. and tenOever, B.R. (2015) 'In vivo RNAi screening identifies MDA5 as a significant contributor to the cellular defence against influenza A virus', Cell Reports, 11(11), pp. 1714–1726. doi:10.1016/j.celrep.2015.05.032.

Berera, D. and Zambon, M. (2013) 'Antivirals in the 2009 pandemic—lessons and implications for future strategies', Influenza and Other Respiratory Viruses, 7(Suppl. 3), pp. 72–79. doi:10.1111/irv.12172.

Bermingham, A. and Collins, P.L. (1999) 'The M2-2 protein of human respiratory syncytial virus is a regulatory factor involved in the balance between RNA replication and transcription', Proceedings of the National Academy of Sciences of the United States of America, 96(20), pp. 11259–11264. doi:10.1073/pnas.96.20.11259.

Berna-Erro, A., Braun, A., Kraft, R., Kleinschnitz, C., Schuhmann, M.K., Stegner, D., Wultsch, T., Eilers, J., Meuth, S.G., Stoll, G., Nieswandt, B. and Freichel, M. (2017) 'Role of STIM2 in cell function and physiopathology', The Journal of Physiology, 595(10), pp. 3111–3128. doi:10.1113/jp273889.

Bernales, S., Papa, F.R. and Walter, P. (2006) 'Intracellular signalling by the unfolded protein response', Annual Review of Cell and Developmental Biology, 22(1), pp. 487–508. doi:10.1146/annurev.cellbio.21.122303.120200.

Berridge, M.J., Lipp, P. and Bootman, M.D. (2000) 'The versatility and universality of calcium signalling', Nature Reviews Molecular Cell Biology, 1(1), pp. 11–21. doi:10.1038/35036035.

Bertherand, E.L. (1857) 'Notice sur la résine de Thapsia garganica et son emploi comme emplâtre révulsif', Journal de Médecine, de Chirurgie et de Pharmacologie, 24, pp. 273–274.

Biondo, C., Lentini, G., Beninati, C. and Teti, G. (2019) 'The dual role of innate immunity during influenza', Biomedical Journal, 42(1), pp. 8–18. doi:10.1016/j.bj.2018.12.009.

Bohmwald, K., Gálvez, N.M.S., Ríos, M. and Kalergis, A.M. (2019) 'Contribution of cytokines to tissue damage during human respiratory syncytial virus infection', Frontiers in Immunology, 10, 452. doi:10.3389/fimmu.2019.00452.

Boni, M.F., Lemey, P., Jiang, X., Lam, T.T.-Y., Perry, B.W., Castoe, T.A., Rambaut, A. and Suchard, M.A. (2020) 'Evolutionary origins of the SARS-CoV-2 sarbecovirus lineage responsible for the COVID-19 pandemic', Nature Microbiology, 5(11), pp. 1408–1417. doi:10.1038/s41564-020-0771-4.

Böttcher, E., Freuer, C., Steinmetzer, T., Klenk, H.-D. and Garten, W. (2006) 'Proteolytic activation of influenza viruses by serine proteases TMPRSS2 and HAT from human airway epithelium', Journal of Virology, 80(19), pp. 9896–9898. doi:10.1128/jvi.01118-06.

Boyer, J.-C. and Haenni, A.-L. (1994) 'Infectious transcripts and cDNA clones of RNA viruses', Virology, 198(2), pp. 415–426. doi:10.1006/viro.1994.1053.

Benitez, A.A., Panis, M., Xue, J., Varble, A., Shim, J.V., Frick, A.L., López, C.B. and tenOever, B.R. (2015) 'In vivo RNAi screening identifies MDA5 as a significant contributor to the cellular defence against influenza A virus', Cell Reports, 11(11), pp. 1714–1726. doi:10.1016/j.celrep.2015.05.032.

Berera, D. and Zambon, M. (2013) 'Antivirals in the 2009 pandemic—lessons and implications for future strategies', Influenza and Other Respiratory Viruses, 7(Suppl. 3), pp. 72–79. doi:10.1111/irv.12172.

Bermingham, A. and Collins, P.L. (1999) 'The M2-2 protein of human respiratory syncytial virus is a regulatory factor involved in the balance between RNA replication and transcription', Proceedings of the National Academy of Sciences of the United States of America, 96(20), pp. 11259–11264. doi:10.1073/pnas.96.20.11259.

Berna-Erro, A., Braun, A., Kraft, R., Kleinschnitz, C., Schuhmann, M.K., Stegner, D., Wultsch, T., Eilers, J., Meuth, S.G., Stoll, G., Nieswandt, B. and Freichel, M. (2017) 'Role of STIM2 in cell function and physiopathology', The Journal of Physiology, 595(10), pp. 3111–3128. doi:10.1113/jp273889.

Bernales, S., Papa, F.R. and Walter, P. (2006) 'Intracellular signalling by the unfolded protein response', Annual Review of Cell and Developmental Biology, 22(1), pp. 487–508. doi:10.1146/annurev.cellbio.21.122303.120200.

Berridge, M.J., Lipp, P. and Bootman, M.D. (2000) 'The versatility and universality of calcium signalling', Nature Reviews Molecular Cell Biology, 1(1), pp. 11–21. doi:10.1038/35036035.

Bertherand, E.L. (1857) 'Notice sur la résine de Thapsia garganica et son emploi comme emplâtre révulsif', Journal de Médecine, de Chirurgie et de Pharmacologie, 24, pp. 273–274.

Biondo, C., Lentini, G., Beninati, C. and Teti, G. (2019) 'The dual role of innate immunity during influenza', Biomedical Journal, 42(1), pp. 8–18. doi:10.1016/j.bj.2018.12.009.

Bohmwald, K., Gálvez, N.M.S., Ríos, M. and Kalergis, A.M. (2019) 'Contribution of cytokines to tissue damage during human respiratory syncytial virus infection', Frontiers in Immunology, 10, 452. doi:10.3389/fimmu.2019.00452.

Boni, M.F., Lemey, P., Jiang, X., Lam, T.T.-Y., Perry, B.W., Castoe, T.A., Rambaut, A. and Suchard, M.A. (2020) 'Evolutionary origins of the SARS-CoV-2 sarbecovirus lineage responsible for the COVID-19 pandemic', Nature Microbiology, 5(11), pp. 1408–1417. doi:10.1038/s41564-020-0771-4.

Böttcher, E., Freuer, C., Steinmetzer, T., Klenk, H.-D. and Garten, W. (2006) 'Proteolytic activation of influenza viruses by serine proteases TMPRSS2 and HAT from human airway epithelium', Journal of Virology, 80(19), pp. 9896–9898. doi:10.1128/jvi.01118-06.

Boyer, J.-C. and Haenni, A.-L. (1994) 'Infectious transcripts and cDNA clones of RNA viruses', Virology, 198(2), pp. 415–426. doi:10.1006/viro.1994.1053.

Brandman, O., Liou, J., Park, W.S. and Meyer, T. (2007) 'STIM2 is a feedback regulator that stabilizes basal cytosolic and endoplasmic reticulum Ca2+ levels', Cell, 131(7), pp. 1327–1339. doi:10.1016/j.cell.2007.11.039.

Breen, M., Nogales, A., Baker, S.F. and Martínez-Sobrido, L. (2016) 'Replication-competent influenza A viruses expressing reporter genes', Viruses, 8(7), 179. doi:10.3390/v8070179.

Breskin, A., Adimora, A.A. and Westreich, D. (2017) 'Women and HIV in the United States', PLOS ONE, 12(2), e0172367. doi:10.1371/journal.pone.0172367.

Brown, D. and Rose, J. (1992) 'Sorting of GPI-anchored proteins to glycolipid-enriched membrane subdomains during transport to the apical cell surface', Trends in Cell Biology, 2(5), p. 132. doi:10.1016/0962-8924(92)90095-5.

Brown, G., Rixon, H., Steel, J., McDonald, T., Pitt, A., Graham, S. and Sugrue, R. (2005) 'Evidence for an association between heat shock protein 70 and the respiratory syncytial virus polymerase complex within lipid-raft membranes during virus infection', Virology, 338(1), pp. 69–80. doi:10.1016/j.virol.2005.05.004.

Buckley, B.J. and Whorton, A.R. (1997) 'Tunicamycin increases intracellular calcium levels in bovine aortic endothelial cells', American Journal of Physiology – Cell Physiology, 273(4), pp. C1298–C1305. doi:10.1152/ajpcell.1997.273.4.C1298.

Burnet, F. and Clark, E. (1942) 'Influenza: a survey of the last 50 years in the light of modern work on the virus of epidemic influenza', JAMA: The Journal of the American Medical Association, 120(5), p. 408. doi:10.1001/jama.1942.02830400082031.

Byerly, C.R. (2010) 'The U.S. military and the influenza pandemic of 1918–1919', Public Health Reports, 125(Suppl. 3), pp. 81–91. doi:10.1177/00333549101250S311.

Böttcher-Friebertshäuser, E., Garten, W., Matrosovich, M. and Klenk, H.-D. (2014) 'The hemagglutinin: a determinant of pathogenicity', in Compans, R.W. and Oldstone, M.B.A. (eds) Influenza Pathogenesis and Control – Volume I. Current Topics in Microbiology and Immunology, 385. Cham: Springer, pp. 3–34. doi:10.1007/82_2014_384.

Caly, L., Ghildyal, R. and Jans, D.A. (2015) 'Respiratory virus modulation of host nucleocytoplasmic transport; target for therapeutic intervention?', Frontiers in Microbiology, 6, 848. doi:10.3389/fmicb.2015.00848.

Caminade, C., McIntyre, K.M. and Jones, A.E. (2018) 'Impact of recent and future climate change on vector-borne diseases', Annals of the New York Academy of Sciences, 1436(1), pp. 157–173. doi:10.1111/nyas.13950.

Campbell-Yesufu, O.T. and Gandhi, R.T. (2011) 'Update on human immunodeficiency virus (HIV)-2 infection', Clinical Infectious Diseases, 52(6), pp. 780–787. doi:10.1093/cid/ciq248.

Canedo-Marroquín, G., Acevedo-Acevedo, O., León, M.A., Gómez, R.S., Salazar-Ardiles, C., Bueno, S.M., Kalergis, A.M. and Bozinovic, F. (2017) 'Modulation of host immunity by human respiratory syncytial virus virulence factors: a synergic inhibition of both innate and adaptive immunity', Frontiers in Cellular and Infection Microbiology, 7, 367. doi:10.3389/fcimb.2017.00367.

Carlson, C.J., Albery, G.F., Merow, C., Trisos, C.H., Zipfel, C.M., Eskew, E.A., Olival, K.J., Ross, N., Bansal, S. and Gehman, A.-L.M. (2020) 'Climate change will drive novel cross-species viral transmission', bioRxiv [Preprint]. doi:10.1101/2020.01.24.918755.

Carrasco-Hernandez, R., Jácome, R., López Vidal, Y. and Ponce de León, S. (2017) 'Are RNA viruses candidate agents for the next global pandemic? A review', ILAR Journal, 58(3), pp. 343–358. doi:10.1093/ilar/ilx026.

Carromeu, C., Simabuco, F.M., Tamura, R.E., Farinha Arcieri, L.E., Ventura, A.M. and Bianconi, M.L. (2007) 'Intracellular localization of human respiratory syncytial virus L protein', Archives of Virology, 152(12), pp. 2259–2263. doi:10.1007/s00705-007-1048-4.

Cascella, M., Rajnik, M., Aleem, A., Dulebohn, S.C. and Di Napoli, R. (2022) 'Features, evaluation, and treatment of coronavirus (COVID-19)', StatPearls Publishing [Preprint]. Available at: https://www.ncbi.nlm.nih.gov/books/NBK554776/ (Accessed: 24 August 2022).

Caul, E.O., Smyth, E.T.M., Clarke, S.K.R., Egglestone, S.I. and Darville, J.M. (1976) 'A comparison of influenza and respiratory syncytial virus infections among infants admitted to hospital with acute respiratory infections', Journal of Hygiene, 77(3), pp. 383–392. doi:10.1017/s0022172400055765.

Centers for Disease Control and Prevention (CDC) (2009) 'Update: infections with a swine-origin influenza A (H1N1) virus — United States and other countries', Morbidity and Mortality Weekly Report, 58(16), pp. 453–458. Available at: https://www.cdc.gov/mmwr/preview/mmwrhtml/mm5816a5.htm (Accessed: 11 August 2022).

Cervantes-Ortiz, S., Zamorano Cuervo, N. and Grandvaux, N. (2016) 'Respiratory syncytial virus and cellular stress responses: impact on replication and physiopathology', Viruses, 8(5), p. 124. doi:10.3390/v8050124.

Chaipan, C., Kobasa, D., Bertram, S., Glowacka, I., Steffen, I., Tsegaye, T.S., Takeda, M., Bugge, T.H., Kim, S., Park, Y., Marzi, A., Pöhlmann, S. and Simmons, G. (2009) 'Proteolytic activation of the 1918 influenza virus hemagglutinin', Journal of Virology, 83(7), pp. 3200–3211. doi:10.1128/jvi.02205-08.

Chan, J.F.-W., Kok, K.-H., Zhu, Z., Chu, H., To, K.K.-W., Yuan, S., Yuen, K.-Y. (2020) 'Genomic characterization of the 2019 novel human-pathogenic coronavirus isolated from a patient with atypical pneumonia after visiting Wuhan', Emerging Microbes & Infections, 9(1), pp. 221–236. doi:10.1080/22221751.2020.1719902.

Chan, J.F.-W., Yuan, S., Kok, K.-H., To, K.K.-W., Chu, H., Yang, J., Xing, F., Liu, J., Yip, C.C.-Y., Poon, R.W.-S., Tsoi, H.-W., Lo, S.K.-F., Chan, K.-H., Poon, V.K.-M., Chan, W.-M., Ip, J.D., Cai, J.-P., Cheng, V.C.-C., Chen, H., Hui, C.K.-M. and Yuen, K.-Y. (2020) 'A familial cluster of pneumonia associated with the 2019 novel coronavirus indicating person-to-person transmission: a study of a family cluster', The Lancet, 395(10223), pp. 514–523. doi:10.1016/s0140-6736(20)30154-9.

Chan, S. and Egan, P.A. (2005) 'Hepatitis C virus envelope proteins regulate CHOP via induction of the unfolded protein response', The FASEB Journal, 19(11), pp. 1510–1512. doi:10.1096/fj.04-3455fje.

Chaudhuri, S., Symons, J.A. and Deval, J. (2018) 'Innovation and trends in the development and approval of antiviral medicines: 1987–2017 and beyond', Antiviral Research, 155, pp. 76–88. doi:10.1016/j.antiviral.2018.05.005.

Chen, B.J. and Lamb, R.A. (2008) 'Mechanisms for enveloped virus budding: can some viruses do without an ESCRT?', Virology, 372(2), pp. 221–232. doi:10.1016/j.virol.2007.11.008.

Chen, B.J., Leser, G.P., Morita, E. and Lamb, R.A. (2007) 'Influenza virus hemagglutinin and neuraminidase, but not the matrix protein, are required for assembly and budding of plasmid-derived virus-like particles', Journal of Virology, 81(13), pp. 7111–7123. doi:10.1128/jvi.00361-07.

Chen, D. and Evans, P.A. (2017) 'A concise, efficient and scalable total synthesis of thapsigargin and nortrilobolide from (R)-(−)-carvone', Journal of the American Chemical Society, 139(17), pp. 6046–6049. doi:10.1021/jacs.7b01734.

Chen, S., Zhang, J., Fang, S., Wang, J., Cui, Y., Xiao, M., Li, S. and Wang, J. (2015) 'Endoplasmic reticulum stress and store-operated calcium entry contribute to usnic acid-induced toxicity in hepatic cells', Toxicological Sciences, 146(1), pp. 116–126. doi:10.1093/toxsci/kfv075.

Cheng, V.C.C., Lau, S.K.P., Woo, P.C.Y. and Yuen, K.-Y. (2013) 'Clinical management and infection control of SARS: lessons learned', Antiviral Research, 100(2), pp. 407–419. doi:10.1016/j.antiviral.2013.08.016.

Chenon, M., Camborde, L., Cheminant, S., Jupin, I. and Martin, C. (2011) 'A viral deubiquitylating enzyme targets viral RNA-dependent RNA polymerase and affects viral infectivity', The EMBO Journal, 31(3), pp. 741–753. doi:10.1038/emboj.2011.424.

Chlanda, P., Schraidt, O., Kummer, S., Richert, L., Veith, T., Bleck, C.-K.E., Weissenhorn, W. and Rohr, K. (2015) 'Structural analysis of the roles of influenza A virus membrane-associated proteins in assembly and morphology', Journal of Virology, 89(17), pp. 8957–8966. doi:10.1128/jvi.00592-15.

Christensen, S.B., Andersen, A., Smitt, U.W., Nissen, P., Thastrup, O., Foder, B. and Bjerrum, P.J. (1982) 'Thapsigargin and thapsigargicin, two histamine liberating sesquiterpene lactones from Thapsia garganica. X-ray analysis of the 7,11-epoxide of thapsigargin', The Journal of Organic Chemistry, 47(4), pp. 649–652. doi:10.1021/jo00343a009.

Christensen, S.B., Jensen, R.B., Sørensen, T., Purup, S., Thastrup, O., Møller, J.V. and Nissen, P. (2021) 'From plant to patient: thapsigargin, a tool for understanding natural product chemistry, total syntheses, biosynthesis, taxonomy, ATPases, cell death, and drug development', Progress in the Chemistry of Organic Natural Products, 115, pp. 59–114. doi:10.1007/978-3-030-64853-4_2.

Christensen, S.B., Andersen, A. and Smitt, U.W. (1997) 'Sesquiterpenoids from Thapsia species and medicinal chemistry of the thapsigargins', Fortschritte der Chemie organischer Naturstoffe / Progress in the Chemistry of Organic Natural Products, 71, pp. 129–167. doi:10.1007/978-3-7091-6529-4_2.

Chu, H., Liu, S., Deng, J., Sun, Y., Ji, J., Chai, Y., Zhang, X., He, J., Li, J., Tian, L., Zhao, J., Wang, X. and Chen, X. (2016) 'Scalable synthesis of (−)-thapsigargin', ACS Central Science, 3(1), pp. 47–51. doi:10.1021/acscentsci.6b00313.

Cockburn, C., Delon, P.J. and Ferreira, W. (1969) 'Origin and progress of the 1968–69 Hong Kong influenza epidemic', Bulletin of the World Health Organization [Preprint].

Cohen, M.S., Chen, Y.Q., McCauley, M., Gamble, T., Hosseinipour, M.C., Kumarasamy, N., Hakim, J.G., Kumwenda, J., Grinsztejn, B., Pilotto, J.H.S., Godbole, S.V., Mehendale, S., Chariyalertsak, S., Santos, B.R., Mayer, K.H., Hoffman, I.F., Eshleman, S.H., Piwowar-Manning, E., Wang, L., Makhema, J., Mills, L.A., de Bruyn, G., Sanne, I., Eron, J., Gallant, J., Havlir, D., Swindells, S., Ribaudo, H., Elharrar, V., Burns, D., Taha, T.E., Nielsen-Saines, K., Celentano, D.D., Essex, M. and Fleming, T.R. (2016) 'Antiretroviral therapy for the prevention of HIV-1 transmission', New England Journal of Medicine, 375(9), pp. 830–839. doi:10.1056/nejmoa1600693.

Collignon, P. (2010) 'H1N1 immunisation: too much too soon?', Australian Prescriber, 33(2), pp. 30–31. doi:10.18773/austprescr.2010.011.

Collins, P.L. and Graham, B.S. (2007) 'Viral and host factors in human respiratory syncytial virus pathogenesis', Journal of Virology, 82(5), pp. 2040–2055. doi:10.1128/jvi.01625-07.

Collins, P.L. and Melero, J.A. (2011) 'Progress in understanding and controlling respiratory syncytial virus: still crazy after all these years', Virus Research, 162(1–2), pp. 80–99. doi:10.1016/j.virusres.2011.09.020.

Collins, P.L., Fearns, R. and Graham, B.S. (2013) 'Respiratory syncytial virus: virology, reverse genetics, and pathogenesis of disease', Current Topics in Microbiology and Immunology, 372, pp. 3–38. doi:10.1007/978-3-642-38919-1_1.

Cong, B., Yu, X., Teng, L., Dong, H., Wang, C., Huang, S., Zhao, L., Tian, J. and Zhang, Y. (2022) 'The role of respiratory co-infection with influenza or respiratory syncytial virus in the clinical severity of COVID-19 patients: a systematic review and meta-analysis', Journal of Global Health, 12, 05040. doi:10.7189/jogh.12.05040.

Covington, E.D., Wu, M.M. and Lewis, R.S. (2010) 'Essential role for the CRAC activation domain in store-dependent oligomerization of STIM1', Molecular Biology of the Cell, 21(11), pp. 1897–1907. doi:10.1091/mbc.e10-02-0145.

Cowton, V.M. (2006) ‘Unravelling the complexities of respiratory syncytial virus RNA synthesis’, Journal of General Virology, 87(7), pp. 1805–1821. doi:10.1099/vir.0.81786-0.

Cox, N.J. and Subbarao, K. (1999) ‘Influenza’, The Lancet, 354(9186), pp. 1277–1282. doi:10.1016/s0140-6736(99)01241-6.

Dakhama, A., Kaan, P.M. and Hegele, R.G. (1998) ‘Permissiveness of guinea pig alveolar macrophage subpopulations to acute respiratory syncytial virus infection in vitro’, Chest, 114(6), pp. 1681–1688. doi:10.1378/chest.114.6.1681.

Daszak, P., Zambrana-Torrelio, C., Bogich, T.L., Fernandez, M., Epstein, J.H., Murray, K.A. and Hamilton, H. (2012) ‘Interdisciplinary approaches to understanding disease emergence: the past, present, and future drivers of Nipah virus emergence’, Proceedings of the National Academy of Sciences of the United States of America, 110(Suppl. 1), pp. 3681–3688. doi:10.1073/pnas.1201243109.

Dawson, S. (2017) ‘Bushmeat’, in Thompson, P.B. and Kaplan, D.M. (eds) Encyclopedia of Food and Agricultural Ethics. Cham: Springer, pp. 209–220. doi:10.1007/978-3-319-64738-8_12.

de Graaff, P.M.A., de Jong, E.C., van Capel, T.M.M., van Dijk, M.E.A., Roholl, P.J.M., Boes, J., Luytjes, W. and Kimpen, J.L.L. (2005) ‘Respiratory syncytial virus infection of monocyte-derived dendritic cells decreases their capacity to activate CD4 T cells’, The Journal of Immunology, 175(9), pp. 5904–5911. doi:10.4049/jimmunol.175.9.5904.

Demoor, T., Petersen, B.C., Morris, S., Mukherjee, S., Ptaschinski, C., De Almeida Nagata, D.E., Kawai, T., Ito, T., Lukacs, N.W. and Rosenberg, H.F. (2012) ‘IPS-1 signalling has a nonredundant role in mediating antiviral responses and the clearance of respiratory syncytial virus’, The Journal of Immunology, 189(12), pp. 5942–5953. doi:10.4049/jimmunol.1201763.

Deng, T., Vreede, F.T. and Brownlee, G.G. (2006) ‘Different de novo initiation strategies are used by influenza virus RNA polymerase on its cRNA and viral RNA promoters during viral RNA replication’, Journal of Virology, 80(5), pp. 2337–2348. doi:10.1128/jvi.80.5.2337-2348.2006.

Denmeade, S.R. and Isaacs, J.T. (2005) ‘The SERCA pump as a therapeutic target: making a “smart bomb” for prostate cancer’, Cancer Biology & Therapy, 4(1), pp. 21–29. doi:10.4161/cbt.4.1.1505.

Deshaies, R.J. and Schekman, R. (1987) ‘A yeast mutant defective at an early stage in import of secretory protein precursors into the endoplasmic reticulum’, The Journal of Cell Biology, 105(2), pp. 633–645. doi:10.1083/jcb.105.2.633.

Dias, A., Bouvier, D., Crépin, T., McCarthy, A.A., Hart, D.J., Baudin, F., Cusack, S. and Ruigrok, R.W.H. (2009) 'The cap-snatching endonuclease of influenza virus polymerase resides in the PA subunit', Nature, 458(7240), pp. 914–918. doi:10.1038/nature07745.

Dobson, A.P. and Carper, E.R. (1996) 'Infectious diseases and human population history', BioScience, 46(2), pp. 115–126. doi:10.2307/1312814.

Dou, D., Revol, R., Östbye, H., Wang, H., Daniels, R. and Krammer, F. (2017) 'Analysis of IAV replication and co-infection dynamics by a versatile RNA viral genome labeling method', Cell Reports, 20(1), pp. 251–263. doi:10.1016/j.celrep.2017.06.021.

Dou, D., Revol, R., Östbye, H., Wang, H., Daniels, R. and Krammer, F. (2018) 'Influenza A virus cell entry, replication, virion assembly and movement', Frontiers in Immunology, 9, 1581. doi:10.3389/fimmu.2018.01581.

Du, W., Guo, H., Nijman, V.S., Doedt, J., van der Vries, E., van der Lee, J., Li, Z., van Kuppeveld, F.J.M., de Vries, E. and de Haan, C.A.M. (2019) 'The 2nd sialic acid-binding site of influenza A virus neuraminidase is an important determinant of the hemagglutinin–neuraminidase–receptor balance', PLOS Pathogens, 15(6), e1007860. doi:10.1371/journal.ppat.1007860.

Dunn, F.L. (1958) 'Pandemic influenza in 1957', Journal of the American Medical Association, 166(10), p. 1140. doi:10.1001/jama.1958.02990100028006.

Duvergé, A. and Negroni, M. (2020) 'Pseudotyping lentiviral vectors: when the clothes make the virus', Viruses, 12(11), p. 1311. doi:10.3390/v12111311.

Eisfeld, A.J., Kawakami, E., Watanabe, T., Neumann, G. and Kawaoka, Y. (2011) 'RAB11A is essential for transport of the influenza virus genome to the plasma membrane', Journal of Virology, 85(13), pp. 6117–6126. doi:10.1128/jvi.00378-11.

Eisfeld, A.J., Neumann, G. and Kawaoka, Y. (2014) 'At the centre: influenza A virus ribonucleoproteins', Nature Reviews Microbiology, 13(1), pp. 28–41. doi:10.1038/nrmicro3367.

Elleman, C.J. and Barclay, W.S. (2004) 'The M1 matrix protein controls the filamentous phenotype of influenza A virus', Virology, 321(1), pp. 144–153. doi:10.1016/j.virol.2003.12.009.

Ellgaard, L. and Helenius, A. (2003) 'Quality control in the endoplasmic reticulum', Nature Reviews Molecular Cell Biology, 4(3), pp. 181–191. doi:10.1038/nrm1052.

Emeny, J.M. and Morgan, M.J. (1979) 'Regulation of the interferon system: evidence that vero cells have a genetic defect in interferon production', Journal of General Virology, 43(1), pp. 247–252. doi:10.1099/0022-1317-43-1-247.

Esakandari, H., Nabi-Afjadi, M., Fakkari-Afjadi, J., Farahmandian, N., Miresmaeili, S.M. and Bahreini, E. (2020) 'A comprehensive review of COVID-19 characteristics', Biological Procedures Online, 22(1), 19. doi:10.1186/s12575-020-00128-2.

U.S. Food and Drug Administration (FDA) (2022) 'Know your treatment options for COVID-19'. Available at: https://www.fda.gov/consumers/consumer-updates/know-your-treatment-options-covid-19 (Accessed: 24 August 2022).

Fearns, R. and Deval, J. (2016) 'New antiviral approaches for respiratory syncytial virus and other mononegaviruses: inhibiting the RNA polymerase', Antiviral Research, 134, pp. 63–76. doi:10.1016/j.antiviral.2016.08.006.

Fearns, R., Collins, P.L. and Peeples, M.E. (2000) 'Functional analysis of the genomic and antigenomic promoters of human respiratory syncytial virus', Journal of Virology, 74(13), pp. 6006–6014. doi:10.1128/jvi.74.13.6006-6014.2000.

Feehan, J. and Apostolopoulos, V. (2021) 'Is COVID-19 the worst pandemic?', Maturitas, 149, pp. 56–58. doi:10.1016/j.maturitas.2021.02.001.

Fischer, C.P. and Romero, L.M. (2019) 'Chronic captivity stress in wild animals is highly species-specific', Conservation Physiology, 7(1), coz093. doi:10.1093/conphys/coz093.

Fodor, E. (2013) 'The RNA polymerase of influenza A virus: mechanisms of viral transcription and replication', Acta Virologica, 57(2), pp. 113–122. doi:10.4149/av_2013_02_113.

Francis, T. and Salk, J.E. (1942) 'A simplified procedure for the concentration and purification of influenza virus', Science, 96(2500), pp. 499–500. doi:10.1126/science.96.2500.499.

Francis, T., Pearson, H.E., Salk, J.E. and Brown, P.N. (1945) 'Protective effect of vaccination against induced influenza A1', Journal of Clinical Investigation, 24(4), pp. 536–546. doi:10.1172/jci101633.

Franz, A., Adams, O., Willems, R., Bonzel, L., Neuhausen, N., Schweizer-Krantz, S., Ruggeberg, J.U., Tenenbaum, T., Schroten, H., Schildgen, V., Schildgen, O. and Eis-Hübinger, A.M. (2010) 'Correlation of viral load of respiratory pathogens and co-infections with disease severity in children hospitalized for lower respiratory tract infection', Journal of Clinical Virology, 48(4), pp. 239–245. doi:10.1016/j.jcv.2010.05.007.

França, M., Stallknecht, D.E. and Howerth, E.W. (2012) 'Expression and distribution of sialic acid influenza virus receptors in wild birds', Avian Pathology, 42(1), pp. 60–71. doi:10.1080/03079457.2012.759176.

Frensing, T., Kupke, S.Y., Bachmann, M., Fritzsche, S., Gallo-Ramírez, L.E., Reichl, U. and Genzel, Y. (2016) 'Influenza virus intracellular replication dynamics, release kinetics, and particle morphology during propagation in MDCK cells', Applied Microbiology and Biotechnology, 100(16), pp. 7181–7192. doi:10.1007/s00253-016-7542-4.

Fricke, J., Koo, L.Y., Brown, M., Collins, P.L. and Peeples, M.E. (2012) 'p38 and OGT sequestration into viral inclusion bodies in cells infected with human respiratory syncytial virus suppresses MK2 activities and stress granule assembly', Journal of Virology, 87(3), pp. 1333–1347. doi:10.1128/jvi.02263-12.

Gamblin, S.J. and Skehel, J.J. (2010) 'Influenza hemagglutinin and neuraminidase membrane glycoproteins', Journal of Biological Chemistry, 285(37), pp. 28403–28409. doi:10.1074/jbc.r110.129809.

Gao, F., Bailes, E., Robertson, D.L., Chen, Y., Rodenburg, C.M., Michael, S.F., Cummins, L.B., Arthur, L.O., Peeters, M., Shaw, G.M., Sharp, P.M. and Hahn, B.H. (1999) 'Origin of HIV-1 in the chimpanzee Pan troglodytes troglodytes', Nature, 397(6718), pp. 436–441. doi:10.1038/17130.

Gerard, J., Dodoens, R. and Priest, R. (1597) The herball, or, generall historie of plantes / gathered by John Gerarde of London, master in chirurgerie. [Preprint]. doi:10.5962/bhl.title.51606.

Gerl, M.J., Sachsenheimer, T., Grzybek, M., Coskun, Ü., Wieland, F.T., Brügger, B. and Simons, K. (2012) 'Quantitative analysis of the lipidomes of the influenza virus envelope and MDCK cell apical membrane', The Journal of Cell Biology, 196(2), pp. 213–221. doi:10.1083/jcb.201108175.

Gillespie, D. and Fill, M. (2008) 'Intracellular calcium release channels mediate their own countercurrent: the ryanodine receptor case study', Biophysical Journal, 95(8), pp. 3706–3714. doi:10.1529/biophysj.108.131987.

Glaser, C.A., Gilliam, S., Thompson, W.W., Dassey, D.E., Waterman, S.H., Saruwatari, M., Shapiro, S., Xia, D., Bridges, C.B., Uyeki, T.M. and Harper, S.A. (2002) 'Medical care capacity for influenza outbreaks, Los Angeles', Emerging Infectious Diseases, 8(6), pp. 569–574. doi:10.3201/eid0806.010370.

Goka, E.A., Vallely, P.J., Mutton, K.J. and Klapper, P.E. (2014) 'Single, dual and multiple respiratory virus infections and risk of hospitalization and mortality', Epidemiology and Infection, 143(1), pp. 37–47. doi:10.1017/s0950268814000302.

Goldenring, J.R., Smith, J., Vaughan, H.D., Cameron, P., Hawkins, W. and Navarre, J. (1996) 'Rab11 is an apically located small GTP-binding protein in epithelial tissues', American Journal of Physiology – Gastrointestinal and Liver Physiology, 270(3), pp. G515–G525. doi:10.1152/ajpgi.1996.270.3.g515.

Goldman, A., Krider, R. and Ramaswami, S. (1999) 'The persistent competitive advantage of traditional food retailers in Asia: wet markets' continued dominance in Hong Kong', Journal of Macromarketing, 19(2), pp. 126–139. doi:10.1177/0276146799192004.

Goritzka, M., Durant, L.R., Pereira, C., Salek-Ardakani, S., Openshaw, P.J.M. and Johansson, C. (2015) 'Alveolar macrophage–derived type I interferons orchestrate innate immunity to RSV through recruitment of antiviral monocytes', The Journal of Experimental Medicine, 212(5), pp. 699–714. doi:10.1084/jem.20140825.

Goulding, L.V., Yang, Z., Tutt, C.E.M., Badhan, A., Cross, M.J., Davidson, A.D., Hulswit, R.J.G., Depledge, D.P., Bhella, D., Bushell, E., Pizzorno, A., Terrier, O., Lina, B., Dunning, J., Malim, M.H., Barclay, W.S. and Chang, K.-C. (2020) 'Thapsigargin at non-cytotoxic levels induces a potent host antiviral response that blocks influenza A virus replication', Viruses, 12(10), p. 1093. doi:10.3390/v12101093.

Govaerts, R., Nic Lughadha, E., Black, N., Turner, R. and Paton, A. (2021) 'The World Checklist of Vascular Plants, a continuously updated resource for exploring global plant diversity', Scientific Data, 8(1), 215. doi:10.1038/s41597-021-00997-6.

Greene, W.C. (2007) 'A history of AIDS: looking back to see ahead', European Journal of Immunology, 37(S1), pp. S94–S102. doi:10.1002/eji.200737441.

Grennan, D. (2019) 'What is a pandemic?', JAMA, 321(9), p. 910. doi:10.1001/jama.2019.0700.

Griffiths, C., Drews, S.J. and Marchant, D.J. (2016) 'Respiratory syncytial virus: infection, detection, and new options for prevention and treatment', Clinical Microbiology Reviews, 30(1), pp. 277–319. doi:10.1128/cmr.00010-16.

Groskreutz, D.J., Babor, E.C., Monick, M.M., Varga, S.M., Hunninghake, G.W. and Hostetter, S.J. (2010) 'Respiratory syncytial virus limits α subunit of eukaryotic translation initiation factor 2 (eIF2α) phosphorylation to maintain translation and viral replication', Journal of Biological Chemistry, 285(31), pp. 24023–24031. doi:10.1074/jbc.m109.077321.

Gruszczynska-Biegala, J., Pomorski, P., Wisniewska, M.B. and Kuznicki, J. (2011) 'Differential roles for STIM1 and STIM2 in store-operated calcium entry in rat neurons', PLOS ONE, 6(4), e19285. doi:10.1371/journal.pone.0019285.

Guan, Y., Vijaykrishna, D., Bahl, J., Zhu, H., Wang, J., Smith, G.J.D. and Chen, H. (2010) 'The emergence of pandemic influenza viruses', Protein & Cell, 1(1), pp. 9–13. doi:10.1007/s13238-010-0008-z.

Guilligay, D., Tarendeau, F., Resa-Infante, P., Coloma, R., Crepin, T., Sehr, P., Lewis, J., Ruigrok, R.W.H., Ortin, J. and Cusack, S. (2008) 'The structural basis for cap binding by influenza virus polymerase subunit PB2', Nature Structural & Molecular Biology, 15(5), pp. 500–506. doi:10.1038/nsmb.1421.

Gutiérrez-Ortega, A., Sánchez-Hernández, C. and Gómez-García, B. (2008) 'Respiratory syncytial virus glycoproteins uptake occurs through clathrin-mediated endocytosis in a human epithelial cell line', Virology Journal, 5, 127. doi:10.1186/1743-422x-5-127.

Görlich, D., Prehn, S., Hartmann, E., Kalies, K.U., Rapoport, T.A. and Wiedmann, M. (1992) 'A mammalian homolog of SEC61p and SECYp is associated with ribosomes and nascent polypeptides during translocation', Cell, 71(3), pp. 489–503. doi:10.1016/0092-8674(92)90517-g.

Haider, N., Osman, A.Y., Gadzekpo, A., de Souza, C., Kayali, A.Y., Rao, A.S.S., Das, J.K. and Nooh, H.Z. (2022) 'The global case-fatality rate of COVID-19 has been declining disproportionately between top vaccinated countries and the rest of the world', medRxiv [Preprint]. doi:10.1101/2022.01.19.22269493.

Hale, B.G., Randall, R.E., Ortín, J. and Jackson, D. (2008) 'The multifunctional NS1 protein of influenza A viruses', Journal of General Virology, 89(10), pp. 2359–2376. doi:10.1099/vir.0.2008/004606-0.

Hamilton, B.S., Whittaker, G.R. and Daniel, S. (2012) 'Influenza virus-mediated membrane fusion: determinants of hemagglutinin fusogenic activity and experimental approaches for assessing virus fusion', Viruses, 4(7), pp. 1144–1168. doi:10.3390/v4071144.

Han, E., Tan, M.M.J., Turk, E., Sridhar, D., Leung, G.M., Shibuya, K., Asgari, N., Oh, J., García-Basteiro, A.L., Hanefeld, J., Cook, A.R., Hsu, L.Y., Teo, Y.Y., Heymann, D., Clark, H., McKee, M. and Legido-Quigley, H. (2020) 'Lessons learnt from easing COVID-19 restrictions: an analysis of countries and regions in Asia Pacific and Europe', The Lancet, 396(10261), pp. 1525–1534. doi:10.1016/s0140-6736(20)32007-9.

Haney, J., Stone, R., Perron, M., Aicher, S., Foote, K., Schiffer, J., Tyagi, S., Baker, S.C., Martínez-Sobrido, L. and Manicassamy, B. (2022) 'Coinfection by influenza A virus and respiratory syncytial virus produces hybrid virus

particles', Nature Microbiology, 7(11), pp. 1879–1890. doi:10.1038/s41564-022-01242-5.

Hanley, L.L., McGivern, D.R., McGivern, T., Mackenzie, J., Baker, S.C. and Hardy, R.W. (2010) 'Roles of the respiratory syncytial virus trailer region: effects of mutations on genome production and stress granule formation', Virology, 406(2), pp. 241–252. doi:10.1016/j.virol.2010.07.006.

Hansen, O. and Jensen, J. (1995) 'Binding of ADP to sarcoplasmic reticulum Ca2+-ATPase in the absence of Mg2+ is specifically inhibited by thapsigargin: observations on the ligand stoichiometry', Cell Calcium, 18(6), pp. 557–568. doi:10.1016/0143-4160(95)90017-9.

Harrison, S.C. (2015) 'Viral membrane fusion', Virology, 479–480, pp. 498–507. doi:10.1016/j.virol.2015.03.043.

Hassan, I., Luo, X., Keeney, F., Wilson, D., Morris, G. and McKimm-Breschkin, J. (2014) 'Inositol-requiring enzyme 1 inhibits respiratory syncytial virus replication', Journal of Biological Chemistry, 289(11), pp. 7537–7546. doi:10.1074/jbc.m113.510594.

Hassan, I.H., Zhang, M.S., Powers, L.S., Shao, J.Q., Baltrusaitis, J., Rutkowski, D.T., Legge, K., Monick, M.M., Hunninghake, G.W. and Carter, A.B. (2011) 'Influenza A viral replication is blocked by inhibition of the inositol-requiring enzyme 1 (IRE1) stress pathway', Journal of Biological Chemistry, 287(7), pp. 4679–4689. doi:10.1074/jbc.m111.284695.

Hause, B.M., Collin, E.A., Liu, R., Huang, B., Sheng, Z., Lu, W., Wang, D., Nelson, E.A., Li, F. and Anderson, G. (2014) 'Characterization of a novel influenza virus in cattle and swine: proposal for a new genus in the Orthomyxoviridae family', mBio, 5(2), e00031-14. doi:10.1128/mbio.00031-14.

Hayden, M.S. and Ghosh, S. (2008) 'Shared principles in NF-κB signaling', Cell, 132(3), pp. 344–362. doi:10.1016/j.cell.2008.01.020.

He, B. (2006) 'Viruses, endoplasmic reticulum stress, and interferon responses', Cell Death & Differentiation, 13(3), pp. 393–403. doi:10.1038/sj.cdd.4401833.

Henderson, D.A. (2016) 'The development of surveillance systems', American Journal of Epidemiology, 183(5), pp. 381–386. doi:10.1093/aje/kwv229.

Henderson, D.A., Courtney, B., Inglesby, T.V., Toner, E., Nuzzo, J.B., Scheckel, J., Gayle, H., Gubler, D.J., Norwood, A., O'Toole, T., Osterholm, M.T., Pettit, D., Schoch-Spana, M., Siegel, J.D., Stoto, M., Troutman, A., Vukotich, C. and Watson, M. (2009) 'Public health and medical responses to the 1957–58 influenza pandemic', Biosecurity and Bioterrorism: Biodefense Strategy, Practice, and Science, 7(3), pp. 265–273. doi:10.1089/bsp.2009.0729.

Hetz, C. (2012) ‘The unfolded protein response: controlling cell fate decisions under ER stress and beyond’, Nature Reviews Molecular Cell Biology, 13(2), pp. 89–102. doi:10.1038/nrm3270.

Hetz, C., Chevet, E. and Oakes, S.A. (2011) ‘The unfolded protein response: integrating stress signals through the stress sensor IRE1α’, Physiological Reviews, 91(4), pp. 1219–1243. doi:10.1152/physrev.00001.2011.

Hilsch, M., Goldenbogen, B., Sieben, C., Höfer, C.T., Rabe, A., Klipp, E. and Herrmann, A. (2014) ‘Influenza A matrix protein M1 multimerizes upon binding to lipid membranes’, Biophysical Journal, 107(4), pp. 912–923. doi:10.1016/j.bpj.2014.06.042.

Hogan, P.G. and Rao, A. (2015) ‘Store-operated calcium entry: mechanisms and modulation’, Biochemical and Biophysical Research Communications, 460(1), pp. 40–49. doi:10.1016/j.bbrc.2015.02.110.

Hollien, J. and Weissman, J.S. (2006) ‘Decay of endoplasmic reticulum-localized mRNAs during the unfolded protein response’, Science, 313(5783), pp. 104–107. doi:10.1126/science.1129631.

Holmes, E.C. (2009) ‘The evolutionary genetics of emerging viruses’, Annual Review of Ecology, Evolution, and Systematics, 40(1), pp. 353–372. doi:10.1146/annurev.ecolsys.110308.120248.

Hoppe, T. (2018) ‘“Spanish flu”: when infectious disease names blur origins and stigmatize those infected’, American Journal of Public Health, 108(11), pp. 1462–1464. doi:10.2105/ajph.2018.304645.

Hotamisligil, G.S. (2010) ‘Endoplasmic reticulum stress and the inflammatory basis of metabolic disease’, Cell, 140(6), pp. 900–917. doi:10.1016/j.cell.2010.02.034.

Hoth, M. and Penner, R. (1992) ‘Depletion of intracellular calcium stores activates a calcium current in mast cells’, Nature, 355(6358), pp. 353–356. doi:10.1038/355353a0.

Hou, X., Pedi, L., Diver, M.M. and Long, S.B. (2012) ‘Crystal structure of the calcium release–activated calcium channel Orai’, Science, 338(6112), pp. 1308–1313. doi:10.1126/science.1228757.

Hua, S. and Inesi, G. (1997) ‘Synthesis of a radioactive azido derivative of thapsigargin and photolabeling of the sarcoplasmic reticulum ATPase’, Biochemistry, 36(39), pp. 11865–11872. doi:10.1021/bi970105n.

Huang, K., Incognito, L., Cheng, X., Ulbrandt, N.D., Wu, H., Snavely, M., Wan, J., Wilson, S., Li, H., Generaux, C., Ueda, A., Tang, X., Swanson, K.A., Allerson, C.R. and Olson, W. (2010) ‘Respiratory syncytial virus-neutralizing monoclonal antibodies motavizumab and palivizumab inhibit fusion’, Journal of Virology, 84(16), pp. 8132–8140. doi:10.1128/jvi.02699-09.

Hutchinson, E. and Fodor, E. (2013) 'Transport of the influenza virus genome from nucleus to nucleus', Viruses, 5(10), pp. 2424–2446. doi:10.3390/v5102424.

Iuliano, A.D., Roguski, K.M., Chang, H.H., Muscatello, D.J., Palekar, R., Tempia, S., Cohen, C., Gran, J.M., Schanzer, D., Cowling, B.J., Wu, P., Kyncl, J., Ang, L.W., Park, M., Redlberger-Fritz, M., Yu, H., Espenhain, L., Krishnan, A., Emukule, G., van Asten, L., Silva, S., Aungkulanon, S., Buchholz, U., Widdowson, M.-A. and Bresee, J.S. (2018) 'Estimates of global seasonal influenza-associated respiratory mortality: a modelling study', The Lancet, 391(10127), pp. 1285–1300. doi:10.1016/s0140-6736(17)33293-2.

Iwata, Y. and Koizumi, N. (2012) 'Plant transducers of the endoplasmic reticulum unfolded protein response', Trends in Plant Science, 17(12), pp. 720–727. doi:10.1016/j.tplants.2012.06.014.

Jackson, C. (2009) 'History lessons: the Asian flu pandemic', British Journal of General Practice, 59(565), pp. 622–623. doi:10.3399/bjgp09x453882.

Jaskulska, A., Janecka, A.E. and Gach-Janczak, K. (2020) 'Thapsigargin—from traditional medicine to anticancer drug', International Journal of Molecular Sciences, 22(1), p. 4. doi:10.3390/ijms22010004.

Jheng, J.-R., Ho, J.-Y. and Horng, J.-T. (2014) 'ER stress, autophagy, and RNA viruses', Frontiers in Microbiology, 5, 388. doi:10.3389/fmicb.2014.00388.

Johnson, N.P.A.S. and Mueller, J. (2002) 'Updating the accounts: global mortality of the 1918–1920 "Spanish" influenza pandemic', Bulletin of the History of Medicine, 76(1), pp. 105–115. doi:10.1353/bhm.2002.0022.

Jorba, N., Coloma, R. and Ortín, J. (2009) 'Genetic trans-complementation establishes a new model for influenza virus RNA transcription and replication', PLOS Pathogens, 5(5), e1000462. doi:10.1371/journal.ppat.1000462.

Jori, F., Galvez, H., Mendoza, J., Jiménez, J., Hurtado, A., Peralta, J.L., Perera, C.L., Herrera, C., Hidalgo, H., Aguirre, A.A., Vila, J., Cordero, J., Ramon, J., Jiménez, F., Alvarado, J., Aguayo, V., Llanos, C., Pizarro, G., Gonzales, L. and Rivera, H. (2013) 'An assessment of zoonotic and production limiting pathogens in rusa deer (Cervus timorensis rusa) from Mauritius', Transboundary and Emerging Diseases, 61, pp. 31–42. doi:10.1111/tbed.12206.

Joseph, U., Su, Y.C.F., Vijaykrishna, D. and Smith, G.J.D. (2016) 'The ecology and adaptive evolution of influenza A interspecies transmission', Influenza and Other Respiratory Viruses, 11(1), pp. 74–84. doi:10.1111/irv.12412.

Karamyshev, A.L., Karamysheva, Z.N., Kajava, A.V., Ksenzenko, V.N., Nirenberg, M., Shabalina, S.A. and Ogurtsov, A.Y. (2014) 'Inefficient SRP interaction with a nascent chain triggers a mRNA quality control pathway', Cell, 156(1–2), pp. 146–157. doi:10.1016/j.cell.2013.12.017.

Kelleher, K., Subramaniam, N. and Drysdale, S.B. (2025) 'The recent landscape of RSV vaccine research', Therapeutic Advances in Vaccines and Immunotherapy, 13. doi:10.1177/25151355241310601.

Kilbourne, E.D. (2006) 'Influenza pandemics of the 20th century', Emerging Infectious Diseases, 12(1), pp. 9–14. doi:10.3201/eid1201.051254.

Kilpatrick, A.M. and Randolph, S.E. (2012) 'Drivers, dynamics, and control of emerging vector-borne zoonotic diseases', The Lancet, 380(9857), pp. 1946–1955. doi:10.1016/s0140-6736(12)61151-9.

Kim, I., Xu, W. and Reed, J.C. (2008) 'Cell death and endoplasmic reticulum stress: disease relevance and therapeutic opportunities', Nature Reviews Drug Discovery, 7(12), pp. 1013–1030. doi:10.1038/nrd2755.

Knobler, S.L., Mack, A., Mahmoud, A. and Lemon, S.M. (2005) The threat of pandemic influenza: are we ready? Workshop summary. Washington, DC: National Academies Press. doi:10.17226/11150.

Kochs, G., Garcia-Sastre, A. and Martinez-Sobrido, L. (2007) 'Multiple anti-interferon actions of the influenza A virus NS1 protein', Journal of Virology, 81(13), pp. 7011–7021. doi:10.1128/jvi.02581-06.

Koenig, P.-A. and Ploegh, H.L. (2014) 'Protein quality control in the endoplasmic reticulum', F1000Prime Reports, 6, 49. doi:10.12703/p6-49.

Kokame, K., Agarwala, K.L., Kato, H. and Miyata, T. (2000) 'Herp, a new ubiquitin-like membrane protein induced by endoplasmic reticulum stress', Journal of Biological Chemistry, 275(42), pp. 32846–32853. doi:10.1074/jbc.m002063200.

Kool, A., de Boer, H.J., Krüger, Å., Rydberg, A., Abbad, A., Björk, L. and Martin, G. (2012) 'Molecular identification of commercialized medicinal plants in southern Morocco', PLOS ONE, 7(6), e39459. doi:10.1371/journal.pone.0039459.

Krilov, L.R. (2011) 'Respiratory syncytial virus disease: update on treatment and prevention', Expert Review of Anti-infective Therapy, 9(1), pp. 27–32. doi:10.1586/eri.10.140.

Krishnan, A., Hamilton, J.P., Alqahtani, S.A. and Woreta, T.A. (2021) 'COVID-19: an overview and a clinical update', World Journal of Clinical Cases, 9(1), pp. 8–23. doi:10.12998/wjcc.v9.i1.8.

Krug, R.M. (2015) ‘Functions of the influenza A virus NS1 protein in antiviral defense’, Current Opinion in Virology, 12, pp. 1–6. doi:10.1016/j.coviro.2015.01.007.

Krzyzaniak, M.A., Zumstein, M.T., Gerez, J.A., Picotti, P. and Helenius, A. (2013) ‘Host cell entry of respiratory syncytial virus involves macropinocytosis followed by proteolytic activation of the F protein’, PLOS Pathogens, 9(4), e1003309. doi:10.1371/journal.ppat.1003309.

Kuchipudi, S.V., Tellabati, M., Sebastian, S., Londt, B.Z., Jansen, C., Vervelde, L., Brookes, S.M., Brown, I.H., Dunham, S.P. and Chang, K.C. (2012) ‘18s rRNA is a reliable normalisation gene for real time PCR based on influenza virus infected cells’, Virology Journal, 9, 230. doi:10.1186/1743-422x-9-230.

Kuchipudi, S.V., Nelli, R.K. and White, G.A. (2009) ‘Differences in influenza virus receptors in chickens and ducks: implications for interspecies transmission’, Journal of Molecular and Genetic Medicine, 3(1), pp. 143–151. doi:10.4172/1747-0862.1000026.

Kumlin, U., Olofsson, S., Dimock, K. and Arnberg, N. (2008) ‘Sialic acid tissue distribution and influenza virus tropism’, Influenza and Other Respiratory Viruses, 2(5), pp. 147–154. doi:10.1111/j.1750-2659.2008.00051.x.

Kuo, R.-L., Zhao, C., Malur, M., Krug, R.M. and Chen, C.-J. (2010) ‘Influenza A virus strains that circulate in humans differ in the ability of their NS1 proteins to block the activation of IRF3 and interferon-β transcription’, Virology, 408(2), pp. 146–158. doi:10.1016/j.virol.2010.09.012.

Kümpel, N.F., Milner-Gulland, E.J., Cowlishaw, G. and Rowcliffe, J.M. (2010) ‘Incentives for hunting: the role of bushmeat in the household economy in rural Equatorial Guinea’, Human Ecology, 38(2), pp. 251–264. doi:10.1007/s10745-010-9316-4.

Lakadamyali, M., Rust, M.J., Babcock, H.P. and Zhuang, X. (2003) ‘Visualizing infection of individual influenza viruses’, Proceedings of the National Academy of Sciences of the United States of America, 100(16), pp. 9280–9285. doi:10.1073/pnas.0832269100.

Lambert, L., Sagfors, A.M., Openshaw, P.J.M. and Culley, F.J. (2014) ‘Immunity to RSV in early life’, Frontiers in Immunology, 5, 466. doi:10.3389/fimmu.2014.00466.

Langmuir, A.D. and Schoenbaum, S.C. (1976) ‘The epidemiology of influenza’, Hospital Practice, 11(10), pp. 49–56. doi:10.1080/21548331.1976.11707011.

Lay, M.K., Céspedes, P.F., Palavecino, C.E., León, M.A., Díaz, R.A., Salazar, F.J., Méndez, G.P., Bueno, S.M. and Kalergis, A.M. (2013) 'Advances in understanding respiratory syncytial virus infection in airway epithelial cells and consequential effects on the immune response', Microbes and Infection, 15(3), pp. 230–242. doi:10.1016/j.micinf.2012.11.012.

Lee, A.-H., Iwakoshi, N.N. and Glimcher, L.H. (2003) 'XBP-1 regulates a subset of endoplasmic reticulum resident chaperone genes in the unfolded protein response', Molecular and Cellular Biology, 23(21), pp. 7448–7459. doi:10.1128/mcb.23.21.7448-7459.2003.

Lee, A.S. (2005) 'The ER chaperone and signalling regulator GRP78/BiP as a monitor of endoplasmic reticulum stress', Methods, 35(4), pp. 373–381. doi:10.1016/j.ymeth.2004.10.010.

Lee, W.J., Monteith, G.R. and Roberts-Thomson, S.J. (2006) 'Calcium transport and signalling in the mammary gland: targets for breast cancer', Biochimica et Biophysica Acta (BBA) - Reviews on Cancer, 1765(2), pp. 235–255. doi:10.1016/j.bbcan.2005.12.001.

Li, F., Ma, C. and Wang, J. (2015) 'Inhibitors targeting the influenza virus hemagglutinin', Current Medicinal Chemistry, 22(11), pp. 1361–1382. doi:10.2174/0929867322666150227153919.

Li, Q., Guan, X., Wu, P., Wang, X., Zhou, L., Tong, Y., Ren, R., Leung, K.S.M., Lau, E.H.Y., Wong, J.Y., Xing, X., Xiang, N., Wu, Y., Li, C., Chen, Q., Li, D., Liu, T., Zhao, J., Liu, M., Tu, W., Chen, C., Jin, L., Yang, R., Wang, Q., Zhou, S., Wang, R., Liu, H., Luo, Y., Liu, Y., Shao, G., Li, H., Tao, Z., Yang, Y., Deng, Z., Liu, B., Ma, Z., Zhang, Y., Shi, G., Lam, T.T.-Y., Wu, J.T., Gao, G.F., Cowling, B.J., Yang, B., Leung, G.M. and Feng, Z. (2020) 'Early transmission dynamics in Wuhan, China, of novel coronavirus–infected pneumonia', New England Journal of Medicine, 382(13), pp. 1199–1207. doi:10.1056/nejmoa2001316.

Li, Z., Lu, J., Xu, P., Xie, X., Chen, L., Zhu, Q., Luo, L., Sun, H., Wang, H., Tian, J., Zhang, W., Li, D., Chen, J., Xu, T. and Xu, P. (2010) 'Graded activation of CRAC channel by binding of different numbers of STIM1 to Orai1 subunits', Cell Research, 21(2), pp. 305–315. doi:10.1038/cr.2010.131.

Lifland, A.W., Jung, J., Alonas, E., Zurla, C., Crowe, J.E. and Santangelo, P.J. (2012) 'Human respiratory syncytial virus nucleoprotein and inclusion bodies antagonize the innate immune response mediated by MDA5 and MAVS', Journal of Virology, 86(15), pp. 8245–8258. doi:10.1128/jvi.00215-12.

Lindquist, M.E., Lifland, A.W., Utley, T.J., Santangelo, P.J. and Crowe, J.E. (2010) 'Respiratory syncytial virus induces host RNA stress granules to facilitate viral replication', Journal of Virology, 84(23), pp. 12274–12284. doi:10.1128/jvi.00260-10.

Lindquist, M.E., Mainou, B.A., Dermody, T.S., Santangelo, P.J. and Crowe, J.E. (2011) 'Activation of protein kinase R is required for induction of stress granules by respiratory syncytial virus but dispensable for viral replication', Virology, 413(1), pp. 103–110. doi:10.1016/j.virol.2011.02.009.

Ling, Z., Tran, K.C. and Teng, M.N. (2009) 'Human respiratory syncytial virus nonstructural protein NS2 antagonizes the activation of beta interferon transcription by interacting with RIG-I', Journal of Virology, 83(8), pp. 3734–3742. doi:10.1128/jvi.02434-08.

Lingwood, D. and Simons, K. (2009) 'Lipid rafts as a membrane-organizing principle', Science, 327(5961), pp. 46–50. doi:10.1126/science.1174621.

Liou, J., Kim, M.L., Do Heo, W., Jones, J.T., Myers, J.W., Ferrell, J.E. and Meyer, T. (2005) 'STIM is a Ca2+ sensor essential for Ca2+-store-depletion-triggered Ca2+ influx', Current Biology, 15(13), pp. 1235–1241. doi:10.1016/j.cub.2005.05.055.

Liou, J., Fivaz, M., Inoue, T. and Meyer, T. (2007) 'Live-cell imaging reveals sequential oligomerization and local plasma membrane targeting of stromal interaction molecule 1 after Ca2+ store depletion', Proceedings of the National Academy of Sciences of the United States of America, 104(22), pp. 9301–9306. doi:10.1073/pnas.0702866104.

Littler, E. and Oberg, B. (2005) 'Achievements and challenges in antiviral drug discovery', Antiviral Chemistry and Chemotherapy, 16(3), pp. 155–168. doi:10.1177/095632020501600302.

Liu, G., Park, H.-S., Pyo, H.-M., Liu, Q., Zhou, Y. and Song, J. (2015) 'Influenza A virus panhandle structure is directly involved in RIG-I activation and interferon induction', Journal of Virology, 89(11), pp. 6067–6079. doi:10.1128/jvi.00232-15.

Liu, M., Li, X., Zheng, Q., Xu, Y., Zhang, M., Wang, C., Ding, H., Luo, X., Liu, Q., Yang, Z., Gao, G.F. and Qi, J. (2022) 'Human-type sialic acid receptors contribute to avian influenza A virus binding and entry by hetero-multivalent interactions', Nature Communications, 13(1), 4056. doi:10.1038/s41467-022-31840-0.

Liu, Q., Zhou, Y. and Yang, Z. (2015) 'The cytokine storm of severe influenza and development of immunomodulatory therapy', Cellular & Molecular Immunology, 13(1), pp. 3–10. doi:10.1038/cmi.2015.74.

Livak, K.J. and Schmittgen, T.D. (2001) 'Analysis of relative gene expression data using real-time quantitative PCR and the 2−ΔΔCT method', Methods, 25(4), pp. 402–408. doi:10.1006/meth.2001.1262.

Lo, M.Y., Ho, J.Y., Hung, P., Wu, S.C. and Lau, T.C. (2019) 'A field study into Hong Kong's wet markets: raised questions into the hygienic maintenance of meat contact surfaces and the dissemination of microorganisms associated with nosocomial infections', Frontiers in Microbiology, 10, 2618. doi:10.3389/fmicb.2019.02618.

Longini, I.M., Fine, P.E.M. and Thacker, S.B. (1986) 'Predicting the global spread of new infectious agents', American Journal of Epidemiology, 123(3), pp. 383–391. doi:10.1093/oxfordjournals.aje.a114253.

Luik, R.M., Wu, M.M., Buchanan, J. and Lewis, R.S. (2008) 'Oligomerization of STIM1 couples ER calcium depletion to CRAC channel activation', Nature, 454(7203), pp. 538–542. doi:10.1038/nature07065.

Lukacs, N.W., Moore, M.L., Rudd, B.D., Berlin, A.A., Collins, R.D., Olson, S.J., Ho, S.B. and Peebles, R.S. (2010) 'Respiratory virus-induced TLR7 activation controls IL-17–associated increased mucus via IL-23 regulation', The Journal of Immunology, 185(4), pp. 2231–2239. doi:10.4049/jimmunol.1000733.

Lytton, J., Westlin, M. and Hanley, M.R. (1991) 'Thapsigargin inhibits the sarcoplasmic or endoplasmic reticulum Ca-ATPase family of calcium pumps', Journal of Biological Chemistry, 266(26), pp. 17067–17071. doi:10.1016/S0021-9258(18)98692-1.

Mabuka, J., Nduati, R., Odem-Davis, K., Peterson, D., Overbaugh, J. and John-Stewart, G. (2012) 'HIV-specific antibodies capable of ADCC are common in breastmilk and are associated with reduced risk of transmission in women with high viral loads', PLOS Pathogens, 8(6), e1002739. doi:10.1371/journal.ppat.1002739.

Magouras, I., Brookes, V.J., Jori, F., Martin, A., Pfeiffer, D.U., Dürr, S., Grace, D., Dominguez, M., De Meneghi, D., Kaszubski, P.A., Häsler, B., Rushton, J., Berezowski, J., Stark, K.D.C. and Keeling, M.J. (2020) 'Emerging zoonotic diseases: should we rethink the animal–human interface?', Frontiers in Veterinary Science, 7, 582743. doi:10.3389/fvets.2020.582743.

Mahase, E. (2020) 'Covid-19: WHO declares pandemic because of "alarming levels" of spread, severity, and inaction', BMJ, 368, m1036. doi:10.1136/bmj.m1036.

Malhotra, J.D. and Kaufman, R.J. (2007) 'The endoplasmic reticulum and the unfolded protein response', Seminars in Cell & Developmental Biology, 18(6), pp. 716–731. doi:10.1016/j.semcdb.2007.09.003.

Manivannan, P., Siddiqui, M.A. and Malathi, K. (2020) 'RNase L amplifies interferon signalling by inducing protein kinase R-mediated antiviral stress granules', Journal of Virology, 94(13), e00205-20. doi:10.1128/jvi.00205-20.

Marc, D. (2016) ‘Stop-codon variations in non-structural protein NS1 of avian influenza viruses’, Virulence, 7(5), pp. 498–501. doi:10.1080/21505594.2016.1175802.

Marlink, R., Kanki, P., Thior, I., Travers, K., Eisen, G., Siby, T., Traore, I., Hsieh, C.C., Dia, M.C., Gueye, E.H., Essex, M. and Ndoye, I. (1994) ‘Reduced rate of disease development after HIV-2 infection as compared to HIV-1’, Science, 265(5178), pp. 1587–1590. doi:10.1126/science.7915856.

Marlowe, F.W. (2005) ‘Hunter-gatherers and human evolution’, Evolutionary Anthropology: Issues, News, and Reviews, 14(2), pp. 54–67. doi:10.1002/evan.20046.

Marr, N., Turvey, S.E. and Grandvaux, N. (2013) ‘Pathogen recognition receptor crosstalk in respiratory syncytial virus sensing: a host and cell type perspective’, Trends in Microbiology, 21(11), pp. 568–574. doi:10.1016/j.tim.2013.08.006.

Martin, G., Yanez-Arenas, C., Plowright, R.K., Chen, C., Roberts, B.J., Skerratt, L.F., Becker, D.J., Goldstein, T., Tabor, G.M., Lunney, D., Schloegel, L.M., Shearer, T., Plummer, C., Broderick, C., Hart, K., Jenkins, S., McCallum, H. and Field, H.E. (2018) ‘Climate change could increase the geographic extent of Hendra virus spillover risk’, EcoHealth, 15(3), pp. 509–525. doi:10.1007/s10393-018-1322-9.

Martin, K. and Helenius, A. (1991) ‘Nuclear transport of influenza virus ribonucleoproteins: the viral matrix protein (M1) promotes export and inhibits import’, Cell, 67(1), pp. 117–130. doi:10.1016/0092-8674(91)90576-k.

Martin, L.B. (2009) ‘Stress and immunity in wild vertebrates: timing is everything’, General and Comparative Endocrinology, 163(1–2), pp. 70–76. doi:10.1016/j.ygcen.2009.03.008.

Martinez-Swatson, K., Hodge, S., Wilson, T.M.A., Clarkson, J.J., Hartley, S.E. and Johnson, S.N. (2019) ‘Exploring evolutionary theories of plant defence investment using field populations of the deadly carrot’, Annals of Botany, 125(5), pp. 737–750. doi:10.1093/aob/mcz151.

McAuley, J.L., Gilbertson, B.P., Trifkovic, S., Brown, L.E. and McKimm-Breschkin, J.L. (2019) ‘Influenza virus neuraminidase structure and functions’, Frontiers in Microbiology, 10, 39. doi:10.3389/fmicb.2019.00039.

McDonald, T.P., Pitt, A., Guy, M., Simmonds, P., Simmonds, M., Sugrue, R.J. and Collins, P.L. (2004) ‘Evidence that the respiratory syncytial virus polymerase complex associates with lipid rafts in virus-infected cells: a proteomic analysis’, Virology, 330(1), pp. 147–157. doi:10.1016/j.virol.2004.09.034.

McGivern, D.R., Collins, P.L. and Fearns, R. (2005) ‘Identification of internal sequences in the 3′ leader region of human respiratory syncytial virus that enhance transcription and confer replication processivity’, Journal of Virology, 79(4), pp. 2449–2460. doi:10.1128/jvi.79.4.2449-2460.2005.

Meanwell, N.A. and Krystal, M. (1996) ‘Taking aim at a moving target—inhibitors of influenza virus. Part 1: virus adsorption, entry and uncoating’, Drug Discovery Today, 1(8), pp. 316–324. doi:10.1016/1359-6446(96)10029-5.

Meng, J., Stobart, C.C., Hotard, A.L. and Moore, M.L. (2014) ‘An overview of respiratory syncytial virus’, PLOS Pathogens, 10(4), e1004016. doi:10.1371/journal.ppat.1004016.

Meusser, B., Hirsch, C., Jarosch, E. and Sommer, T. (2005) ‘ERAD: the long road to destruction’, Nature Cell Biology, 7(8), pp. 766–772. doi:10.1038/ncb0805-766.

Michelangeli, F. and East, J.M. (2011) ‘A diversity of SERCA Ca2+ pump inhibitors’, Biochemical Society Transactions, 39(3), pp. 789–797. doi:10.1042/bst0390789.

Momose, F., Kikuchi, Y., Komase, K., Morikawa, Y., Ishihama, A. and Nagata, K. (2011) ‘Apical transport of influenza A virus ribonucleoprotein requires Rab11-positive recycling endosome’, PLOS ONE, 6(6), e21123. doi:10.1371/journal.pone.0021123.

Monk, P.D., Marsden, R.J., Tear, V.J., Brookes, J., Batten, T.N., Mankowski, M., Gabbay, F.J., Davies, D.E., Holgate, S.T., Ho, L.-P., Clark, T., Djukanovic, R. and Wilkinson, T.M.A.; Inhaled Interferon Beta COVID-19 Study Group (2021) ‘Safety and efficacy of inhaled nebulised interferon beta-1a (SNG001) for treatment of SARS-CoV-2 infection: a randomised, double-blind, placebo-controlled, phase 2 trial’, The Lancet Respiratory Medicine, 9(2), pp. 196–206. doi:10.1016/S2213-2600(20)30511-7.

Monteith, G.R., McAndrew, D., Faddy, H.M. and Roberts-Thomson, S.J. (2007) ‘Calcium and cancer: targeting Ca2+ transport’, Nature Reviews Cancer, 7(7), pp. 519–530. doi:10.1038/nrc2171.

Monto, A.S. and Sullivan, K.M. (1993) ‘Acute respiratory illness in the community: frequency of illness and the agents involved’, Epidemiology and Infection, 110(1), pp. 145–160. doi:10.1017/s0950268800050779.

Morens, D.M. and Taubenberger, J.K. (2018) ‘The mother of all pandemics is 100 years old (and going strong)!’, American Journal of Public Health, 108(11), pp. 1449–1454. doi:10.2105/ajph.2018.304631.

Morens, D.M., Taubenberger, J.K. and Fauci, A.S. (2009) ‘The persistent legacy of the 1918 influenza virus’, New England Journal of Medicine, 361(3), pp. 225–229. doi:10.1056/nejmp0904819.

Mostafa, A., Abdelwhab, E.-S.M., Mettenleiter, T.C. and Pleschka, S. (2018) 'Zoonotic potential of influenza A viruses: a comprehensive overview', Viruses, 10(9), 497. doi:10.3390/v10090497.

Møller, J.V., Olesen, C., Winther, A.-M.L. and Nissen, P. (2010) 'The sarcoplasmic Ca2+-ATPase: design of a perfect chemo-osmotic pump', Quarterly Reviews of Biophysics, 43(4), pp. 501–566. doi:10.1017/s003358351000017x.

Nakada, R., Hirano, H. and Matsuura, Y. (2015) 'Structure of importin-α bound to a non-classical nuclear localization signal of the influenza A virus nucleoprotein', Scientific Reports, 5, 15055. doi:10.1038/srep15055.

Nakatsu, S., Murakami, S., Shindo, K., Horimoto, T. and Sagara, H. (2018) 'Influenza C and D viruses package eight organized ribonucleoprotein complexes', Journal of Virology, 92(6), e02084-17. doi:10.1128/jvi.02084-17.

Nelli, R.K., Kuchipudi, S.V., White, G.A., Perez, B.B., Dunham, S.P. and Chang, K.-C. (2010) 'Comparative distribution of human and avian type sialic acid influenza receptors in the pig', BMC Veterinary Research, 6, 4. doi:10.1186/1746-6148-6-4.

Newcomb, L.L., Kuo, R.-L., Ye, Q., Jiang, Y., Tao, Y.J. and Krug, R.M. (2008) 'Interaction of the influenza A virus nucleocapsid protein with the viral RNA polymerase potentiates unprimed viral RNA replication', Journal of Virology, 83(1), pp. 29–36. doi:10.1128/jvi.02293-07.

Nickbakhsh, S., Mair, C., Matthews, L., Reeve, R., Johnson, P.C.D., Thorburn, F., von Wissmann, B., Reynolds, A., McMenamin, J., Gunson, R.N. and Murcia, P.R. (2016) 'Extensive multiplex PCR diagnostics reveal new insights into the epidemiology of viral respiratory infections', Epidemiology and Infection, 144(10), pp. 2064–2076. doi:10.1017/s0950268816000339.

Nishitoh, H. (2011) 'CHOP is a multifunctional transcription factor in the ER stress response', Journal of Biochemistry, 151(3), pp. 217–219. doi:10.1093/jb/mvr143.

Noton, S.L., Medcalf, E., Fisher, D., Mullin, A.E., Elton, D., Digard, P. and Killip, M.J. (2007) 'Identification of the domains of the influenza A virus M1 matrix protein required for NP binding, oligomerization and incorporation into virions', Journal of General Virology, 88(8), pp. 2280–2290. doi:10.1099/vir.0.82809-0.

Oh, D., Kim, T. and Lee, H. (2019) 'Differential role of anti-viral sensing pathway for the production of type I interferon β in dendritic cells and macrophages against respiratory syncytial virus A2 strain infection', Viruses, 11(1), 62. doi:10.3390/v11010062.

Ohn, T., Kedersha, N., Hickman, T., Tisdale, S. and Anderson, P. (2008) 'A functional RNAi screen links O-GlcNAc modification of ribosomal proteins to stress granule and processing body assembly', Nature Cell Biology, 10(10), pp. 1224–1231. doi:10.1038/ncb1783.

Oliveira, M., Mesquita, J.R., Abreu-Silva, J., Ferreira, P. and Teixeira, J.P. (2020) 'Biowarfare, bioterrorism and biocrime: a historical overview on microbial harmful applications', Forensic Science International, 314, 110366. doi:10.1016/j.forsciint.2020.110366.

Olowokure, B., Clark, C., Isherwood, H., Elliot, A.J., Fleming, D.M. and Smith, G.E. (2004) 'Focus: SARS', Nature Reviews Microbiology, 2(2), p. 92. doi:10.1038/nrmicro824.

Oreshkova, N., Molenaar, R.J., Vreman, S., Harders, F., Oude Munnink, B.B., Hakze-van der Honing, R.W., Gerhards, N., Tolsma, P., Bouwstra, R., Sikkema, R.S., Tacken, M.G., de Rooij, M.M., Weesendorp, E., Engelsma, M.Y., Bruschke, C.J., Smit, L.A., Koopmans, M. and Stegeman, A. (2020) 'SARS-CoV-2 infection in farmed minks, the Netherlands, April and May 2020', Eurosurveillance, 25(23), 2001005. doi:10.2807/1560-7917.es.2020.25.23.2001005.

Pahl, H.L. and Baeuerle, P.A. (1996) 'Activation of NF-κB by ER stress requires both Ca2+ and reactive oxygen intermediates as messengers', FEBS Letters, 392(2), pp. 129–136. doi:10.1016/0014-5793(96)00800-9.

Palty, R., Stanley, C. and Isacoff, E.Y. (2015) 'Critical role for Orai1 C-terminal domain and TM4 in CRAC channel gating', Cell Research, 25(8), pp. 963–980. doi:10.1038/cr.2015.80.

Park, C.Y., Hoover, P.J., Mullins, F.M., Bachhawat, P., Covington, E.D., Raunser, S., Walz, T., Garcia, K.C., Dolmetsch, R.E. and Lewis, R.S. (2009) 'STIM1 clusters and activates CRAC channels via direct binding of a cytosolic domain to Orai1', Cell, 136(5), pp. 876–890. doi:10.1016/j.cell.2009.02.014.

Patz, J.A. (1996) 'Global climate change and emerging infectious diseases', JAMA: The Journal of the American Medical Association, 275(3), p. 217. doi:10.1001/jama.1996.03530270057032.

Pavia, A.T. (2011) 'Viral infections of the lower respiratory tract: old viruses, new viruses, and the role of diagnosis', Clinical Infectious Diseases, 52(Suppl. 4), pp. S284–S289. doi:10.1093/cid/cir043.

Peiris, J.S.M., Lai, S.T., Poon, L.L.M., Guan, Y., Yam, L.Y.C., Lim, W., Nicholls, J., Yee, W.K.S., Yan, W.W., Cheung, M.T., Cheng, V.C.C., Chan, K.H., Tsang, D.N.C., Yung, R.W.H., Ng, T.K., Yuen, K.Y. and SARS study group (2003) 'The severe acute respiratory syndrome', New England Journal of Medicine, 349(25), pp. 2431–2441. doi:10.1056/nejmra032498.

Peiris, M., Yuen, K.Y., Leung, C.W., Chan, K.H., Ip, P.L.S., Lai, R.W.M., Orr, W.K. and Shortridge, K.F. (1999) 'Human infection with influenza H9N2', The Lancet, 354(9182), pp. 916–917. doi:10.1016/s0140-6736(99)03311-5.

Peng, A.W., Milleri, S. and Stein, D.S. (2000) 'Direct measurement of the anti-influenza agent zanamivir in the respiratory tract following inhalation', Antimicrobial Agents and Chemotherapy, 44(7), pp. 1974–1976. doi:10.1128/AAC.44.7.1974-1976.2000.

Penna, A., Demuro, A., Yeromin, A.V., Zhang, S.L., Safrina, O., Parker, I. and Cahalan, M.D. (2008) 'The CRAC channel consists of a tetramer formed by STIM-induced dimerization of Orai dimers', Nature, 456(7218), pp. 116–120. doi:10.1038/nature07338.

Periasamy, M. and Kalyanasundaram, A. (2007) 'SERCA pump isoforms: their role in calcium transport and disease', Muscle & Nerve, 35(4), pp. 430–442. doi:10.1002/mus.20745.

Perrot, E. (1943) Matières premières usuelles du règne végétal: thérapeutique – hygiène – industrie, vol. 2. Paris: Masson et Cie.

Persson, B.D., Jaffe, A.B., Fearns, R. and Johnson, J.E. (2014) 'Respiratory syncytial virus can infect basal cells and alter human airway epithelial differentiation', PLOS ONE, 9(7), e102368. doi:10.1371/journal.pone.0102368.

Peset, J.L. (2015) 'Plagues and diseases in history', in Wright, J.D. (ed.) International encyclopedia of the social & behavioral sciences. 2nd edn. Amsterdam: Elsevier, pp. 174–179. doi:10.1016/b978-0-08-097086-8.62050-0.

Peters, L.R. and Raghavan, M. (2011) 'Endoplasmic reticulum calcium depletion impacts chaperone secretion, innate immunity, and phagocytic uptake of cells', The Journal of Immunology, 187(2), pp. 919–931. doi:10.4049/jimmunol.1100690.

Pflug, A., Guilligay, D., Reich, S. and Cusack, S. (2014) 'Structure of influenza A polymerase bound to the viral RNA promoter', Nature, 516(7531), pp. 355–360. doi:10.1038/nature14008.

Pflug, A., Guilligay, D., Reich, S. and Cusack, S. (2017) 'Structural insights into RNA synthesis by the influenza virus transcription–replication machine', Virus Research, 234, pp. 103–117. doi:10.1016/j.virusres.2017.01.013.

Pinto, L.H. and Lamb, R.A. (2005) 'The M2 proton channels of influenza A and B viruses', Journal of Biological Chemistry, 281(14), pp. 8997–9000. doi:10.1074/jbc.r500020200.

Piret, J. and Boivin, G. (2021) 'Pandemics throughout history', Frontiers in Microbiology, 11, 631736. doi:10.3389/fmicb.2020.631736.

Plotch, S.J., Bouloy, M., Ulmanen, I. and Krug, R.M. (1981) 'A unique cap(m7GpppXm)-dependent influenza virion endonuclease cleaves capped RNAs to generate the primers that initiate viral RNA transcription', Cell, 23(3), pp. 847–858. doi:10.1016/0092-8674(81)90449-9.

Potter, C.W. (2001) 'A history of influenza', Journal of Applied Microbiology, 91(4), pp. 572–579. doi:10.1046/j.1365-2672.2001.01492.x.

Powell, M.K., Aung, H., Griffin, J., O'Reilly, R., Morgan, S. and Cooper, D.A. (2016) 'Opportunistic infections in HIV-infected patients differ strongly in frequencies and spectra between patients with low CD4+ cell counts examined postmortem and compensated patients examined antemortem irrespective of the HAART era', PLOS ONE, 11(9), e0162704. doi:10.1371/journal.pone.0162704.

Plants of the World Online (no date) Facilitated by the Royal Botanic Gardens, Kew. Available at: http://www.plantsoftheworldonline.org/ (Accessed: 27 February 2023).

Prakriya, M. and Lewis, R.S. (2003) 'CRAC channels: activation, permeation, and the search for a molecular identity', Cell Calcium, 33(5–6), pp. 311–321. doi:10.1016/s0143-4160(03)00045-9.

Primeau, J.O., Armanious, G.P., Fisher, M.E., Young, H.S. and Squier, T.C. (2018) 'The sarco/endoplasmic reticulum calcium ATPase', Subcellular Biochemistry, 87, pp. 229–258. doi:10.1007/978-981-10-7757-9_8.

Putney, J.W. (1986) 'A model for receptor-regulated calcium entry', Cell Calcium, 7(1), pp. 1–12. doi:10.1016/0143-4160(86)90026-6.

Qi, L., Kash, J.C., Dugan, V.G., Jagger, B.W., Lau, Y.-F., Sheng, Z.-M., Crouch, E.C., Hartshorn, K.L., Taubenberger, J.K. and Basler, C.F. (2012) 'Analysis by single-gene reassortment demonstrates that the 1918 influenza virus is functionally compatible with a low-pathogenicity avian influenza virus in mice', Journal of Virology, 86(17), pp. 9211–9220. doi:10.1128/jvi.00887-12.

Rabadan, R., Levine, A.J. and Robins, H. (2006) 'Comparison of avian and human influenza A viruses reveals a mutational bias on the viral genomes', Journal of Virology, 80(23), pp. 11887–11891. doi:10.1128/jvi.01414-06.

Raffaello, A., Mammucari, C., Gherardi, G. and Rizzuto, R. (2016) 'Calcium at the center of cell signaling: interplay between endoplasmic reticulum, mitochondria, and lysosomes', Trends in Biochemical Sciences, 41(12), pp. 1035–1049. doi:10.1016/j.tibs.2016.09.001.

Rajsbaum, R., Albrecht, R.A., Wang, M.K., Maharaj, N.P., Versteeg, G.A., Nistal-Villán, E., García-Sastre, A. and Gack, M.U. (2012) 'Species-specific inhibition of RIG-I ubiquitination and IFN induction by the influenza A virus NS1 protein', PLOS Pathogens, 8(11), e1003059. doi:10.1371/journal.ppat.1003059.

Rajão, D.S. and Pérez, D.R. (2018) 'Universal vaccines and vaccine platforms to protect against influenza viruses in humans and agriculture', Frontiers in Microbiology, 9, 123. doi:10.3389/fmicb.2018.00123.

Rameix-Welti, M.-A., Le Goffic, R., Hervé, P.-L., Moules, V., Gruenert, D.C., Madelaine, M.-F., Dausset, J., Chignard, M., Pothlichet, J., Si-Tahar, M. and Eléouët, J.-F. (2014) 'Visualizing the replication of respiratory syncytial virus in cells and in living mice', Nature Communications, 5, 5104. doi:10.1038/ncomms6104.

Rappuoli, R. and Del Giudice, G. (2019) 'Inhibiting neuraminidase can make the difference', Journal of Experimental Medicine, 216(2), pp. 251–252. doi:10.1084/jem.20182245.

Rasmussen, U., Broegger Christensen, S. and Sandberg, F. (1978) 'Thapsigargine and thapsigargicine, two new histamine liberators from Thapsia garganica L.', Acta Pharmaceutica Suecica, 15(2), pp. 133–140.

Reeves, J.D. and Doms, R.W. (2002) 'Human immunodeficiency virus type 2', Journal of General Virology, 83(6), pp. 1253–1265. doi:10.1099/0022-1317-83-6-1253.

Reich, S., Guilligay, D., Pflug, A. and Cusack, S. (2014) 'Structural insight into cap-snatching and RNA synthesis by influenza polymerase', Nature, 516(7531), pp. 361–366. doi:10.1038/nature14009.

Reich, S., Guilligay, D. and Cusack, S. (2017) 'An in vitro fluorescence-based study of initiation of RNA synthesis by influenza B polymerase', Nucleic Acids Research, 45(6), pp. 3353–3368. doi:10.1093/nar/gkx043.

Reperant, L.A., Moesker, F.M. and Osterhaus, A.D.M.E. (2016) 'Influenza: from zoonosis to pandemic', ERJ Open Research, 2(1), 00013–2016. doi:10.1183/23120541.00013-2016.

Riedel, S. (2005) 'Edward Jenner and the history of smallpox and vaccination', Baylor University Medical Center Proceedings, 18(1), pp. 21–25. doi:10.1080/08998280.2005.11928028.

Robb, N.C., Smith, M., Vreede, F.T. and Fodor, E. (2009) 'NS2/NEP protein regulates transcription and replication of the influenza virus RNA genome', Journal of General Virology, 90(6), pp. 1398–1407. doi:10.1099/vir.0.009639-0.

Robb, N.C., Chase, G., Bier, K., Vreede, F.T., Shaw, P.C., Naffakh, N., Schwemmle, M. and Fodor, E. (2016) 'Single-molecule FRET reveals the pre-initiation and initiation conformations of influenza virus promoter RNA', Nucleic Acids Research, 44(2), pp. 1034–1042. doi:10.1093/nar/gkw884.

Rodger, A.J., Cambiano, V., Bruun, T., Vernazza, P., Collins, S., van Lunzen, J., Corbelli, G.M., Degen, O., Raben, D., Prins, J.M., Di Caro, A., Fuentes, A.C., Bogner, J.R., Estrada, V., Geretti, A.M., Beloukas, A., Asboe, D., Viciana, P., Gutiérrez, F., Weber, R., Westling, K., Wandeler, G., Geretti, A.M., Collins, S., Lundgren, J. and PARTNER Study Group (2019) 'Risk of HIV transmission through condomless sex in serodifferent gay couples with the HIV-positive partner taking suppressive antiretroviral therapy (PARTNER): final results of a multicentre, prospective, observational study', The Lancet, 393(10189), pp. 2428–2438. doi:10.1016/s0140-6736(19)30418-0.

Romero-Tejeda, A. and Capua, I. (2013) 'Virus-specific factors associated with zoonotic and pandemic potential', Influenza and Other Respiratory Viruses, 7, pp. 4–14. doi:10.1111/irv.12075.

Ron, D. and Walter, P. (2007) 'Signal integration in the endoplasmic reticulum unfolded protein response', Nature Reviews Molecular Cell Biology, 8(7), pp. 519–529. doi:10.1038/nrm2199.

Roos, J., DiGregorio, P.J., Yeromin, A.V., Ohlsen, K., Lioudyno, M., Zhang, S., Safrina, O., Kozak, J.A., Wagner, S.L., Cahalan, M.D. and Stauderman, K.A. (2005) 'STIM1, an essential and conserved component of store-operated Ca2+ channel function', Journal of Cell Biology, 169(3), pp. 435–445. doi:10.1083/jcb.200502019.

Rosenberg, H.F. and Domachowske, J.B. (2012) 'Inflammatory responses to respiratory syncytial virus (RSV) infection and the development of immunomodulatory pharmacotherapeutics', Current Medicinal Chemistry, 19(10), pp. 1424–1431. doi:10.2174/092986712799828346.

Rosenberg, R. (2014) 'Detecting the emergence of novel, zoonotic viruses pathogenic to humans', Cellular and Molecular Life Sciences, 72(6), pp. 1115–1125. doi:10.1007/s00018-014-1785-y.

Rossman, J.S. and Lamb, R.A. (2013) 'Viral membrane scission', Annual Review of Cell and Developmental Biology, 29(1), pp. 551–569. doi:10.1146/annurev-cellbio-101011-155838.

Rota, P.A., Wallis, T.R., Harmon, M.W., Rota, J.S., Kendal, A.P. and Nerome, K. (1990) 'Cocirculation of two distinct evolutionary lineages of influenza type B virus since 1983', Virology, 175(1), pp. 59–68. doi:10.1016/0042-6822(90)90186-u.

Rothberg, B.S., Wang, Y. and Gill, D.L. (2013) 'Orai channel pore properties and gating by STIM: implications from the Orai crystal structure', Science Signaling, 6(267), ra24. doi:10.1126/scisignal.2003971.

Roy, A.-M.M., Parker, J.S., Parrish, C.R., Whittaker, G.R. and Compans, R.W. (2000) 'Early stages of influenza virus entry into Mv-1 lung cells: involvement of dynamin', Virology, 267(1), pp. 17–28. doi:10.1006/viro.1999.0109.

Sagara, Y. and Inesi, G. (1991) 'Inhibition of the sarcoplasmic reticulum Ca2+ transport ATPase by thapsigargin at subnanomolar concentrations', Journal of Biological Chemistry, 266(21), pp. 13503–13506. doi:10.1016/s0021-9258(18)92726-2.

Sagara, Y., Wade, J.B. and Inesi, G. (1992) 'A conformational mechanism for formation of a dead-end complex by the sarcoplasmic reticulum ATPase with thapsigargin', Journal of Biological Chemistry, 267(2), pp. 1286–1292. doi:10.1016/s0021-9258(18)48427-x.

Sakaguchi, T. (1996) 'The ion channel activity of the influenza virus M2 protein affects transport through the Golgi apparatus', The Journal of Cell Biology, 133(4), pp. 733–747. doi:10.1083/jcb.133.4.733.

Saleh, N., Van Petegem, F., Despa, S., Weiss, J.N. and Bers, D.M. (2019) 'Allosteric modulation of the sarcoplasmic reticulum Ca2+ ATPase by thapsigargin via decoupling of functional motions', Physical Chemistry Chemical Physics, 21(39), pp. 21991–21995. doi:10.1039/c9cp04736k.

Salvatore, M., Basler, C.F., O'Neill, R.E., Ilyushina, N., Harris, A., Ambrose, M., Rehg, J.E. and Palese, P. (2002) 'Effects of influenza A virus NS1 protein on protein expression: the NS1 protein enhances translation and is not required for shutoff of host protein synthesis', Journal of Virology, 76(3), pp. 1206–1212. doi:10.1128/jvi.76.3.1206-1212.2002.

Salzberg, S. (2009) 'Faculty opinions recommendation of origins and evolutionary genomics of the 2009 swine-origin H1N1 influenza A epidemic', Faculty Opinions – Post-Publication Peer Review of the Biomedical Literature [Preprint]. doi:10.3410/f.1162111.622575.

Sampath, S., Khedr, A., Chidambaram, S.A., Chidambaram, S., Ravichandran, J., Maheshwari, R., Sahoo, S., Adinarayanan, S., Ganesan, S. and Subramanian, M. (2021) 'Pandemics throughout the history', Cureus [Preprint]. doi:10.7759/cureus.18136.

Satterly, N., Tsai, P.-L., van Deursen, J., Nussenzveig, D.R., Wang, Y., Faria, P.A., Levay, A., Levy, D.E. and Fontoura, B.M.A. (2007) 'Influenza virus targets the mRNA export machinery and the nuclear pore complex', Proceedings of the National Academy of Sciences of the United States of America, 104(6), pp. 1853–1858. doi:10.1073/pnas.0610977104.

Saunders-Hastings, P. and Krewski, D. (2016) 'Reviewing the history of pandemic influenza: understanding patterns of emergence and transmission', Pathogens, 5(4), 66. doi:10.3390/pathogens5040066.

Schildgen, V., Simon, A. and Williams, J. (2011) 'Human metapneumovirus: lessons learned over the first decade', Clinical Microbiology Reviews, 24(4), pp. 734–754. doi:10.1128/cmr.00015-11.

Schäffr, J.R., Webster, R.G., Bean, W.J., Kawaoka, Y., Kendal, A.P. and Shortridge, K.F. (1993) 'Origin of the pandemic 1957 H2 influenza A virus and the persistence of its possible progenitors in the avian reservoir', Virology, 194(2), pp. 781–788. doi:10.1006/viro.1993.1319.

Schögler, A., Kopf, B.S., Edwards, M.R., Johnston, S.L., Casaulta, C., Kieninger, E., Jung, A., Moeller, A., Geiser, T., Regamey, N. and Alves, M.P. (2019) 'Modulation of the unfolded protein response pathway as an antiviral approach in airway epithelial cells', Antiviral Research, 162, pp. 44–50. doi:10.1016/j.antiviral.2018.12.007.

Schönthal, A.H. (2012) 'Endoplasmic reticulum stress: its role in disease and novel prospects for therapy', Scientifica, 2012, 857516. doi:10.6064/2012/857516.

Sehgal, P., Szalai, P., Olesen, C., Praetorius, H.A., Nissen, P., Christensen, S.B. and Engedal, N. (2017) 'Inhibition of the sarco/endoplasmic reticulum (ER) Ca2+-ATPase by thapsigargin analogues induces cell death via ER Ca2+ depletion and the unfolded protein response', Journal of Biological Chemistry, 292(48), pp. 19656–19673. doi:10.1074/jbc.m117.796920.

Sempere Borau, M. and Stertz, S. (2021) 'Entry of influenza A virus into host cells — recent progress and remaining challenges', Current Opinion in Virology, 48, pp. 23–29. doi:10.1016/j.coviro.2021.03.001.

Sharp, P.M. and Hahn, B.H. (2011) 'Origins of HIV and the AIDS pandemic', Cold Spring Harbor Perspectives in Medicine, 1(1), a006841. doi:10.1101/cshperspect.a006841.

Shaw, P.J., Weidinger, C., Vaeth, M., Luethy, K., Kaech, S.M., Hancock, W.W., Hoth, M., Feske, S. and Rothermel, B.A. (2014) 'CD4+ and CD8+ T cell–dependent antiviral immunity requires STIM1 and STIM2', Journal of Clinical Investigation, 124(10), pp. 4549–4563. doi:10.1172/jci76602.

Shen, J., Chen, X., Hendershot, L.M. and Prywes, R. (2002) 'ER stress regulation of ATF6 localization by dissociation of BiP/GRP78 binding and unmasking of Golgi localization signals', Developmental Cell, 3(1), pp. 99–111. doi:10.1016/s1534-5807(02)00203-4.

Shinya, K., Ebina, M., Yamada, S., Ono, M., Kasai, N. and Kawaoka, Y. (2006) 'Influenza virus receptors in the human airway', Nature, 440(7083), pp. 435–436. doi:10.1038/440435a.

Shope, R.E. (1931) ‘Swine influenza’, Journal of Experimental Medicine, 54(3), pp. 373–385. doi:10.1084/jem.54.3.373.

Short, K.R., Richard, M., Verhagen, J.H., van Riel, D., Schrauwen, E.J.A. and van den Brand, J.M.A. (2015) ‘One health, multiple challenges: the inter-species transmission of influenza A virus’, One Health, 1, pp. 1–13. doi:10.1016/j.onehlt.2015.03.001.

Shuttleworth, T.J. (2012) ‘Orai3 — the “exceptional” Orai?’, The Journal of Physiology, 590(2), pp. 241–257. doi:10.1113/jphysiol.2011.220574.

Siegert, W., Bauer, G. and Hofschneider, P.H. (1973) ‘Direct evidence for messenger activity of influenza virion RNA’, Proceedings of the National Academy of Sciences of the United States of America, 70(10), pp. 2960–2963. doi:10.1073/pnas.70.10.2960.

Simonsen, L., Spreeuwenberg, P., Lustig, R., Taylor, R.J., Fleming, D.M., Kroneman, M., Van Kerkhove, M.D., Mounts, A.W., Paget, W.J. and GLaMOR Collaborating Teams (2013) ‘Global mortality estimates for the 2009 influenza pandemic from the GLaMOR project: a modelling study’, PLOS Medicine, 10(11), e1001558. doi:10.1371/journal.pmed.1001558.

Smith, J.A. (2014) ‘A new paradigm: innate immune sensing of viruses via the unfolded protein response’, Frontiers in Microbiology, 5, 222. doi:10.3389/fmicb.2014.00222.

Smith, W., Andrewes, C.H. and Laidlaw, P.P. (1933) ‘A virus obtained from influenza patients’, The Lancet, 222(5732), pp. 66–68. doi:10.1016/s0140-6736(00)78541-2.

Smitt, U. and Christensen, S. (1991) ‘Nortrilobolide, a new potent guaianolide secretagogue from Thapsia garganica’, Planta Medica, 57(2), pp. 196–197. doi:10.1055/s-2006-960067.

Smitt, U.W., Jäger, A.K. and Nyman, U. (1996) ‘Thapsia garganica L.: in vitro culture, somatic embryogenesis, and the production of thapsigargins’, Biotechnology in Agriculture and Forestry, 38, pp. 402–409. doi:10.1007/978-3-662-08618-6_24.

Smyth, J.T., Hwang, S.-Y., Tomita, T., DeHaven, W.I., Mercer, J.C. and Putney, J.W. (2010) ‘Activation and regulation of store-operated calcium entry’, Journal of Cellular and Molecular Medicine, 14(10), pp. 2337–2349. doi:10.1111/j.1582-4934.2010.01168.x.

Soboloff, J., Rothberg, B.S., Madesh, M. and Gill, D.L. (2012) ‘STIM proteins: dynamic calcium signal transducers’, Nature Reviews Molecular Cell Biology, 13(9), pp. 549–565. doi:10.1038/nrm3414.

Sorci, G., Faivre, B. and Morand, S. (2020) ‘Explaining among-country variation in COVID-19 case fatality rate’, Scientific Reports, 10, 18909. doi:10.1038/s41598-020-75848-2.

Srikanth, S., Woo, J.S., Wu, B., El-Sherbiny, Y.M., Leung, J., Chupradit, K., Rice, L., Seo, G.J., Calmettes, G., Ramakrishna, C., Cantor, J., Jonsson, C.B., Cameron, C.E., Bergelson, J.M., Shumilina, E., Lang, F., Yoo, J.S., John, S., Wu, T.T., Arvan, P., Hwang, S., Nicholls, P.K., Choi, J.-M., He, L., Luo, X., Feske, S. and Gwack, Y. (2019) ‘The Ca2+ sensor STIM1 regulates the type I interferon response by retaining the signalling adaptor STING at the endoplasmic reticulum’, Nature Immunology, 20(2), pp. 152–162. doi:10.1038/s41590-018-0287-8.

Stathopulos, P.B., Zheng, L. and Ikura, M. (2009) ‘Stromal interaction molecule (STIM) 1 and STIM2 calcium sensing regions exhibit distinct unfolding and oligomerization kinetics’, Journal of Biological Chemistry, 284(2), pp. 728–732. doi:10.1074/jbc.c800178200.

Steinhauer, D.A., Wharton, S.A., Skehel, J.J., Wiley, D.C. and Hay, A.J. (1991) ‘Amantadine selection of a mutant influenza virus containing an acid-stable hemagglutinin glycoprotein: evidence for virus-specific regulation of the pH of glycoprotein transport vesicles’, Proceedings of the National Academy of Sciences of the United States of America, 88(24), pp. 11525–11529. doi:10.1073/pnas.88.24.11525.

Stevens, F.J. and Argon, Y. (1999) ‘Protein folding in the ER’, Seminars in Cell & Developmental Biology, 10(5), pp. 443–454. doi:10.1006/scdb.1999.0315.

Stieneke-Gröber, A., Vey, M., Angliker, H., Shaw, E., Thomas, G., Roberts, C., Klenk, H.D. and Garten, W. (1992) ‘Influenza virus hemagglutinin with multibasic cleavage site is activated by furin, a subtilisin-like endoprotease’, The EMBO Journal, 11(7), pp. 2407–2414. doi:10.1002/j.1460-2075.1992.tb05305.x.

Stockman, L.J., Bellamy, R. and Garner, P. (2006) ‘SARS: systematic review of treatment effects’, PLOS Medicine, 3(9), e343. doi:10.1371/journal.pmed.0030343.

Stridh, S., Datema, R. and Scholtissek, C. (1985) ‘The influenza A virus protein PB1 undergoes a conformational rearrangement during mRNA primed influenza virus mRNA synthesis’, Virus Research, 3(1), pp. 17–32. doi:10.1016/0168-1702(85)90286-2.

Su, G., Jin, H., Zhang, L., Xu, H., Wang, D., Lin, W., Chen, P., Wang, Y., Gao, G.F. and Liu, W. (2024) ‘Virus versus host: influenza A virus circumvents the immune responses’, Frontiers in Microbiology, 15, 1394510. doi:10.3389/fmicb.2024.1394510.

Summerfield, A. and McCullough, K. (2009) ‘Dendritic cells in innate and adaptive immune responses against influenza virus’, Viruses, 1(3), pp. 1022–1034. doi:10.3390/v1031022.

Suzuki, Y., Ito, T., Suzuki, T., Holland, R.E., Chambers, T.M., Kiso, M., Ishida, H. and Kawaoka, Y. (2000) ‘Sialic acid species as a determinant of the host range of influenza A viruses’, Journal of Virology, 74(24), pp. 11825–11831. doi:10.1128/jvi.74.24.11825-11831.2000.

Sze, S., Pan, D., Nevill, C.R., Gray, L.J., Martin, C.A., Nazareth, J., Minhas, J.S., Divall, P., Khunti, K. and Abrams, K.R. (2020) ‘Ethnicity and clinical outcomes in COVID-19: a systematic review and meta-analysis’, EClinicalMedicine, 29–30, 100630. doi:10.1016/j.eclinm.2020.100630.

Takemura, H. and Putney, J.W. (1989) ‘Capacitative calcium entry in parotid acinar cells’, Biochemical Journal, 258(2), pp. 409–412. doi:10.1042/bj2580409.

Takemura, H., Hughes, A.R., Thastrup, O. and Putney, J.W. (1989) ‘Activation of calcium entry by the tumour promoter thapsigargin in parotid acinar cells’, Journal of Biological Chemistry, 264(21), pp. 12266–12271. doi:10.1016/s0021-9258(18)63852-9.

Taubenberger, J.K. and Morens, D.M. (2006) ‘1918 influenza: the mother of all pandemics’, Emerging Infectious Diseases, 12(1), pp. 15–22. doi:10.3201/eid1209.05-0979.

Taubenberger, J.K. and Morens, D.M. (2008) ‘The pathology of influenza virus infections’, Annual Review of Pathology: Mechanisms of Disease, 3, pp. 499–522. doi:10.1146/annurev.pathmechdis.3.121806.154316.

Taubenberger, J.K. and Morens, D.M. (2010) ‘Influenza: the once and future pandemic’, Public Health Reports, 125(Suppl. 3), pp. 15–26. doi:10.1177/00333549101250s305.

Taylor, L.H., Latham, S.M. and Woolhouse, M.E.J. (2001) ‘Risk factors for human disease emergence’, Philosophical Transactions of the Royal Society of London. Series B: Biological Sciences, 356(1411), pp. 983–989. doi:10.1098/rstb.2001.0888.

Tayyari, F., Marchant, D., Moraes, T.J., Duan, W., Mastrangelo, P. and Hegele, R.G. (2011) ‘Identification of nucleolin as a cellular receptor for human respiratory syncytial virus’, Nature Medicine, 17(9), pp. 1132–1135. doi:10.1038/nm.2444.

Thacker, S.B. (1987) ‘The diffusion of influenza: patterns and paradigms’, JAMA: The Journal of the American Medical Association, 258(3), p. 389. doi:10.1001/jama.1987.03400030105046.

Thastrup, O., Cullen, P.J., Drøbak, B.K., Hanley, M.R. and Dawson, A.P. (1989) 'Thapsigargin, a novel molecular probe for studying intracellular calcium release and storage', Agents and Actions, 27(1–2), pp. 17–23. doi:10.1007/bf02222186.

Thastrup, O., Dawson, A.P., Scharff, O., Foder, B., Cullen, P.J., Drøbak, B.K., Bjerrum, P.J., Christensen, S.B. and Hanley, M.R. (1990) 'Thapsigargin, a tumour promoter, discharges intracellular Ca2+ stores by specific inhibition of the endoplasmic reticulum Ca2+-ATPase', Proceedings of the National Academy of Sciences of the United States of America, 87(7), pp. 2466–2470. doi:10.1073/pnas.87.7.2466.

Theophrastus and Hort, A. (1916) Enquiry into plants and minor works on odours and weather signs, with an English translation by Sir Arthur Hort, Bart. [Preprint]. doi:10.5962/bhl.title.27820.

Tompa, D.R., Immanuel, T.J., Srikanth, M., Natarajan, S. and Karthikeyan, M. (2021) 'Trends and strategies to combat viral infections: a review on FDA approved antiviral drugs', International Journal of Biological Macromolecules, 172, pp. 524–541. doi:10.1016/j.ijbiomac.2021.01.076.

Tong, S., Li, Y., Rivailler, P., Conrardy, C., Castillo, D.A., Chen, L.-M., Recuenco, S., Ellison, J.A., Davis, C.T., York, I.A., Turmelle, A.S., Moran, D., Rogers, S., Shi, M., Tao, Y., Weil, M.R., Tang, K., Rowe, L.A., Sammons, S., Xu, X., Frace, M., Lindblade, K.A., Cox, N.J., Anderson, L.J., Rupprecht, C.E. and Donis, R.O. (2012) 'A distinct lineage of influenza A virus from bats', Proceedings of the National Academy of Sciences of the United States of America, 109(11), pp. 4269–4274. doi:10.1073/pnas.1116200109.

Toyoshima, C. (2009) 'How Ca2+-ATPase pumps ions across the sarcoplasmic reticulum membrane', Biochimica et Biophysica Acta (BBA) - Molecular Cell Research, 1793(6), pp. 941–946. doi:10.1016/j.bbamcr.2008.10.008.

Toyoshima, C. and Nomura, H. (2002) 'Structural changes in the calcium pump accompanying the dissociation of calcium', Nature, 418(6898), pp. 605–611. doi:10.1038/nature00944.

Tregoning, J.S., Yamaguchi, Y., Harker, J., Wang, B., Openshaw, P.J.M. and Schwarze, J. (2008) 'The role of T cells in the enhancement of respiratory syncytial virus infection severity during adult reinfection of neonatally sensitized mice', Journal of Virology, 82(8), pp. 4115–4124. doi:10.1128/jvi.02313-07.

Trotter, Y., Dull, H.B., Langmuir, A.D., Hedberg, C.L., Witte, J.J. and Hall, H.E. (1959) 'Asian influenza in the United States, 1957–1958', American Journal of Epidemiology, 70(1), pp. 34–50. doi:10.1093/oxfordjournals.aje.a120063.

Tschirch, A. and Stock, E. (1936) Die Harze. Berlin: Verlag von Gebrüder Borntträger, 2nd half, 2nd part, p. 1540.

Turale, S., Meechamnan, C. and Kunaviktikul, W. (2020) 'Challenging times: ethics, nursing and the COVID-19 pandemic', International Nursing Review, 67(2), pp. 164–167. doi:10.1111/inr.12598.

Turner, T., Kinnear, E., Song, A., Akbar, A.N., Harker, J.A. and Tregoning, J.S. (2014) 'Respiratory syncytial virus: current and emerging treatment options', ClinicoEconomics and Outcomes Research, 6, pp. 217–225. doi:10.2147/ceor.s60710.

UNAIDS (2013) UNAIDS report on the global AIDS epidemic 2013. Available at: https://www.unaids.org/sites/default/files/media_asset/UNAIDS_Global_Report_2013_en_1.pdf (Accessed: 5 September 2025).

Utley, T.J., Ducharme, N.A., Varthakavi, V., Shepherd, B.E., Santangelo, P.J., Lindquist, M.E., Goldenring, J.R., Crowe, J.E. and Wright, J.R. (2008) 'Respiratory syncytial virus uses a Vps4-independent budding mechanism controlled by Rab11-FIP2', Proceedings of the National Academy of Sciences of the United States of America, 105(29), pp. 10209–10214. doi:10.1073/pnas.0712144105.

Vaeth, M., Eckstein, M., Shaw, P.J., Kozhaya, L., Yang, J., Berberich-Siebelt, F., Clancy, R., Unutmaz, D., Feske, S. and Kummerow, C. (2017) 'Store-operated Ca2+ entry controls clonal expansion of T cells through metabolic reprogramming', Immunity, 47(4), pp. 664–679.e6. doi:10.1016/j.immuni.2017.09.003.

van Huizen, R., Martindale, J.L., Gorospe, M. and Holbrook, N.J. (2003) 'p58IPK, a novel endoplasmic reticulum stress-inducible protein and potential negative regulator of eIF2α signalling', Journal of Biological Chemistry, 278(18), pp. 15558–15564. doi:10.1074/jbc.m212074200.

Veerapandian, R., Snyder, J.D. and Samarasinghe, A.E. (2018) 'Influenza in asthmatics: for better or for worse?', Frontiers in Immunology, 9, 1843. doi:10.3389/fimmu.2018.01843.

Veit, M. and Thaa, B. (2011) 'Association of influenza virus proteins with membrane rafts', Advances in Virology, 2011, 370606. doi:10.1155/2011/370606.

Viboud, C., Miller, M.A., Olson, D.R., Osterholm, M.T. and Simonsen, L. (2005) 'Multinational impact of the 1968 Hong Kong influenza pandemic: evidence for a smouldering pandemic', The Journal of Infectious Diseases, 192(2), pp. 233–248. doi:10.1086/431150.

Viboud, C., Simonsen, L., Fuentes, R., Flores, J., Miller, M.A. and Chowell, G. (2016) 'Global mortality impact of the 1957–1959 influenza pandemic', Journal of Infectious Diseases, 213(5), pp. 738–745. doi:10.1093/infdis/jiv534.

Viboud, C., Alonso, W.J. and Simonsen, L. (2006) 'Influenza in tropical regions', PLOS Medicine, 3(4), e89. doi:10.1371/journal.pmed.0030089.

Wahlgren, J. (2011) 'Influenza A viruses: an ecology review', Infection Ecology & Epidemiology, 1, 6004. doi:10.3402/iee.v1i0.6004.

Walter, P. and Ron, D. (2011) 'The unfolded protein response: from stress pathway to homeostatic regulation', Science, 334(6059), pp. 1081–1086. doi:10.1126/science.1209038.

Wan, H. and Perez, D.R. (2006) 'Quail carry sialic acid receptors compatible with binding of avian and human influenza viruses', Virology, 346(2), pp. 278–286. doi:10.1016/j.virol.2005.10.035.

Wang, H., Paulson, K.R., Pease, S.A., Watson, S., Comfort, H., Zheng, P., Mullany, E.C., Lindstrom, A., Brolin Ribacke, K., Peacocke, E.F., Gray, G., Bannick, M.S., Barber, R., Carter, A., Chen, C., Fullman, N., Hay, S.I., Lozano, R., Mokdad, A.H., Naghavi, M., Pigott, D.M., Reiner, R.C., Sorensen, R.J.D., Vos, T., Murray, C.J.L. and Collaborators, C.-M. (2022) 'Estimating excess mortality due to the COVID-19 pandemic: a systematic analysis of COVID-19-related mortality, 2020–21', The Lancet, 399(10334), pp. 1513–1536. doi:10.1016/s0140-6736(21)02796-3.

Wang, L.-F. and Eaton, B.T. (2007) 'Bats, civets and the emergence of SARS', Current Topics in Microbiology and Immunology [Preprint].

Weitzel, C., Petersen, G., Jensen, S.R., Möller, B.L. and Christensen, S.B. (2014) 'Resurrecting deadly carrots: towards a revision of Thapsia (Apiaceae) based on phylogenetic analysis of nrITS sequences and chemical profiles', Botanical Journal of the Linnean Society, 174(4), pp. 620–636. doi:10.1111/boj.12144.

World Health Organization (2007) Rapid operations to control the initial emergence of pandemic influenza. Geneva: WHO.

World Health Organization (2009) Recommended use of antivirals: pandemic (H1N1) 2009 briefing note 8. Geneva: WHO.

World Health Organization (2010) H1N1 in post-pandemic period. Available at: https://www.who.int/news/item/10-08-2010-h1n1-in-post-pandemic-period (Accessed: 11 August 2022).

World Health Organization (2022) HIV. Available at: https://www.who.int/news-room/fact-sheets/detail/hiv-aids(Accessed: 10 August 2022).

Willing, E. (2017) Thapsia garganica L. (Willing 1), Flora of Greece Web – Vascular Plants of Greece: An Annotated Checklist. Available at: https://portal.cybertaxonomy.org/flora-greece/cdm_dataportal/taxon/729f96b7-9d13-4e6a-ad95-7cffb58b3fff (Accessed: 27 February 2023).

Woehlbier, U. and Hetz, C. (2011) 'Modulating stress responses by the UPRosome: a matter of life and death', Trends in Biochemical Sciences, 36(6), pp. 329–337. doi:10.1016/j.tibs.2011.03.001.

Wolfe, N.D., Dunavan, C.P. and Diamond, J. (2007) 'Origins of major human infectious diseases', Nature, 447(7142), pp. 279–283. doi:10.1038/nature05775.

Woolhouse, M.E.J. and Brierley, L. (2018) 'Epidemiological characteristics of human-infective RNA viruses', Scientific Data, 5, 180017. doi:10.1038/sdata.2018.17.

Wright, J. and Priston, N. (2010) 'Hunting and trapping in Lebialem Division, Cameroon: bushmeat harvesting practices and human reliance', Endangered Species Research, 11, pp. 1–12. doi:10.3354/esr00244.

Wu, M.M., Buchanan, J., Luik, R.M. and Lewis, R.S. (2006) 'Ca2+ store depletion causes STIM1 to accumulate in ER regions closely associated with the plasma membrane', The Journal of Cell Biology, 174(6), pp. 803–813. doi:10.1083/jcb.200604014.

Wu, W., Zhang, W., Duggan, E.S., Booth, J.L., Zou, M.H., Metcalf, J.P. and McCrae, K.R. (2016) 'Human primary airway epithelial cells isolated from active smokers have epigenetically impaired antiviral responses', Respiratory Research, 17, 5. doi:10.1186/s12931-016-0428-2.

Wu, W.W.H., Weaver, L.L. and Panté, N. (2007) 'Ultrastructural analysis of the nuclear localization sequences on influenza A ribonucleoprotein complexes', Journal of Molecular Biology, 374(4), pp. 910–916. doi:10.1016/j.jmb.2007.10.022.

Xu, C. (2005) 'Endoplasmic reticulum stress: cell life and death decisions', Journal of Clinical Investigation, 115(10), pp. 2656–2664. doi:10.1172/jci26373.

Xu, C., Ma, H., Inesi, G. and Toyoshima, C. (2004) 'Specific structural requirements for the inhibitory effect of thapsigargin on the Ca2+ ATPase SERCA', Journal of Biological Chemistry, 279(17), pp. 17973–17979. doi:10.1074/jbc.m313263200.

Xu, H. and Van Remmen, H. (2021) 'The sarco/endoplasmic reticulum calcium ATPase (SERCA) pump: a potential target for intervention in ageing and skeletal muscle pathologies', Skeletal Muscle, 11, 13. doi:10.1186/s13395-021-00280-7.

Xu, X., Chen, P., Wang, J., Feng, J., Zhou, H., Li, X., Zhong, W. and Hao, P. (2020) 'Evolution of the novel coronavirus from the ongoing Wuhan outbreak and modelling of its spike protein for risk of human transmission', Science China Life Sciences, 63(3), pp. 457–460. doi:10.1007/s11427-020-1637-5.

Yamashita, M., Yeung, P.S.-W., Ing, C.E., McNally, B.A., Pomès, R. and Prakriya, M. (2017) 'STIM1 activates CRAC channels through rotation of the pore helix to open a hydrophobic gate', Nature Communications, 8, 14512. doi:10.1038/ncomms14512.

Yan, J., Grantham, M., Pantelic, J., Bueno de Mesquita, P.J., Albert, B., Liu, F., Ehrman, S., Milton, D.K. and EMIT Consortium (2018) 'Infectious virus in exhaled breath of symptomatic seasonal influenza cases from a college community', Proceedings of the National Academy of Sciences of the United States of America, 115(5), pp. 1081–1086. doi:10.1073/pnas.1716561115.

Ye, C., Dickman, M.B. and Whitham, S.A. (2011) 'The unfolded protein response is triggered by a plant viral movement protein', Plant Physiology, 156(2), pp. 741–755. doi:10.1104/pp.111.174110.

York, A., Hengrung, N., Vreede, F.T., Huiskonen, J.T. and Fodor, E. (2013) 'Isolation and characterization of the positive-sense replicative intermediate of a negative-strand RNA virus', Proceedings of the National Academy of Sciences of the United States of America, 110(45), pp. E4238–E4245. doi:10.1073/pnas.1315068110.

Yoshida, H., Matsui, T., Yamamoto, A., Okada, T. and Mori, K. (2001) 'XBP1 mRNA is induced by ATF6 and spliced by IRE1 in response to ER stress to produce a highly active transcription factor', Cell, 107(7), pp. 881–891. doi:10.1016/s0092-8674(01)00611-0.

Yu, M., Haslam, R.J., Haslam, J., Crabb, J.W. and Howell, T.W. (1998) 'Specific substitutions at amino acid 256 of the sarcoplasmic/endoplasmic reticulum Ca2+ transport ATPase mediate resistance to thapsigargin in thapsigargin-resistant hamster cells', Journal of Biological Chemistry, 273(6), pp. 3542–3546. doi:10.1074/jbc.273.6.3542.

Yu, X., Carroll, S., Rigaud, J.-L., Inesi, G., Zhang, Z. and Lenoir, C. (1993) 'H+ countertransport and electrogenicity of the sarcoplasmic reticulum Ca2+ pump in reconstituted proteoliposomes', Biophysical Journal, 64(4), pp. 1232–1242. doi:10.1016/s0006-3495(93)81489-9.

Yuan, J.P., Zeng, W., Huang, G.N., Worley, P.F. and Muallem, S. (2009) 'SOAR and the polybasic STIM1 domains gate and regulate Orai channels', Nature Cell Biology, 11(3), pp. 337–343. doi:10.1038/ncb1842.

Yuan, P., Bartlam, M., Lou, Z., Chen, S., Zhou, J., He, X., Lv, Z., Ge, R., Li, X., Deng, T., Fodor, E., Rao, Z. and Liu, Y. (2009) 'Crystal structure of an avian influenza polymerase PA-N reveals an endonuclease active site', Nature, 458(7240), pp. 909–913. doi:10.1038/nature07720.

Yuen, K.Y., Lam, J.S., Wang, L.F., Anderson, D.E., Field, H.E., Barr, J.A., Bingham, J., Marsh, G.A., Wang, L. and Broder, C.C. (2021) 'Hendra virus: epidemiology dynamics in relation to climate change, diagnostic tests and control measures', One Health, 12, 100207. doi:10.1016/j.onehlt.2020.100207.

Zafar, S., Hussain, M., Møller, J.V., Hasler, U., Lenoir, C. and Toyoshima, C. (2008) 'Specificity of ligand binding to transport sites: Ca2+ binding to the Ca2+ transport ATPase and its dependence on H+ and Mg2+', Archives of Biochemistry and Biophysics, 476(1), pp. 87–94. doi:10.1016/j.abb.2008.04.035.

Zavada, J. (1982) 'The pseudotypic paradox', Journal of General Virology, 63(1), pp. 15–24. doi:10.1099/0022-1317-63-1-15.

Zhang, J., Pekosz, A. and Lamb, R.A. (2000) 'Influenza virus assembly and lipid raft microdomains: a role for the cytoplasmic tails of the spike glycoproteins', Journal of Virology, 74(10), pp. 4634–4644. doi:10.1128/jvi.74.10.4634-4644.2000.

Zhang, K. and Kaufman, R.J. (2008) 'From endoplasmic-reticulum stress to the inflammatory response', Nature, 454(7203), pp. 455–462. doi:10.1038/nature07203.

Zhang, L. and Wang, A. (2012) 'Virus-induced ER stress and the unfolded protein response', Frontiers in Plant Science, 3, 293. doi:10.3389/fpls.2012.00293.

Zhang, L. and Yin, F. (2014) 'Wildlife consumption and conservation awareness in China: a long way to go', Biodiversity and Conservation, 23(9), pp. 2371–2381. doi:10.1007/s10531-014-0708-4.

Zhang, S.L., Yu, Y., Roos, J., Kozak, J.A., Deerinck, T.J., Ellisman, M.H., Stauderman, K.A. and Cahalan, M.D. (2005) 'STIM1 is a Ca2+ sensor that activates CRAC channels and migrates from the Ca2+ store to the plasma membrane', Nature, 437(7060), pp. 902–905. doi:10.1038/nature04147.

Zhang, T., Wu, Q. and Zhang, Z. (2020) 'Probable pangolin origin of SARS-CoV-2 associated with the COVID-19 outbreak', Current Biology, 30(7), pp. 1346–1351.e2. doi:10.1016/j.cub.2020.03.022.

Zhao, H., Lu, X., Deng, Y., Tang, Y., Lu, J. and He, J. (2020) 'COVID-19: asymptomatic carrier transmission is an underestimated problem', Epidemiology and Infection, 148, e116. doi:10.1017/s0950268820001235.

Zhong, S., Crang, M. and Zeng, G. (2019) 'Constructing freshness: the vitality of wet markets in urban China', Agriculture and Human Values, 37(1), pp. 175–185. doi:10.1007/s10460-019-09987-2.

Zhou, Y., Meraner, P., Kwon, H.T., Machnes, D., Oh-hora, M., Zimmer, J., Huang, Y., Stura, A., Rao, A. and Hogan, P.G. (2015) 'STIM1 dimers undergo unimolecular coupling to activate Orai1 channels', Nature Communications, 6, 8395. doi:10.1038/ncomms9395.

Book review: Epidemic influenza — A survey. Edwin O. Jordan, Ph.D., Sc.D.' (1928) New England Journal of Medicine, 198(3), pp. 168–168. doi:10.1056/nejm192803081980333.